

NASA Contractor Report No. 180883

# Advanced Gearbox Technology

Advanced Counter-Rotating Gearbox  
Detailed Design Report

D.C. Howe, C.V. Sundt and A.H. McKibbin  
*UNITED TECHNOLOGIES CORPORATION*  
*Pratt & Whitney*  
*East Hartford, Connecticut*

October 1988

Prepared for  
Lewis Research Center  
Under Contract NAS3-24342

(NASA-CR-180883) AGBT ADVANCED  
COUNTER-ROTATING GEARBOX DETAILED  
DESIGN REPORT Report, Aug. 1984 -  
Jan. 1987 (PWA) 164 p

458306 156 p

N94-10400

Unclass

G3/37 0184024

## FOREWORD

The Advanced Gearbox Technology program is currently being conducted by Pratt & Whitney and Allison Gas Turbines under parallel NASA contracts. Mr. Gerald A. Kraft and Mr. Dean C. Reemsnyder, both of the Advanced Turboprop Project Office, NASA-Lewis Research Center, direct the overall effort. The Pratt & Whitney effort is under NASA Contract NAS3-24342. Mr. C. Reynolds is the propfan Program Manager at Pratt & Whitney, and Mr. D. C. Howe is the Project Manager responsible for this specific contractual effort. This report was prepared as a team effort by Messrs. D. C. Howe, C. V. Sundt and A. H. McKibbin of Pratt & Whitney.

Appreciation is extended to Mr. R. A. Stone of Sikorsky Aircraft and Mr. S. Amin of Pratt & Whitney Canada, who assisted in the design of gearbox hardware components described in this report; also to Mr. D. P. Townsend of the NASA-Lewis Research Center, and Mr. W. F. Johnson, Jr., private consultant, whose advice was especially helpful.

**PRECEDING PAGE BLANK NOT FILMED**

## TABLE OF CONTENTS

<u>Section</u>	<u>Page</u>
FOREWORD	iii
1.0 SUMMARY	1
2.0 INTRODUCTION	3
3.0 GEARBOX CONCEPT STUDIES	4
3.1 Gearbox Concept Screening Process	4
3.2 Gearbox Structural Configuration	7
3.3 Gearbox Concept - Advanced Technologies	13
4.0 TEST GEARBOX DETAILED DESIGN	16
4.1 Design Overview	16
4.1.1 Design Objectives	16
4.1.2 Design Requirements	17
4.2 Test Gearbox Configuration	20
4.2.1 Gearbox Efficiency Prediction	22
4.3 Gearing	24
4.3.1 Ring Gear	25
4.3.2 Planet Gear	25
4.3.3 Gear Tooth Design	27
4.3.3.1 Drive Side Pressure Angle Analysis	32
4.3.3.2 Dynamic Analysis	34
4.3.3.3 Deflection Analysis	41
4.3.3.4 Vibration Analysis	43
4.3.3.5 Sun/Planet Flexibility	44
4.3.4 Planetary Gear/Bearing Assembly Analysis	46
4.3.5 Gear Materials Selection	51
4.4 Bearings	52
4.4.1 Planet Bearings	56
4.4.2 Prop Shaft Support Bearings	58
4.4.3 Bearing Materials	66
4.5 Lubrication and Scavenging	66
4.5.1 System Description	66
4.5.2 Oil Transfer Unit	71
4.5.3 Bearing Lubrication	75
4.5.4 Gear Mesh Lubrication	80
4.5.5 Scavenging	84

TABLE OF CONTENTS (Continued)

<u>Section</u>	<u>Page</u>
4.6 Shafts and Housing	87
4.6.1 Shafts Design	89
4.6.1.1 Propeller Shaft Analysis	89
4.6.1.2 Carrier Shaft Analysis	96
4.6.1.3 Sun Shaft Analysis	100
4.6.1.4 Bearing Retaining Nut Analysis	103
4.6.1.5 Shaft Materials Selection	104
4.6.2 Housing Design	104
4.6.2.1 Prop-Side Housing	104
4.6.2.2 Engine-Side Housing	106
4.6.2.3 Housing Structural Analysis	106
4.6.2.4 Housing Materials Selection	108
4.7 Instrumentation	108
4.8 Weights and Materials Summary	112
4.9 Code Development	114
5.0 TEST FACILITY AND MULTIPURPOSE TEST RIG	116
5.1 Test Facility	116
5.2 Multipurpose Test Rig	120
5.3 Preliminary Test Plan	125
6.0 SUPPORTING TECHNOLOGY PROGRAMS	128
6.1 Scavenge Rig Test Program	128
6.1.1 Test Rig Description	128
6.1.2 Test Plan	130
6.1.3 Test Results	130
6.2 Lubrication Rig Test Program	131
6.2.1 Test Rig Description	134
6.2.2 Gear Lubrication Test Plan	135
6.2.3 Gear Lubrication Test Results	135
6.2.4 Windage Loss Test Plan	143
6.2.5 Windage Loss Test Results	143
7.0 SUMMARY AND CONCLUSIONS	145
REFERENCES	146
LIST OF SYMBOLS	147

## LIST OF ILLUSTRATIONS

<u>Number</u>	<u>Title</u>	<u>Page</u>
1	Offset Counter-Rotating Gearbox Candidates - Concepts Were Rejected by the Forced Decision Methodology	5
2	In-Line Counter-Rotating Gearbox Candidates - The Differential Planetary Concept Was Rated Best by the Forced Decision Methodology	5
3	Differential Planetary Concept Has Greatest Overall Potential. This concept is superior in reliability, efficiency, maintenance and acquisition cost.	7
4	Straddle-Mounted Differential Planetary. In this design, the prop shaft/ring gear support bearings are fore and aft of the gear set.	8
5	Cantilevered (Ring Gear/Carrier) Differential Planetary Gearbox Concept. In this design, the rear support bearings for the prop shaft/ring gear and carrier are forward of the gear set.	8
6	Close Coupled Differential Planetary Gearbox Concept. In this design, the reduction gearing is attached directly to the second stage propfan through the ring drive shaft.	9
7	Inter Prop Differential Planetary Gearbox Concept. In this design carrier support and interprop bearing functions are combined in one set of bearings of the five candidates, this arrangement is the most compact.	9
8	Grounded Planetary Gearbox. This concept converts the differential planetary configuration into a grounded system with a fixed speed ratio for each prop.	10
9	Counter-Rotating Gearbox, Forced Decision Analysis Comparison. The straddle-mounted and cantilevered arrangements were chosen for further study.	11
10	Straddle-Mounted Concept Shell Analysis. The analysis shows acceptable gear slope/misalignment from prop loads.	12
11	Cantilever System Shell Analysis. The analysis shows no significant misalignment from prop load, but the calculated slope for the seal arrangement is excessive.	12

LIST OF ILLUSTRATIONS (Continued)

<u>Number</u>	<u>Title</u>	<u>Page</u>
12	AGBT Gearbox Incorporates Advanced Technologies Identified in APET Studies	15
13	Selected Gearbox Configuration from Conceptual Design Studies Embodies Counter-Rotating, In-Line Planetary Gear System	20
14	On-Wing Maintenance Capabilities - Easy access is provided to carbon seals, oil pumps, last-chance filters and oil supply jets.	21
15	Test Gearbox Configuration Showing Major Design Features	22
16	External Details of Engine-Side and Prop-Side Housings	23
17	Basic Functioning Characteristics of the Differential Planetary Gear System - Viewed from engine toward gearbox assuming a tractor installation	24
18	Comparison of Standard Involute and High Contact Ratio Gear Tooth Designs - High contact ratio teeth improve load-carrying ability.	28
19	Advanced Buttress Tooth Form - At least 2 gear tooth pairs are always in contact at one time.	29
20	Advanced Buttress Tooth Form Specimen Test Results Show Significant Life Improvement Over Standard Involute Form	29
21	Contact Ratio and Addendum Geometry Combinations Showing Region of Acceptable Candidates	31
22	Drive Side Pressure Angle Selection - 20 Degrees provides best combinations of minimum bending stress and low critical contact temperature rise.	34
23	GEARDYN Tooth Compliance Results Showing Gear Tooth Contact Pattern Along Line of Action	35
24	GEARDYN Tooth Load Distribution Results Showing Smoothing Effect Caused by Tip Relief	35
25	Calculated Tooth Loading Profiles With No Tooth Spacing Error Accounted For	36

LIST OF ILLUSTRATIONS (Continued)

<u>Number</u>	<u>Title</u>	<u>Page</u>
26	Calculated Tooth Loading Profiles With Tooth Spacing Error of 0.00076 cm (0.0003 in)	37
27	Ring Gear Deflection Analysis	41
28	Comparison of Rigid and Flexible Ring Gear Designs - The flexible design is more accommodating of spacing errors and has been designed as backup.	43
29	Gear Vibration Excitation Frequencies - Analysis showed that vibration frequencies are well above excitation frequency.	43
30	Finite Element Analysis Model Used to Assess Sun/Planet Flexibility	44
31	Load Distribution Across Sun/Planet Gear Mesh - Load is more nearly uniform with flexible ring gear support.	45
32	Finite Element Model Used for Planet Gear and Bearing Load and Stress Analysis	47
33	Comparison of Spherical Roller Load Distributions - Finite element analysis results show the same number of rollers in the loaded zone as that determined by the PLANETSYS analysis method.	49
34	Distribution of Combined Stresses in the Tooth Root Fillets at the Sun/Planet Gear Mesh and the Ring/Planet Gear Mesh	50
35	Combined Stresses in Planet Gear Tooth Root Fillets Are Acceptable Even With a Factor of 1.5 Included - More flexibility could be incorporated in the bearing outer race without critically influencing the maximum fillet stress.	51
36	High Hot Hardness Steels Improve Scoring Resistance and Fatigue Life Relative to Standard AISI-9310 Gear Materials	52
37	Bearing Arrangement for Differential Planetary Gearbox - Four bearing sets encompass eight separate bearing locations.	53

LIST OF ILLUSTRATIONS (Continued)

<u>Number</u>	<u>Title</u>	<u>Page</u>
38	Integral Planet Gear/Bearing Configuration - This single unit construction provides lowest weight design.	57
39	Roller Cage Design - Features shown enhance strength while achieving minimum weight and adequate cage support surface area.	58
40	Tapered Roller Bearings (Spaced Apart) - Provides potential benefits in reliability and maintainability, but with a risk of increased power loss.	60
41	Duplex Tapered Bearings - Transfers shaft bending moments directly to the housing, potentially reducing prop shaft bending and ring gear distortion, but with a risk of increased power loss.	61
42	Prop Shaft Section Deformation at Ball and Roller Bearing Locations - Ovality is not a serious limitation on bearing life.	64
43	Selected Oil Cooling System for Advanced Turboprop Engine - Separate gearbox and engine supplies offer flexibility in configuring air/oil coolers and managing heat loads throughout the flight cycle.	67
44	Lubrication System Schematic Designed for the Gearbox Uses a Positive Displacement Pump and Pressure Regulating Valve to Ensure Adequate Oil Supply	68
45	"Last-Chance" Filters Screen Foreign Particles Too Large to Pass Through the Smallest Lubricant Metering Jets	69
46	Modulated Lubrication System Provides Recovery of Gearbox Efficiency at Cruise Power	70
47	Oil Transfer Unit - Transfers high pressure oil from a stationary source to rotating parts.	72
48	Journal Bearing Design Approach Selected for Oil Transfer Unit - Effectively controls friction at transfer sleeve-support housing interface.	73
49	Transfer Sleeve Force Balance Results In Acceptable Oil Leakage Rates	74

LIST OF ILLUSTRATIONS (Continued)

<u>Number</u>	<u>Title</u>	<u>Page</u>
50	Distribution of Oil Transfer Unit Flows and Pressures - All are acceptable.	74
51	Bearings and Bearing Locations Serviced by the Lubricant Supply System	75
52	Lubricant Distribution Through Oil Transfer Unit	76
53	Lubrication Schemes for the Number 5, 6, 7 and 8 Bearings	76
54	Lubrication Schemes for the Number 2, 3 and 4 Bearings	78
55	Summary of Bearing Oil Flows and Temperatures - Positive bearing lubrication is provided and temperature rise is acceptable.	79
56	Number 1 (Planet) Bearing Lubrication Scheme	80
57	Oil Distribution System for the Sun and Planet Gear Meshes - Primary and secondary jets provide modulated flow capability.	81
58	Initial Oil Spray Pattern Into Gear Meshes - Testing may lead to a more optimum pattern.	81
59	Possible Modification to the Primary Jet Flow Passage - Reduces the risk of plugging from particulate matter entrained in the oil stream.	83
60	Scavenge System Features - Collector cartridge directs scavenged oil to magnetic chip detector and scavenge pumps.	85
61	Scavenge Collector Cartridge Details - Deflectors direct captured lubricant into flow discharge ports.	85
62	Scheme for Injecting Air Into the Gear Mesh - Tests showed that this had little or no effect on scavenge effectiveness.	86
63	Scavenge Route for Oil Exiting the Gear Mesh and Number 1, 5 and 6 Bearings	87
64	Deflection and Stress Analysis - The design meets structural requirements.	88

LIST OF ILLUSTRATIONS (Continued)

<u>Number</u>	<u>Title</u>	<u>Page</u>
65	Propeller Shaft Finite Element Model	90
66	Torque Tube Cyclic Fatigue Results	91
67	Torque Tube Stress Analysis Results	91
68	Prop Mount Flange Details	92
69	Mount Flange Stress Analysis Results at Nominal Operating Conditions Are Well Within Allowable Limits	93
70	Mount Flange Stress Analysis Results at Maximum Maneuver and Blade Loss Conditions - Bolt stresses are within allowable limits.	93
71	Torque Tube/Prop-Side Ring Gear Support Shaft Interface Showing Locations of Highest Contact Stresses	94
72	Cycle Slip Analysis Results for Front and Rear Connection Cones - Shows acceptable results for rear cone but unacceptable for a front cone design.	95
73	Cyclic Stress and Contact Stress Analyses Show Acceptable Results	95
74	Propeller Shaft Deflection Analysis Results Show Deflection Consistent With Allowable Levels	96
75	Carrier Shaft Finite Element Model	97
76	Carrier Shaft Deflection Analysis Results Show Acceptable Slope Deflection of 0.0004 at Planetary Gear Support Posts	98
77	Locations of Potential Maximum Stress on Carrier Shaft	98
78	Carrier Shaft Stress Analysis Results Show Stresses to be Within Allowable Limits	99
79	Carrier Shaft Showing Area Thickened to Meet Critical Speed Margin Requirements	100
80	Sun Shaft Showing Regions of Potential Maximum Stress	101
81	Sun Shaft Stress Analysis Results Show That Life Requirements are Met	102

LIST OF ILLUSTRATIONS (Continued)

<u>Number</u>	<u>Title</u>	<u>Page</u>
82	Gearbox Bearing Retaining Nut Locations	103
83	Typical Bearing Configuration (Location 2)	103
84	Gearbox Housing Assembly Showing Three Major Components	105
85	Prop-Side Housing Details	105
86	Engine-Side Housing Details	106
87	Housing Assembly Finite Element Analysis Model	107
88	Housing Assembly Finite Element Analysis Showing Regions of Maximum Potential Stress	107
89	Housing Stress Analysis Results Show Acceptable Cyclic Life Under the Most Limiting Load Condition	108
90	Location of Instrumentation Used Primarily for Performance Measurement	109
91	Location of Instrumentation Used Primarily for Structural and Mechanical Assessment	110
92	Location of Instrumentation Used Primarily for Condition Monitoring	110
93	Rig Telemetry System	111
94	Advanced Gearbox Technology Test Facilities: Overall View with Rotating Testbed Tilted at a 45 Degree Angle	117
95	Rotating Testbed Drive and Braking Systems	118
96	Advanced Gearbox Technology Test Facilities: Rotating Testbed, Bottom View	118
97	Advanced Gearbox Technology Test Facilities: Test Stand Computer Control System	119
98	Advanced Gearbox Technology Test Facilities: Portable Data Recording System	119
99	Multipurpose Test Rig as Assembled for Test	121

LIST OF ILLUSTRATIONS (Continued)

<u>Number</u>	<u>Title</u>	<u>Page</u>
100	Test Rig Showing Principal Interfaces Where Quick Disconnects Are Utilized	122
101	Torquer Unit: Test Gearbox View	123
102	Torquer Unit: Slave Gearbox View	123
103	Multipurpose Test Rig as Mounted on Test Facility Testbed (Top View)	124
104	Collector Insert Configurations - Designs to evaluate scavenging effectiveness.	128
105	Test Rig - Configured for Scavenge Tests	129
106	Power Consumption Versus Oil Flow - Power increased 15% when 18.1 kg/min (40 ppm) auxiliary oil was introduced into the double scroll configuration.	131
107	Oil Scavenge Design Effectiveness - Constant volume collector configuration was best.	132
108	Oil Scavenge Design Effectiveness - Constant volume collector configuration was best.	132
109	Power Consumption with Added Air - No impact on scavenge effectiveness.	133
110	Planetary Lubrication Rig Gear Configuration	133
111	Test Rig as Configured for Lubrication Tests	134
112	Planetary Lubrication Rig Spray Bar Out-of-Mesh Configurations - For testing effectiveness in reducing losses in triangular spaces between gears.	137
113	Lubrication Spray Angle Test - To evaluate effectiveness of an axial component of flow.	137
114	Pressure Transducer Locations for Gear Mesh Scavenge Oil Pressure Measurements - Provides an indication of gear tooth pumping work.	138
115	Planetary Lubrication Rig: Input Power Versus Sun Gear Speed; Primary and Secondary Spray Bars Installed - Power consumption increases by 30% at takeoff oil flows.	139

LIST OF ILLUSTRATIONS (Continued)

<u>Number</u>	<u>Title</u>	<u>Page</u>
116	Planetary Lubrication Rig: Comparison of Results With and Without Primary Spray Bars Installed - Power consumption was relatively insensitive to removal of the primary spray bar.	140
117	Angled Oil Jets Versus Radial Oil Jets - No change is evident with primary oil flow only.	141
118	Angled Oil Jets Versus Radial Oil Jets - A 10% reduction in power consumption is achieved with angled jets when secondary flow is added.	142
119	Planetary Lubrication Rig: Effect of Air Windage on Power Losses - A nominal 15% reduction in power consumption was achieved with 37.1 cm (14.6 in) Hg vacuum.	144

## LIST OF TABLES

<u>Table</u>	<u>Title</u>	<u>Page</u>
1	Counter-Rotating Reduction Gear Forced Decision Evaluation Parameters	6
2	Gearbox Technical Comparison	13
3	Basic Design Requirements	17
4	CR Propfan Characteristics Influencing Gearbox Design	18
5	Flight Mission Profile for 120 Passenger Aircraft	19
6	Flight Attitude and Maneuver Loads	19
7	AGBT Build 1 Loss Prediction (Values at Design Speed and 12,000 SHP Sea Level Takeoff Power)	22
8	Comparison of Conventional and High Contact Ratio Gear Geometries Showing Selected Ring Gear Pitch Diameter	26
9	Comparison of Four and Five Planet Gear Design: The Five Planet Design Was Selected	27
10	Constraints Affecting Gear Design Optimization	30
11	Acceptable Tooth Count Combinations: The Sun/Planet/Ring Tooth Count of 73/97/267 Was Selected As Best	32
12	Stress and Temperature Rise Variations With Change In Gear Tooth Drive Side Pressure Angle	33
13	Comparison of Allowable Gear Tooth Stresses As Calculated Using AGMA and GEARDYN Analytical Codes	38
14	Summary of Gear Dynamic Analysis Results - Stresses and Scoring Temperature Rise Are Within Allowable Levels	39
15	Comparison of Preliminary Design and Finalized Detail Design High Contact Ratio Gear Characteristics	40
16	Bearing Selection Summary (Preliminary Design)	54
17	Bearing Selection (Detail Design) Gear and Shaft Support Bearing Configurations	55
18	Bearing Operation: Durability Objectives Are Met	59
19	Optimal Bearing System Risk/Benefit Analysis	62

LIST OF TABLES (Continued)

<u>Table</u>	<u>Title</u>	<u>Page</u>
20	Summary of Bearing Loads and Fit-Ups	65
21	Advanced Turboprop Engine Oil System Requirements (12,000 Horsepower Size Engine)	67
22	Calculated Power Loss, Oil Flow and Temperature Rise Summary at Takeoff Power Conditions	84
23	Summary of Instrumentation Used in Build 1 Test Rig	109
24	Gearbox Weight and Material Summary	113
25	Pretest Calibrations and Functional System Checks	126
26	Test Parameters to Be Investigated and Monitored During Gearbox Build 1 Testing	127
27	Scavenge Rig Test Plan	130
28	Gear Mesh Scavenge - Phase I Test Plan (Oil Supply Temperature = 93°C (200°F))	136

## 1.0 SUMMARY

In earlier NASA-sponsored studies, fuel burn benefits on the order of 21% and direct operating cost benefits on the order of 10% were identified for geared, propfan-powered transport aircraft when compared with comparable technology high bypass ratio turbofan engines. Under this current contract, an Advanced, In-Line Counter-Rotating (CR) Differential Planetary Gearbox has been designed and fabricated to evaluate the efficiency, durability and weight characteristics of the gearbox as they relate to emerging propfan-powered airplane performance and flight worthiness requirements. The Counter-Rotating In-Line Differential Planetary Gear System was selected as the best of ten candidate arrangements studied in an earlier conceptual design study phase. It was superior in reliability, efficiency, weight, maintenance and acquisition cost. Principal features of the design include:

- o 8.315 reduction ratio
- o remote pitch control
- o straddle-mounted prop shaft/ring gear support bearings
- o 5 planet gear planetary system
- o high contact ratio buttress gear tooth form
- o single row spherical roller planet bearings integral with planet gears
- o combination ball/roller prop shaft support bearings
- o modulated gearbox lubrication supply system separate from the engine lube system

The test gearbox was designed for 12,000 HP (nominal) with growth capability to 15,000 HP. It is compatible with the Hamilton Standard CR-geared propfans. The principal design criteria were based on meeting a fully developed gearbox durability goal of 30,000 hours mean-time-between-unplanned-removals (MTBUR) and an efficiency goal equal to or greater than 99%. The gearbox design meets structural and reliability goals when applied to the aircraft mission and duty cycle requirements of a competitive 155 passenger aircraft design. Advanced technology materials applicable to the durability goal include high strength CRB7 bearing materials and high strength, high hot hardness Carpenter EX-53 steel gear material. A high contact ratio buttress tooth form is used to reduce tooth stress, thereby increasing durability, and provision is made for advanced high temperature capability lubricants. Bearing life predictions exceed the L10 life goal of 18,000 hours. Advanced technologies applicable to the efficiency goal include a modulated lubricant supply system coupled to an aerodynamic scavenge system and spherical roller bearings integral with the planet gears.

Instrumentation design was an integral part of the overall gearbox design effort, with the objective to provide sufficient instrumentation to accurately assess the performance and structural-dynamic characteristics of the gearbox and to provide essential on-line condition monitoring during gearbox testing.

A fully automated test facility and multipurpose test rig were provided by the Contractor and are available for future test evaluation of the gearbox. The facility and rig are capable of meeting the full range of gearbox test operational requirements; including power capacity up to 20,000 SHP and torque loads up to 56,492 Nm (500,000 in-lb). Other capabilities include simulation of propeller thrust, side and torque loads as well as simulation of aircraft attitude.

Two contractor-funded supporting technology programs provided data to assist in the gearbox design definition. The first, a scavenge test program, showed that a constant volume collector configuration had the highest scavenge effectiveness of the three configurations tested, and that the addition of airflow had no noticeable impact on scavenge effectiveness. The second, a lubrication test program, showed that gearbox losses could be reduced by controlling the air/oil mixture ratio of the gearbox lubricant and by imparting an axial component to the oil jets flowing into the sun/planet gear mesh. The lubrication tests confirmed the benefits associated with a modulated lubrication supply system.

The detailed analyses, design and fabrication work conducted under this contract have further substantiated the conclusions drawn from previous studies that substantial improvements in fuel burned and direct operating costs can be made with a geared, propfan-powered transport aircraft. Full realization of this potential is dependent on development testing of the gearbox and advanced technologies.

## 2.0 INTRODUCTION

The NASA Advanced Turboprop (ATP) program has the objective to establish both single-rotation and counter-rotation propfan technology for Mach 0.65 to 0.85 aircraft applications. As part of the ATP program, NASA sponsored the Advanced Propfan Engine Technology (APET) definition studies (Reference 1), which defined the potential of an advanced, geared propfan propulsion system to offer significant savings in fuel burn and operating cost when compared with turbofan propulsion systems. The APET program was conducted, under parallel contracts, by Pratt & Whitney, Allison Gas Turbines and General Electric. These studies corroborated the beneficial aspects of a propfan system, and identified critical technologies necessary to enable propfan propulsion systems to be available for commercial airline usage in the early 1990s.

An advanced technology gearbox was identified as a critical technology. A gearbox enables optimizing the design of the two major components: the power turbine and propfan. A reduction gearbox uniquely permits: (1) a high-speed power turbine with a smaller diameter and fewer stages for the best efficiency; and (2) a low speed, lightly loaded propfan for maximum efficiency and lower noise levels. In order to develop an efficient, durable and low maintenance gearbox, the APET program was extended to conduct a conceptual and preliminary design study of both single- and counter-rotation gearboxes, as well as propfan pitch change systems in the 10,000 SHP class. Pratt & Whitney and Allison Gas Turbines conducted parallel efforts through the preliminary design of a large-scale, flight design, advanced CR gearbox.

Both phases of the APET program verified large potential payoffs for an advanced technology gearbox counter-rotation propfan system relative to a turbofan propulsion system. In addition, the studies quantified and qualified the use of advanced technologies in the design of future propfan gearboxes. Overall, the APET Definition Study and the preliminary gearbox design efforts provided an essential technology base for the conduct of the AGBT contract effort reported herein.

The Advanced Gearbox Technology (AGBT) program was initiated in 1984 under the joint sponsorship of NASA and Pratt & Whitney. The original objectives of the AGBT program were to design, fabricate and test the in-line, 12,000 SHP advanced counter-rotation gearbox.

This report documents the detail design and fabrication of the counter-rotation test gearbox. In addition, the test rig design, installation and checkout, and supporting technology programs are described.

### 3.0 GEARBOX CONCEPT STUDIES

The APET counter-rotating propeller/gearbox study (NASA Contract NAS3-23045), which Pratt & Whitney conducted in 1983, included concept studies which provided the starting point for the subsequent gearbox design efforts described in Section 4.0 of this report. Study results were reported in Reference 1 and are summarized in the following sections.

#### 3.1 Gearbox Concept Screening Process

A screening process was conducted to evaluate candidate gearbox concepts and to select the best of these for further analyses and design. Basic turboprop design requirements were established for a commercial (120 passenger) transport, 1800 nautical mile design range, short mission lengths ( 1 hour), 0.75 Mach at 10,668 m (35,000 ft) cruise, two wing-mounted 12,000 SHP engines and Hamilton Standard 10 blade single-rotating or counter-rotating propfan.

A survey of all known gearbox drive concepts identified five offset and five in-line concepts for further study. These concepts are listed below and shown in Figures 1 and 2. At the conclusion of this study the Differential Planetary In-line Gear System was selected as being the best choice for counter-rotation propfans.

The five offset gearbox candidates were:

- o The dual compound idler
- o The dual compound idler with reversing idler
- o The spur with reversing idler
- o The dual compound bevel
- o The spur-differential planetary

The five in-line gearbox candidates were:

- o The differential planetary
- o The split path planetary
- o The compound planetary
- o The planetary with reversing bevel
- o The multiple compound idler

A forced decision selection methodology was used to evaluate the candidate concepts. In this process, rating parameters, summarized in Table 1, were selected and ranked in terms of their importance in meeting the objectives of a successful counter-rotating propfan transport aircraft. The weighting factors were determined by a Delphi statistical analysis, using the team of experienced engineers assigned to the program. (In the Delphi process, each team member provides his/her weighted opinion on the candidate elements of the topic. The results are statistically analyzed and returned to the members, who after reconsideration are polled again to obtain a final statistical ranking).

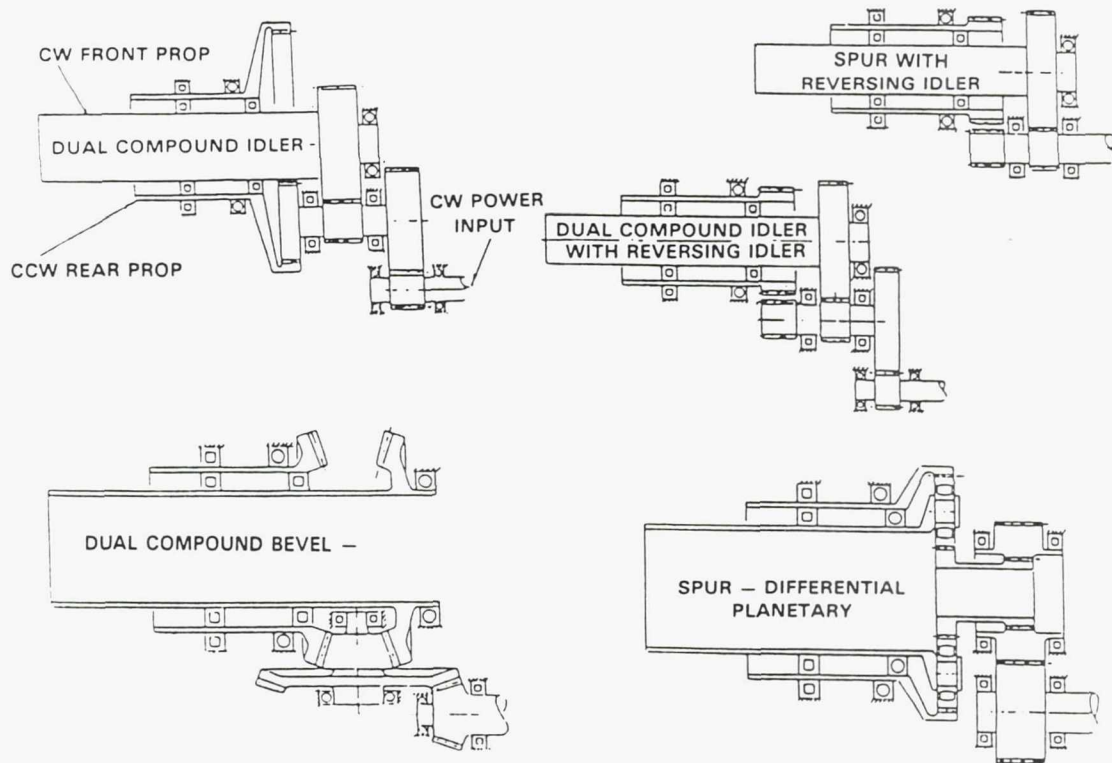


Figure 1 Offset Counter-Rotating Gearbox Candidates - Concepts Were Rejected by the Forced Decision Methodology

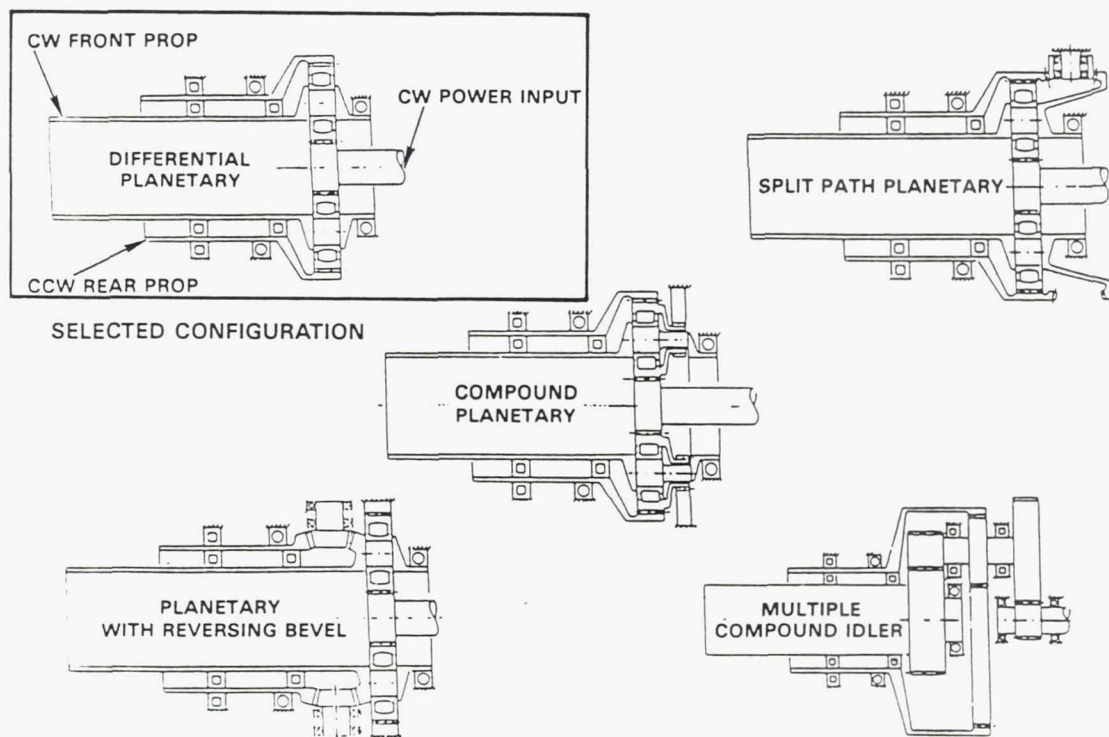


Figure 2 In-Line Counter-Rotating Gearbox Candidates - The Differential Planetary Concept Was Rated Best by the Forced Decision Methodology

Table 1 Counter-Rotating Reduction Gear Forced Decision Evaluation Parameters

	Weighting Factor (Property Emphasis Coefficient)
Reliability	0.18
Efficiency	0.17
Maintenance	0.13
Acquisition Cost	0.12
Pitch Control Accessibility	0.12
Weight	0.11
Technical Risk	0.08
Ease of Scaling	0.04
Acoustic Signature	0.03
Spatial Envelope	0.02
Total	1.00

Figure 3 summarizes the results of the Delphi statistical analysis conducted by the team members to compare the relative merits of the most promising candidate systems. The Differential Planetary In-line Gear System received the highest figure of merit. It was judged to be superior in all categories except Pitch Control Access, which was complicated by its location inside the gearbox. Subsequently, the design was changed to provide for an accessible remotely located pitch control system.

Of the offset concepts, the dual compound idler and the dual compound idler with reversing idler were rejected because they are relatively heavy, complex and have large diameters. The compound bevel was rejected because it is very heavy, and the spur with reversing gear was rejected because it is too large. The spur-differential planetary concept was the most attractive.

Of the in-line candidates, the planetary with reversing bevel was rejected because it is heavy and inefficient. The compound planetary was rejected because it is relatively complex and less reliable. The multiple compound idler and the split path planetary were rejected because they are heavy, complex and difficult to maintain. The differential planetary was chosen because it is simple, light, efficient and offers the greatest overall potential of the in-line and offset gear systems.

LEGEND:  
 1 = RELIABILITY  
 2 = EFFICIENCY  
 3 = MAINTENANCE  
 4 = ACQUISITION COSTS  
 5 = PITCH CONTROL RISK  
 6 = WEIGHT  
 0 = INSTALLATION CONSIDERATIONS

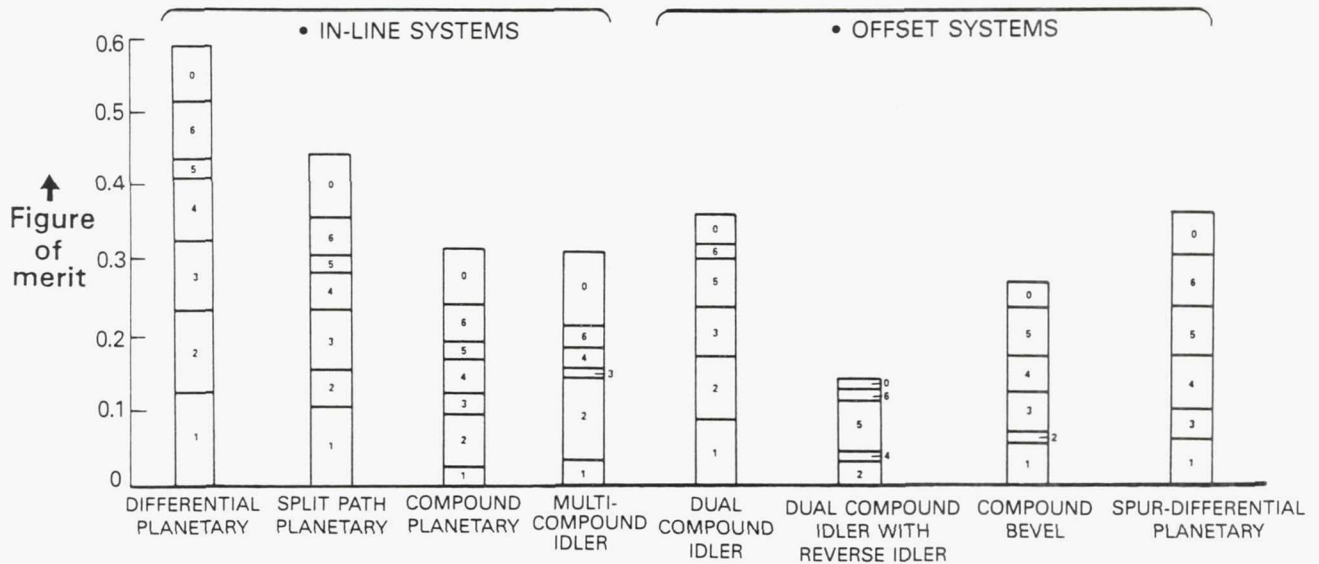


Figure 3 Differential Planetary Concept Has Greatest Overall Potential. This concept is superior in reliability, efficiency, maintenance and acquisition cost.

### 3.2 Gearbox Structural Configuration

Once the differential planetary in-line arrangement was selected, design refinement studies were initiated to provide a basis for selecting the best structural configuration to continue into detail design. This process resulted in selection of the straddle-mounted structural configuration shown in Figure 4.

Four different structural arrangements were configured using the differential gearing to optimize the differential planetary in-line concept. Each system has a unique support structure, and each was evaluated using the critical parameters from the conceptual studies. A fifth gearbox arrangement (the nondifferential grounded system) was included in this study to address a concern over controlling rotor speeds in a failure mode. Subsequent failure mode and effects analysis indicated that design features incorporated into the propfan pitch change mechanism and control logic were adequate to assure safe operation with the ungrounded system. The five structural candidates studied are illustrated in Figures 4 through 8.

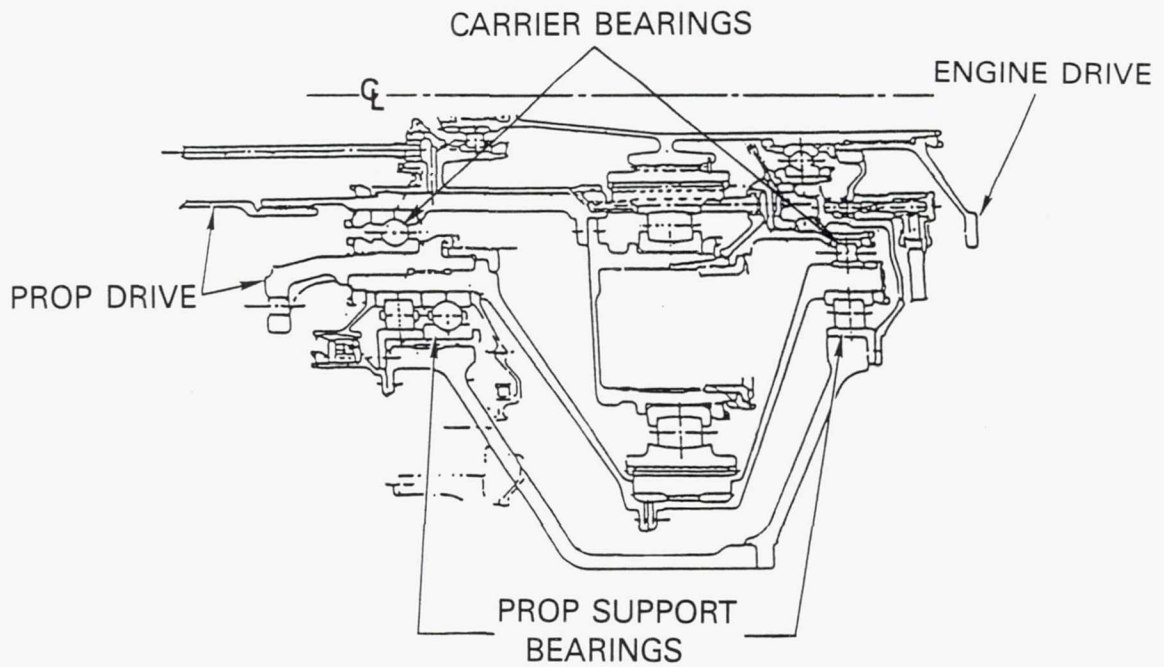


Figure 4 Straddle-Mounted Differential Planetary. In this design, the prop shaft/ring gear support bearings are fore and aft of the gear set.

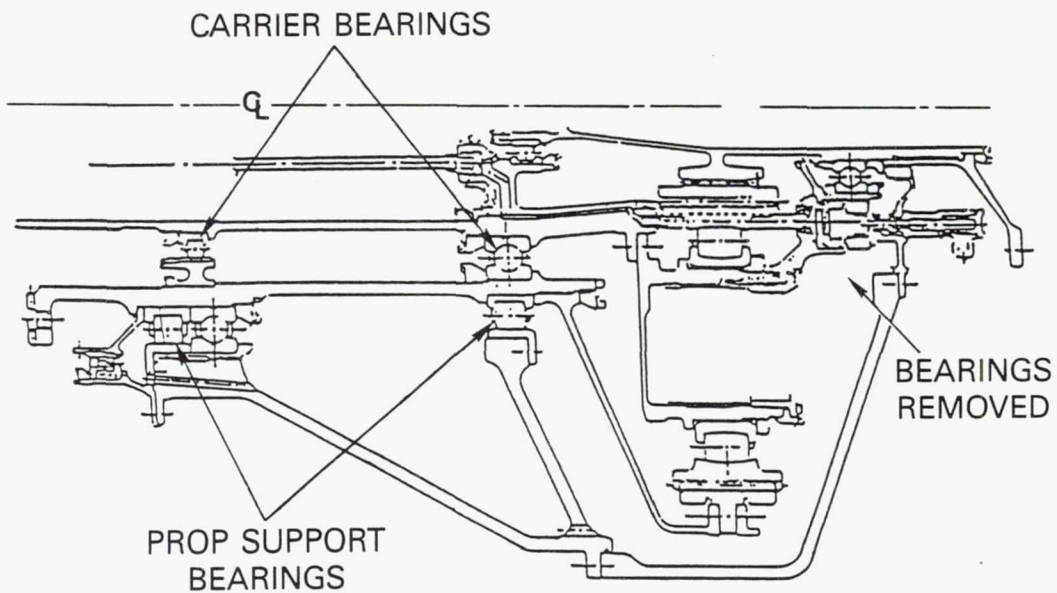


Figure 5 Cantilevered (Ring Gear/Carrier) Differential Planetary Gearbox Concept. In this design, the rear support bearings for the prop shaft/ring gear and carrier are forward of the gear set.

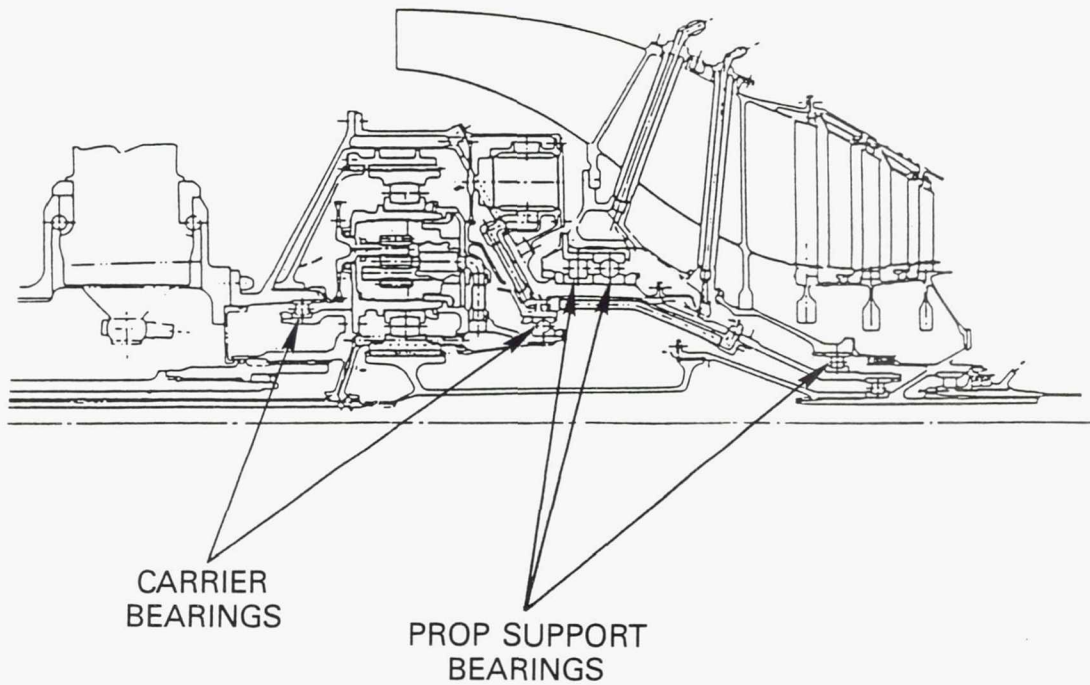


Figure 6 Close Coupled Differential Planetary Gearbox Concept. In this design, the reduction gearing is attached directly to the second stage propfan through the ring drive shaft.

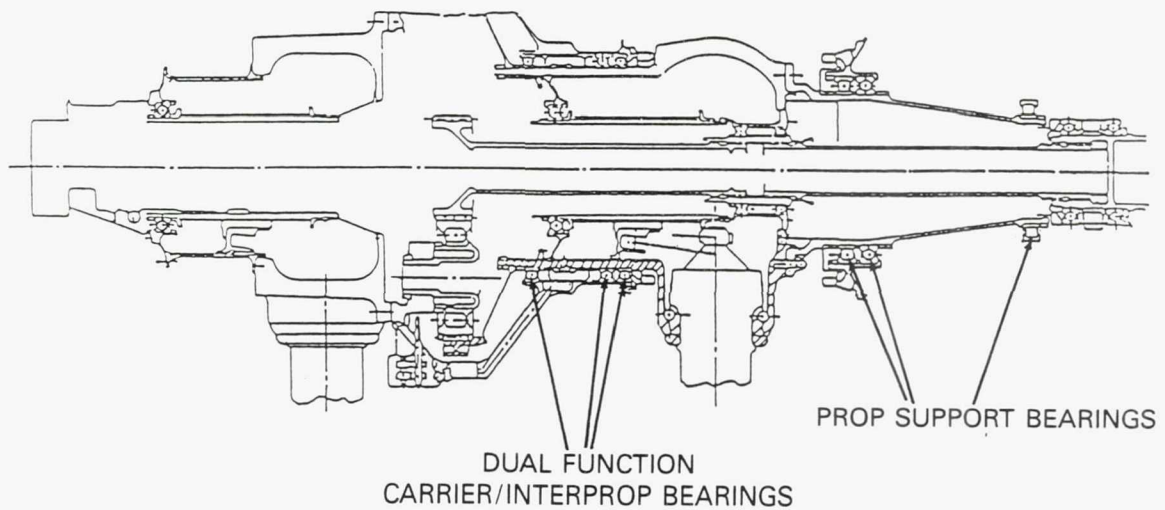


Figure 7 Inter Prop Differential Planetary Gearbox Concept. In this design, carrier support and interprop bearing functions are combined in one set of bearings. Of the five candidates, this arrangement is the most compact.

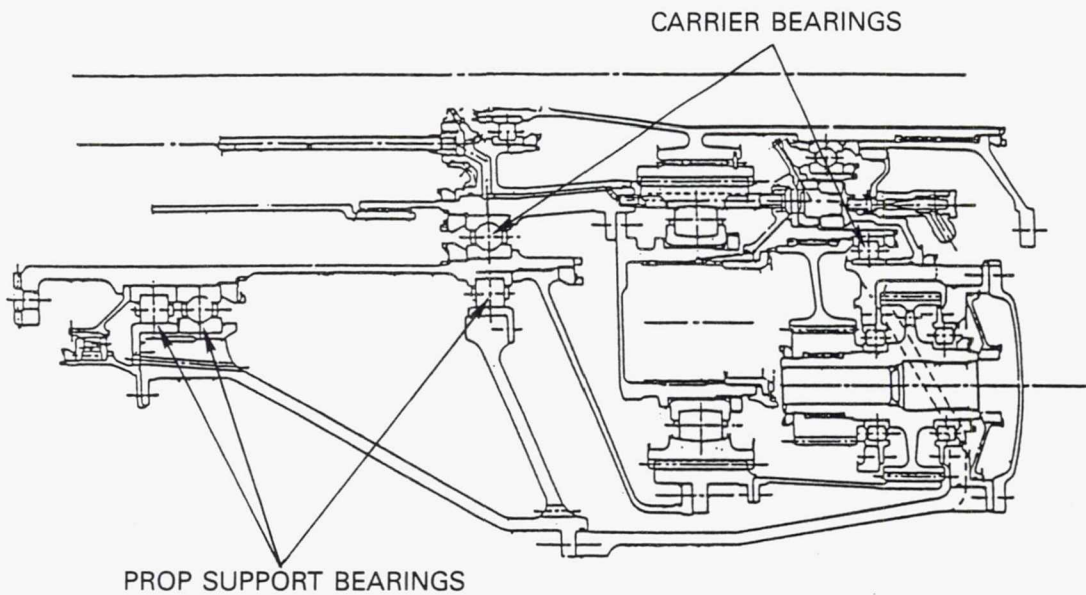


Figure 8 Grounded Planetary Gearbox. This concept converts the differential planetary configuration into a grounded system with a fixed speed ratio for each prop.

The five concepts were evaluated using the forced decision screening methodology described earlier. The analysis included sizing the gears and bearings and conceptually designing each configuration to identify the number of gears, bearings and spatial envelope requirements. This information provided preliminary estimates to assess the reliability, technical risk and installation considerations.

Figure 9 summarizes the results of this evaluation. Note that the split path grounded system did not compare well with the other arrangements. Weight, maintainability, reliability and efficiency parameters penalized this arrangement. The straddle-mounted and cantilevered arrangements rated closely, with a slight advantage given to the straddle-mounted because it has a shorter installation length. The forced decision analysis identified both of these designs as being superior in most categories, so both were chosen for further study before a final selection was made.

A technical and economic evaluation was made to compare the straddle-mounted and cantilevered arrangements on the basis of aircraft mission fuel burn and direct operating costs. To compare fuel burn and direct operating costs, additional analysis of the straddle-mounted and cantilevered arrangements was conducted to evaluate the impact of the prop shaft loading on the gear mesh and on the overall system. A shell analysis was conducted under a 1.5G and 1P shear load of 26,689 N (6,000 lb) to determine the impact of shaft and hub deflection on the gear mesh misalignment. A slope of 0.0004 is judged by experience to be acceptable in normal crowned gear operation. The analysis showed that the resultant 0.00014 misalignment slope is well within this

allowable limit. Figure 10 shows graphically the results of the straddle-mounted analysis. Figure 11 represents the cantilevered analysis, where an excessive slope at the drive coupling end was calculated. The slope and deflection analysis highlights the major advantages and disadvantages of each arrangement. The cantilevered arrangement supports the gear package as a unit. Deflection of the prop shaft cannot generate slope differences between gears because all gears move as a unit. However, the carbon seal located on the input shaft is grounded to the housing; therefore, there is a slope difference generated between the carbon seal land located on the rotor and the seal. The calculated slope is 0.001 which experience has shown to be excessive for this type of seal arrangement.

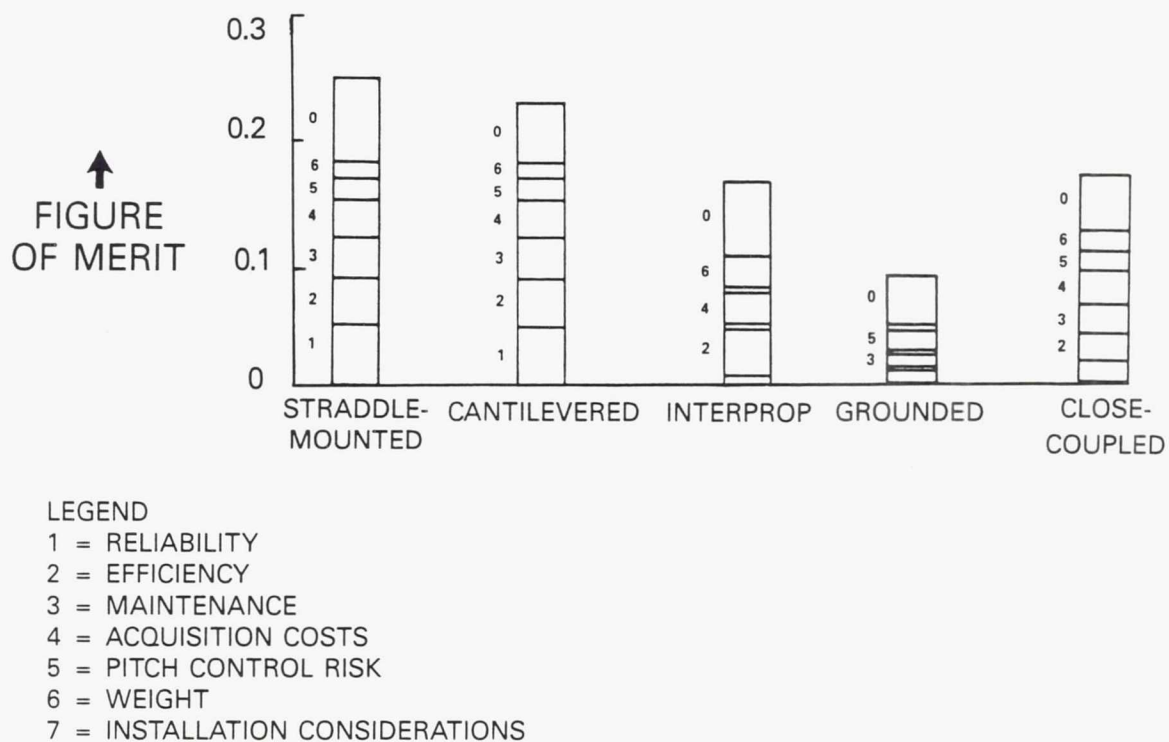
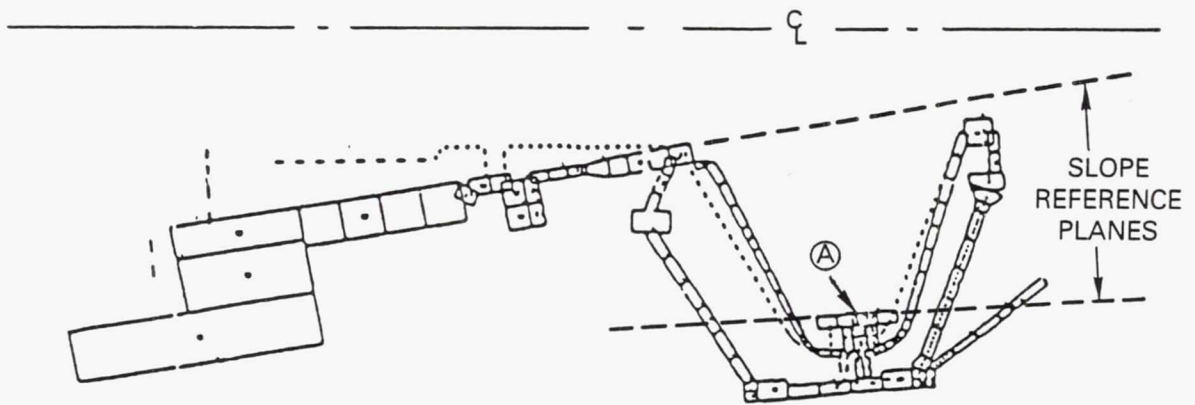
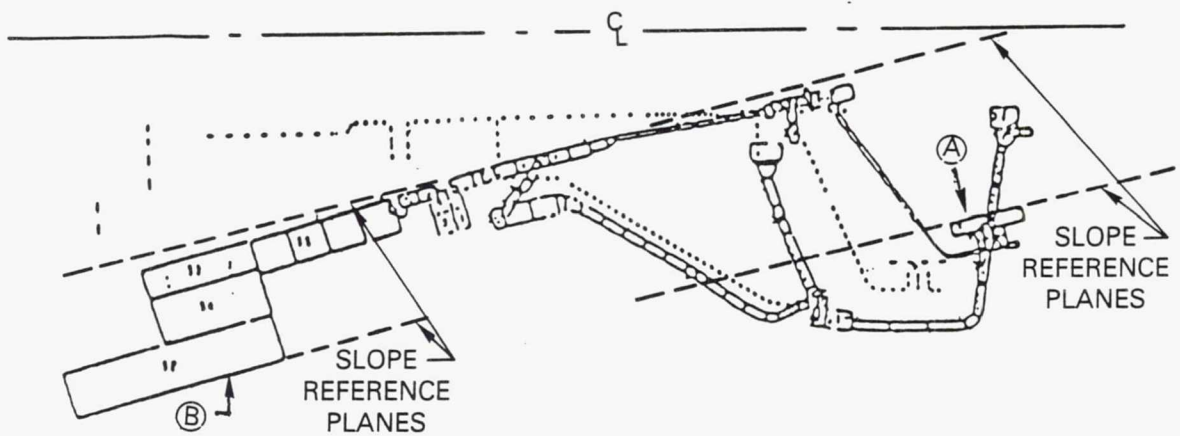


Figure 9 Counter-Rotating Gearbox, Forced Decision Analysis Comparison. The straddle-mounted and cantilevered arrangements were chosen for further study.



Ⓐ RELATIVE SLOPE AT RING/PLANET GEAR MESH — 0.00014

Figure 10 Straddle-Mounted Concept Shell Analysis. The analysis shows acceptable gear slope/misalignment from prop loads.



Ⓐ RELATIVE SLOPE AT RING/PLANET GEAR MESH = 0.0

Ⓑ SLOPE AT DRIVE COUPLING END = 0.001

Figure 11 Cantilever System Shell Analysis. The analysis shows no significant misalignment from prop load, but the calculated slope for the seal arrangement is excessive.

Table 2 shows the gearbox technical and economic evaluation comparison between the straddle-mounted and cantilevered designs. The ratings of the two designs are essentially equal in terms of fuel burn and direct operating costs. A slight advantage in reliability, maintainability, weight and length is achieved in selection of the straddle-mounted arrangement.

Table 2 Gearbox Technical Comparison

	Straddle	Cantilever
Efficiency	Base	Base
Reliability (MTBUR), hours	Base	-5800
Maintainability, \$/EFH	Base	-0.25
Weight, kg (lb)	Base	+9.1 (+20)
Cost difference	Base	-4%
Technical risk	--	Ring shaft vibration
Gear mesh misalignment	Acceptable	0
Shaft seal alignment	Acceptable	Unacceptable
Installation length, cm (in)	Base	+15.2 (+6)
Fuel burn	Base	+0.04%
Direct operating cost	Base	-0.03%

### 3.3 Gearbox Concept - Advanced Technologies

Advanced technologies identified in the APET program were carried forward in the detail design of the advanced counter-rotating test gearbox described in Section 4.0 of this report. Principal among these are the technologies shown in Figure 12.

CRB7 Bearing Material - This advanced material has a potential life improvement over M-50 currently in use. It is being utilized in the planet bearing outer ring of the test gearbox first build and may have application in the planet bearing inner ring as well. M-50-NiL (a case-hardened material) is also a candidate for both highly loaded propshaft bearings and integral gear planet bearings.

Integral Planet Gear/Bearing Design - This approach results in a more compact, lighter weight and durable configuration compared to separate bearings and gears. It also provides the increased bearing load capacity needed in the high centrifugal load field of the planet gear system. (See Sections 4.3 and 4.4 for detailed discussion of gear and bearing designs.)

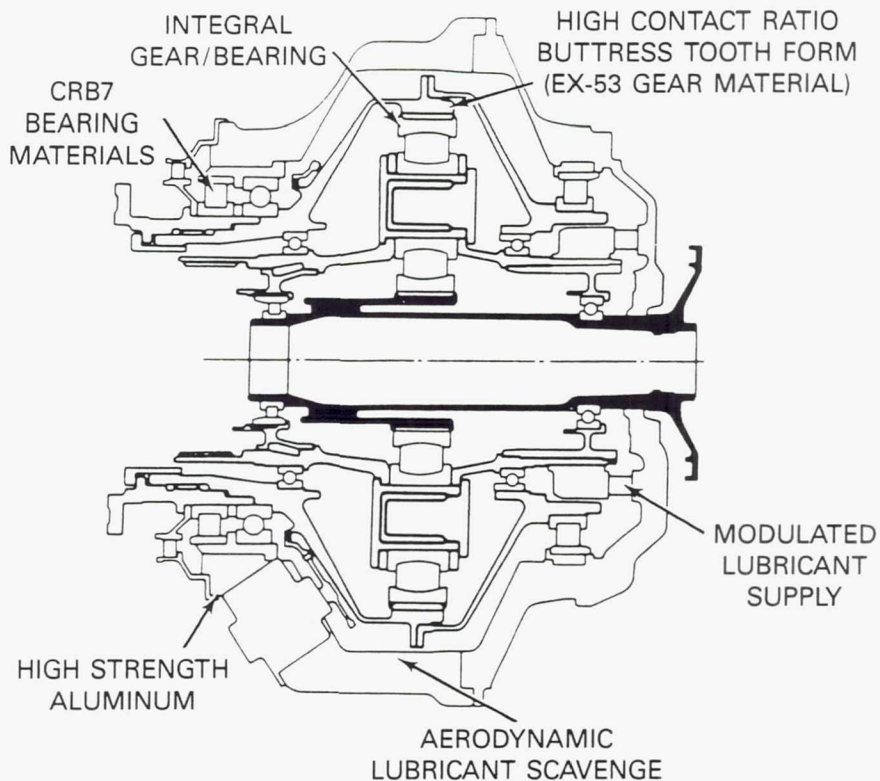
High Contact Ratio Buttress Tooth Form and Carpenter EX-53 Gear Material - The high contact ratio tooth form shows a 15% strength advantage over the more conventional standard involute tooth form and EX-53 material has a 20% or greater increase in pitting fatigue strength capability relative to the current AISI-9310 gear materials. (See Section 4.3 for detailed discussion of gear design.)

High Strength Aluminum - Cast aluminum was selected for the gearbox housing components because it is a lightweight material that is less prone to corrosion than magnesium and has capability for weld repair. (See Section 4.6.2 for detailed discussion of housing design.)

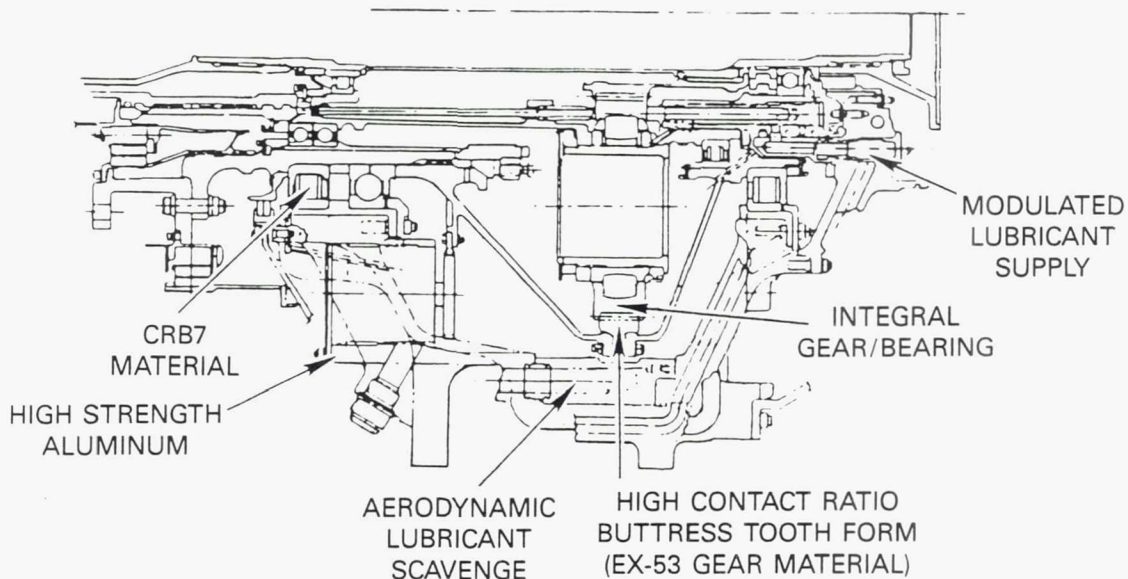
Aerodynamic Lubricant Scavenge - This technology may have some potential for reducing power losses associated with inefficient scavenging of oil from the sun/planet gear mesh and the ring gear scavenge collector. Lubrication rig tests (see Section 6.0) showed no clear benefit for the initial schemes tested. Testing of additional schemes may yield more promising design concepts. Improved lubricants are expected to yield 50 degree higher temperature capability and improved load carrying capability relative to current gear lubricants. These lubricants are not expected to be available for the first build of the test gearbox, but will be incorporated in subsequent builds as they become available.

Modulated Lubricant Supply - Use of a modulated lubricant supply system is expected to improve gearbox efficiency at cruise power by a nominal 0.8% over a constant flow system. Rig testing (see Section 6.0) verified that gearbox power losses could, indeed, be reduced with a modulated system.

Verification of the benefits associated with these technology advancements is the purpose of the gearbox test program described in Section 5.3. As indicated, some investigations have already been initiated through the supporting technology rig tests described in Section 6.0.



APET GEARBOX (CONFIGURATION RESULTING FROM PRELIMINARY DESIGN STUDIES)



AGBT GEARBOX (CONFIGURATION RESULTING FROM DETAIL DESIGN STUDIES)

Figure 12 AGBT Gearbox Incorporates Advanced Technologies Identified in APET Studies

## 4.0 TEST GEARBOX DESIGN

### 4.1 Design Overview

With the selection of the straddle-mounted, differential planetary in-line gearbox configuration, design studies were initiated to effect refinements in the major gearbox subsystems. These studies focused on the planetary gear configuration, gear tooth form, bearings, lubrication system, and shaft and housing structural analysis.

This section describes these studies as they relate to the technology demonstrator test gearbox. It includes design objectives and requirements, an overview of the basic design, a discussion of the design characteristics of the major sub-components and test instrumentation, a weight and materials summary, and a brief discussion of the principal analytical design codes and suggested code modifications.

#### 4.1.1 Design Objectives

The design approach for the test gearbox focused on three primary objectives: (1) simulate as nearly as practical flight gearbox requirements, (2) ensure successful demonstration testing and (3) minimize risk and cost of the program. Emphasis was therefore placed on factors affecting flight worthiness, durability, efficiency, safety, operability, design data acquisition and cost reduction. Specific objectives related to each of these are described briefly as follows:

Flight worthiness: This objective will be achieved through use of flight weight materials where practical, design for realistic flight loads (prop, gust, maneuver), consideration of extreme failure conditions (i.e., propfan shell and fill loss, slam-feather over-torque and loss of lubrication), low noise and minimum vibration.

Durability: The gearbox durability goal is 30,000 hours MTBUR. Design lives for the gearbox components reflect the requirements of this goal and include gear tooth design within acceptable stress limits, bearings with high life, direct lubrication of the planetary bearing, minimum shaft deflections to ensure that gears run true, minimum shaft stresses to assure long shaft lives and vibration dampers on ring and sun gears.

Efficiency: The gearbox design efficiency goal is 99%. This will be achieved through a simple, compact design with a modulated flow lubrication system, direct lubrication of the sun/planet gear mesh, rolling element bearings throughout and design to accommodate high temperature capability lubricants.

Safety: This objective will be met through use of bearings that are tolerant to loss of lubricant, design to anticipated extreme failure modes, provisions for condition monitoring during test and instrumentation for rig protection.

Operability: Operability will be addressed through design of the gearbox as a self-contained test unit with easy-access inspection ports to enhance on-stand inspection of internal parts. Replaceable lubrication supply and scavenge units will also be incorporated.

Design Data Acquisition: Design data quality will be enhanced through use of extensive instrumentation directed toward meeting data analysis requirements, an insulated test gearbox to ensure accurate efficiency measurements, design for compatibility with an automatic data recording system and computer linked operating system.

Cost Reduction: Existing tooling and component hardware will be used wherever practical.

#### 4.1.2 Design Requirements

To satisfy the design objectives, specific design requirements were formulated. These encompassed basic design requirements as well as special requirements to consider both pusher and tractor installations and 25% horsepower growth potential within the basic 12,000 SHP gearbox housing envelope.

The basic design requirements are listed in Table 3.

Table 3 Basic Design Requirements

<ul style="list-style-type: none"><li>o Output power: 12,000 HP (nominal) - - 15,000 HP (growth)</li><li>o Shaft speeds: Output - 1,280 RPM maximum      1,235 RPM normal Input - 10,700 RPM maximum      10,250 RPM normal</li><li>o 15% critical speed margin</li><li>o 177°C (350°F) maximum oil temperature</li><li>o ±30 degrees attitude operation</li><li>o Counter-rotation propfan based on SR-7 single-rotation propfan blade type</li><li>o Duty cycle defined by flight mission profile (commercial)</li><li>o Maneuver loading (commercial and military)</li></ul>
---

At the start of the detailed design effort, assumptions for propfan characteristics were made based on aircraft flight attitude and maneuver data generated through the use of generalized characteristics for propeller-driven transport aircraft in the 120 passenger size. This established the data shown in Table 4 under the column "Start of Design". The 1P moment and shear loads reflect the conservatively high propeller air inlet angles resulting from the use of the generalized aircraft characteristics. The flight mission profile in Table 5 represents a typical short range 644 km (400 miles) mission with most of the time spent climbing and descending from a cruise altitude of 10,668 m (35,000 ft). A cruise Mach number of 0.8 was assumed, though the data are not significantly changed for a Mach number of 0.7. Maneuver loads in Table 6 are based on current Federal Airworthiness Regulations.

Late in the design effort, more specific propfan characteristics data were generated from flight attitude and maneuver profiles supplied by an aircraft designer for a specific propfan-driven transport aircraft in the 155 passenger size. These characteristics resulted in less severe propeller air inlet angles with a subsequent reduction in 1P moment and shear loads as shown in Table 4 under the column "Revised Data". No fundamental changes to the design were required as a result of introducing this more refined flight data; the major effect was to improve the calculated bearing design lives by removing an otherwise marginal situation.

Table 4 CR Propfan Characteristics Influencing Gearbox Design

Configurational:	Start of Design	Revised Data
Prop diameter, m (ft)	3.5 (11.6)	3.35 (11.0)
Blade type/number	SR-7/6x6	SR-7/6x6
Blade weight, airfoil + attachment, kg (lb)	29 (64)	22.7 (50)
Tip speed, m/sec (FPS)	229 (750)	197 (645)
Maximum oil temperature, °C (°F)	177 (350)	177 (350)
Prop Loads (Normal):		
Prop weight, kg (lb)	1,179 (2,600)	1,095 (2,414)
1P moment (scalar sum), SLTO, Nm (ft-lb)	Net 8,257 (6,090)	3,539 (2,610)
1P shear, SLTO, kg (lb)	Net 1,828 (4,030)	835 (1,840)
Gyro moment at 1 rad/sec, Nm (ft-lb)	Fwd 20,202 (14,900)	20,202 (14,900)
	Aft 20,202 (14,900)	20,202 (14,900)
	Net 0 (0)	0 (0)
Maximum torque, Nm (ft-lb)	Fwd (carrier) 38,747 (28,578)	38,055 (28,068)
	Aft (ring gear) 31,826 (23,474)	31,136 (22,965)
Thrust, Takeoff Static Conditions, N (lb)	97,861 (22,000)	84,516 (19,000)
At 0.2 Mn, N (lb)	76,509 (17,200)	72,951 (16,400)
Reverse thrust, At 0.2 Mn, N (lb)	77,844 (17,500)	60,051 (13,500)
At 0 Mn (approximately), N (lb)	10,008 (2,250)	8,896 (2,000)

Table 5 Flight Mission Profile for 120 Passenger Aircraft

Condition	Duration (minutes)	Altitude km (1000 ft)	Flight Speed (Mn)	Power (% max)	Propfan Speed (% max)
Taxi (ground idle)	5.0	0	0	2-5	20-70
Takeoff	1.5	0-0.46 (0-1.5)	0.00-0.39	100	95-100
Climb	2.4	0.46-3.05 (1.5-10)	0.39-0.50	88.0-81.3	100
	3.8	3.05-6.10 (10-20)	0.50-0.60	81.3-70.0	100
	8.9	6.10-9.14 (20-30)	0.60-0.74	70.0-58.7	100
	5.9	9.14-10.67 (30-35)	0.74-0.80	58.7-53.3	100
Cruise	20.0	10.67 (35)	0.8	43.3	100
Descent	20.0	Variable	Variable	2-5	30-70
Approach	3.0	Variable	Variable	20-25	75-100
Reverse	0.5	0	0.2-0	22-6	60-80
Taxi (ground idle)	5.0	0	0	2-5	20-70

Table 6 Flight Attitude and Maneuver Loads

Load Case Description	Load Case	Load Factors	Remarks
Malfunction torque	1	2.0 x takeoff torque + 1G down	FAR 25.361 with amendment 46
Maximum maneuver and gust	2	4.5G down + (TH or TR)	FAR 25 requirements
	3	-2.5G up + (TH or TR)	
	4	2.85G down + takeoff thrust and takeoff torque	
	5	-1.32G up + takeoff thrust and takeoff torque	
Gyroscopic loads	6	3.2G down + (TH or TR) = ( $\pm 1$ rad/sec) + ( $\pm 1.5$ rad/sec)	FAR 25 requirements
Side load	7	$\pm 1.33$ side factor + (TH or TR) + 1G down	-FAR 25.363 -Military spec -Possible dynamic case
	8	10G down $\pm 2$ G fore and aft	
	9	-6G up + (TH or TR)	
1P moment continuous	10	(Bending nacelle) + (TH or TR) + 1G down	
Crash case	11	20G down + 12G forward	BCAR spec
Engine seizure	12	Torque due to stoppage from speed in 0.3 seconds (including turbines and prop) + 1G down	FAR: (no time is specified in FAR)

## 4.2 Test Gearbox Configuration

The concept studies, coupled with the design objectives and requirements described in the previous sections, were the determining factors in selection of the test gearbox configuration to be carried forward into detailed design. Figure 13 illustrates the conceptual design and highlights its significant features, which are as follows:

- o Counter-rotating, in-line differential planetary gear system
- o Remote pitch control
- o Straddle-mounted prop shaft/ring gear support bearings
- o 5 planet gear planetary system
- o High contact ratio buttress gear tooth form
- o Single row spherical roller planet bearings
- o Combination ball/roller prop shaft support bearings
- o Modulated gearbox lubrication system separate from the engine system

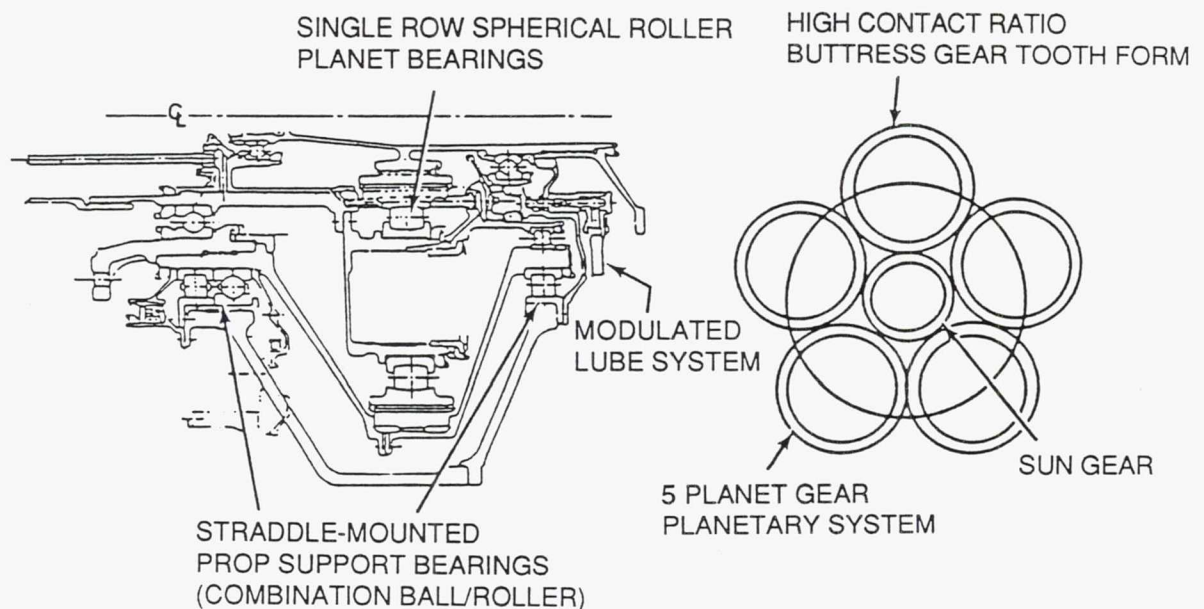


Figure 13 Selected Gearbox Configuration from Conceptual Design Studies Embodies Counter-Rotating, In-Line Planetary Gear System

Installation studies conducted as part of the Reference 1 effort indicated that the counter-rotation gearbox adapts easily to both tractor and pusher aircraft installations. In addition, maintainability of the differential planetary gearbox presents a substantial improvement over gearboxes used in current turboprop aircraft installations. The differential planetary gearbox is much simpler than previously designed gearboxes, having fewer parts contained in the single stage gear set. It has 7 gears and 12 bearings, and it is a concept that lends itself to on-wing maintenance, illustrated in Figure 14. This has been achieved by providing easy access to normal maintenance items such as carbon seals, oil pumps, last-chance filters and oil supply jets.

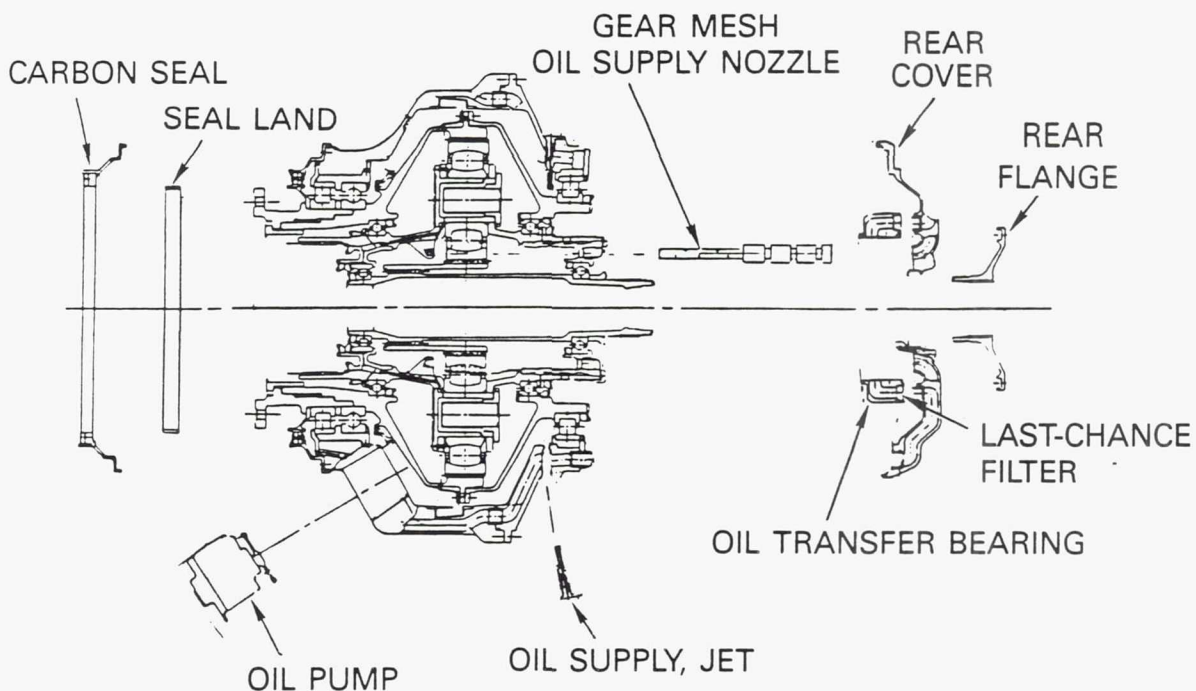


Figure 14 On-Wing Maintenance Capabilities - Easy access is provided to carbon seals, oil pumps, last-chance filters and oil supply jets.

The differential planetary test gearbox configuration and its major features are illustrated in Figures 15 and 16. The features include those necessary to facilitate back-to-back testing in the multipurpose test rig described in Section 5.2. Figure 16 identifies external details on the engine-side and prop-side housings that accommodate gearbox lubrication and scavenge system pumps and flow interfaces, chip detectors, speed sensors and viewing ports for inspection of the gear train while the gearbox is assembled. Configurational characteristics of the conceptual design were retained in the test gearbox. The major sub-components include the gearing, shafting, bearings, housing, lubrication system and scavenge system. These, together with the instrumentation required to conduct an operational test program, are discussed in more detail in Sections 4.3 through 4.7.

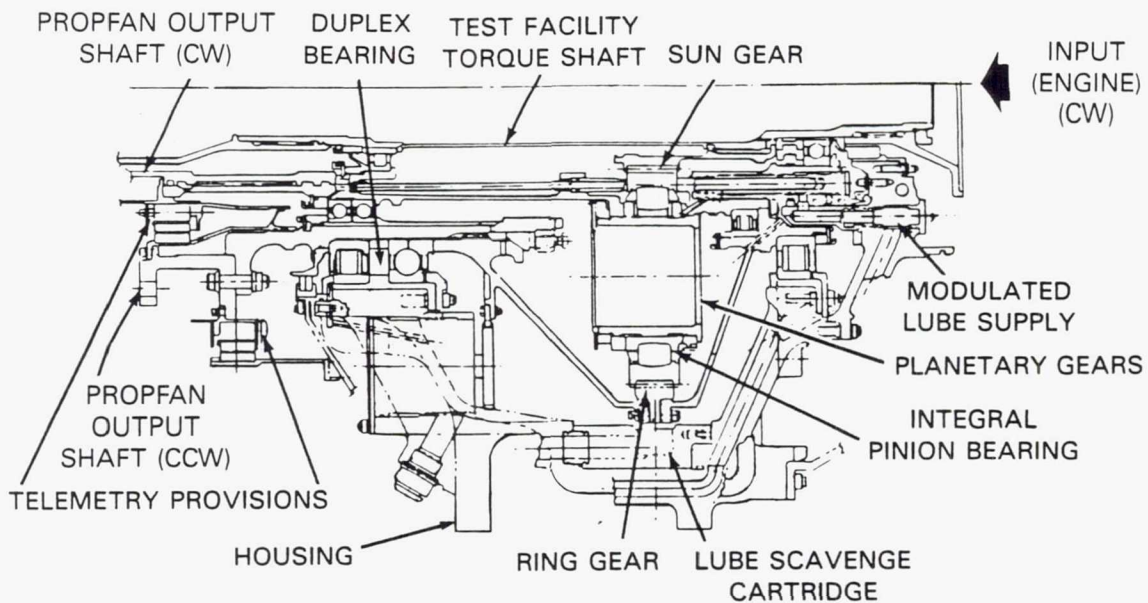


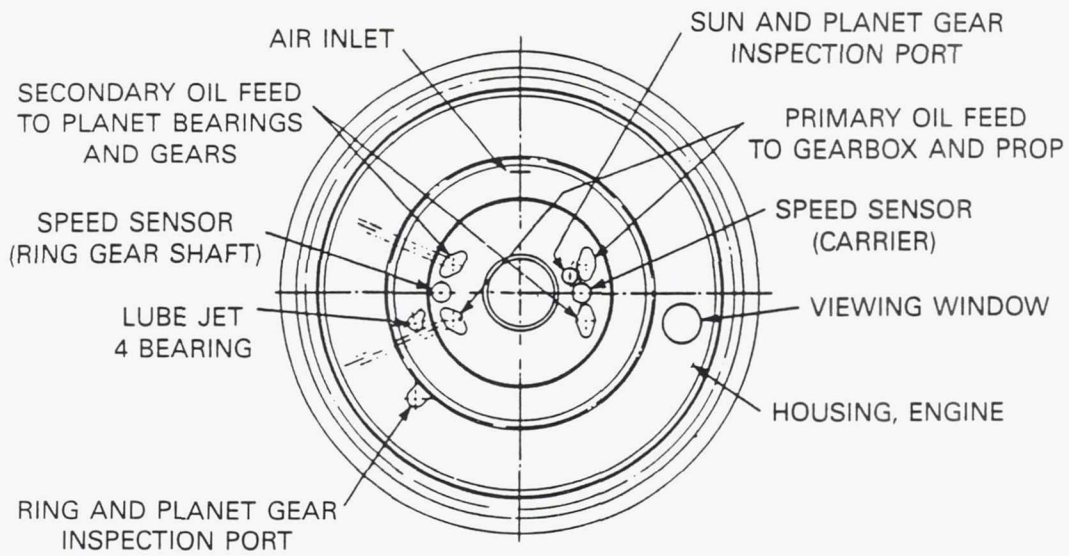
Figure 15 Test Gearbox Configuration Showing Major Design Features

#### 4.2.1 Gearbox Efficiency Prediction

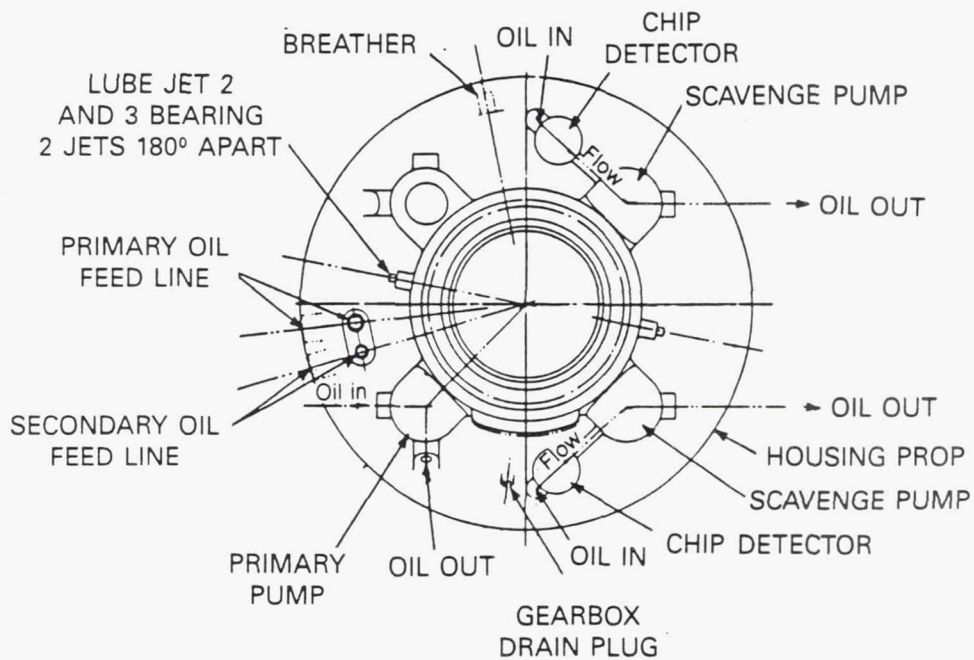
Gearbox efficiency is directly related to the loss mechanisms inherent in the gear train, bearings and lubrication system. These mechanisms are summarized in Table 7, together with the predicted losses for Build 1 of the test gearbox. As noted in the table, some of the losses are predicted based on existing Pratt & Whitney analytical design codes and experience with similar hardware. Data from the lubrication rig tests, described in Section 6, have also been utilized in the estimates. Although the predicted efficiency shown is 0.3% below the goal of 99%+ for a fully-developed flight design gearbox, planned gearbox testing and continuing supporting technology tests are expected to provide the data base necessary to achieve the goal efficiency.

Table 7 AGBT Build 1 Loss Prediction (Values at Design Speed and 12,000 SHP Sea Level Takeoff Power)

Loss Mechanism	Power Loss (HP)	Prediction Base
o Sun/planet gear mesh friction	49.6	Analytical code
o Planet/ring gear mesh friction		
o Planet bearing churning and friction	33.5	Analytical code
o Shaft bearings churning and friction	8.9	Analytical code
o Sun/planet churning	18.5	Lube rig data
o Sun/planet windage	21.5	Lube rig data
o Ring shaft windage	2.1	Lube rig data
o Pumps	12.0	Existing pump data
o Ring shaft pumping	9.4	Lube rig data
o Oil transfer bearing	2.4	Analytical code
Total losses	157.9	
Predicted efficiency	98.7%	



## ENGINE-SIDE



## PROP-SIDE

Figure 16 External Details of Engine-Side and Prop-Side Housings

### 4.3 Gearing

As noted in Section 4.2, the differential planetary gear system using 5 planet gears and high contact ratio gear tooth form was selected. The detailed design process reaffirmed this choice and provided the comprehensive design analyses required to achieve success in the proof-of-concept test gearbox program.

The basic functioning characteristics of the gear system are shown in Figure 17. The system is driven clockwise by an engine shaft-coupled sun gear, which at design speed rotates at 10,270 RPM. This, drives the planetary pinion gears which turn the carrier clockwise at 1235 RPM and the ring gear counterclockwise at 1235 RPM. The differential planetary system has a fixed torque ratio between the carrier output and the ring gear output of 1.2734:1 but the speed ratio between these two outputs is variable. The relative speed of these two outputs, and thereby the speeds of the two counter-rotating propellers, are determined by the propeller blade pitch settings. These blade pitch settings of the separate propellers determine their relative power absorption levels, their torque/speed gradients and hence, their relative speeds to achieve the fixed torque ratio.

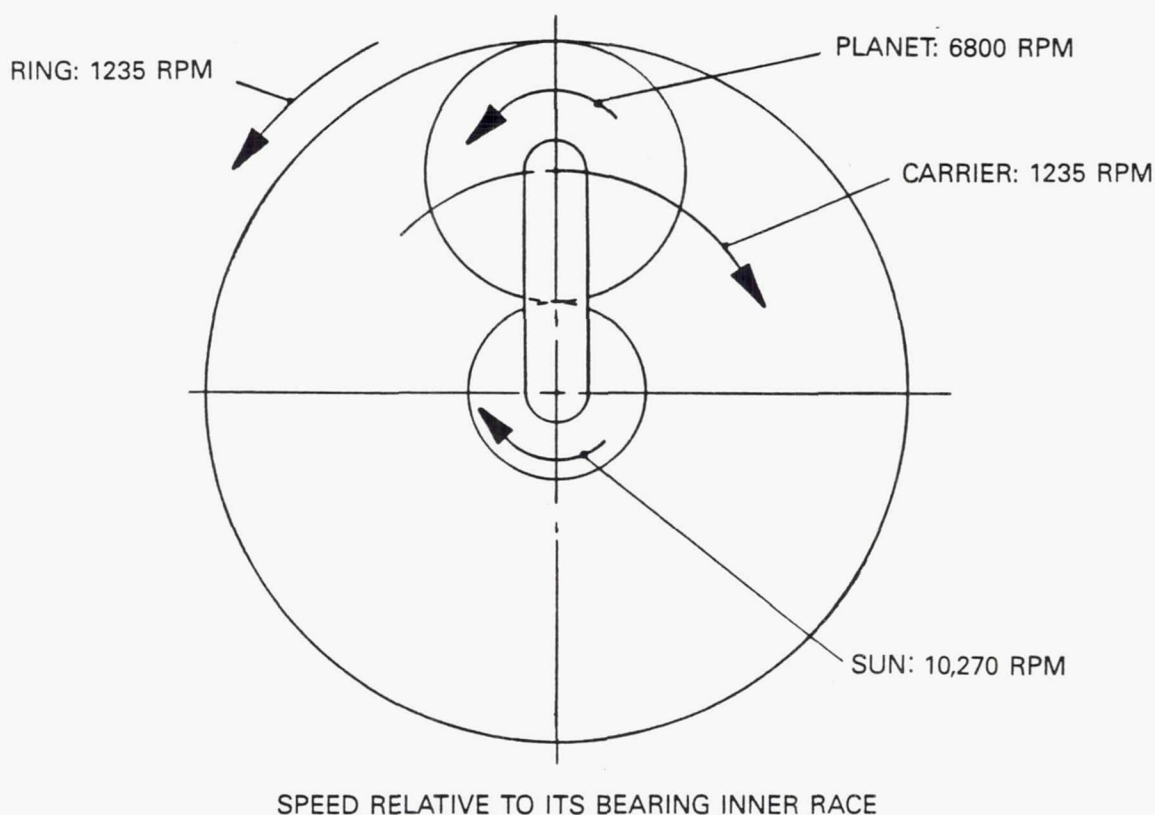


Figure 17 Basic Functioning Characteristics of the Differential Planetary Gear System - Viewed from engine toward gearbox assuming a tractor installation.

A major consideration in the durability of a geared propfan system is gear tooth design, which significantly affects weight and durability of the system. An advanced high contact ratio gear tooth design was selected for the AGBT gearbox because this design results in lower tooth stress for a given load, which in turn can be translated into beneficial weight or life factors.

The principal areas of gearing design requiring detailed design analyses are described in the following subsections.

#### 4.3.1 Ring Gear

Experience with manufacturing large ring gears for Sikorsky helicopters has demonstrated the difficult task of developing and tailoring the manufacturing processes to achieve the necessary tolerances. These considerations include both the quench operation, which requires accurate tooling to hold the ring gear true and prevent it from distorting during the quench operation, and the gear grind operation which must maintain very accurate tooth geometry. In selecting the diameter of the ring gear for this test gearbox, a decision was made to use the in-place Sikorsky manufacturing technology for their Black Hawk helicopter gear system. This minimizes the risk to program cost and schedule. Table 8 compares conventional gearing and high contact ratio spur gears that were investigated in preliminary design studies. The notable difference between them is the gear tooth profile. The conventional planetary gearset uses a low contact ratio (1.676, 1.771) gear tooth profile, and the advanced planetary gearset uses high contact ratio (2.087, 2.077) gear teeth. The significance of this comparison is that it shows the advantage of high contact ratio gear teeth in lowering stress loads. This translates directly into the ability to reduce gear face widths and, subsequently, to reduce weight. Stress level reductions with high contact ratio vary from 20 to 40 percent at equivalent face widths. The table also shows a 65.3 cm (25.7 in) pitch diameter ring gear. This diameter is several inches larger than the optimum design for the AGBT and results in a significantly higher weight, but represents faithful demonstration of proof-of-concept. The Sikorsky experience in designing a high contact ratio gear system supported the selection of a high contact ratio system for the AGBT design.

#### 4.3.2 Planet Gear

Preliminary design of the planetary gear set included a planet pinion optimization study and a review of the arrangement's effect on the gas generator power turbine. Prop speed was a fundamental design consideration, to fix the prop tip speed at a low enough level to ensure meeting noise criteria. This, in turn, established the gearbox ratio. Based on a preliminary power turbine design study and propfan RPM requirements, a reduction ratio of 8.6 to 1 was initially proposed. This reduction ratio limited the planetary pinion count to a maximum of four. A small change in the reduction ratio (i.e., 8.315 to 1) allowed the use of five pinions with a potential weight savings.

Table 8 Comparison of Conventional and High Contact Ratio Gear Geometries Showing Selected Ring Gear Pitch Diameter

Conventional Planetary Gears

	Sun	Planet	Ring
Number of teeth	62	83	228
Module, mm (in)	2.868 (0.113)	2.868 (0.113)	2.868 (0.113)
Diametral Pitch, 1/cm (1/in)	3.487 (8.857)	3.487 (8.857)	3.487 (8.857)
Pitch diameter, cm (in)	17.780 (7.000)	23.803 (9.371)	65.385*(25.742)
Pressure angle	22°30'	22°30'	22°30'
Face width, cm (in)	9.144 (3.600)	7.531 (2.965)	7.569 (2.980)
Bending stress, MPa (psi)	321.7 (46,654)	381.2/368.1 (55,289/53,382)	334.6 (48,527)
Contact stress, MPa (psi)	954.0 (138,367)	953.9/504.2 (138,347/73,154)	503.7 (73,050)
Contact ratio	1.676		1.771

High Contact Ratio Gears

	Sun	Planet	Ring
Number of teeth	62	83	228
Module, mm (in)	2.868 (0.113)	2.868 (0.113)	2.868 (0.113)
Diametral Pitch, 1/cm (1/in)	3.487 (8.857)	3.487 (8.857)	3.487 (8.857)
Pitch diameter, cm (in)	17.780 (7.000)	23.803 (9.371)	65.385 (25.742)
Pressure angle	20°	20°/23°	23°
Face width, cm (in)	9.144 (3.600)	7.531 (2.965)	7.569 (2.980)
Bending stress, MPa (psi)	224.6 (32,573)	277.4/272.6 (40,227/39,532)	239.8 (34,787)
Contact stress, MPa (psi)	793.7 (115,114)	794.4/409.7 (115,211/59,421)	409.6 (59,408)
Contact ratio (Minimum)	2.087		2.0771

A trade study considering the power turbine speed, flowpath modification, efficiency and weight was undertaken. As a result of this study, the smaller five planet design was selected for the final design because it has a slight advantage in weight, fuel burn and direct operating costs (Table 9).

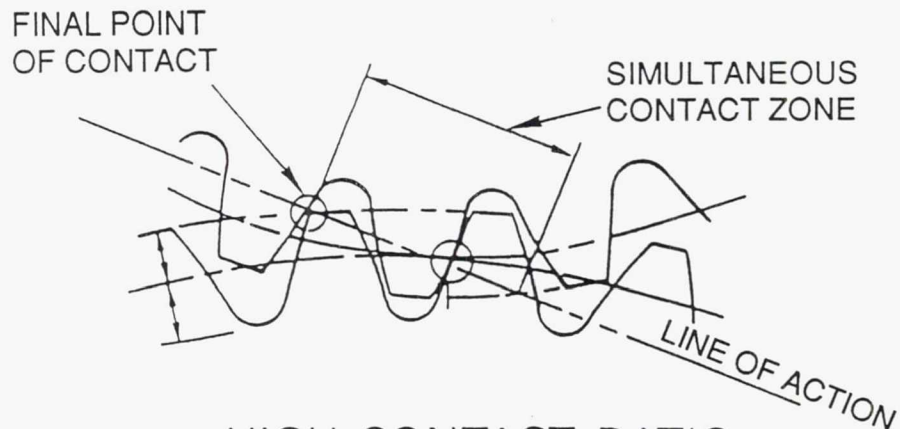
Table 9 Comparison of Four and Five Planet Gear Designs: The Five Planet Design Was Selected

	Four Planet	Five Planet
Number of bearings	6	7
Number of gears	11	12
Efficiency	Base	Base
MTBUR, hours	31,800	30,000
Acquisition cost, \$	Base	-1,000
Maintenance cost, \$	Base	+0.16
Weight, kg (lb)	Base	-11.3 (-25)
Fuel burn	Base	-0.03%
Direct operating cost + interest (DOC + I)	Base	-0.001%

#### 4.3.3 Gear Tooth Design

The high power and high speed levels of the proposed propfan installations require larger gears and faster pitch line velocities than are currently used in turboprop transmissions. The proposed counter-rotating gearbox will have gear pitch line velocities nearly twice those of existing transmissions. The gear tooth dynamic loading is directly related to both speed and accountable tooth tolerances. As gear speeds increase, the dynamic increment on the nominal loading increases. The dynamic increment is that part of the load induced by imperfections in gear manufacturing (tooth profile and relative position). Another contributing factor to dynamic loading is elastic bending deformation of the tooth profile, which distorts the involute form. This can be controlled by proper profile modification in the detail manufacturing drawings. Due to the high pitch line velocities inherent in the counter-rotating gearbox, the dynamic load requires very precise control. The greatest single contribution to this control is tooth form. Conventional (standard involute) spur gears operate with contact ratios of 1.4 to 1.7 and are noisy and prone to vibration at high speeds. There are two possible approaches to resolving these problems: one is to use single helical gearing; the other is to use high contact ratio (HCR) spur gears. Single helical gears require a more complex bearing support system to accommodate parasitic axial load components; therefore, the high contact ratio approach was used. High contact ratios are achieved by using teeth of a relatively low pressure angle, which brings about a tall, slender, compliant configuration somewhat more tolerant of the nonuniformities in involute form and tooth spacing caused by manufacturing dimensional tolerances. This longer tooth form experiences higher tooth bending moments and thus higher root bending stress for the same tooth loading at the tip. To compensate for this, a buttress tooth form was used to lower stress levels in the root area. Standard involute and high contact ratio gear tooth designs and meshing characteristics are illustrated in Figure 18.

## STANDARD INVOLUTE



## HIGH CONTACT RATIO

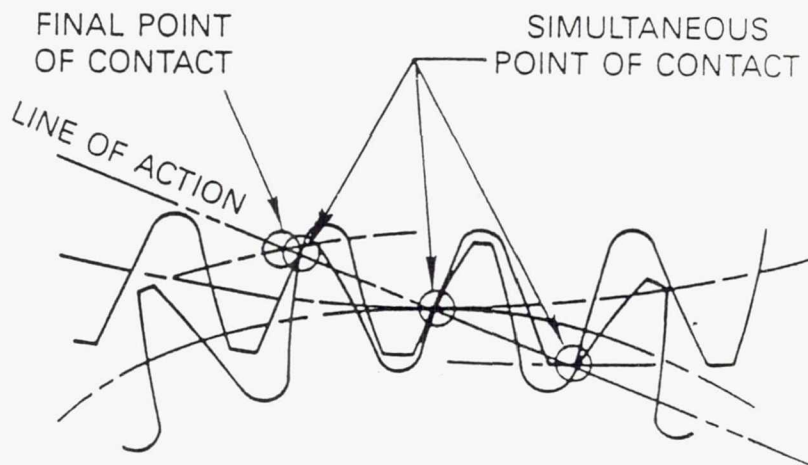


Figure 18 Comparison of Standard Involute and High Contact Ratio Gear Tooth Designs - High contact ratio teeth improve load-carrying ability.

As previously noted, the advantage of a high contact ratio gear system is that for a given mesh load level, the gear tooth stresses are significantly lower because of the extra teeth in contact that share the load. This leads to longer gear life or, conversely, the opportunity to design narrower face widths, resulting in a lighter weight gear system. In a standard involute gear system, when the retreating gear tooth is going out of contact, the advancing gear tooth is starting contact, resulting in one tooth pair taking the load during much of the rotation of the gear system. On the other hand, in the high contact ratio system, when the retreating gear tooth is just going out of contact, the middle gear tooth pair is in contact, near the pitch point, while the advancing gear tooth is making contact. The result of this latter mesh system is that at least two gear tooth pairs are always in contact at one time, producing a much smoother load versus time characteristic. This characteristic is summarized in Figure 19, which shows that in the tip area of the tooth there are 3 teeth in contact; in the outer third of the tooth there are always 2 teeth in contact, in the middle of the tooth for a short period of time there are 3 teeth in contact, toward the inner third of the tooth there are 2 teeth in contact and finally near the root of the tooth for a short period of time there are 3 teeth in contact. Some results of specimen tests conducted on high contact ratio gears relative to standard low contact ratio gears are summarized in Figure 20, which shows that the high contact

ratio gears tested to the same mesh load level as the standard gear teeth survived beyond  $10^7$  cycles without failure while the standard involute gear systems failed in the  $10^5$  to  $10^6$  cycle range.

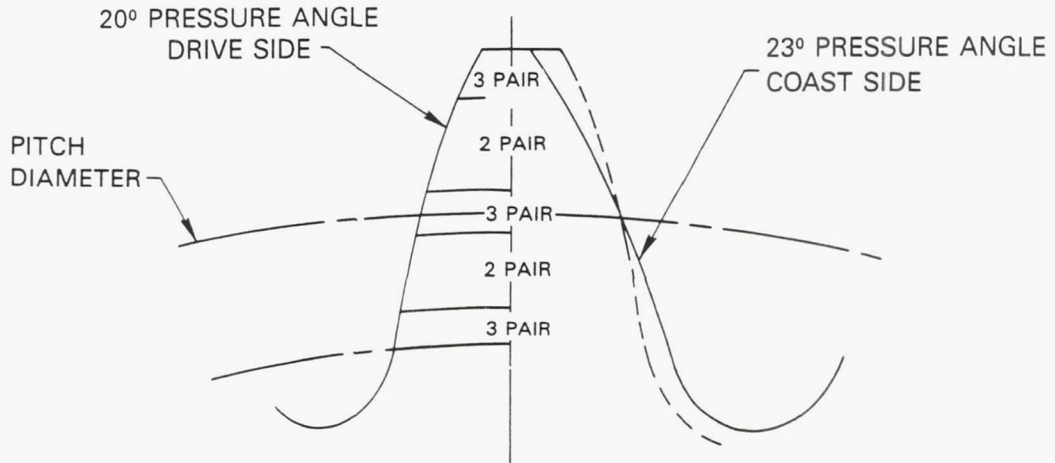


Figure 19 Advanced Buttress Tooth Form - At least 2 gear tooth pairs are always in contact at one time.

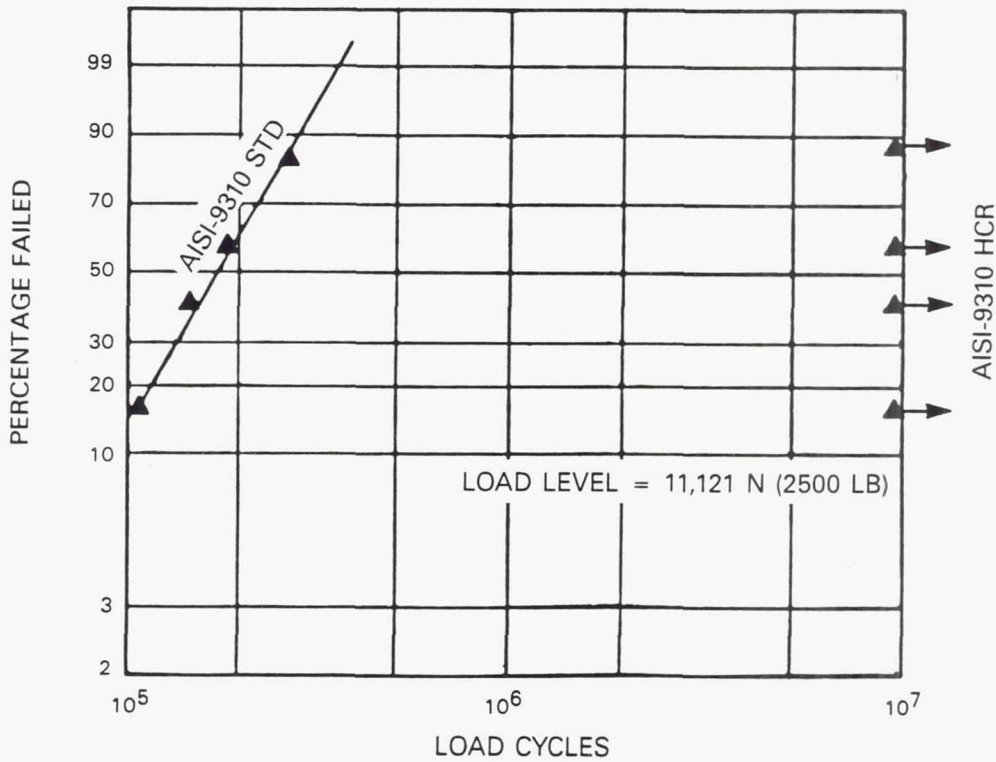


Figure 20 Advanced Buttress Tooth Form Specimen Test Results Show Significant Life Improvement Over Standard Involute Form

Consideration of design requirement constraints or limiting conditions entered into the final tooth design selection. Table 10 summarizes the various constraints placed on the gear design optimization procedure. Tooth combination constraints included: reduction ratio range (8.315 was selected to set the propeller speed required to meet noise criteria); hunting tooth criteria to minimize tooth wear through progressive nonrepeating meshing; sequence meshing to provide phase shifting in engagement so that no two teeth engage simultaneously; and planet equal circumferential spacing.

Table 10 Constraints Affecting Gear Design Optimization

Tooth Combination Constraints
<ul style="list-style-type: none"> <li>o Reduction ratio spread - 8.2 to 8.4</li> <li>o Hunting tooth</li> <li>o Sequence meshing</li> <li>o Planet equal spacing</li> </ul>
Geometric Constraints
<ul style="list-style-type: none"> <li>o Sliding velocity at tip of planet and at tip of sun are the same</li> <li>o Equal contact ratio in sun/planet mesh and planet/ring mesh</li> <li>o Pitch diameter of ring gear shall not vary more than 0.635 cm (0.25 in)</li> <li>o Minimum clearance between planets = 0.127 cm (0.05 in)</li> </ul>

The geometric constraints affecting gear design optimization are also shown in Table 10. With these constraints, a number of gear systems were identified for various contact ratios and addendum (length of tooth above the pitch line) geometries. These combinations are summarized in Figure 21, where the region of acceptable candidates is shown in the shaded area. The lower end of the shaded area was set by choosing a contact ratio greater than 2.3 to insure there would always be at least a 2.0 contact ratio for the worst combination of tolerances. The limit on the right of the shaded area was set to insure that the teeth tips had sufficient width. As shown to the right of the shaded area, a gear with an addendum in the 1.6 to 1.8 range would result in teeth with unacceptably sharp points at the tip. This is to be avoided because the tip would have a tendency to fracture due to internal separation between the

carburized case and core. The high compressive prestress, created in the hardened case by the carburizing and quenching process, puts the remaining thin core in tension near the very tip of the tooth. When this tension is excessive, internal separation cracks can originate at the case/core interface and propagate, even under normal tooth loading, to result in loss of the tip of the tooth. Such debris caught in an engaging mesh can be destructive. A tip geometry with a tooth thickness at the tip of not less than 0.635 cm (0.25 in) per diametral pitch was therefore selected to ensure adequate tip strength. This results in the limit at the right of the shaded area. Within this band are four different acceptable candidate tooth count combinations satisfying these constraints. The sun/planet/ring tooth count of 73/97/267 was selected as best from the standpoints of low scoring (metal-to-metal radial scratch) index and acceptable fillet stress levels. In Table 11, the four candidate tooth count combinations are shown. Even though the 88/117/322 combination, with finer teeth, was lowest in scoring temperature rise, it showed significantly higher stresses than the selected combination of 73/97/267.

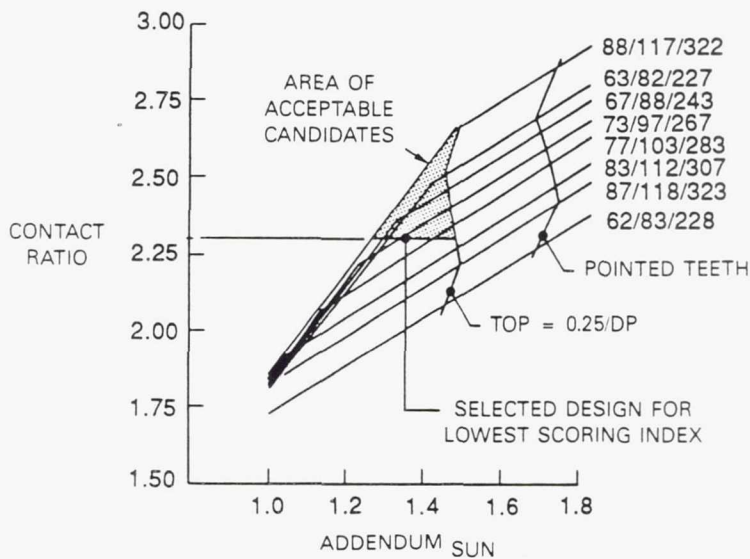


Figure 21 Contact Ratio and Addendum Geometry Combinations Showing Region of Acceptable Candidates

Table 11 Acceptable Tooth Count Combinations: The Sun/Planet/Ring Tooth Count of 73/97/267 Was Selected As Best

Mesh	63-82-227	67-88-243	73-97-267	88-117-322
Module, mm (in)	2.881 (0.1134)	2.692 (0.1060)	2.450 (0.0970)	2.031 (0.0800)
Diametral Pitch, 1/cm (1/in)	3.471 (8.816)	3.715 (9.437)	4.082 (10.369)	4.923 (12.505)
Contact Ratio	2.352	2.367	2.292	2.344
Sun To Planet Gear Mesh				
Fb sun, MPa (psi)	205.0 (29,370)	218.6 (31,700)	234.0 (33,940)	290.6 (42,150)
Fb plan, MPa (psi)	252.0 (36,550)	277.4 (40,230)	324.3 (47,040)	418.5 (60,700)
Fc s-p, MPa (psi)	654.9 (94,980)	654.8 (94,970)	670.2 (97,200)	659.4 (95,640)
$\Delta T$ s-p, degrees	187	176	143	133
Planet To Ring Gear Mesh				
Fb plan, MPa (psi)	233.3 (33,840)	257.0 (37,270)	296.0 (42,930)	386.1 (56,000)
Fb ring, MPa (psi)	304.3 (44,140)	325.1 (47,150)	346.4 (50,240)	460.1 (66,730)
Fc p-r, MPa (psi)	356.1 (51,650)	353.8 (51,310)	353.7 (51,300)	351.7 (51,010)
$\Delta T$ p-r, degrees	44	41	38	30

$\phi_{drive} = 20^\circ$   
 $\phi_{coast} = 23^\circ$   
 25 rms surface finish

FWsun, cm (in) = 5.398 (2.125)  
 FWpin, cm (in) = 4.763 (1.875)  
 FWring, cm (in) = 3.810 (1.500)

#### 4.3.3.1 Drive Side Pressure Angle Analysis

Table 12 summarizes stress and temperature rise data for several different drive side pressure angles. As pressure angle increases, the critical contact temperature rise generally decreases so that large pressure angles are advantageous for a low scoring temperature index. On the other hand, the bending stresses tend to decrease for a while but then start increasing as the drive side pressure angle gets larger than 20 degrees. This is illustrated in Figure 22, which shows that a 20 degree drive side pressure angle provides a minimum bending stress and also a relatively low critical contact temperature rise. This optimization procedure was conducted using static analysis

procedures. Further optimization of the gear system required consideration of both surface finish as well as dynamic tooth contact behavior. Initially, a gear tooth surface finish profilometer measurement of 25 rms was assumed, but this level resulted in a scoring related temperature rise that was marginal at about 65.6°C (150°F). A surface finish of 15 rms was subsequently found to provide acceptable temperature rise and still be within manufacturing capabilities.

Table 12 Stress and Temperature Rise Variations With Change In Gear Tooth Drive Side Pressure Angle

Drive Side Pressure Angle, degrees	Contact ratio	Fb sun Fb plan MPa (psi)	Fc s-p MPa (psi)	$\Delta T$ s-p degrees	Fb plan Fb ring MPa (psi)	Fc p-r MPa (psi)	$\Delta T$ p-r degrees
15	2.291	196.2 (28,460) 366.6 (53,170)	746.4 (108,260)	252	307.9 (44,660) 400.3 (58,060)	348.8 (50,590)	41
18	2.294	213.2 (30,920) 319.8 (46,390)	688.2 (99,820)	189	287.0 (41,620) 354.5 (51,420)	352.5 (51,130)	39
20	2.292	234.0 (33,940) 324.3 (47,040)	670.2 (97,200)	143	296.0 (42,930) 346.4 (50,240)	353.7 (51,300)	38
22	2.308	255.1 (37,000) 505.3 (73,290)	677.5 (98,260)	135	434.6 (63,030) 368.7 (53,470)	349.6 (50,710)	39

Module, mm (in) = 2.45 (0.097)

Diametral Pitch,

1/cm (1/in) = 4.082 (10.369)

$\phi_{\text{coast}} = 23^\circ$

25 rms surface finish

FWsun, cm (in) = 5.398 (2.125)

FWpin, cm (in) = 4.763 (1.875)

FWring, cm (in) = 3.810 (1.500)

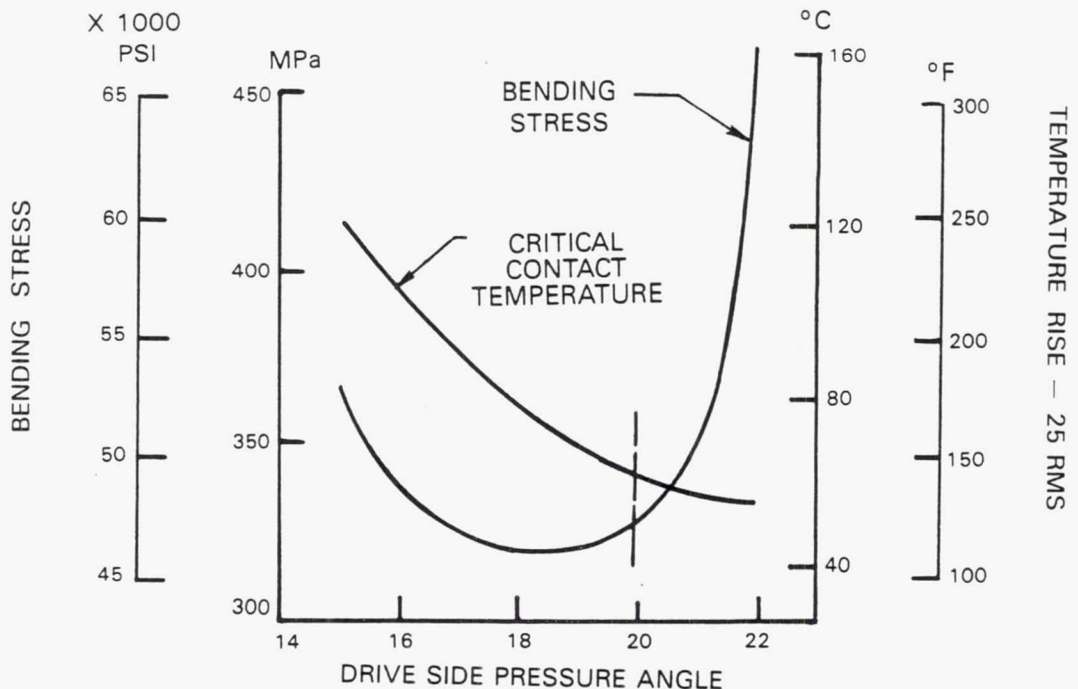


Figure 22 Drive Side Pressure Angle Selection - 20 Degrees provides best combinations of minimum bending stress and low critical contact temperature rise.

#### 4.3.3.2 Dynamic Analysis

A dynamic analysis was next conducted to determine what involute tooth profile modification would be necessary to minimize dynamic stress levels. This analysis was conducted through use of an analytical code called GEARDYN that was developed under contract to NASA by the Hamilton Standard Division of United Technologies. Figure 23 illustrates tooth compliance (spring rate) as contact progresses from the tip of the pinion tooth to the tip of the sun tooth along the line of action and summarizes how during the mesh action 3 pairs of teeth are in contact at first, then 2 pairs, then 3 pairs, then 2 pairs and finally 3 pairs at the end of the mesh of the given tooth. The results of the GEARDYN analysis of this mesh action compliance are shown in Figure 24. During the initial contact, the load suddenly builds up on the contacting tooth; coming up to roughly 20% level of the total mesh load and then, as 3 teeth are in contact, a fairly shallow load increase until 2 teeth have to take the full load. This results again in a rapid load increase, up to about a 40% level, where the two teeth continue taking the load as the gear rotates to the mid point of the contact and all three teeth are now in contact. At this point, the load decreases rapidly to about a 45% level for a short period of time and then rapidly increases to a 60% level as the rest of the mesh continues in a mirror image of the loading experienced during the advancing action. By removing some metal in the tip region, a profile modification, shown in Figure 24, was obtained to soften the engagement; tip relief of 0.00127 cm (0.0005 in) to 0.0203 cm (0.0008 in) was chosen to smooth out this load curve.

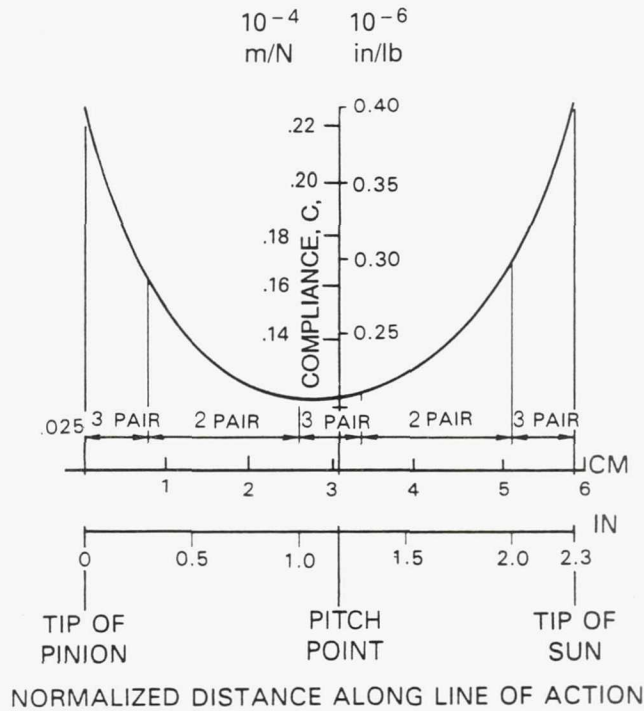


Figure 23 GEARDYN Tooth Compliance Results Showing Gear Tooth Contact Pattern Along Line of Action

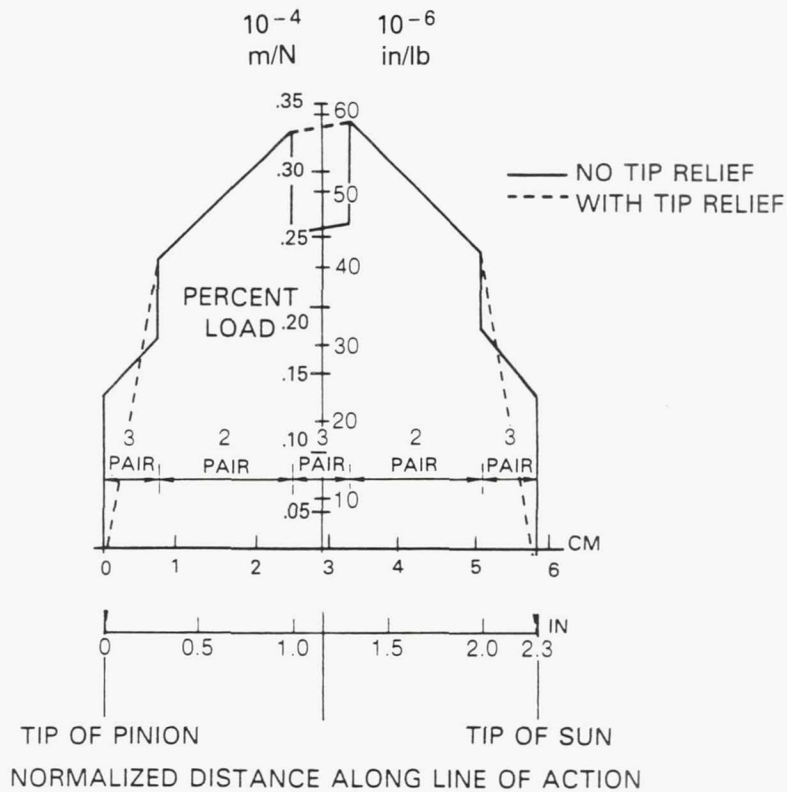


Figure 24 GEARDYN Tooth Load Distribution Results Showing Smoothing Effect Caused by Tip Relief

The dynamic analysis made with the Hamilton Standard program used a different set of equations to calculate stresses than the American Gear Manufacturers Association (AGMA) method used previously to calculate the stresses for Sikorsky helicopter gear designs for which there was direct proof by successful test and operating experience. This required a comparative analysis, by the new method, of the previous successful Black Hawk production helicopter planetary system to establish allowable stress levels calculated by the new method.

The calibrated Hamilton Standard dynamic analysis method (GEARDYN) was then used to calculate, more precisely, the successive tooth loading profiles while passing along the line of action under dynamic conditions, considering tooth compliance with the selected profile modification, rotating element spring rates and inertias, etc.

This analysis was conducted both without, Figure 25, and with a tooth spacing error of 0.00076 cm (0.0003 in), Figure 26, to show the magnitude of the stress level differences caused by the spacing inaccuracy excitation. As can be seen by observing the stress variation levels, a relatively smooth load transfer occurs during the mesh action as a result of the involute profile modification.

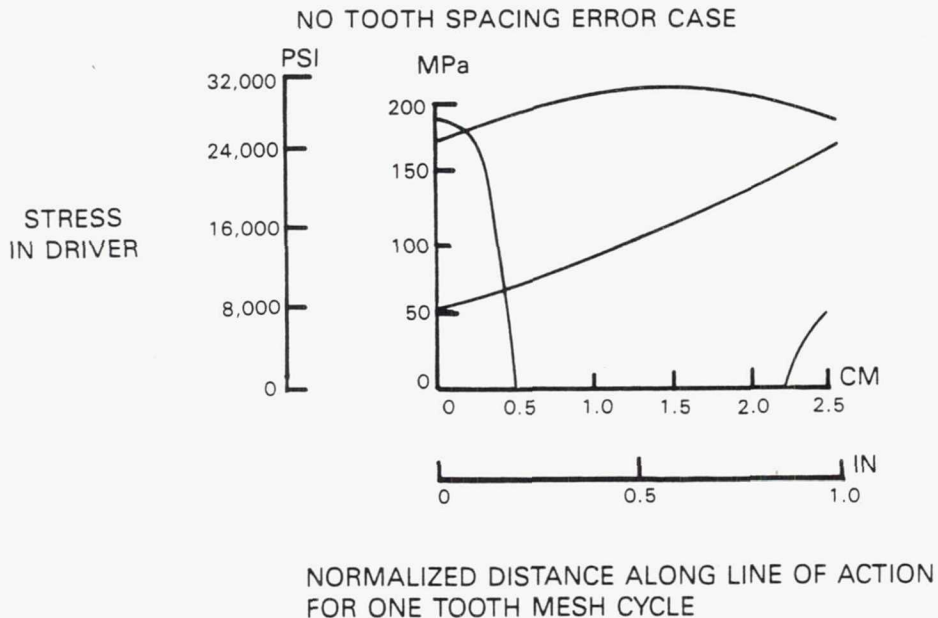
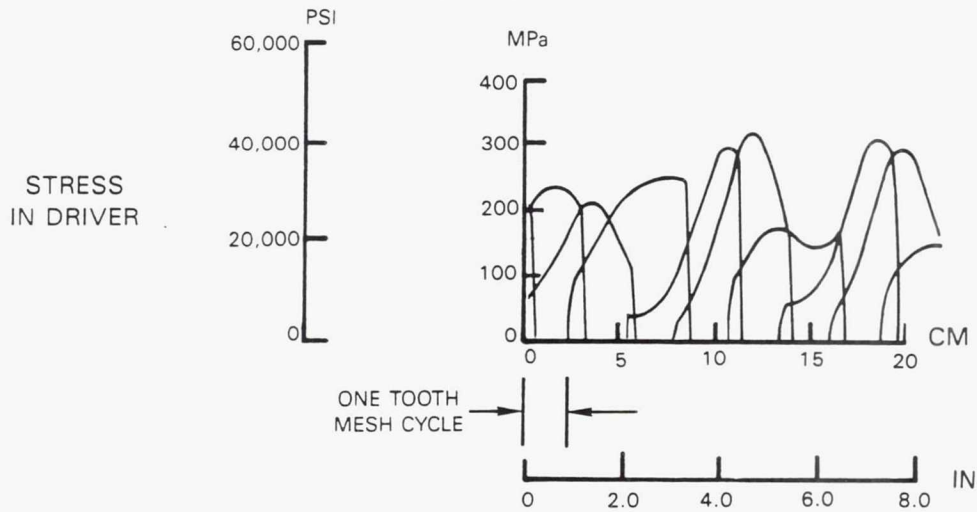


Figure 25 Calculated Tooth Loading Profiles With No Tooth Spacing Error Accounted For

0.00076 CM (0.0003 IN) TOOTH SPACING ERROR CASE



NORMALIZED DISTANCE ALONG LINE OF ACTION  
8 SUCCESSIVE TOOTH MESHING CYCLES

Figure 26 Calculated Tooth Loading Profiles With Tooth Spacing Error of 0.00076 cm (0.0003 in)

Comparison of the AGMA and GEARDYN analytical methods (Table 13), by application of both to successful design experience, provided acceptability limits for stresses calculated by the new, more extensive dynamic analysis method.

Table 13 Comparison of Allowable Gear Tooth Stresses As Calculated Using AGMA and GEARDYN Analytical Codes

Black Hawk production planetary

Standard tooth form	module, mm (in)	2.868 (0.113)
62/83/228	diametral pitch, 1/cm (1/in)	3.487 (8.857)
pressure angle = 22.5°		

Stress prediction by AGMA formulation

	Fbending, MPa (psi)	Fhertz, MPa (psi)
Sun	309.8 (44,930)	947.8 (137,460)
Planet	340.8/313.6 (49,430/45,490)	
Ring	368.0 (53,380)	554.1 (80,370)

Stress prediction by Hamilton Standard Dynamic Program (GEARDYN) incorporated in AGBT Design

	Fbending, MPa (psi)	Fhertz, MPa (psi)
Sun	392.2 (56,880)	990.9 (143,720)
Planet	422.0/376.7 (61,200/54,630)	
Ring	474.2 (68,780)	755.8 (109,620)

Gear analysis results, summarized in Table 14, show that both the bending stress and the contact stress levels are below the allowable levels established by the GEARDYN analysis. In addition, the scoring temperature rise is below the 43.3°C (110°F) level that is considered acceptable for scoring temperature rise. Acceptable pitch-line velocities and sliding velocities were maintained. Final gear geometry was selected following detailed design optimization of the gear system and dynamic analysis of this system. This geometry is summarized in Table 15. Face widths shown are relatively narrow and are a result of the initial decision to maintain ring gear diameter to the dimensions of existing manufacturing tooling.

Table 14 Summary of Gear Dynamic Analysis Results - Stresses and Scoring Temperature Rise Are Within Allowable Levels

Allowables:

Fbending = 475.7 MPa (69,000 psi) one way bending  
 = 420.6 MPa (61,000 psi) two way bending  
 Fhertz = 992.8 MPa (144,000 psi)  
 Flash temperature rise = 110 degrees

	No Tooth Spacing Error		.00076 cm (.0003 in) Spacing Error		Temperature Rise
	Fbending MPa (psi)	Fhertz MPa (psi)	Fbending MPa (psi)	Fhertz MPa (psi)	degrees
Sun	209.5 (30,390)	615.0 (89,200)	281.1 (40,770)	730.3 (105,920)	104
Planet	246.6/271.9 (35,770/39,440)		365.2/420.1 (52,970/60,930)		
Ring	283.2 (41,070)	472.4 (68,510)	432.8 (62,770)	581.0 (84,270)	26

15 rms surface finish

Operating Conditions:

	Sun	Planet	Ring
RPM About Own Center	10,269	6,800	1,235
Pitch Line Velocity, m/min (ft/min)	5,075 (16,651)		5,075 (16,651)
Sliding Velocity, m/min (ft/min)	863 (2,830)		247 (810)

Table 15 Comparison of Preliminary Design and Finalized Detail Design High Contact Ratio Gear Characteristics

Preliminary Design

	Sun	Planet	Ring
Number of teeth	62	83	228
Module, mm (in)	2.868 (0.113)	2.868 (0.113)	2.868 (0.113)
Diametral Pitch, 1/cm (1/in)	3.487 (8.857)	3.487 (8.857)	3.487 (8.857)
Pitch diameter, cm (in)	17.780 (7.000)	23.803 (9.371)	65.385 (25.742)
Pressure angle	20°	20°/23°	23°
Face width, cm (in)	9.144 (3.600)	7.531 (2.965)	7.569 (2.980)
Contact Ratio	2.087		2.0771

Finalized Detail Design

Center Distance, cm(in)	20.822 (8.1976)	Backlash, cm(in)	.00968 (.00381)
-------------------------	-----------------	------------------	-----------------

	Sun	Planet	Ring
Number of teeth	62	83	228
Module, mm (in)	2.450 (0.097)	2.450 (0.097)	2.450 (0.097)
Diametral Pitch, 1/cm (1/in)	4.082 (10.369)	4.082 (10.369)	4.082 (10.369)
Pitch diameter, cm (in)	17.882 (7.040)	23.761 (9.355)	65.405 (25.750)
Pressure Angle	20°Drive/ 23°Coast	20°Drive/ 23°Drive	23°Drive/ 20°Coast
Face Width,	6.033 (2.375)	5.398 (2.125)	4.128 (1.625)
Contact Ratio	2.292		2.292
Tip Diameter, cm (in)	18.544/18.531 (7.3007/7.2957)	24.350/24.338 (9.5868/9.5818)	64.725/64.712 (25.4823/25.4773)
Root Diameter, cm (in)	17.195/17.170 (6.7697/6.7597)	22.971/22.945 (9.0436/9.0336)	66.117/66.092 (26.0305/26.0205)
Tooth Thickness, cm (in)	.381/.378 (.1500/.1490)	.381/.378 (.1500/.1490)	.381/.378 (.1500/.1490)
Fillet Radius, cm (in)	.069/.094 (.027/.037)	.043/.069 (.017/.027)	.048/.074 (.019/.029)
Tip Relief, cm (in)	.00127/.00203 (.0005/.0008)	.00127/.00203 (.0005/.0008)	.00152/.00229 (.0006/.0009)

### 4.3.3.3 Deflection Analysis

A review of important gear system deflections was made in conjunction with the finite element stress analysis of the various shaft assemblies to assess how these deflections might influence the accuracy of gear tooth meshing.

A very detailed finite element analysis of the ring gear shaft and prop shaft assembly was made, assuring that operating stress levels in the shafting elements are within allowables and that the design of the cone/nut attachment of the prop shaft to the ring gear shaft avoids fretting. As part of this analysis, the slope of the ring gear shaft at the bearing mounting lands and the slope of the ring gear pitch cylinder were derived. Another result was the ovality induced in the ring gear pitch cylinder by the propeller moment and shear loads on the propeller mounting flange (under the initial assumption of equally distributed planet gear loads on the ring gear). The method of ring gear tooth loading and the radial and tangential deflections of the ring gear backing resulting from this analysis are illustrated in Figure 27. Deflection analysis results indicate acceptable levels compared to Sikorsky experience.

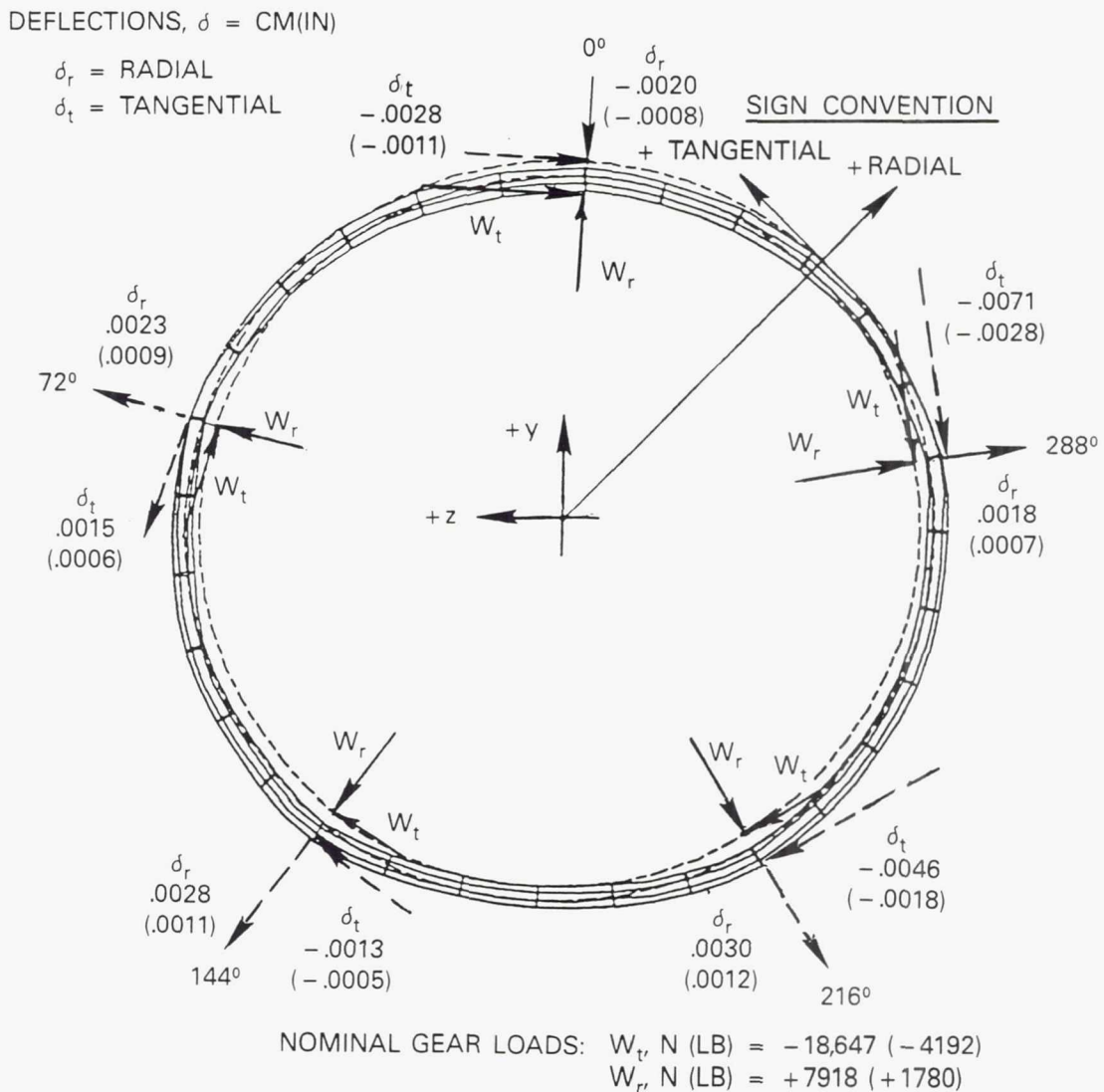


Figure 27 Ring Gear Deflection Analysis

The radial components of the ovality of the ring gear (in the order of 0.0018 cm (0.0007 in) to 0.0028 cm (0.0012 in)) are negligible in that they relate only to center distance changes for the meshes between the ring and the planets; changes to which the involute profiles of the teeth are quite insensitive. Only the difference between these radial deflections and their average value (related to the effective center of the oval pitch cylinder) has any influence on load sharing between planets and this is reduced further by the low pressure angle of these high contact ratio teeth.

The tangential components of the displacements, as derived from the analysis, are small in value also (in the order of -0.0013 cm (-0.0005 in) to -0.0071 cm (-0.0028 in)). These values are relative to the point of fixity in the coordinate system of the ring gear shaft model which was defined to facilitate the derivation of stress values. Further work is needed to provide transformation of these deflection values to a coordinate system related to an effective center of the oval pitch cylinder and relative to the centerline of rotation of the carrier defined by the two inter-shaft support bearings. Then their differences (obviously smaller numerical values) can be evaluated as a measure of their influence on load sharing between planets.

Some additional analysis was done by exercising this same ring gear shaft model with an estimated incremental maldistribution of radial and tangential loads (related to positioning errors resulting from machining tolerances) applied, without constraints, to the same meshing points in the ring gear. The resulting incremental radial and tangential deflections at each of these load points provided a measure of the sensitivity of the ring gear pitch cylinder to further deformation by planet-to-planet load maldistribution. With the relative stiffness of the rigid ring gear mounting, this sensitivity was low, in the order of 10% of the deflections induced by the propeller loads on the shaft. This indicated the tendency of a reduced ability to alleviate planet-to-planet load maldistributions. It also indicated the tendency of the propeller shaft loads to impose an interaction on the uniformity of planet gear load sharing through the forced ovality. These deviations from the nominal planet gear tooth loads in the ring gear meshes are reflected in comparable deviations from nominal tooth loads in the sun/planet meshes, which are more critical. The instrumentation and the tooth pattern changes for each planet in the initial AGBT testing will be monitored closely to provide an experimental indication of how important these deflections are.

An alternate ring gear mounting has been designed, as a back-up, in case the initial AGBT experimental data indicate that the propeller loads excessively influence planet load uniformity, or, that ring gear compliance is inadequate to alleviate planet positioning tolerance errors. This design is shown in Figure 28.

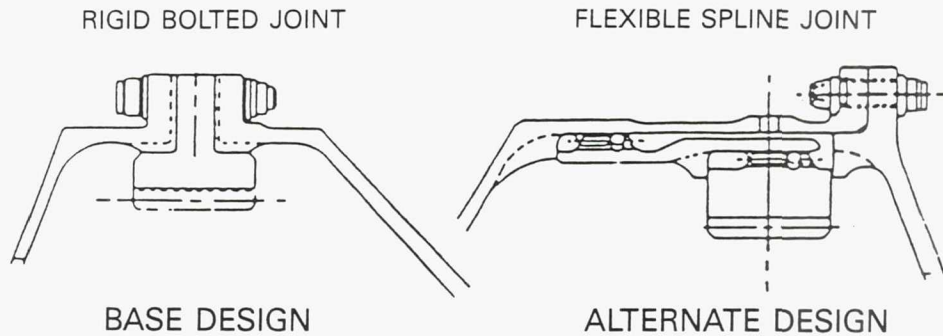


Figure 28 Comparison of Rigid and Flexible Ring Gear Designs - The flexible design is more accommodating of spacing errors and has been designed as backup.

This alternate flexible ring gear design, with its flexible spline connection, provides more independence of the ring gear pitch cylinder from the oval deformations and eccentricity of the ring gear shaft due to the propeller loads. The relatively thin gear backing ring allows more radial compliance and some additional tangential compliance of the ring (through wave bending) to alleviate planet-to-planet position-related tooth load nonuniformities.

#### 4.3.3.4 Vibration Analysis

A shell vibration analysis of the ring gear system indicated that at design operating speeds, there were no first order resonances at the basic rotational excitation frequencies generated by the sun-to-planet or planet-to-ring gear mesh action (Figure 29). To compensate for forced vibration modes that may become excited during operation of the gearbox, both the ring gear and the sun gear were designed with grooves to accommodate ring dampers.

EXCITATION FREQUENCY : (as a function of rotational speeds,  $N_n$ )

- SUN GEAR =  $5 \times (N_1 + N_2)$
- PLANET GEAR = 2 per revolution of planet gear
- RING GEAR =  $5 \times (N_2 + N_3)$

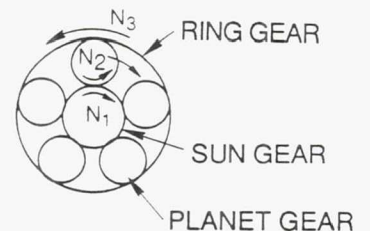


Figure 29 Gear Vibration Excitation Frequencies - Analysis showed that vibration frequencies are well above excitation frequency.

The ring gear was analyzed for possible vibration resonances in the out-of-round wave bending modes due to: (1) the planet passage excitation frequencies created by sun/planet meshes, (2) planet gear rotational eccentricities and (3) the planet passage frequencies created by the planet/ring meshes. All of the resonant gear shell vibration frequencies are well above these basic excitation frequencies.

#### 4.3.3.5 Sun/Planet Flexibility

The sun/planet gear mesh system was analyzed to determine its flexibility characteristics and their influence on the uniformity of loading across the facewidth of the teeth of the sun/planet mesh. A three dimensional finite element analysis model, illustrated in Figure 30, showed that, for a rigidly supported ring gear with zero angular misalignment between its centerline and that of the sun gear, the torsional and radial deflection of the sun gear (supported at one end by its shaft) distorted the uniformity of load across the facewidth of the sun/planet mesh about 12% above nominal loading, as shown in Figure 31. It also showed that a flexibly supported ring gear, with zero axial misalignment with the sun, provided enough compliance to reduce that nonuniformity to about 3% above nominal.

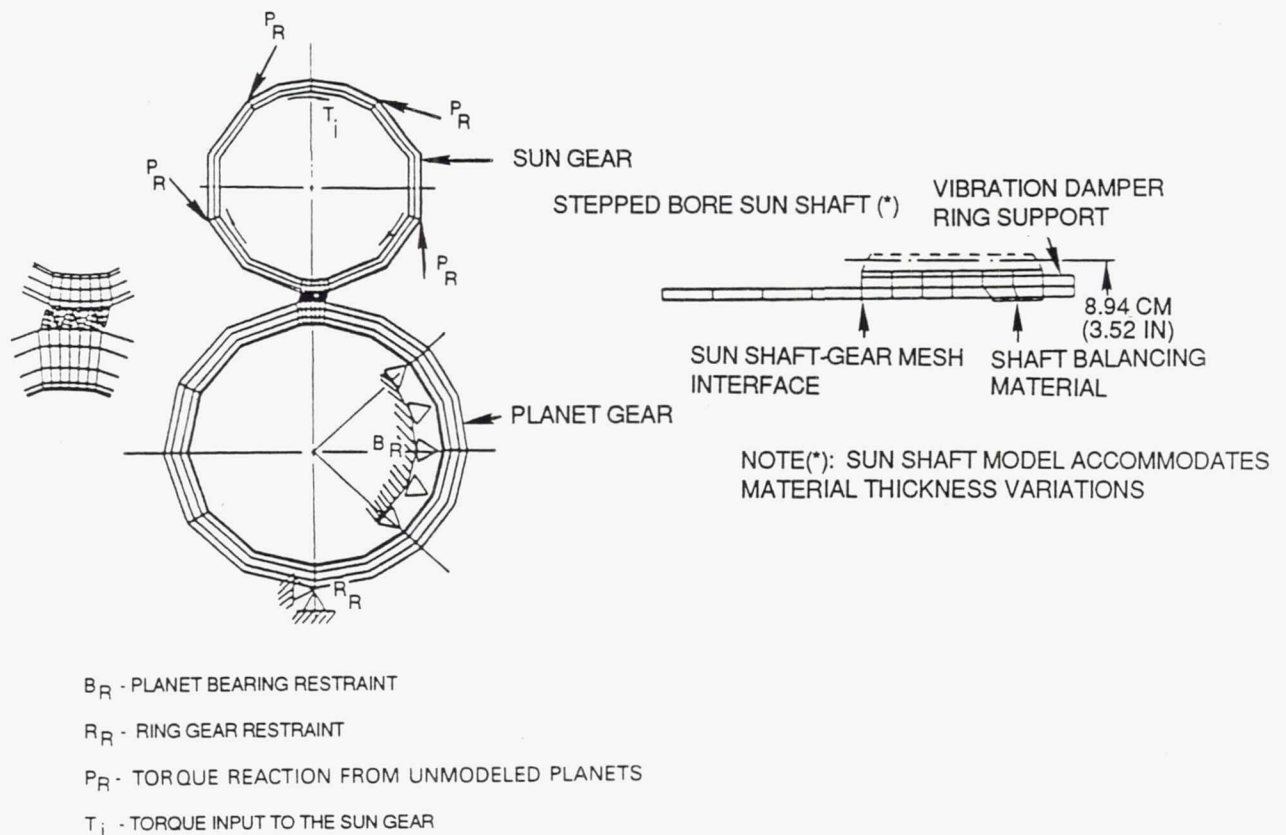


Figure 30 Finite Element Analysis Model Used to Assess Sun/Planet Flexibility

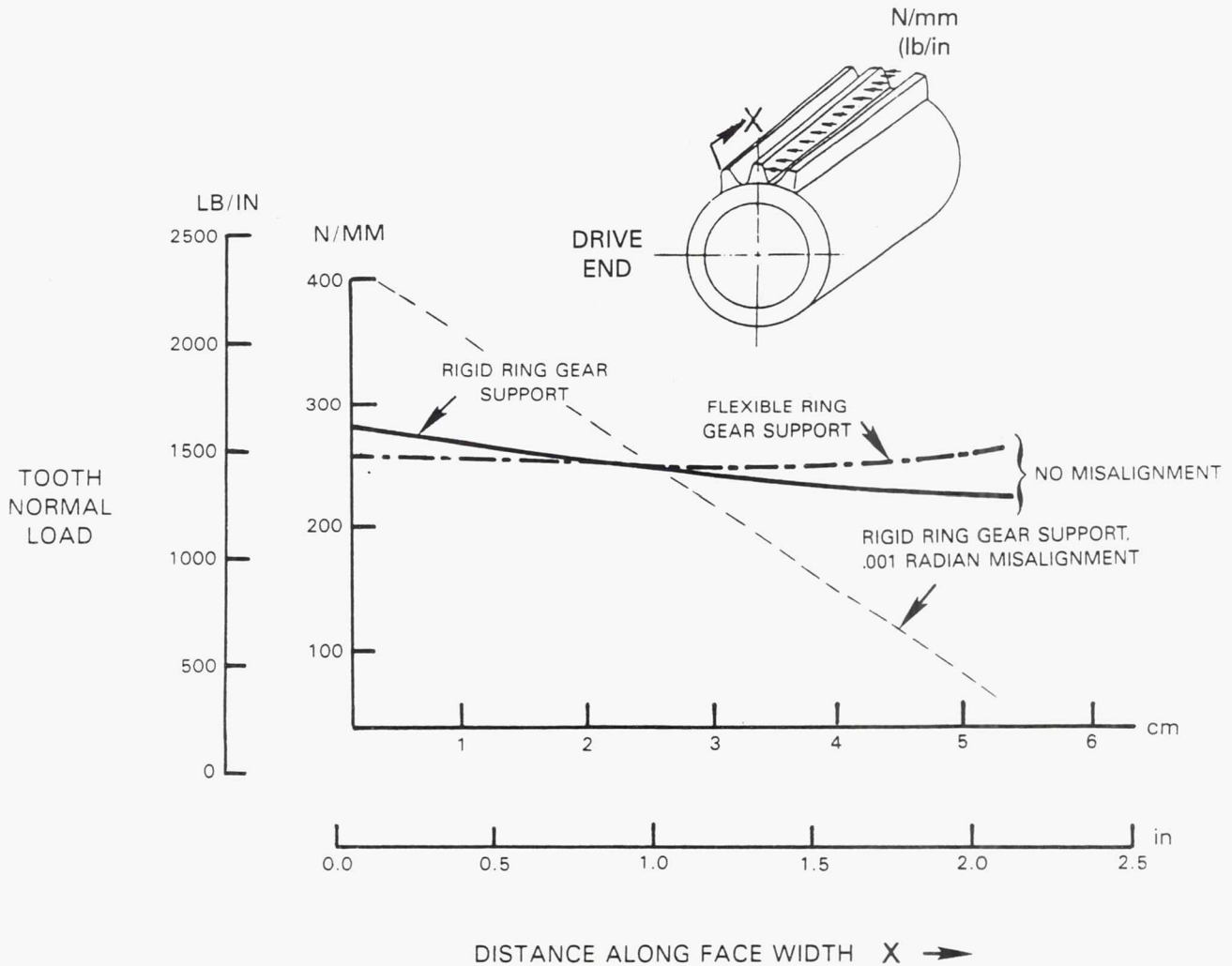


Figure 31 Load Distribution Across Sun/Planet Gear Mesh - Load is more nearly uniform with flexible ring gear support.

One of the important reasons for the relative uniformity of load across the face width of the sun/planet meshes is the independence from carrier journal centerline deflections provided by the spherical bearing supporting the planet gear. This makes helical lead error between mating teeth in each mesh dependent only on the deformation and alignment of the sun gear teeth with respect to the ring gear teeth. It is of critical concern to keep this effective lead mismatch from causing high end loading of the teeth, a principal cause of tooth failure.

The three dimensional finite element model illustrated in Figure 30 considers the effect of the free end of the sun gear, located radially only by equilibrium with the five planet meshes, with its drive cylinder providing the torque at one end of the sun gear element. It also provides for the flexibility of the planet gear outer race and tooth backing ring as well as the bearing roller support points. These roller bearing support points are modeled as free axially (tangentially in the spherical inner surface, or raceway, of the planet bearing outer ring and integral with the gear tooth backing), thus providing the self aligning feature of the spherical planet bearing. Gear tooth compliance is modeled by extra fine detail in the finite elements comprising the gear teeth themselves. This model can also be used to evaluate the gear tooth load maldistributions caused by angular misalignment of the sun/planet gear mesh. While analysis of this type of misalignment was not extensive, one extreme case, with a 0.001 radian slope forced on the planet at the sun gear mesh, was investigated. The large resultant load maldistribution for a rigid ring gear support, shown in Figure 31, indicates that further consideration should be given to the flexible ring gear support shown in Figure 28.

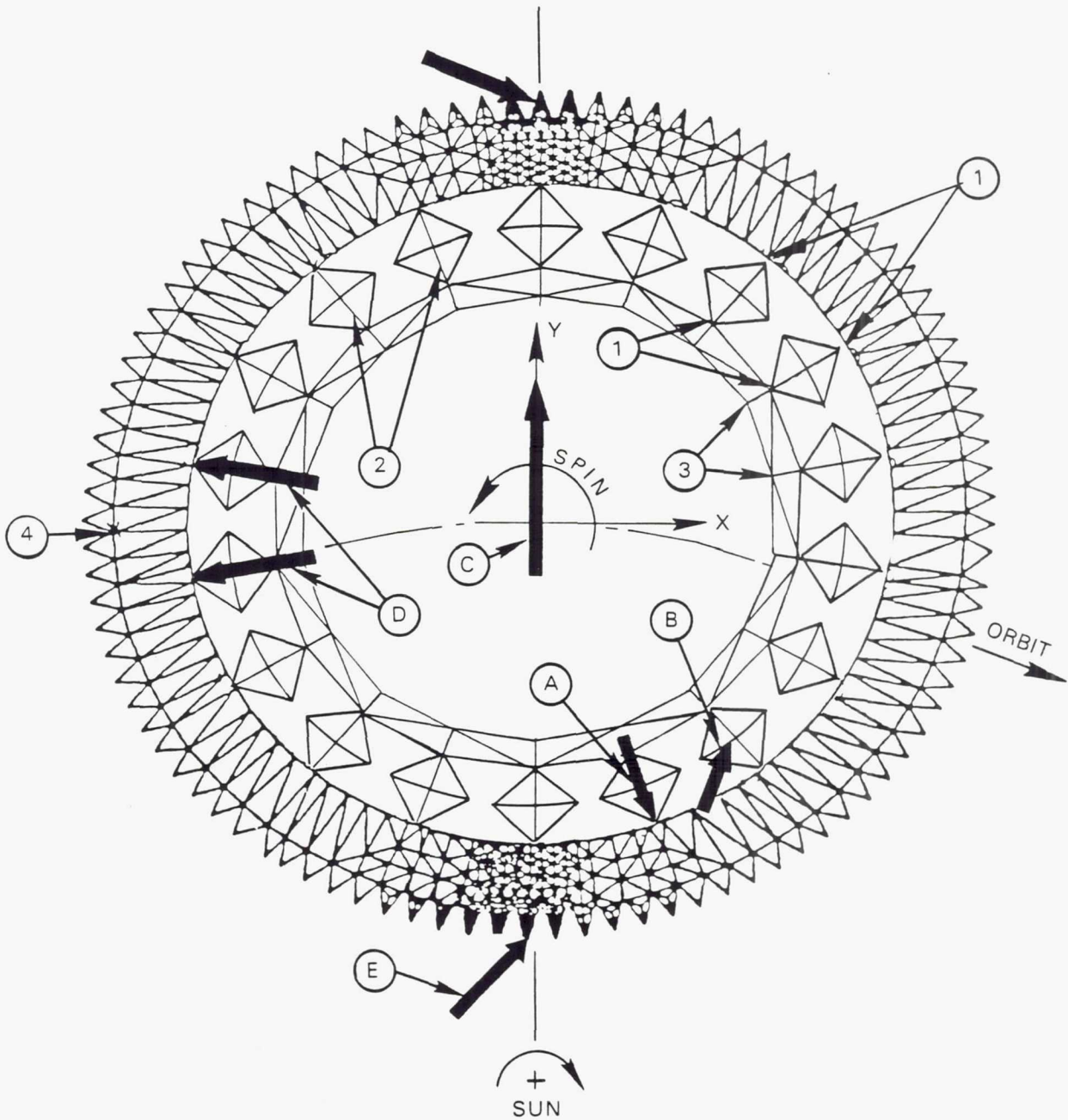
Effective use of some crowning by end relief of the planet gear teeth has been used in the test gearbox to centralize nonuniform loading, making the stresses somewhat higher in the mid-span of the tooth face where there is support of adjacent tooth material on both sides. This crowning can reduce the risk of overloading of the ends of the teeth.

It is a design goal to properly account for deflections of the tooth supporting structures of the gearbox to minimize the nonuniformity of tooth loading across the facewidth to allow the use of a minimal amount of crowning to avoid the higher mid-span stresses created by crowning.

The analysis work done in this particular area has provided, in a relatively short time, access to an understanding and a quantification of the principal problems encountered heretofore in high power density epicyclic gearing. These are problems that have, in the past, only been understood and resolved through extended trial and error development programs. This is a relatively modern and unique use of finite element analysis of the gear tooth supporting structures in a manner to define the deflection modes directly affecting the accuracy of tooth meshing in a very flexible weight-efficient structure. Frequent checks in the progressive changes of tooth mesh contact patterns with changes in loading during development testing will serve to verify and calibrate these analyses for rapid convergence on an optimum design.

#### 4.3.4 Planetary Gear/Bearing Assembly Analysis

The planet gear and bearing assembly was modeled separately, as illustrated in Figure 32, with a finite element analysis to: (1) determine that operating stresses in the bearing and in the gear tooth fillets are held to an acceptable level and (2) determine that the spherical bearing roller load distribution circumferentially around the inner and outer races is acceptable for the required bearing life.



BOUNDARY CONDITIONS

ROLLER LOADS

- ① NODES TIED IN RADIAL DIRECTION AT EACH ROLLER CONTACT WITH RACES
- ② POINTS ON EACH ROLLER LOCKED IN TANGENTIAL DIRECTION (BY CAGE)
- ③ NODES OF BEARING BORE LOCKED IN ALL DEGREES OF FREEDOM
- ④ REFERENCE NODE LOCKED IN "Y" DIRECTION (DIRECTION OF LINE OF CENTERS)

- Ⓐ ROLLER CENTRIFUGAL FORCES DUE TO PLANET SPINNING ABOUT ITS CENTER
- Ⓑ ROLLER CENTRIFUGAL FORCES DUE TO PLANET ORBITING ABOUT THE SUN GEAR
- Ⓒ PLANET GEAR OUTER RACE CENTRIFUGAL FORCE DUE TO ITS ORBITING ABOUT THE SUN
- Ⓓ ROLLER REACTIONS TO EXTERNALLY APPLIED GEAR TOOTH LOADS Ⓔ DERIVED FROM SEPARATE ANALYSIS

Figure 32 Finite Element Model Used for Planet Gear and Bearing Load and Stress Analysis

The results of the completed analysis indicate that, with an allowable stress factor of 1.5 for dynamic loads and planet-to-planet load sharing, the combined tooth bending and backing ring bending stresses in the fillet of the planet gear teeth are acceptable in accordance with the applicable Goodman diagram. The spherical roller load distribution results shown in Figure 33 indicate the same number of rollers in the loaded zone as that determined by the PLANETSYS analysis method which indicated bearing life to be acceptable.

The need to minimize the radial thickness of the integral outer race/gear backing rim for minimum weight and centrifugal loading and for maximum bearing capacity provides the opportunity to influence the local clearances between races and rollers and further to utilize any ring bending flexibility to help alleviate differences in load sharing between planets. The finite element analysis method used provides access to the understanding of the highly interactive elements of the planet gear/bearing assembly.

This modeling of the planet gear/bearing assembly with the detailed centrifugal loads from both the spinning about the inner race and the orbiting around the sun gear, together with multiple tooth loading related to high contact ratio teeth, pioneers such investigation of this kind of gearing configuration.

The information derived from this analysis provides a measure of the magnitudes and sensitivities of the interactive influences of the tooth bending loads and flexibilities and the flexure of the gear backing ring (with the integral outer bearing raceway). It establishes the location and magnitude of the combined resultant maximum stresses in the tooth fillets. It also similarly establishes the interactive influences of the outer race flexibility and the extent of the loaded zone of the bearing, together with the distribution of loads between rollers in this zone.

This understanding will provide a valuable basis for acquiring pertinent data and a more thorough analysis of forthcoming test results. Most importantly, it assists in a more rapid convergence on the optimums in the final design development tradeoffs.

The combined stresses in the tooth root fillets, distributed as shown in Figures 34(a) and 34(b), are shown by the Goodman Diagram of Figure 35 to be acceptable even with the factor of 1.5 included, showing that, if desirable, more flexibility could be incorporated in the bearing outer race without critically influencing the maximum fillet stress.

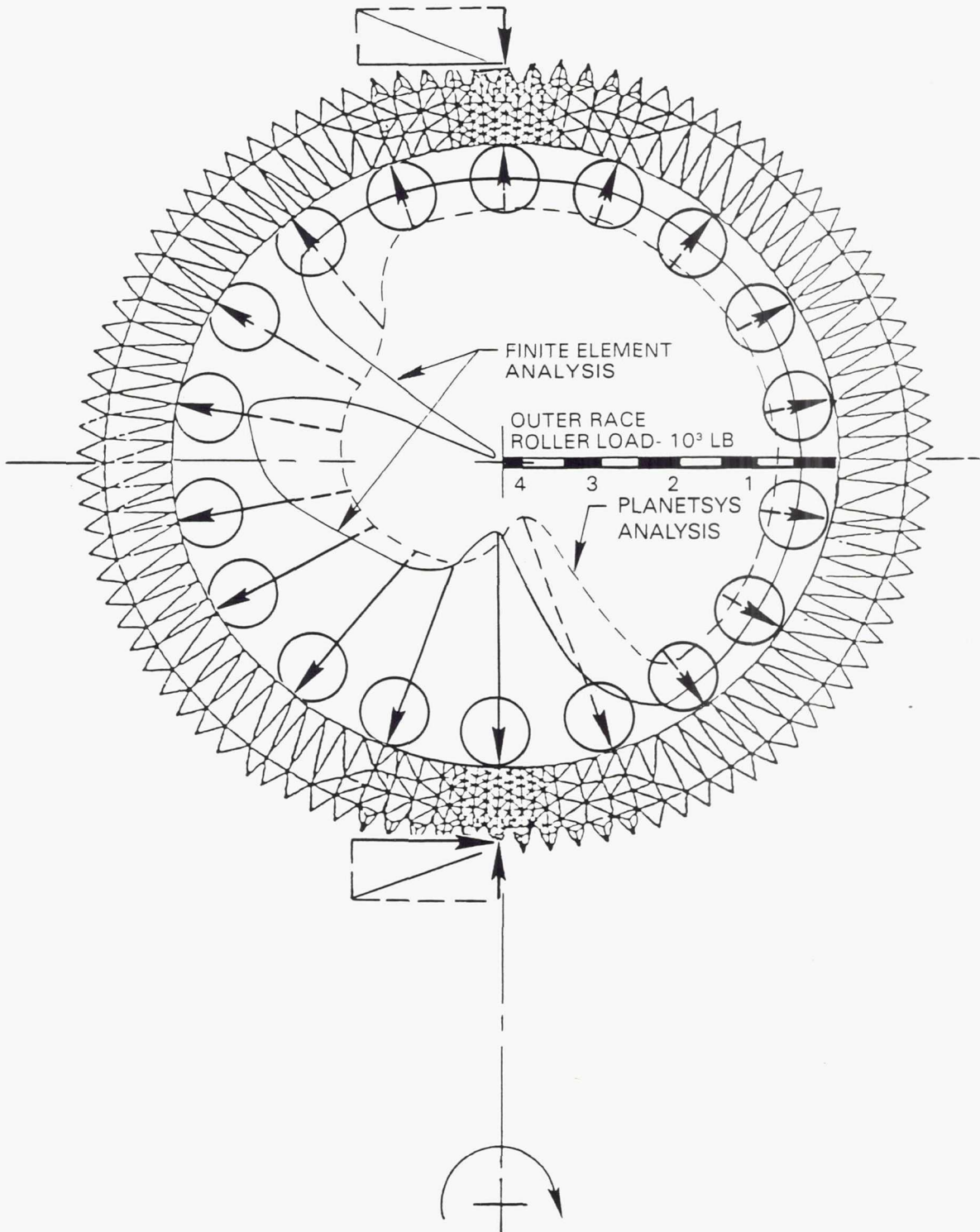
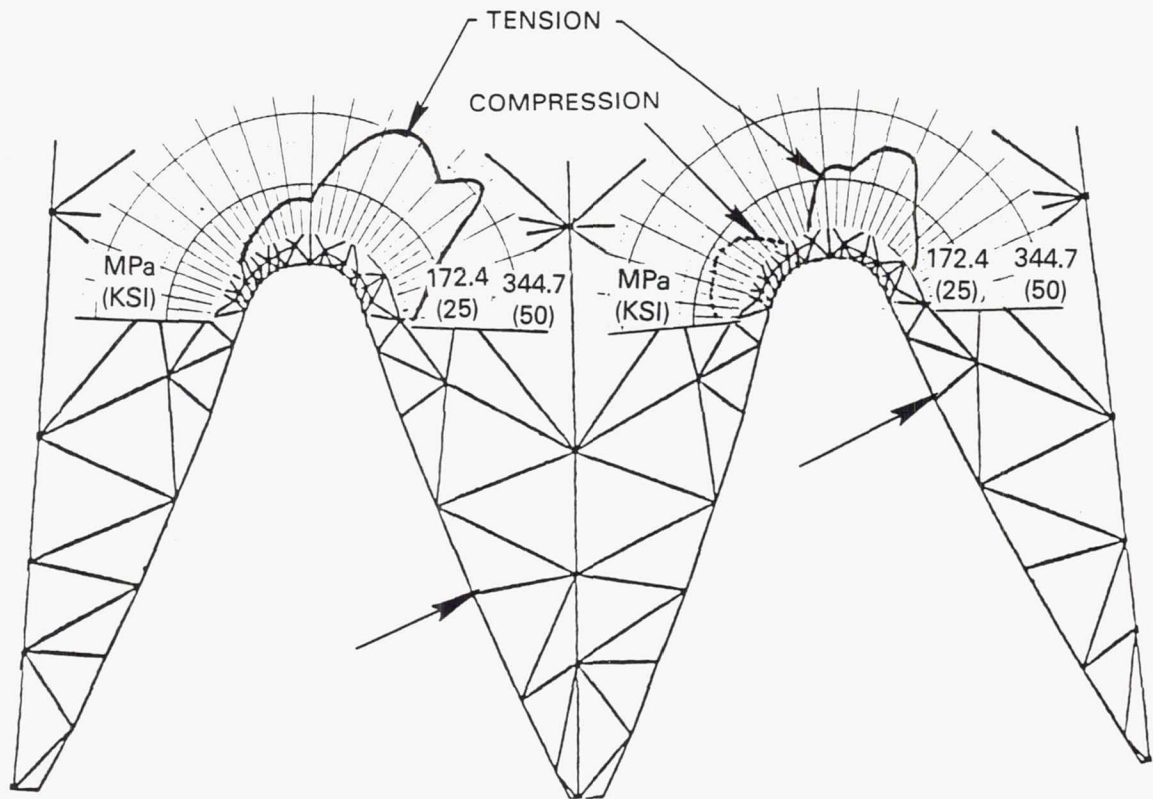
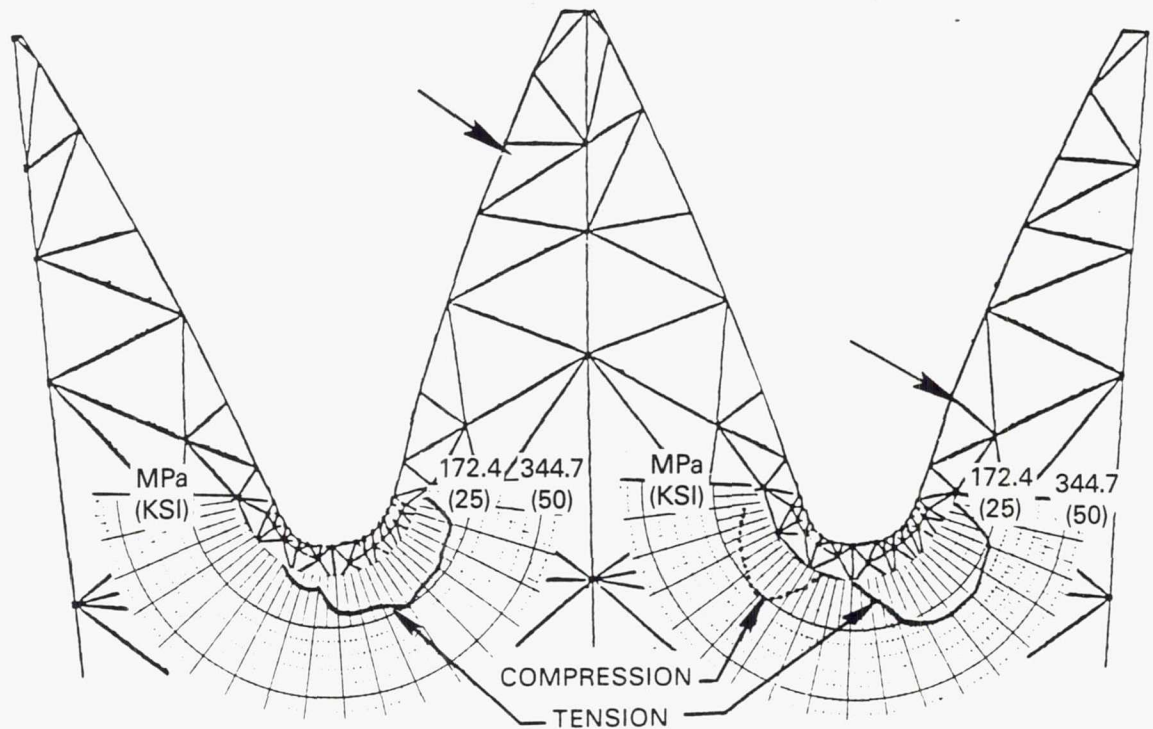


Figure 33 Comparison of Spherical Roller Load Distributions - Finite element analysis results show the same number of rollers in the loaded zone as that determined by the PLANETSYS analysis method.



(a) PLANET GEAR — SUN/PLANET MESH FINITE ELEMENT ANALYSIS ROOT FILLET TOTAL BENDING STRESSES



(b) PLANET GEAR — RING/PLANET MESH FINITE ELEMENT ANALYSIS ROOT FILLET TOTAL BENDING STRESSES

Figure 34 Distribution of Combined Stresses in the Tooth Root Fillets at the Sun/Planet Gear Mesh and the Ring/Planet Gear Mesh

### GOODMAN DIAGRAM

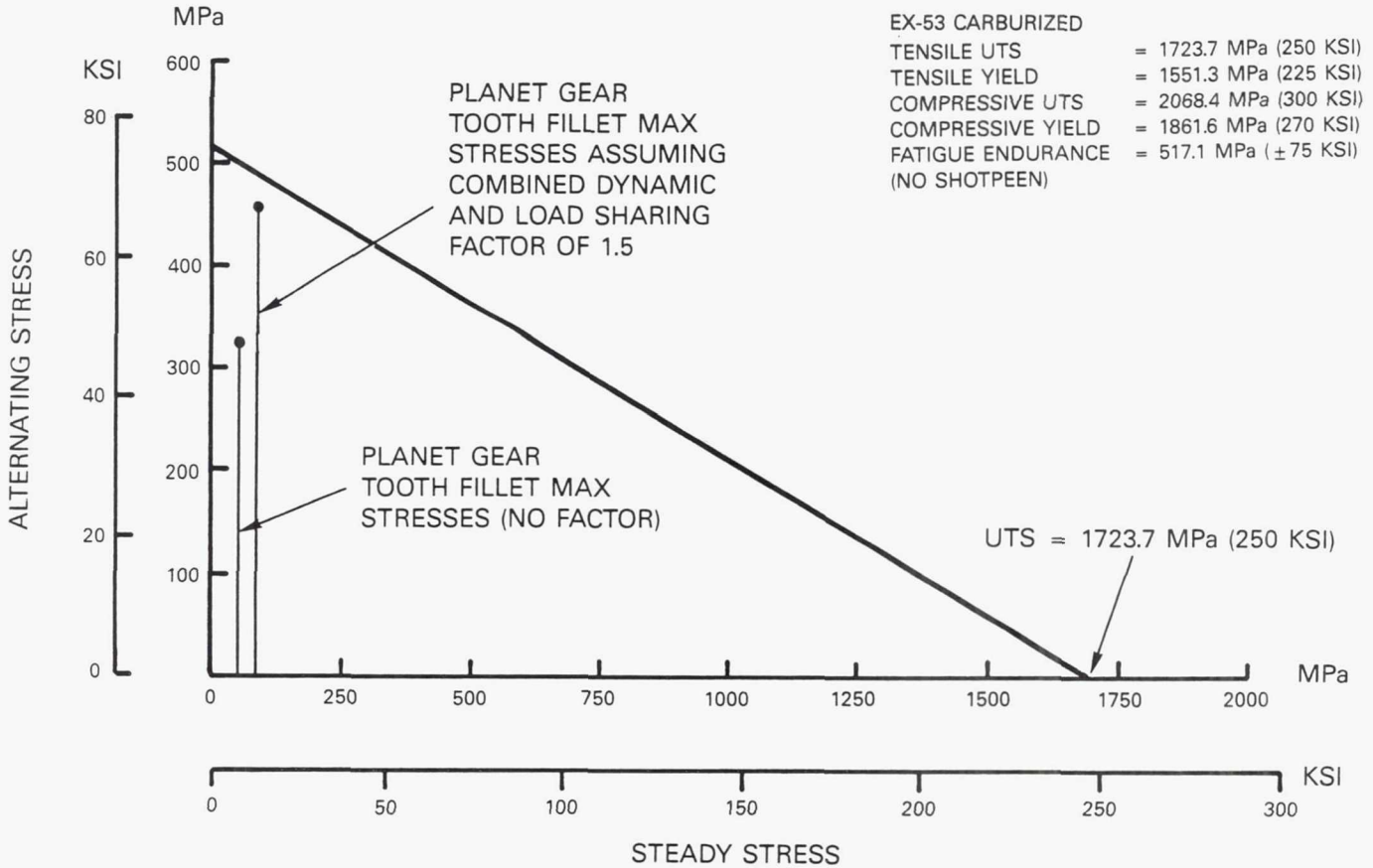


Figure 35 Combined Stresses in Planet Gear Tooth Root Fillets Are Acceptable Even With a Factor of 1.5 Included - More flexibility could be incorporated in the bearing outer race without critically influencing the maximum fillet stress.

#### 4.3.5 Gear Materials Selection

Gear material selection focused on high, hot hardness steels which are being developed in the gear industry to provide higher temperature capability. This permits operation at higher temperatures while at the same time providing better scoring capability. After reviewing several candidate materials, Carpenter EX-53 material was chosen as providing both improved scoring resistance as well as improved fatigue life. The characteristic of this material, as shown in Figure 36, is that it maintains its hardness to a higher temperature level relative to standard AISI-9310 materials.

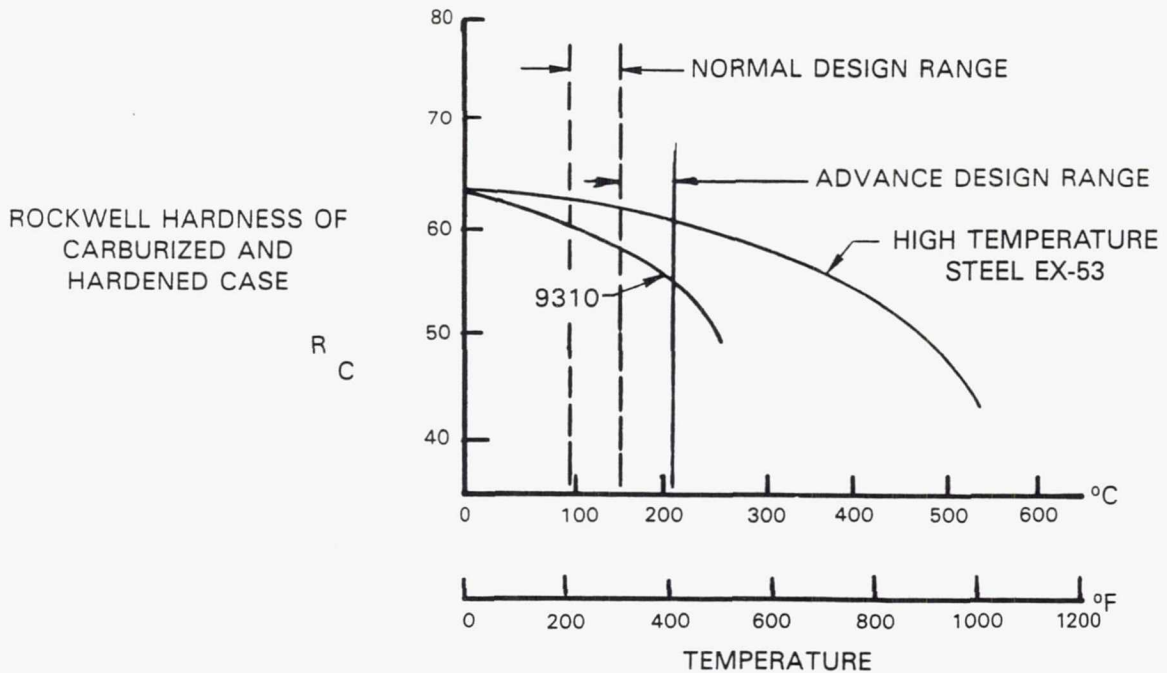


Figure 36 High Hot Hardness Steels Improve Scoring Resistance and Fatigue Life Relative to Standard AISI-9310 Gear Materials

#### 4.4 Bearings

Bearing system life is the single most important factor controlling gearbox durability. The overall gearbox durability design objective of 30,000 hours was apportioned over the subsystems and components, with a requirement for 50,000 hours Mean Time Between Unplanned Removals (MTBUR) assigned to the bearings. This is the equivalent of a 90% survival rate of the bearing system for 18,000 hours\*. This system objective was the governing factor in selecting bearing design and sizes for the highly loaded gearbox application. Bearings critical to achieving this objective were the planetary bearings (integral with the planetary gears) and the bearings supporting the prop shaft.

The gearbox configuration selected during Preliminary Design was a differential planetary gear system with five planet gears and a straddle-mounted prop shaft bearing support. The bearing arrangement required for this configuration was established using four bearing sets (seen as shaded areas in Figure 37) with eight separate bearing locations. These are:

- o Number 1: planet bearings (one in each of 5 planet gears)
- o Number 2, 3 and 4: bearings supporting the outer prop shaft (including the ring gear)
- o Number 5 and 6: bearings for the intermediate planet carrier shaft
- o Number 7 and 8: bearings for the inner sun gear input shaft

\* The conventional measure of bearing life is the time period over which 90% of the bearings survive, i.e. the period incurring 10% failure. This has been labelled the "L10" life, or sometimes the "B10" value. The L10 life of 18,000 hours for rolling element bearings is equivalent to an L50 life of 50,000 hours, the period for survival of 50% of the bearings. The relationship between L10 and L50 lives is based on a Weibull slope of 1.6.

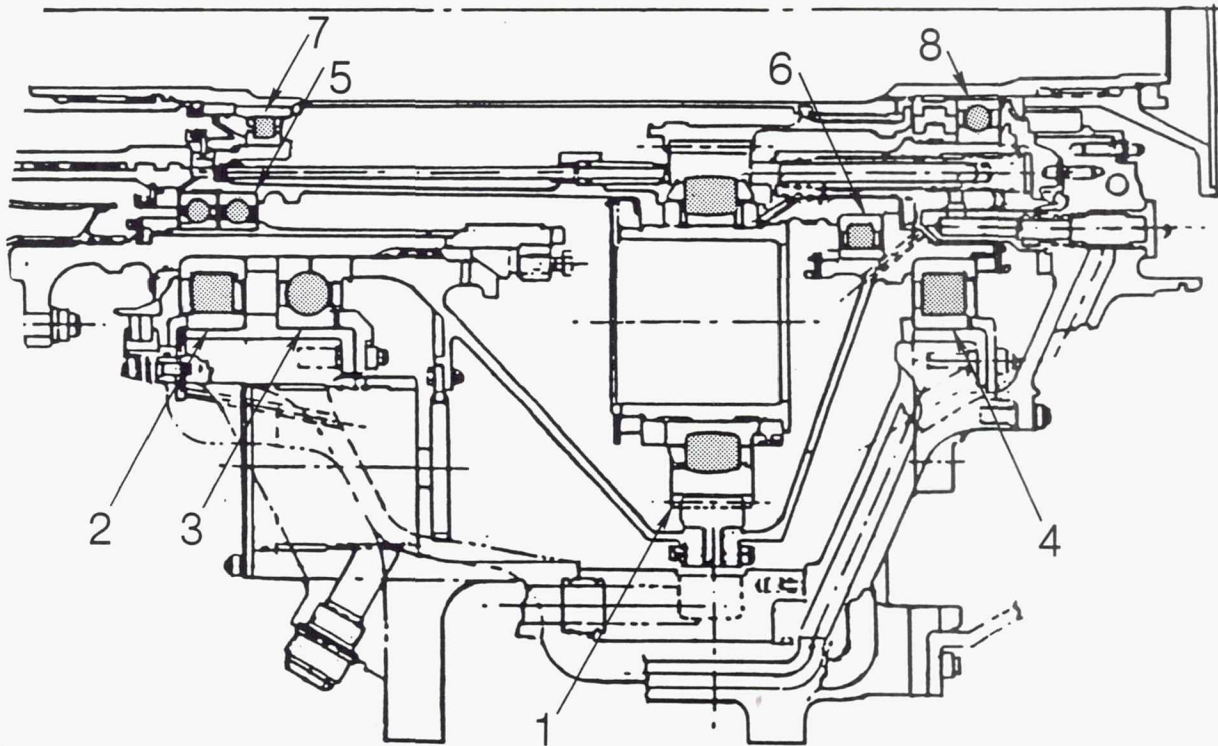


Figure 37 Bearing Arrangement for Differential Planetary Gearbox - Four bearing sets encompass eight separate bearing locations.

A summary of bearing locations and quantities, selected bearing types and sizes, speed factors and lives used in the preliminary design is shown in Table 16. The 18,700 hour calculated fatigue life of the bearing set exceeds the goal of 18,000 hours, for the original 120 passenger aircraft mission profile used at the start of design.

The subsequent AGBT Detailed Design, while changed in some details from the Preliminary Design, nevertheless retains the same basic bearing arrangement and meets all objectives for the system.

Design analyses of this bearing arrangement were performed during the Detailed Design Phase to confirm that the selected Preliminary Design configuration met design objectives, and to establish detailed design data. Analytical results determined rolling element numbers and sizing, load carrying capacity, rolling contact fatigue lives, lubrication, supporting structures and bearing/gear meshing contact geometry. Bearing selection details are shown in Table 17.

Table 16 Bearing Selection Summary (Preliminary Design)

	Location Name (Tractor Installation)	Bearing	Bearing Size, mm			Speed Factor (DN)	Qty	Bearing Life (L10)
	Type	Type	Bore	OD	Width	mmxRPM		hours
1	Planet roller	Spherical, 1 row	75	212.16	72	510,000	5	65,000
2	Rear prop shaft roller, front	Cylindrical, DFI	340	430	42	420,000	1	61,000
3	Rear prop shaft ball, front	Split inner ring	340	430	42	420,000	1	250,000
4	Rear prop shaft roller, rear	Cylindrical, DFI	360	450	42	440,000	1	390,000
5	Front prop shaft ball, front	Split inner ring	254	304.8	25.4	630,000	1	>500,000
6	Front prop shaft roller, rear	Split inner ring	254	304.8	25.4	630,000	1	>500,000
7	Input shaft roller, front	Cylindrical, DFI	100	150	24	900,000	1	>500,000
8	Input shaft ball, rear	Deep groove radial	100	160	28	900,000	1	>500,000

DFI = Double flange inner ring  
(controlling roller alignment)

Bearing Set Life (L10) 18,700  
Set Life Goal (L10) 18,000

Note: Bearing Set Life is calculated according to the methodology described in Chapter 8 of Reference 3.

Table 17 Bearing Selection (Detail Design) Gear and Shaft Support Bearing Configurations

	Bearing Type	Bearing Size			Element			Ball Bearing Contact	Cross-Race Conformity	
		Bore cm (in)	OD cm (in)	Width cm (in)	Qty	Length cm (in)	Diameter cm (in)	Angle deg	Outer Radius	Inner Radius
1	Spherical roller	13.00 ( 5.12)	---	6.17 (2.43)	18	3.51 (1.38)	2.54 (1.00)	--	0.5144	0.5076
2	Cylindrical roller	33.02 (13.00)	42.52 (16.74)	4.29 (1.69)	36	2.79 (1.10)	2.79 (1.10)	--	---	---
3	Ball	33.02 (13.00)	42.52 (16.74)	4.29 (1.69)	34	---	2.87 (1.13)	30	0.5350	0.5200
4	Cylindrical roller	33.02 (13.00)	42.52 (16.74)	4.29 (1.69)	36	2.79 (1.10)	2.79 (1.10)	--	---	---
5	Duplex Ball	24.13 ( 9.50)	29.21 (11.50)	2.54 (1.00)	48	---	1.42 (0.56)	30	0.5200	0.5200
6	Cylindrical roller	27.00 (10.63)	33.02 (13.00)	2.79 (1.10)	48	1.60 (0.63)	1.60 (0.63)	--	---	---
7	Cylindrical roller	13.00 ( 5.12)	18.01 ( 7.09)	2.49 (0.98)	28	1.30 (0.51)	1.30 (0.51)	--	---	---
8	Ball	11.51 ( 4.53)	17.50 ( 6.89)	2.77 (1.09)	16	---	1.60 (0.63)	17.25	0.5200	0.5200

A calculated L10 bearing system life of 22,300 hours was achieved for the revised 150 passenger aircraft mission profile used in the detail design; exceeding the design objective.

Designs of the Number 5 and 6 intermediate shaft bearings, which carry the gearset weight (but not prop loads), and the Number 7 and 8 inner shaft bearings, which support the power turbine drive shaft weight (but not thrust), were straightforward. These sets are characteristically common to aircraft gas turbine bearings. For example, in the test gearbox design, the number 7 and 8 bearings are production parts to save cost. The major design effort was therefore devoted to the planet bearings and the prop shaft support bearings.

#### 4.4.1 Planet Bearings

In a planetary gear system, the technical challenge imposed on the planet bearings is the bearing cage speed and rolling element centrifugal loading caused by the high rotational speed of the carrier. This is true for both single-rotation and counter-rotation applications. However, counter-rotation imposes a greater technical challenge relative to single-rotation because the planet gear rotational speeds and centrifugal loadings are higher in this application. Consequently, appropriate technology programs must assure roller pocket and cage land durability. The planet bearings are required to operate reliably under gear mesh loads generated by the power transmission torque, combined with the centrifugal loading of the gear rim and rollers produced by carrier rotational speed.

The planet bearing system comprises 5 single row spherical roller bearings. Each bearing has a bore diameter of 130 mm (5.12 in), with 2.54 cm (1.00 in) diameter rollers that are 3.493 cm (1.375 in) long. The L10 life of each planet bearing was calculated to be 89,000 hours, using the load distribution from the PLANETSYS computer program.

A major determination in the selection of planet bearings was the choice to use rolling contact bearings rather than journal bearings. Either would function adequately, but the choice was to use rolling contact bearings to achieve lower losses and better reliability. In many earlier high speed, high power transmission gearboxes, journal bearings were favored because of their ability to absorb the high centrifugal loads; however, they introduced significant parasitic power loss from high oil film drag. Additionally, cylindrical journal bearings are sensitive to misalignment. Wear problems have been traditionally experienced with journal bearings that were forced to operate during cold starts, dry starts after prolonged shutdown and short term oil interruption during maneuvers. All of these problem areas are addressed favorably by selecting spherical rolling contact bearings.

Spherical bearings (as opposed to cylindrical bearings) provide better tooth mesh alignment and uniform load distribution across the face width at each gear mesh. The spherical outer race, by allowing rotation of the integral planet gear teeth out of plane of the carrier-mounted inner race, provides for accommodation of the carrier torsional (angular) deflections with better meshing.

Single row (as opposed to double row) spherical rollers were selected for their simpler dynamics and to alleviate gyroscopic effects. In a single row bearing there are virtually no gyroscopic moment loads imposed on the roller, and consequently there is lower friction at the roller-to-guide flange interface and less slip caused by roller drag in the roller-to-race contact. These benefits contribute to minimizing wear and lubrication requirements.

With the planet gear pitch diameter and root diameter established by sun and ring gear selection, the planet bearing size is dictated by establishing adequate gear tooth backing thickness and the desired spherical radius of the outer raceway of the planet bearing for best bearing life. An integral gear/bearing outer ring is achieved by machining gear teeth into external surfaces of the bearing outer ring (see Figure 38). This single unit

construction provides the lowest weight gear/outer ring design. Integral planet gear/bearing construction also avoids the interfacial fretting that occurs when separate parts deflect and rub under working loads and speeds.

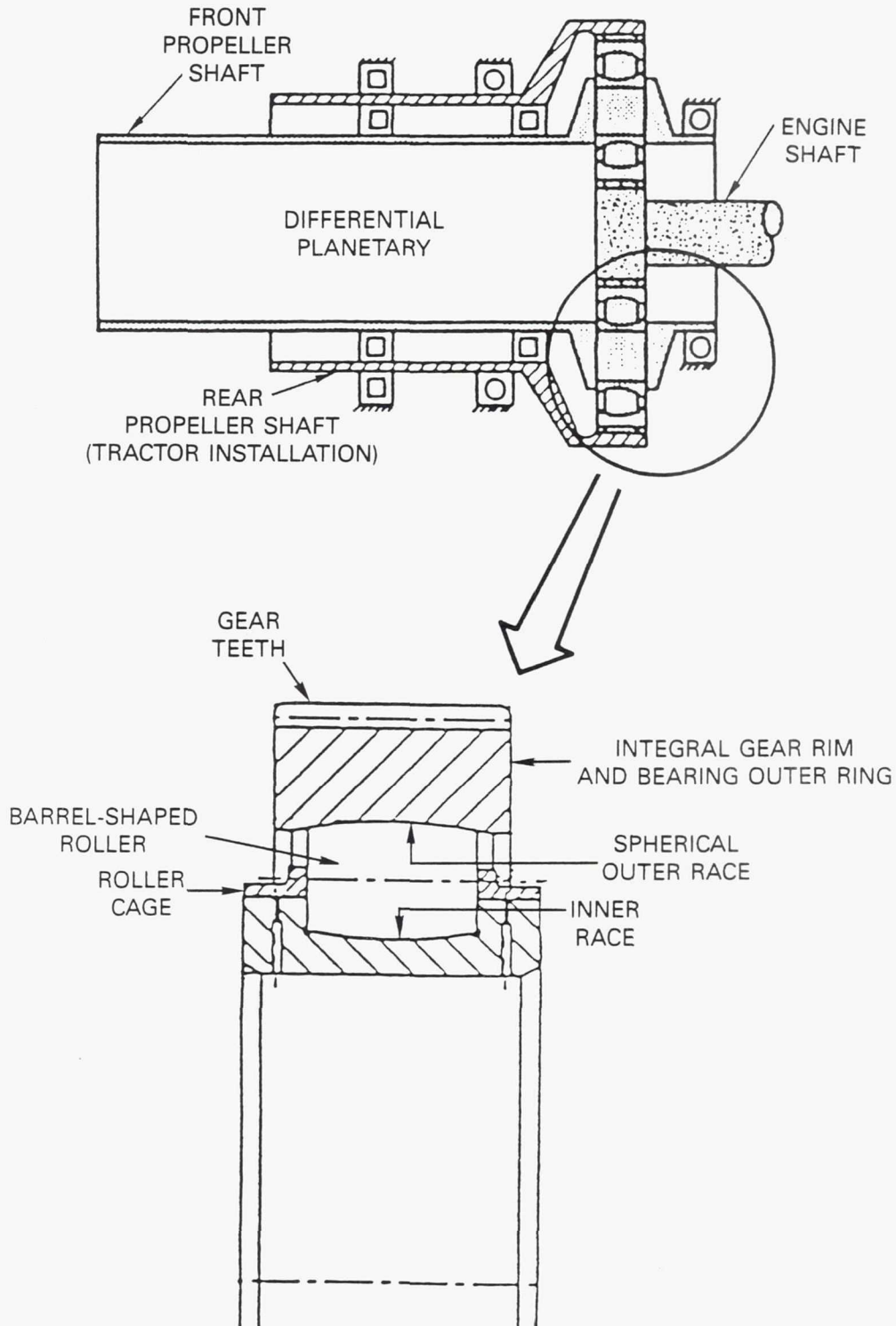


Figure 38 Integral Planet Gear/Bearing Configuration - This single unit construction provides lowest weight design.

A design optimization study was accomplished for the spherical rollers utilizing the SKF Industries, Inc. (Bearing Company) computer program "PLANETSYS" to achieve minimum cage weight and optimum load distribution. Bearing lives were based on the PLANETSYS load distribution as opposed to a load distribution generated by a finite element analysis (see earlier discussion in Section 4.3.4).

Attention to the roller pocket details (shown in Figure 39) follows practices used in aircraft engine mainshaft designs. The roller/web contact surface is curved to maximize the roller contacting area and the strength of the web (or cross-bar). Standoff tabs are employed to allow an increased radius at the corners of the pocket to reduce the likelihood of fracture.

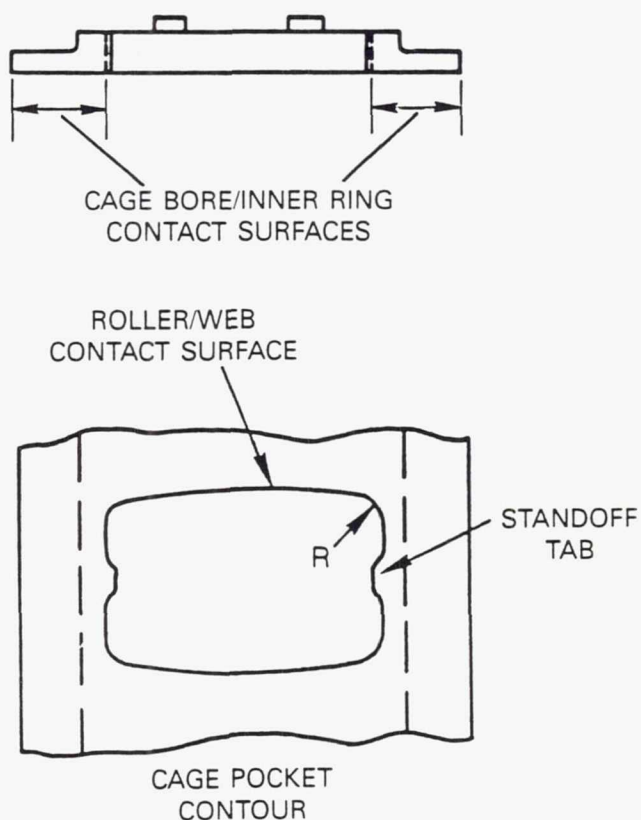


Figure 39 Roller Cage Design - Features shown enhance strength while achieving minimum weight and adequate cage support surface area.

#### 4.4.2 Prop Shaft Support Bearings

The other critical bearings in meeting the counter-rotating gearbox durability objective are the prop shaft support bearings. These bearings must support the large propfan assembly mass and are required to operate stably and predictably during all aircraft operating modes, including high aerodynamic asymmetrical loads from the propeller that occur during maneuvers and high angles of attack that occur during takeoff and climb.

Design of the prop shaft bearing system consists of a front cylindrical roller bearing in combination with a ball bearing, and a rear cylindrical roller bearing. The two cylindrical bearings support the radial reaction loads to the shear and moment forces applied by the propfan and the shaft weight. The ball bearing carries only the fore and aft thrust loads.

The calculated lives of the prop shaft support bearings (Number 2, 3 and 4) can be seen in Table 18. High individual bearing design lives are needed to meet the system objective of 18,000 hours. As noted in the table, the detail design calculated set life is 3600 hours greater than the preliminary design result shown in Table 16. This results from the change in aircraft mission and duty cycle profile (discussed earlier in Section 4.1.2) associated with the 155 passenger aircraft design.

Table 18 Bearing Operation: Durability Objectives Are Met

Bearing Location	Flight Condition	Mean Hertz Stress, MPa (ksi)	Speed Factor, DN mm x RPM	Mission Life, L10, hours
1	SLTO CRUISE	1400 (203) 1317 (191)	884,000	89,000
2	SLTO CRUISE	779 (113) 855 (124)	408,000	192,000
3	SLTO CRUISE	1200 (174) 807 (117)	408,000	75,000
4	SLTO CRUISE	676 ( 98) 738 (107)	408,000	920,000
5		669 (97) 669 (97)	596,000 596,000	1,000,000 1,000,000
6		421 (61)	667,000	40,000,000
7		779 (113)	1,175,000	100,000
8		889 (129)	1,038,000	162,000

Bearing Set Life (L10) = 22,300 hours (exceeds 18,000 hour objective)

In selecting the design configuration during the Preliminary Design phase, concern for bearing misalignment caused by the propfan moment loads and prop shaft angular displacement, as well as the radial clearances necessary to accommodate the high thermal expansion of the lightweight alloy housing, led to a study of alternative configurations.

The alternative concepts studied are shown in Figures 40 and 41. The configuration in Figure 40, with two tapered roller bearings spaced apart, offers two advantages. The number of bearings supporting the prop shaft is reduced by one, improving reliability and maintainability; and the tapered roller bearings increase the effective span between bearings, improving transfer of the propfan loads to the gearbox housing. However, the use of tapered bearings requires that axial load be applied to the large end of each roller in proportion to the roller normal load and roller cone angle, to keep the roller in equilibrium. This axial load is applied through sliding contact with the roller guide flange and causes bearing friction drag and power loss which can be severe if the thermal/mechanical design is not finely tuned. Tapered bearings are also more sensitive to oil supply interruption. These factors represent increased risk for this option.

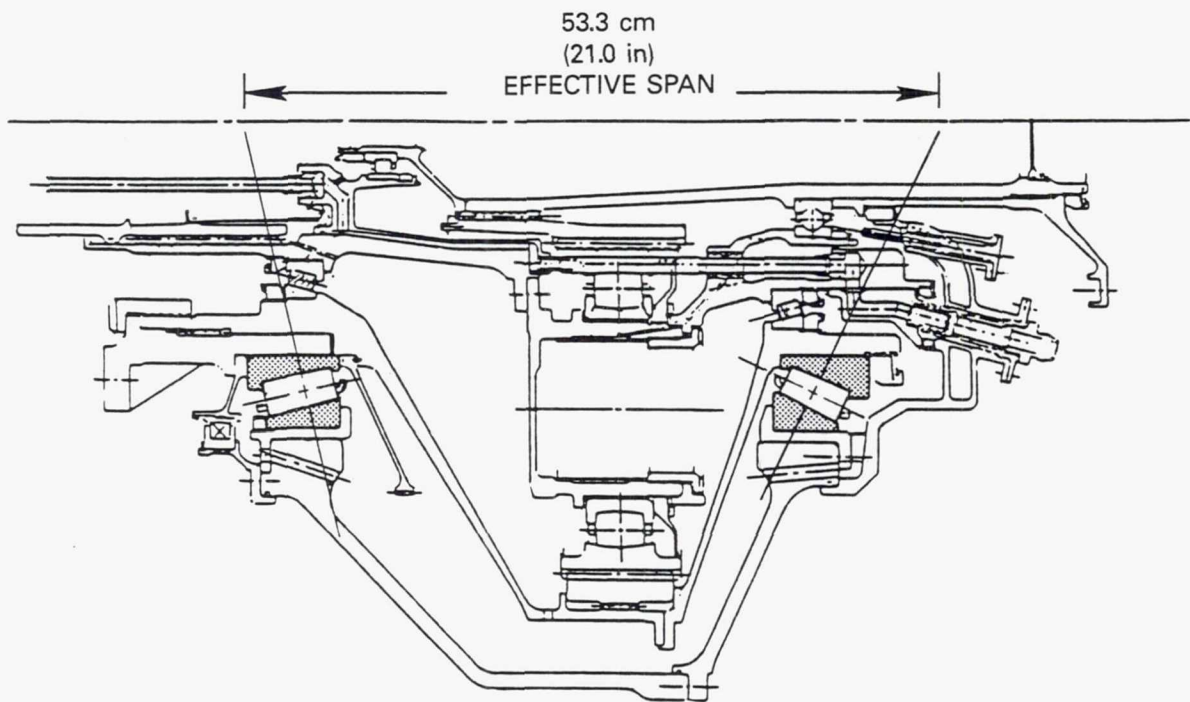


Figure 40 Tapered Roller Bearings (Spaced Apart) - Provides potential benefits in reliability and maintainability, but with a risk of increased power loss.

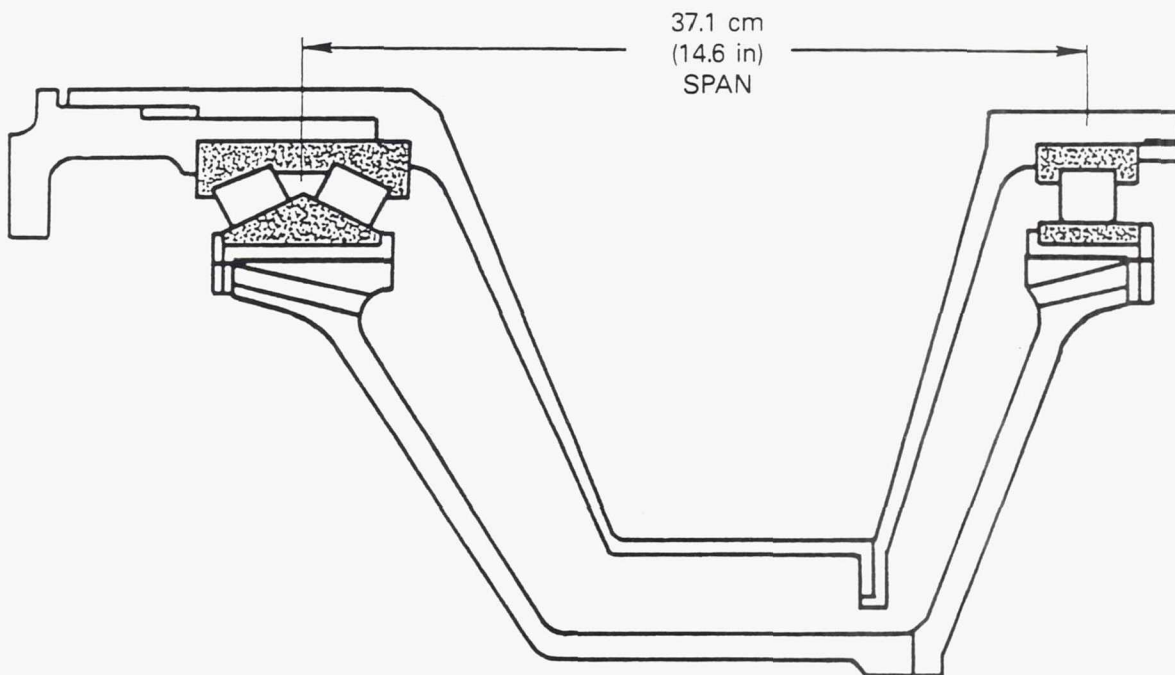


Figure 41 Duplex Tapered Bearings - Transfers shaft bending moments directly to the housing, potentially reducing prop shaft bending and ring gear distortion, but with a risk of increased power loss.

The other option (Figure 41) shows duplex tapered bearings with a cylindrical roller bearing. This is closer to the base design, with some potential advantages. While the effective span is unchanged relative to the base, the duplex bearings provide a more direct path for moment transfer from the shaft to the housing. This effect could potentially reduce prop shaft bending and ring gear distortion, thereby improving load sharing between the planet gears. Shaft displacement and bearing misalignments would be reduced relative to the base but not as much as the first option. Moment loading of the duplex tapered bearings would require increased bearing size and weight relative to both options. Roller end loading, as in the case of the other tapered roller bearing option, would increase power loss.

Table 19 compares the three designs examined for the prop shaft support bearings. A qualitative assessment of the technical risks assigned to each appears in terms of a relative risk/benefit ratio. It was on the basis of this factor that the baseline ball and cylindrical roller bearing option was retained for the counter-rotation gearbox detail design.

Table 19 Optimal Bearing System Risk/Benefit Analysis

	Ball and Cylindrical	Spaced Tapered Rollers	Duplex Tapered Rollers and Cylindrical Roller
Load support	Base	Improved	Improved
Damaged propeller operation	Base	Improved	Improved
Cost	Base	Reduced	Base (+)
Weight	Base	Reduced	Increased
Power loss	Base	Increased	Increased
Risk/benefit ratio	Base	Highest	Increased

The selected bearing arrangement, using a combined angular contact ball thrust bearing and cylindrical roller bearing for the bearing unit at the propeller end, and a cylindrical roller bearing at the engine end, follows historical Pratt & Whitney practice (dating from early piston engine designs to modern turboshaft engines), of separating the thrust and radial component forces so as to take thrust loads through the angular contact ball bearing and radial and moment loads in the two cylindrical bearings. During the detailed design phase, the considerations for using tapered roller bearings were reviewed again. The potential weight, cost and part-count advantages for the configurations shown in Figures 40 and 41 were determined to be small in comparison to the relatively high risks associated with differential radial and axial thermal expansions between the aluminum housings and the steel shafting. The expected magnitude of the range of these differential expansions over the desirably long effective span would seriously compromise the axial preloads required for these tapered roller bearings to operate reliably. Designing for axial travel in an outer ring mounting fit, with low spring rate preloading provisions to ameliorate the thermal preload variation problem, would be contrary to the separate need for minimal outer ring looseness to avoid fretting and galling. This excluded further consideration of the tapered roller bearing configurations.

As noted earlier, changes in mission and duty cycle requirements during the course of the design efforts affected detailed design data, but the basic configuration remained the same. For example, specific prop shaft aircraft design data, obtained for a 155 passenger aircraft from an aircraft company, resulted in more refined flight cycle aerodynamic load values, which led to the extended predicted lives shown in Table 18.

Assymetrical aerodynamic loads are generated by changes in air angles, such as those created at rotation of the aircraft during takeoff. The propeller shear and moment loads associated with these aerodynamic loads are reacted by the

Number 2 and 4 cylindrical bearings. Estimates of maximum prop shear and moment loads for an earlier 120 passenger aircraft were much higher than for the more recent 155 passenger aircraft aerodynamic data, which lowered the maximum propeller shear load from 17,926 N (4,030 lb) to 8,185 N (1,840 lb). Similarly, less severe loads were required by the larger aircraft at other flight conditions. The major effect these changes had on the output results was to increase the earlier life prediction for the critical prop shaft bearing. In the Preliminary Design (see Table 16), the prop shaft bearing lives were adequate to meet system objectives, although the Number 2 prop shaft bearing had a slightly lower life than the planet bearings. The prop shaft bearing lives resulting from detailed design (see Table 18) were well beyond the 18,000 hour system objective although, in this case, the life of the Number 3 prop shaft bearing was somewhat lower than the planet bearings.

A lightweight aluminum gearbox housing is used. The prop shaft bearings are installed inside steel liners which are press-fit into the housing to give proper support and clearances for the bearings. Iterative design analysis determined the proper thickness for the steel liners, to establish thermal stability over the broad range of environmental conditions, i.e., -53.9°C (-65°F) cold soak to 176.7°C (350°F) inlet oil temperatures.

The shaft bearing loadings for life calculations were first determined on an individual bearing basis through equilibrium calculations of the individual shaft assemblies under the mission profile to establish equivalent radial and thrust loads for each bearing. In the Detailed Design phase this was updated using a sophisticated computer analysis that jointly considers a subsystem of shafts, mountings and multiple bearings, together with their individual internal design details, such as race curvatures, rolling element size and geometry, contact angles for ball thrust bearings, diametral clearances, etc. Iterative application of this analysis, using variations in these internal design characteristics for each bearing, provided the optimization of the combination bearing/shaft subsystem for best bearing lives. Revised, more realistic and less conservative propeller loads from the more specifically applicable aircraft installation were applied to the mission profile in the updated bearing loads calculation. This resulted in the significant improvement, noted earlier, in the B10 bearing lives of the propeller supporting bearings 2, 3 and 4.

The limiting operating conditions of angular misalignment between the inner and outer races, caused by shaft bearing seat slopes due to shaft deflections, were determined with the assistance of the finite element analysis of the shafting assemblies under the worst case applied operating loads. Other considerations, such as manufacturing tolerances, bearing internal clearance and bearing contact deformations, were included to arrive at net misalignment values affecting bearing life.

The ovality imposed on the bearings by shaft distortions, defined in the finite element analysis and illustrated in Figure 42, indicated that ovality was not a serious limitation of bearing life, but instead, when properly combined with internal fit-up, could increase bearing capacity by extending the loading zone arc to include a greater number of rolling elements. The values of these imposed race ovalities are available for more informed analyses of track patterns observed on a bearing race after initial test stand

operation. They will also be available for later design optimization refinements of the internal detail design of the bearings for further extending life capabilities.

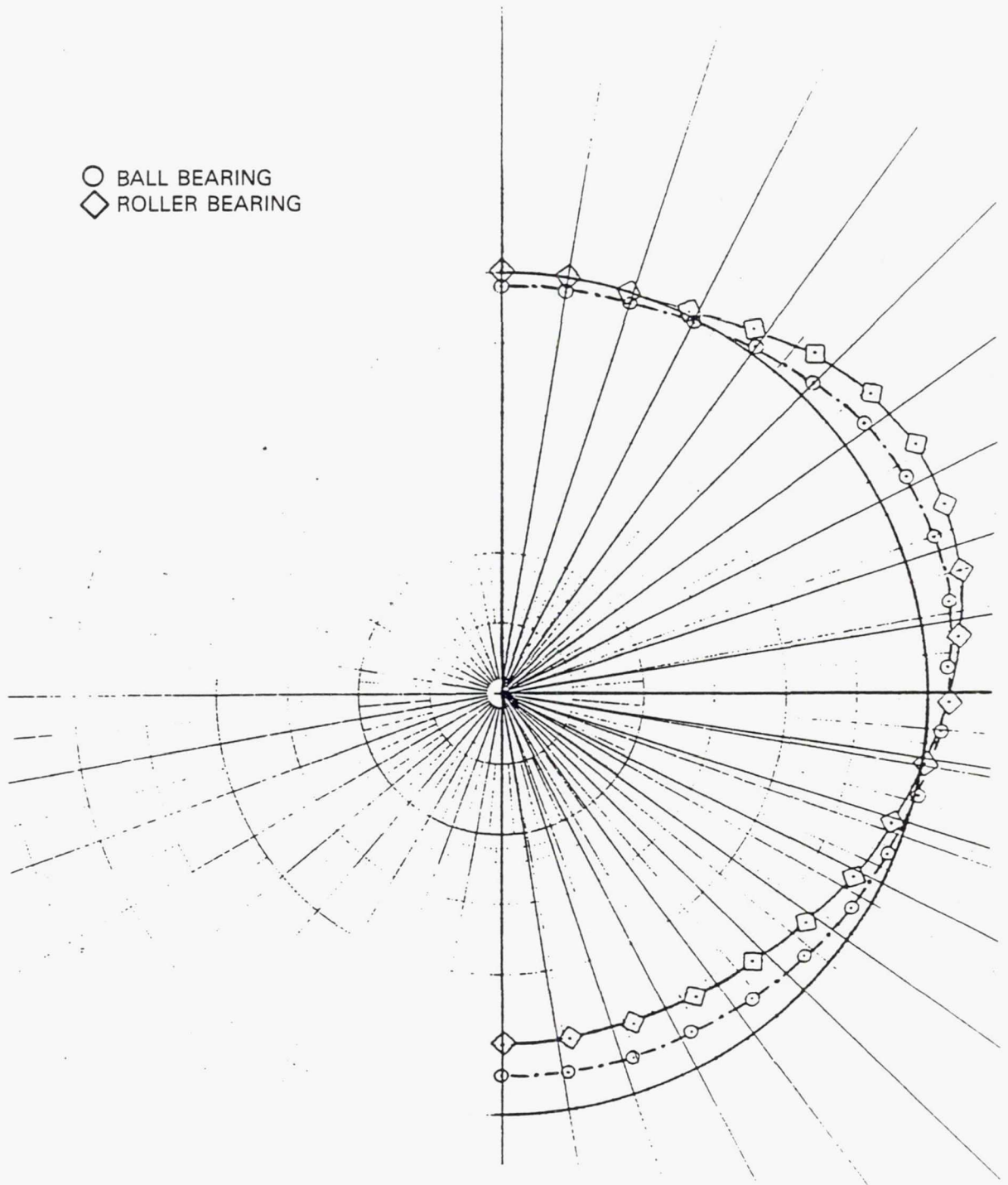


Figure 42 Prop Shaft Section Deformation at Ball and Roller Bearing Locations  
- Ovality is not a serious limitation on bearing life.

The relatively high radial loads on the shafting bearings carrying the propeller shear and moment loads required careful consideration of the special fits between the bearing races and their mounting surfaces on the shafting to avoid excessive creep and attendant fretting or galling of the interfaces. Some of the high interference fits required, as indicated in Table 20, demanded special consideration of the internal fit-up or looseness of the bearings, as manufactured, to provide the proper operating clearances.

Table 20 Summary of Bearing Loads and Fit-Ups

Bearing Number	Radial Load N (lb)	Thrust Load N (lb)	Inner Diameter Fit cm (in)	Outer Diameter Fit cm (in)	Liner Fit cm (in)
2	97,861 (22,000)	--- ---	.0241-.0277 (.0095-.0109)	.0114-.0152 (.0045-.0060)	.0991-.1067 (.0390-.0420)
3	--- ---	97,861 (22,000)	.0051-.0086 (.0020-.0034)	.0100L-.0140L (.0040L-.0055L)	.0991-.1067 (.0390-.0420)
4	71,172 (16,000)	--- ---	.0229-.0264 (.0090-.0104)	.0114-.0152 (.0045-.0060)	.0991-.1067 (.0390-.0420)
5 Front	890-1779 (200- 400)	--- ---	.0005-.0038L (.0002-.0015L)	.0000-.0041L (.0000-.0016L)	--- ---
5 Rear	890-1779 (200- 400)	--- ---	.0005-.0038L (.0002-.0015L)	.0000-.0041L (.0000-.0016L)	--- ---
6	890-1779 (200- 400)	--- ---	.0051-.0084 (.0020-.0033)	.0025-.0063 (.0010-.0025)	--- ---
7	7117 (1600)	--- ---	.0063-.0089 (.0025-.0035)	.0025-.0013L (.0010-.0005L)	--- ---
8	990-1779 (200- 400)	--- ---	.0013-.0038 (.0005-.0015)	.0013-.0013L (.0005-.0005L)	--- ---

L = These dimensions have a loose fit whereas all others are tight

Detail consideration of the expected angular misalignments between races defined the use of open curvatures in the order of 53.5% for the outer race of the angular contact ball thrust bearing rather than the normal race curvatures in the range of 52% +/-0.25% (ratio of raceway transverse radius of curvature to ball diameter). This avoids large changes of operating contact angle between balls and raceway around the circumference of the bearing that could increase ball creep and slippage in the contact areas. This also reduces dynamic loads on the retaining cage and reduces friction losses and energy dissipation within the bearing.

A proprietary P&W empirical database, based on typical bearing operating data, nondimensionalized, was applied to each of the individual bearings to determine the energy losses that must be dissipated from each bearing. The inputs to this analysis include: the operating speed and load, the clearances and curvatures (where applicable), the number of rolling elements and their orbit or "pitch" diameter, the type of cage, the type of oil supply (splash, flood or jet) and the oil supply rate in pounds per minute. The analysis considers the net effect of the rolling coefficient of creep friction in the rolling contact areas as well as cage friction and windage and oil churning. This analysis was used to iterate the requirements for cooling oil flows and to define the resulting oil temperature rise and equilibrium bearing operating temperatures under the worse case loads for each bearing, as discussed in Section 4.5. This information also provided inputs to the design of the oil supply and to the calculated efficiency of the gearbox.

The planet bearing energy dissipation requirements were determined through the use of the PLANETSYS computer program. The iteration of required oil flow versus oil temperature rise and equilibrium bearing temperature was done independently of that for the shafting support bearings. The estimates of the expected L10 life of the planet bearing design used were also provided by the load distribution outputs from iterations of the PLANETSYS program.

#### 4.4.3 Bearing Materials

Advanced bearing materials were selected for the AGBT gearbox design so that they may be included in testing to verify their benefits and compliance for the production gearbox. The integral planet gear/bearing set uses Carpenter EX-53 high hot hardness steel material carburized in the teeth and the bearing raceway of the integral gear and outer bearing ring. Both the Sikorsky and Pratt & Whitney Divisions of United Technologies are gathering experience with this advanced carburized material. Other candidate materials considered for this location included CBS 1000M, Vasco X2M and a carburized M-50 (M-50-NiL). Bearing rollers are made from M-50 steel. The future use of silicon nitride rollers depends on effective quality assurance and production economy. A new, lightweight hot isostatic pressed silicon nitride material under development at Pratt & Whitney and elsewhere is considered to be the leading candidate to replace the present day M-50 material for rolling elements in the planet gears. Silicon nitride has a density approximately 40% that of M-50 and a modulus of elasticity approximately 150% that of M-50. The potential benefit of this material is lighter weight bearings that would reduce the centrifugal forces generated by the rollers; thus reducing the normal components of the centrifugal roller loads on the races and the tangential components of the orbiting centrifugal forces that create loads on the cage pockets.

#### 4.5 Lubrication and Scavenging

##### 4.5.1 System Description

The lubrication and scavenging system must provide positive oil supply, filtration, scavenging and thermal management.

Concept studies of single- and counter-rotation gearbox systems resulted in the recommendation to separate the gearbox oil system from the engine oil system. The system and its requirements, shown in Figure 43 and Table 21, utilize a common fuel/oil cooler and separate air/oil coolers. This approach offers flexibility in configuring air/oil coolers and managing heat loads throughout the flight cycle. It also provides the opportunity to consider testing and using advanced lubricants developed specifically for high power gearbox applications. This design decision will be reviewed again, before committing to a production design, to assess the tradeoff benefits related to air/oil cooler size and life prediction.

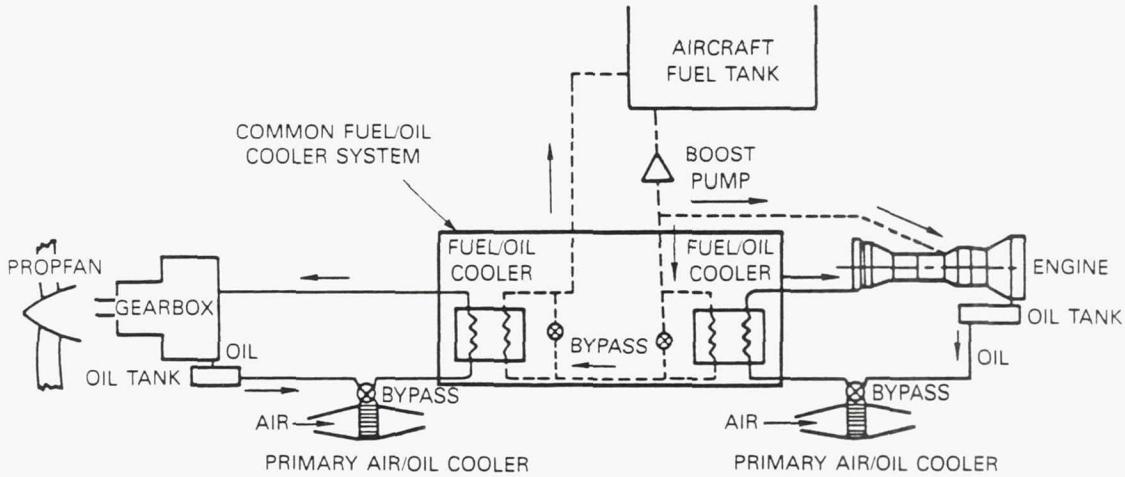


Figure 43 Selected Oil Cooling System for Advanced Turboprop Engine - Separate gearbox and engine supplies offer flexibility in configuring air/oil coolers and managing heat loads throughout the flight cycle.

Table 21 Advanced Turboprop Engine Oil System Requirements (12,000 Horsepower Size Engine)

	Gearbox And Propfan	Engine And Power Turbine
Heat to oil, joules/sec (Btu/min)	89,658-105,480* (5100-6000*)	73,836 (4200)
Oil flow, kg/min (ppm)	68-91* (150-200*)	57 (125)
Oil volume, liters (gallons)	10.6-14.0* (2.8-3.7*)	12.9 (3.4)
Residence time, seconds (full tank)	8	12
Tank Size (oil + air), liters (gallons)	12.9-17.4* (3.4-4.6*)	14.4 (3.8)

\* Higher value includes propfan

Details of the lubrication system designed for the gearbox are illustrated in Figure 44. A high pressure positive displacement gear pump supplies oil to the gearbox in conjunction with a pressure regulating valve which holds a preset discharge pressure. The pressure is set high enough to assure adequate oil jet penetration to gear tooth flanks in the high contact ratio gear mesh planned for this gearbox. The regulating valve bypasses some flow back to the pump inlet, to ensure full flow under all conditions.

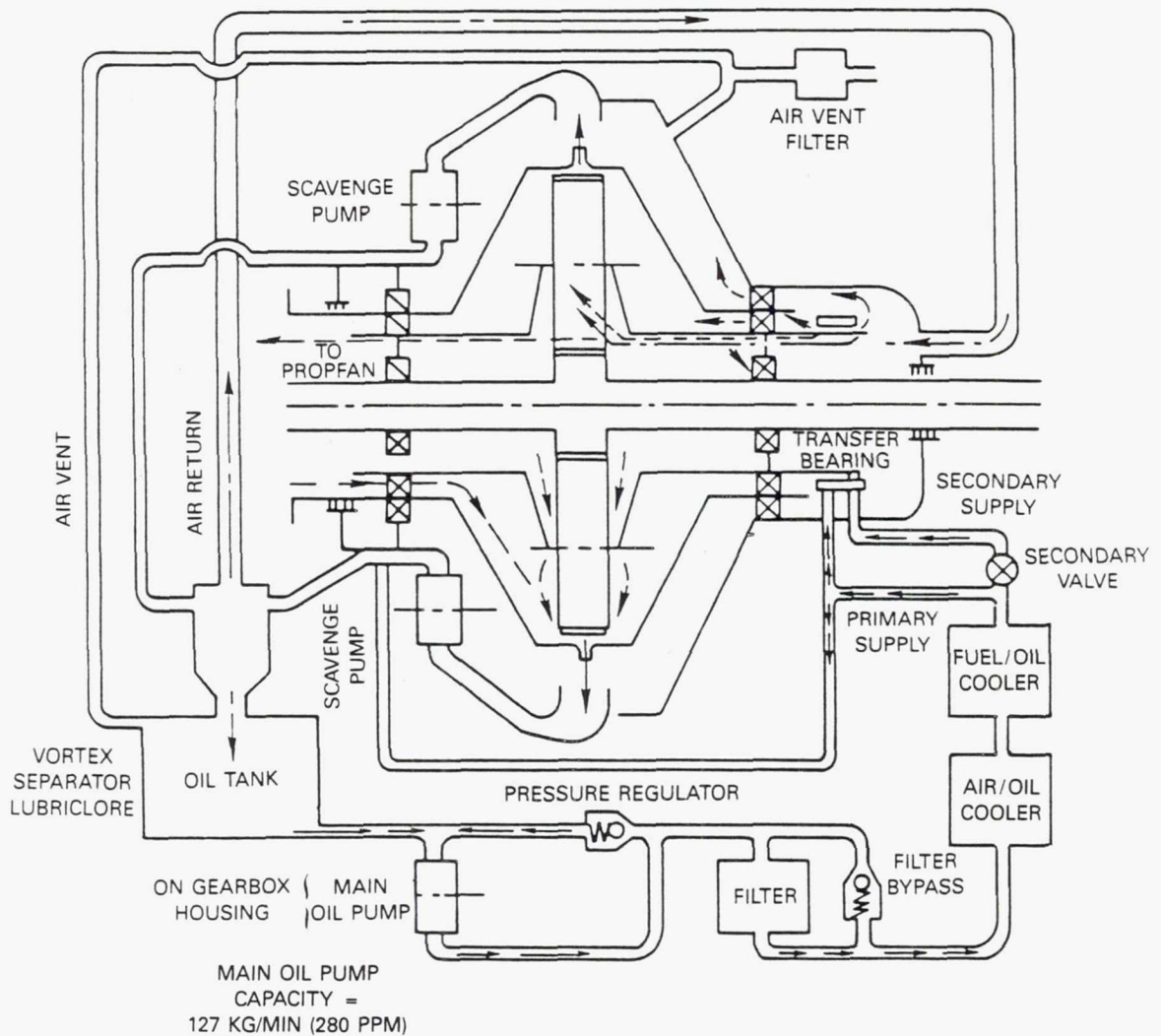


Figure 44 Lubrication System Schematic Designed for the Gearbox Uses a Positive Displacement Pump and Pressure Regulating Valve to Ensure Adequate Oil Supply

High pressure oil is cooled and filtered before delivery to the gearbox. The cooler transfers oil heat to ambient air. The oil filter is an ultra-fine replaceable element with a 3 micron rating. The filter is protected by a warning device which signals excessive pressure drop in advance of filter bypass, should the filter become clogged between normal maintenance actions.

The main oil supply lines to bearings and gears are also equipped with "last-chance" screens (Figure 45) which intercept any foreign particles too large to pass through the smallest of the metering jets in the lubrication system. These screens are accessible for inspection and cleaning from outside of the fully assembled gearbox.

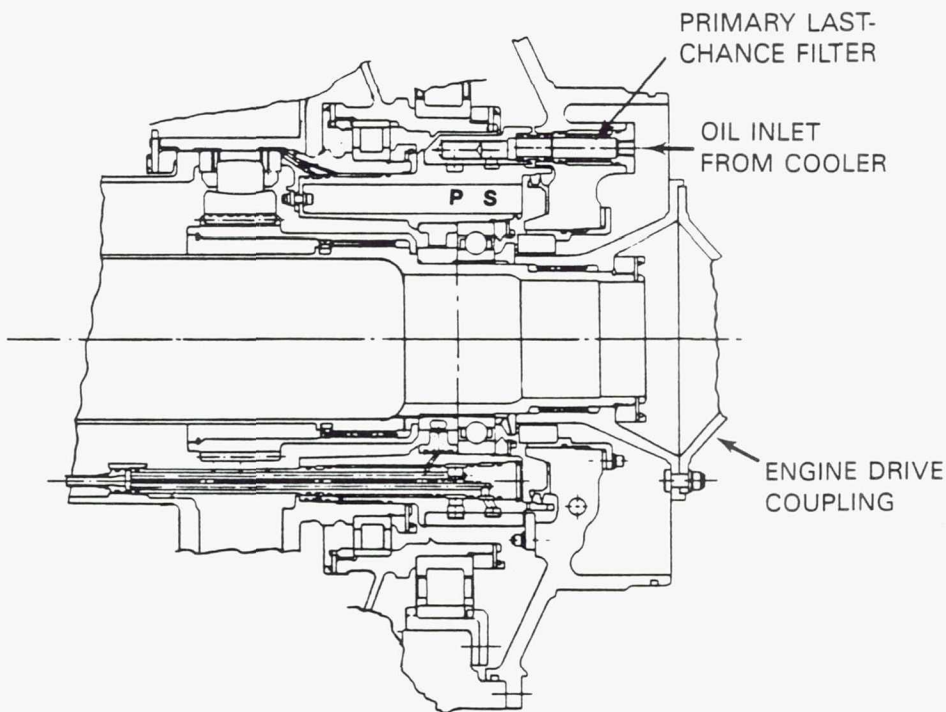


Figure 45 "Last-Chance" Filters Screen Foreign Particles Too Large to Pass Through the Smallest Lubricant Metering Jets

As noted in Section 3.3, one of the features of the lubrication supply system is that it is modulated to recover gearbox efficiency at low power levels; specifically at cruise power. This is illustrated by referring to Figure 46. While gear and bearing friction losses vary linearly with power at constant oil flow, much of the total power loss is due to windage and churning, which are relatively insensitive to input power and are, in fact, the dominant losses at power settings typical of cruise. As noted in the figure, reducing power at constant oil flow results in a degradation of gearbox efficiency, which can be recovered with appropriate oil flow reduction. The modulated flow lubrication system offers this capability and lubrication rig testing (Section 6.0) verified that reduced losses were achievable.

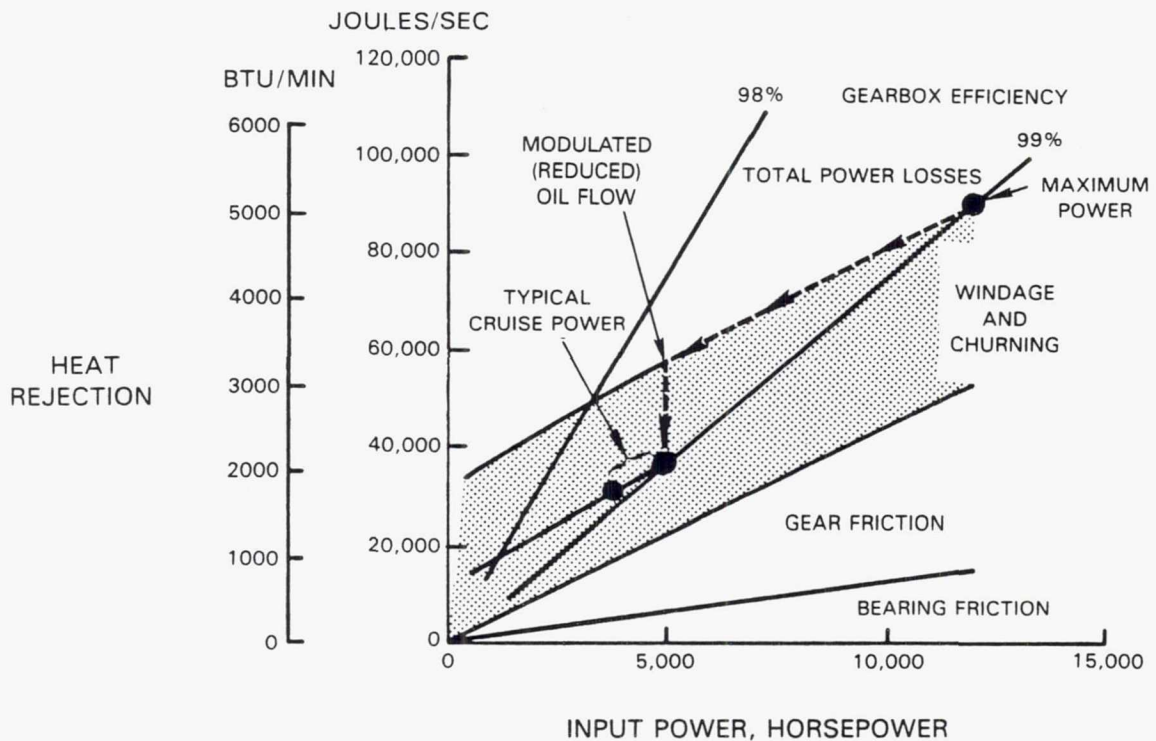


Figure 46 Modulated Lubrication System Provides Recovery of Gearbox Efficiency at Cruise Power

To facilitate modulated lubricant flow in the test gearbox, oil flow exiting the cooler is divided into primary and secondary streams. The primary stream provides lubrication for all the bearings and gear mesh systems. The secondary stream is used only at high power settings (i.e., takeoff) to provide additional cooling for the planetary bearings and the sun/planet gear mesh. Secondary flow in the test gearbox is controlled with a two-position shutoff valve. The valve is designed to fail open and is closed only when gearbox power transmission is at or below cruise level. For a production gearbox, it is conceivable that a control/metering system could be developed to provide modulation over a wide range of power settings.

A major portion of the primary oil supply and all of the secondary oil supply is transferred from stationary flow lines in the housing to rotating passages in the planet gear carrier through the oil transfer unit described in Section 4.5.2.

After passing through the various bearing and gear lubrication sites (see Sections 4.5.3 and 4.5.4), oil is collected by a scroll in the gearbox housing to scavenge. The scavenge collector carries a mixture of air and oil from the interior of the gearbox housing to scavenge pumps. These pumps are sized to accommodate a quantity of air sufficient to promote the scavenge process at critical locations in the gearbox.

The air/oil mixture discharged from the scavenge pumps enters a vortex separator where air is discharged from one outlet and oil from another. Air is returned to the gearbox and oil to the tank. Air entering the gearbox at one end of the planet carrier shaft helps to reduce oil churning around the sun gear.

The vortex separator contains a magnetic chip detector at the oil discharge line for conditioning monitoring. The line is oriented so that dense solid particles are centrifuged toward the detector, increasing its effectiveness.

The oil tank is located close to the gearbox and oriented so that pressure loss to the inlet of the main oil pump is minimal. The hot oil tank arrangement outlined above is commonly used in aircraft engine oil systems.

Gearbox oil temperatures required for this design are higher by 50 to 100 degrees than nominal helicopter experience; peak oil temperatures of 148.9°C (300°F) 176.7°C (350°F) are, however, similar to those in some transport aircraft engine gearboxes. A nominal 55 degree temperature rise was used to set the test gearbox oil supply flow rate. This resulted in a flow rate that was conservatively high to ensure adequate gearbox lubrication during testing. Since gear train churning and windage losses are directly proportional to oil flow rate, the test gearbox would expect to incur a slight efficiency penalty. Further development should permit higher temperature rise (i.e., lower oil flows) with a reduction in churning and windage losses, leading to increased gearbox efficiency.

#### 4.5.2 Oil Transfer Unit

The purpose of the oil transfer unit, illustrated in Figure 47, is to transfer high pressure oil from a stationary source to rotating parts, with minimum leakage at the interfaces, so that required lubricant flows and pressures can be maintained. The principal elements of the unit, as shown, are the stationary transfer sleeve, with its primary and secondary oil supply ports, the rotating oil distribution cylinders and their support housing, and the rotating oil jet nozzle mounted on the support housing. The stationary transfer sleeve receives high pressure oil from the "last-chance" filter, which is supplied from flow passages in the gearbox housing. The transfer sleeve is fitted as closely as possible to the rotating oil distribution cylinder support housing which is, in turn, tied to the carrier shaft. The combination of high pressure oil and high relative part velocities at the sleeve-support housing interface raised the concern that a conventional piston ring seal arrangement would generate too much friction and induce high temperatures and excessive wear. Consequently, a journal bearing design approach with controlled clearances was selected and is illustrated in Figure 48. This approach is not new to Pratt & Whitney, but oil pressures are much higher than previous experience, which places this application in the advanced technology regime. Recent company-funded rig tests using high pressure oil have verified the concept, but additional development work is required before committing to a product design. The sleeve is designed to accommodate small displacements in the support housing that may occur during gearbox operation.

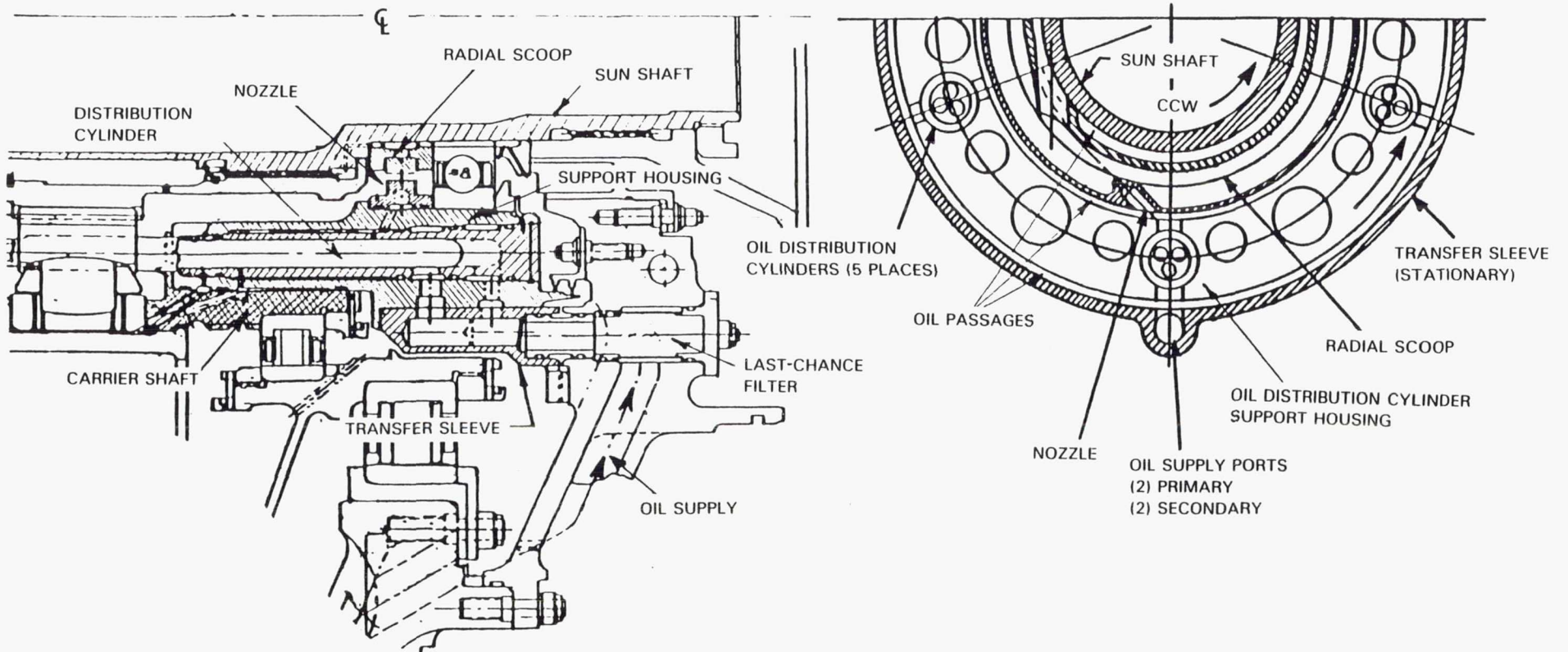


Figure 47 Oil Transfer Unit - Transfers high pressure oil from a stationary source to rotating parts.

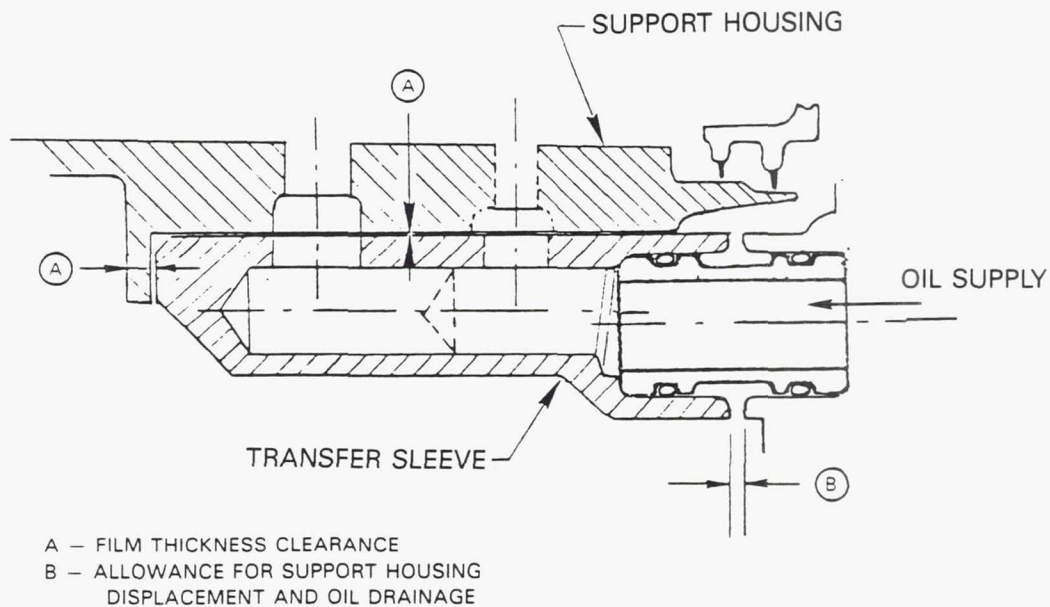
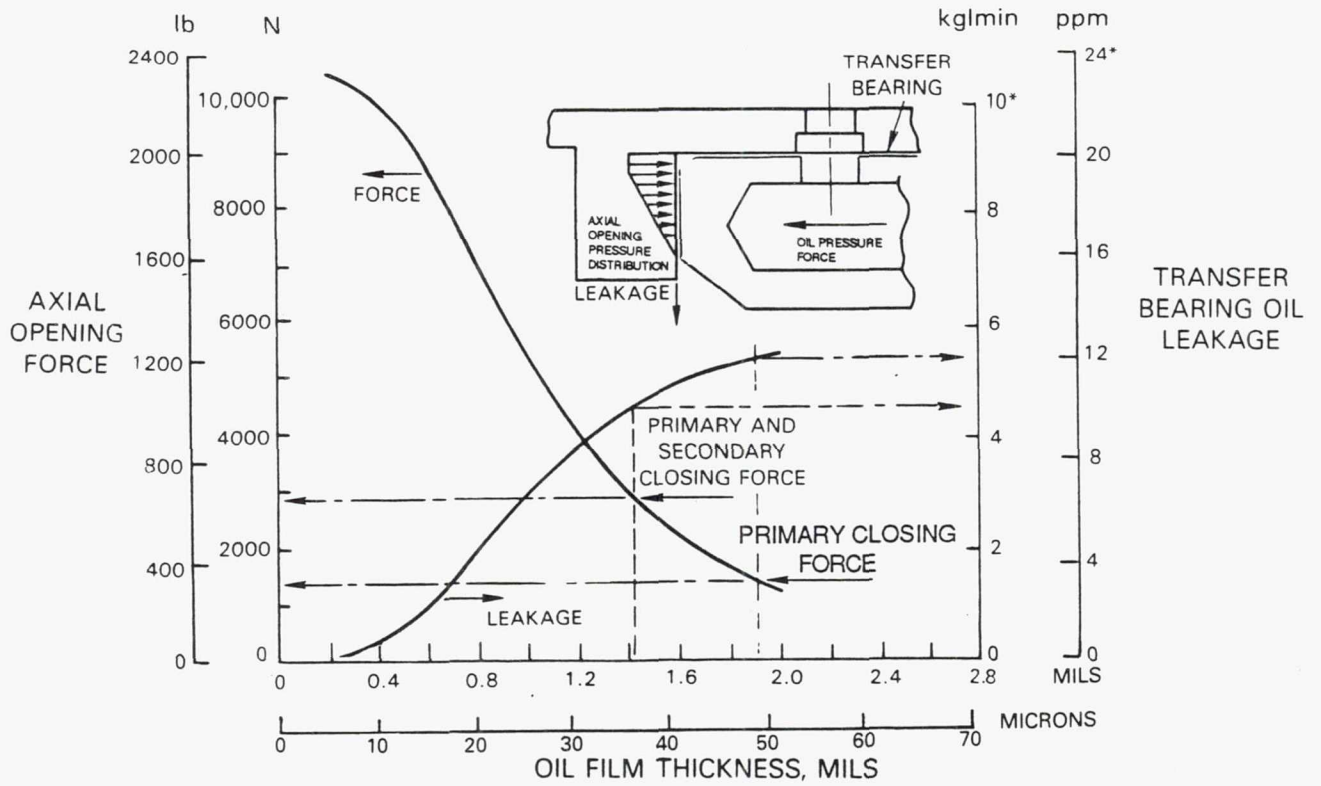


Figure 48 Journal Bearing Design Approach Selected for Oil Transfer Unit - Effectively controls friction at transfer sleeve-support housing interface.

Leakage at the sleeve end face is controlled by the force balance resulting from internal oil pressure in the sleeve supply ports being opposed by the external pressure of the oil film in the clearance passage. Clearance passage width (oil film thickness) is inversely proportional to the closing force imposed by the transfer sleeve and leakage is directly proportional to oil film thickness. These relationships, as calculated for the oil transfer unit configuration, are illustrated in Figure 49. Closing force with primary oil flow only results in an oil film thickness of 0.048 mm (1.9 mils) and a leakage rate of 5.44 kg/min (12.0 pounds per minute (ppm)). Adding secondary oil flow increases the closing force such that oil film thickness is reduced to 0.036 mm (1.4 mils) and leakage is reduced to 4.54 kg/min (10.0 ppm). These leakage rates are sufficiently low to permit acceptable oil pressures and flows throughout the oil transfer unit, as shown in Figure 50.



NOTE (\*): TOTAL SLEEVE LEAKAGE RATE AT TAKEOFF POWER

Figure 49 Transfer Sleeve Force Balance Results In Acceptable Oil Leakage Rates

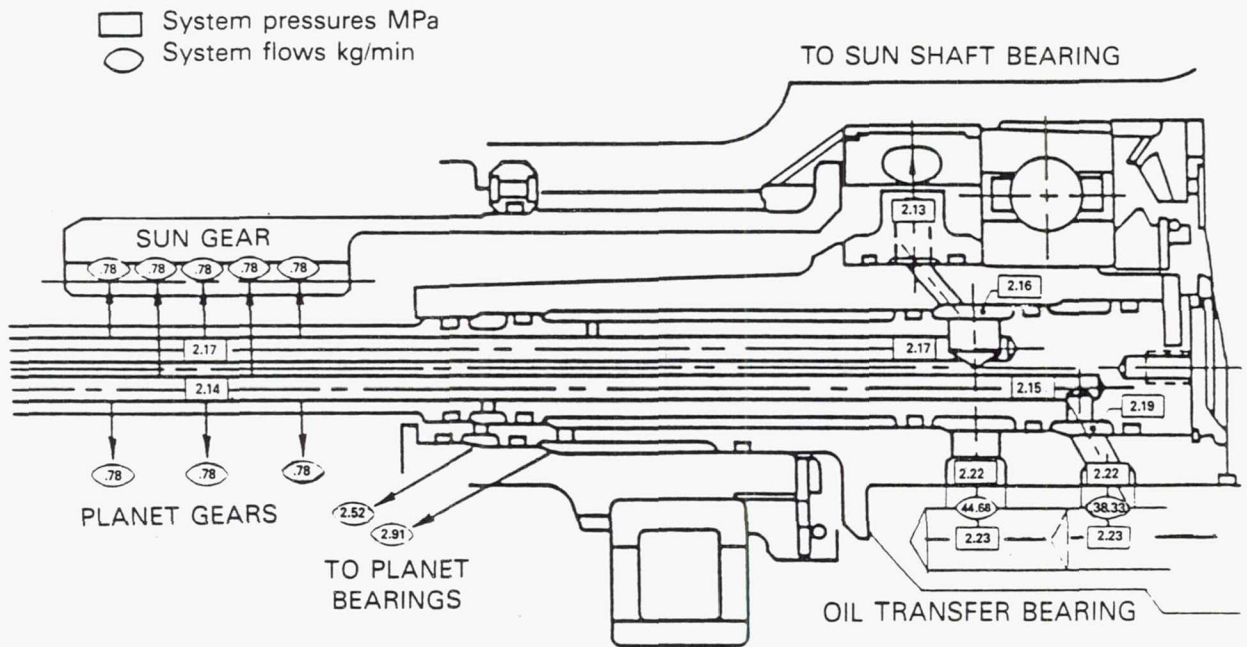


Figure 50 Distribution of Oil Transfer Unit Flows and Pressures - All are acceptable.

### 4.5.3 Bearing Lubrication

The bearings that must be serviced by lubricant flow are shown in Figure 51. Lubricant for the number 1, 5, 6, 7 and 8 bearings is supplied via the oil transfer unit, (which, in a production gearbox, would also provide pressurized oil to the propfan pitch control mechanism) through the rotating oil distribution tubes, as indicated in Figure 52. Figures 53(a) and (b) show the details of the oil supply system feeding the number 5, 6, 7 and 8 bearings. All of this oil passes through the primary "last-chance" filter and is distributed by appropriate passages in the rotating oil distribution cylinders incorporated in the oil transfer unit. Lubrication system design for the number 7 and number 8 (sun shaft) bearings follows normal jet engine practice of using oil jets aimed at rotating scoops, which deliver oil to the inner races of the bearings. Distribution to the bearing surface is through multiple axial grooves. The oil jets are designed to be accessible from the outside for ease of maintenance.

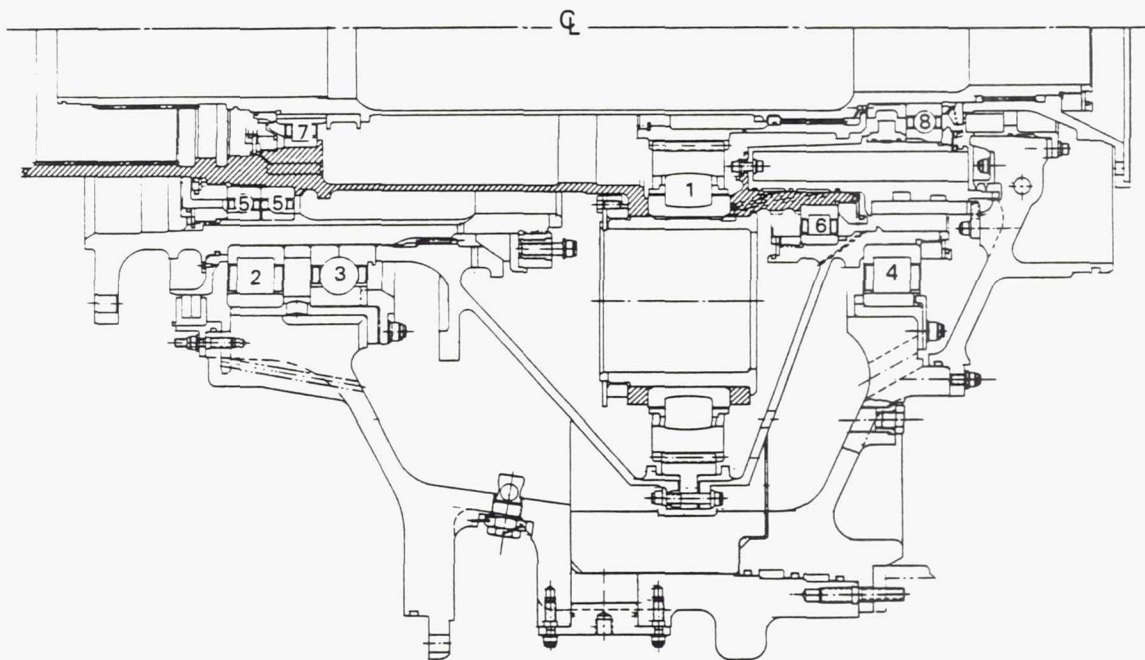


Figure 51 Bearings and Bearing Locations Serviced by the Lubricant Supply System

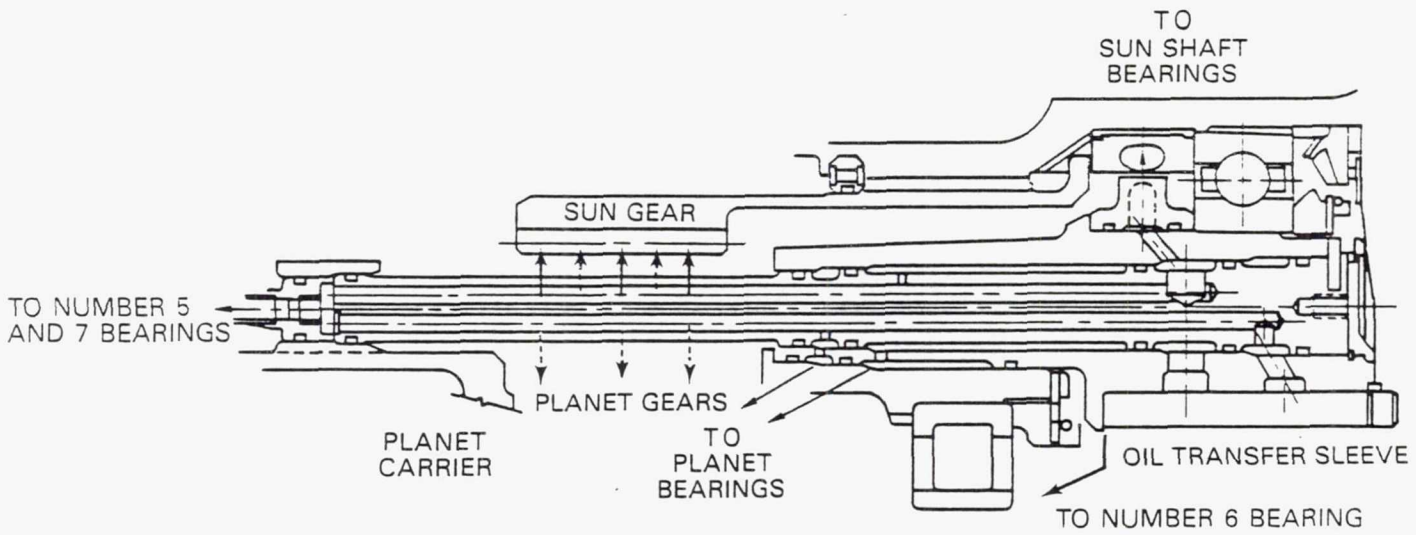


Figure 52 Lubricant Distribution Through Oil Transfer Unit

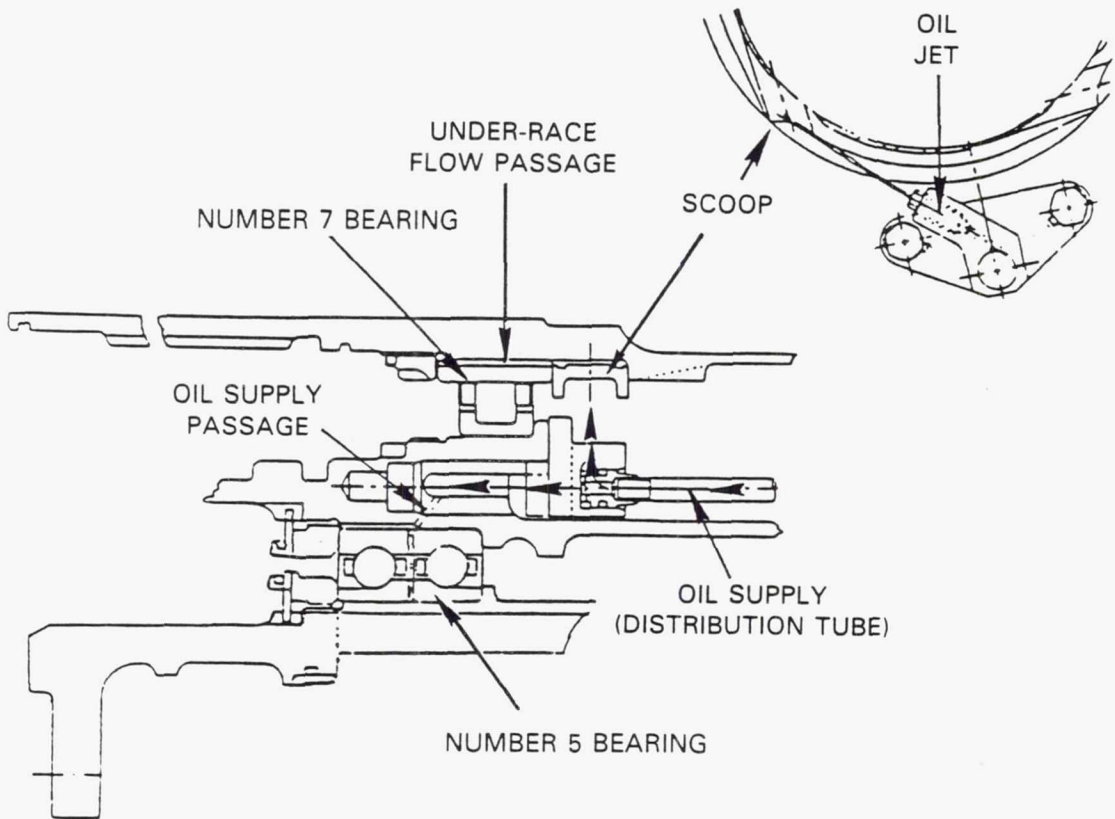


Figure 53(a)

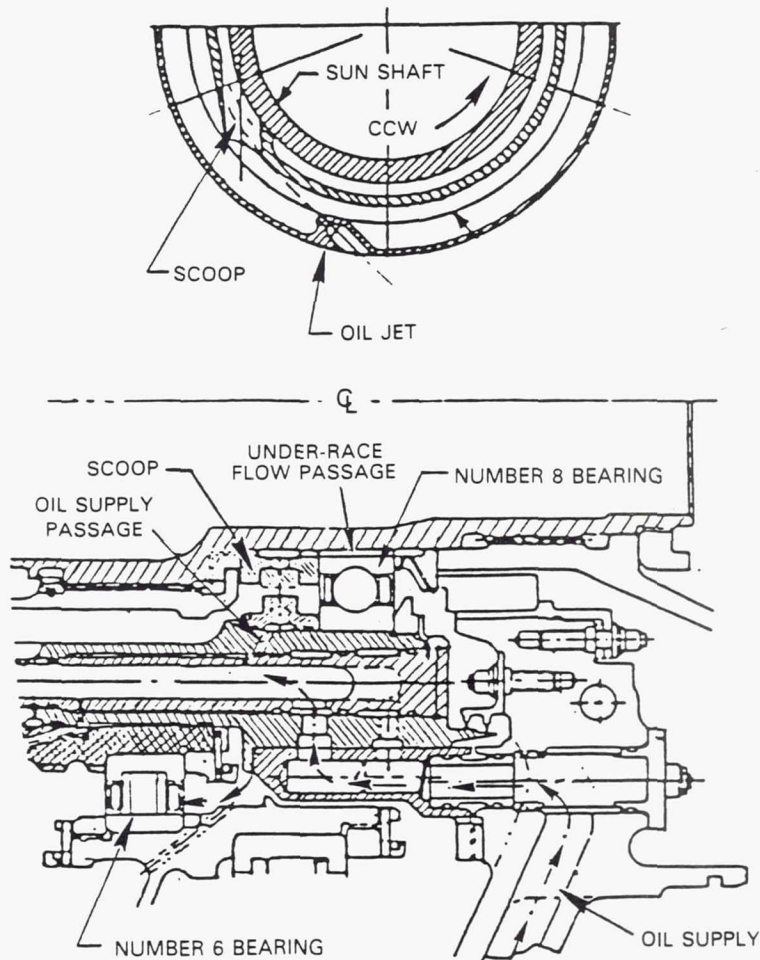


Figure 53(b)

Figure 53 Lubrication Schemes for the Number 5, 6, 7 and 8 Bearings

Oil to the number 5 bearing is also supplied by the rotating distribution tube to the bearing inner race as illustrated in Figure 53(a). Oil leakage at the interface between the transfer sleeve and support housing provides the lubricant for the number 6 bearing, as shown in Figure 53(b).

The number 2, 3 and 4 prop shaft bearings are lubricated by jets mounted externally on the gearbox housing and fed by flow passages integral in the housing. These jets are illustrated in Figure 54 and their mount locations are shown in Figure 16. A single jet, mounted on the engine-side housing, supplies lubricant to the number 4 bearing, whereas two jets, mounted 180 degrees apart on the prop-side housing, supply lubricant to the number 2 and 3 bearings. No "last-chance" filters are currently included in the supply lines for these bearings, but these filters could be added if circumstances and test experience dictate a requirement. External mounting of the jets facilitates

ease of maintenance. Figure 55 summarizes the calculated lubricant flows and bearing temperatures at the locations just discussed for an oil-in temperature of 121.1°C (250°F). Bearing lubrication is adequate and temperature rise is moderate.

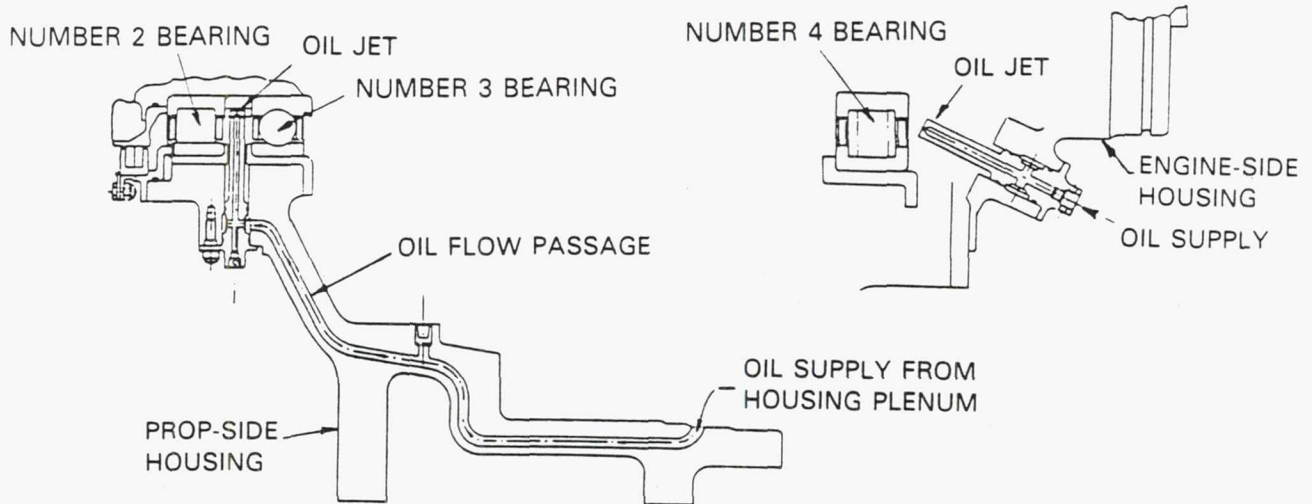


Figure 54 Lubrication Schemes for the Number 2, 3 and 4 Bearings

Lubrication of the planet (number 1) bearings requires special design considerations relative to helicopter practice. The helicopter planet carrier output speed is nominally 250 RPM whereas in the AGBT gearbox it rotates at 1235 RPM. This produces significantly higher centrifugal forces, since these forces are proportional to the square of the carrier speed. Features to ensure proper lubrication of the bearings were therefore introduced. Figure 56 illustrates the lubrication scheme for the planet bearing. High pressure oil from the transfer unit rotating distribution tube is guided to passages under the inner race where it is subsequently distributed to the case and roller interfaces as shown. This distribution system permits tailoring the design to counteract the natural effect of the "g" field to throw oil to the farthest region while starving other locations. Oil holes are located circumferentially to ensure even flow distribution to the loaded regions of the interfaces noted. Oil metering holes were designed to provide adequate film distribution.

ORIGINAL PAGE IS  
OF POOR QUALITY

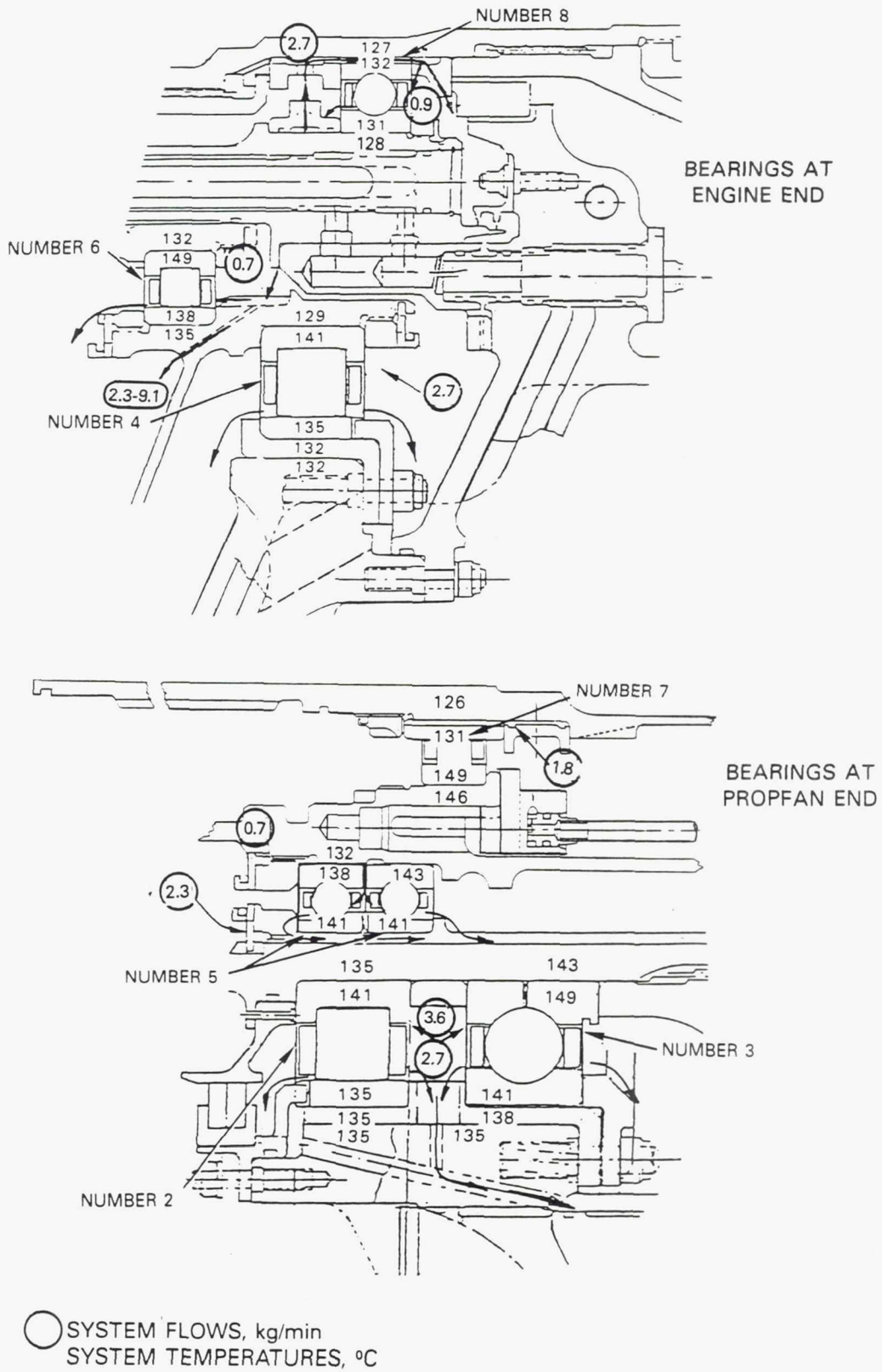


Figure 55 Summary of Bearing Oil Flows and Temperatures - Positive bearing lubrication is provided and temperature rise is acceptable.

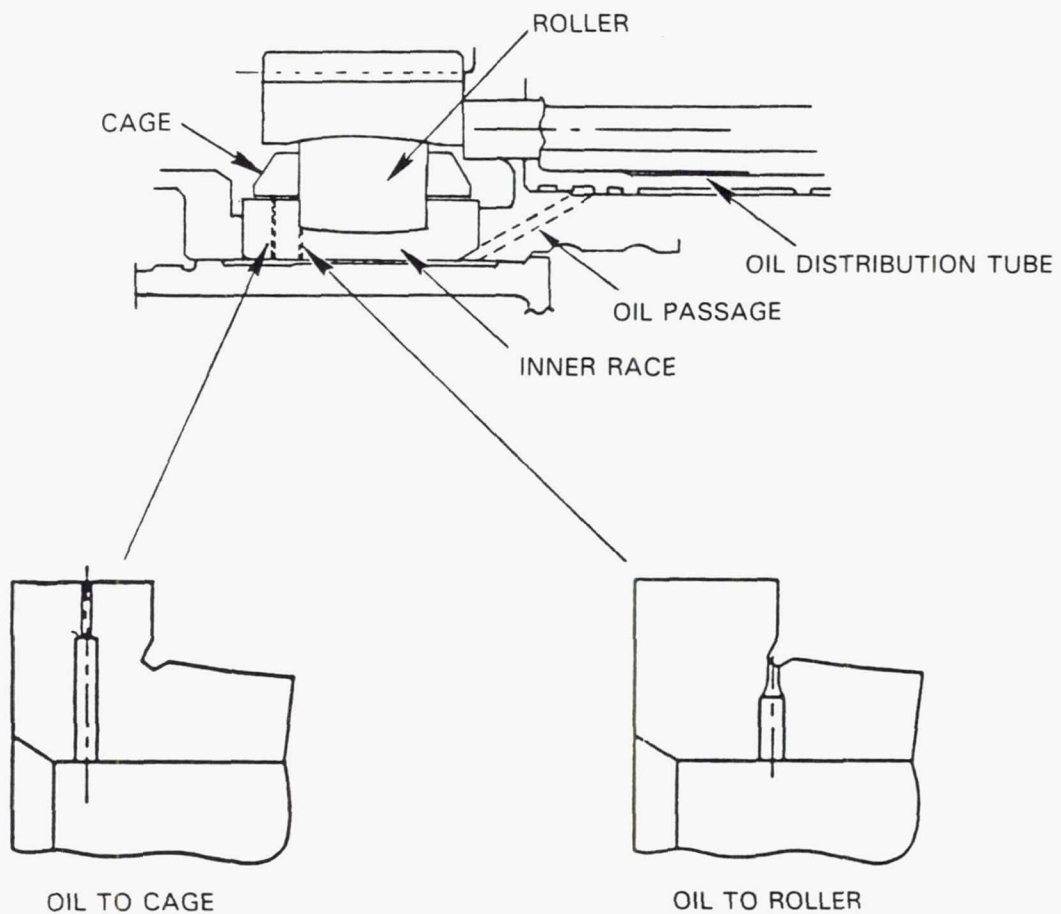


Figure 56 Number 1 (Planet) Bearing Lubrication Scheme

#### 4.5.4 Gear Mesh Lubrication

The design objectives for the gear mesh lubrication system were to (1) ensure positive oil flow penetration into the gear mesh and (2) optimize oil jet size to prevent blockage while maintaining an acceptable spray pattern. The principal parameters controlling adequate penetration are jet angle into the mesh, oil pressure, jet nozzle hole size and jet velocity. Oil supply to the gear mesh is based on the modulated system described in Section 4.5.1 and distribution is through spray bars incorporated into the rotating distribution cylinders mounted in the oil transfer unit. Figure 57 illustrates the flow passages and shows that three primary jets and two secondary jets are aimed at the sun gear with three secondary jets only aimed at the planet gears. Figure 58 illustrates the initial gear tooth impingement pattern established for the jets.

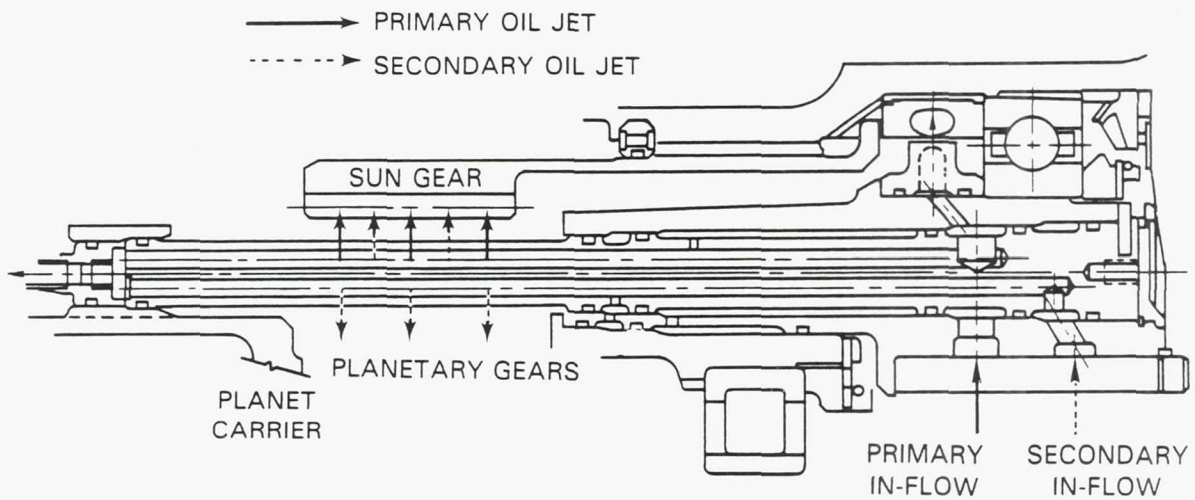


Figure 57 Oil Distribution System for the Sun and Planet Gear Meshes - Primary and secondary jets provide modulated flow capability.

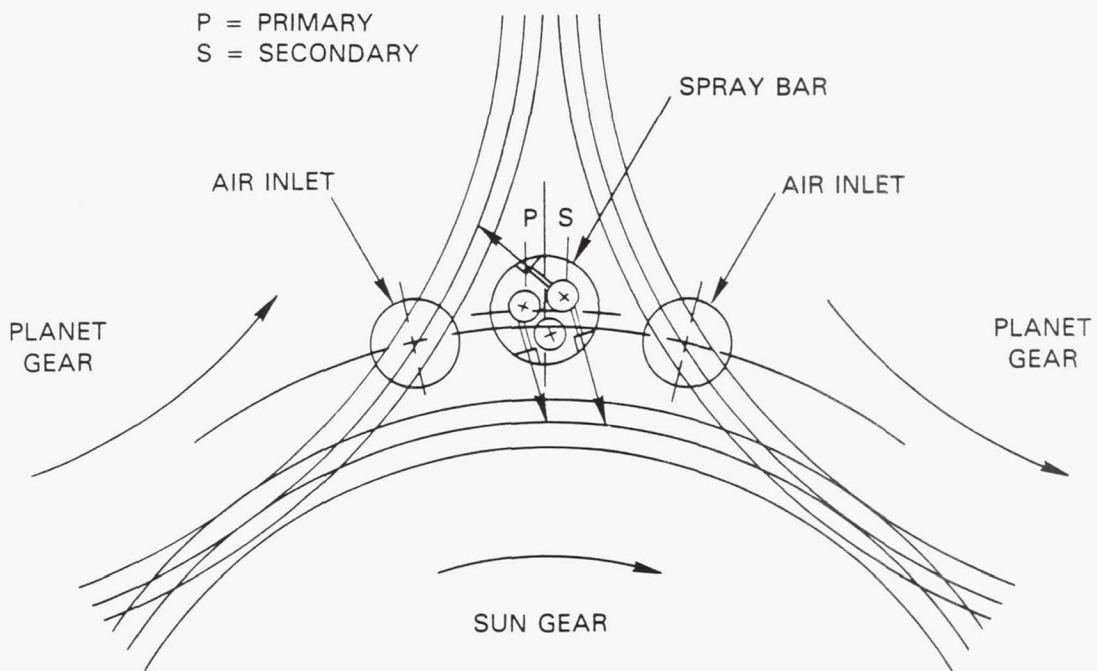


Figure 58 Initial Oil Spray Pattern Into Gear Meshes - Testing may lead to a more optimum pattern.

C-2

An extensive review of the literature was conducted prior to arriving at the lubrication and cooling design for the gear mesh. The work of Akin and Townsend (Reference 2) was particularly valuable in establishing the effectiveness of high velocity, radial oil jets, to relieve gear tooth hot spots. This information, in conjunction with Pratt & Whitney experience, was used to establish the number and location of the primary and secondary oil jets. Jet diameter (hole size) was designed to provide 60% oil spray impingement depth for tooth scoring prevention. Initial calculations indicated a minimum jet diameter of 0.58 mm (23 mils) (see Figure 50) would provide the necessary impingement depth with a 2.068 MPa (300 psig) supply pressure. Subsequent jet nozzle flow calibrations in the lube rig program (Section 6.0) indicated that a 0.64 mm (25 mil) hole size was more suitable. The use of 0.64 mm (25 mil) holes places a priority on design features to prevent plugging of the holes. Four features combine in meeting this requirement; (1) "last-chance" filtration screens of 0.51 mm (20 mils) mesh size in addition to conventional oil filters located in the main oil supply and scavenging passages, (2) 2.068 MPa (300 psi) oil supply pressure which not only inhibits hole plugging but improves the efficiency of spray distribution, (3) multiple holes, reducing the likelihood of oil starvation even if some plugging were to occur and (4) independent (from the engine) oil supply system which eliminates a source of potential contamination and also allows for the use of special lubricants. The multiple hole approach allows for some redundancy should clogging occur. In addition, the influence of the carrier rotational centrifugal field on the spray bar would tend to centrifuge any debris away from the entrance to the primary jets and to allow that debris to be flushed past the jets by the continuing axial oil velocity along the spray bar oil passage. If necessary, the secondary jet could be modified as shown in Figure 59 to further reduce the chance of this set of jets being plugged by debris that might escape the "last-chance" filters. No specific design features were incorporated into the test gearbox condition monitoring system to sense indications of clogging. Condition monitoring in a production gearbox could include these parameters should development testing indicate a need.

Flow and thermal analyses of the lubrication system resulted in the distributions of power loss, oil flow and temperature rise shown in Table 22 at takeoff power conditions; resulting in a gearbox efficiency of 99.06% for a fully-developed gearbox. These results should be compared to those in Table 7, Section 4.2.1, which include power loss adjustments for the test gearbox based on the results of the lube rig testing described in Section 6.0. Significant power loss reductions and efficiency improvements are expected to be achieved with additional technology development testing of the test gearbox.

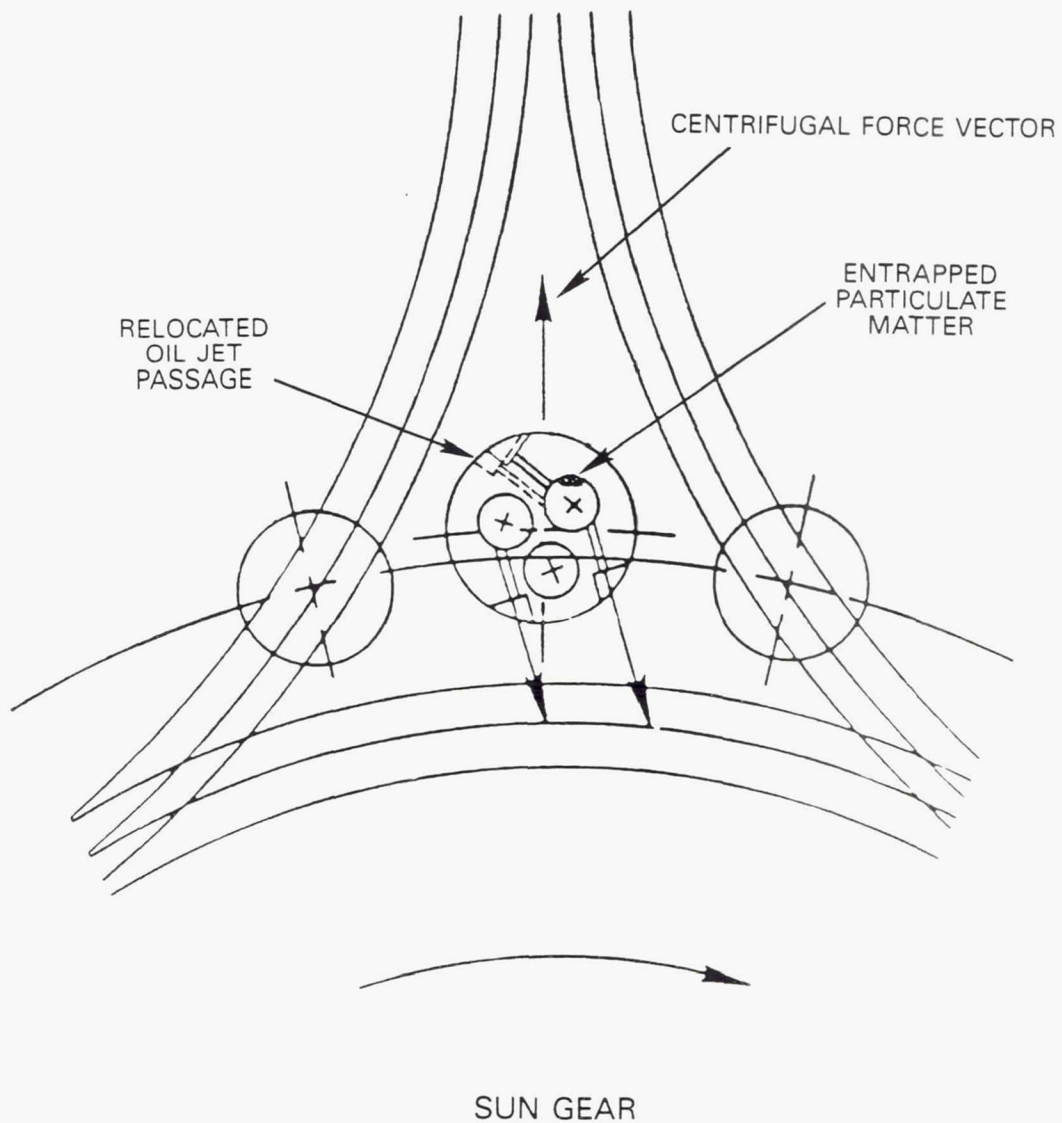


Figure 59 Possible Modification to the Primary Jet Flow Passage - Reduces the risk of plugging from particulate matter entrained in the oil stream.

Table 22 Calculated Power Loss, Oil Flow and Temperature Rise Summary at Takeoff Power Conditions

	Loss, HP	Flow kg/min(ppm)	Temperature Rise, degrees
Gears	49.6	31.3 (69)	58.6
Planet bearings	33.5	27.2 (60)	45.5
Shaft bearings	8.9	17.7 (39)	18.7
Pumps	12.0	---	
Windage	9.0	---	
Transfer bearing leakage	---	10.0 (22)	
Propfan pitch control	---	18.1 (40)	
Gearbox total	113.0	104.3 (230)	40.0

Gearbox efficiency = 99.06%

#### 4.5.5 Scavenging

Scavenge system design was fairly conventional except for oil removal from the sun/planet gear mesh region, which required special design attention. Oil exiting the various bearing locations drains to a collector cartridge inserted at the outer circumference of the prop-side housing, as shown in Figure 60. Cartridge design was based on the results of the scavenge rig tests, described in Section 6.1, which investigated three different collector configurations. Tests results showed that the constant volume collector design had the highest scavenge effectiveness. The collector annulus incorporates flow deflectors, shown in Figure 61, which direct the captured lubricant into flow discharge ports aligned with connecting passages cast in the housing. These passages conduct the lubricant from the scavenge cartridge through the magnetic chip detector and into the scavenge pumps. (The housing also incorporates integral flow passages that route the oil leaving the pressure side of the scavenge pumps across the gearbox to pipe connections on the engine-side, where the oil is subsequently directed to the air/oil cooler). Provisions for mounting two scavenge pumps are included in the housing. However, for the test gearbox in the test stand, these will be fitted with connectors leading to scavenge pumps mounted remotely on the test facility lube skids.

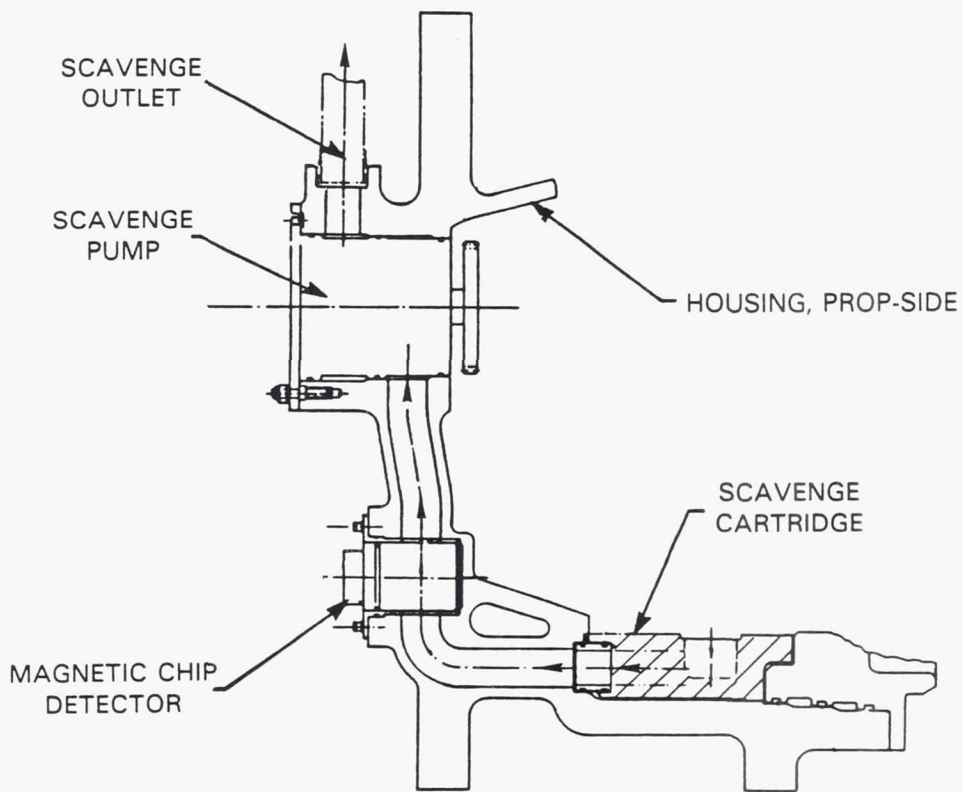


Figure 60 Scavenge System Features - Collector cartridge directs scavenged oil to magnetic chip detector and scavenge pumps.

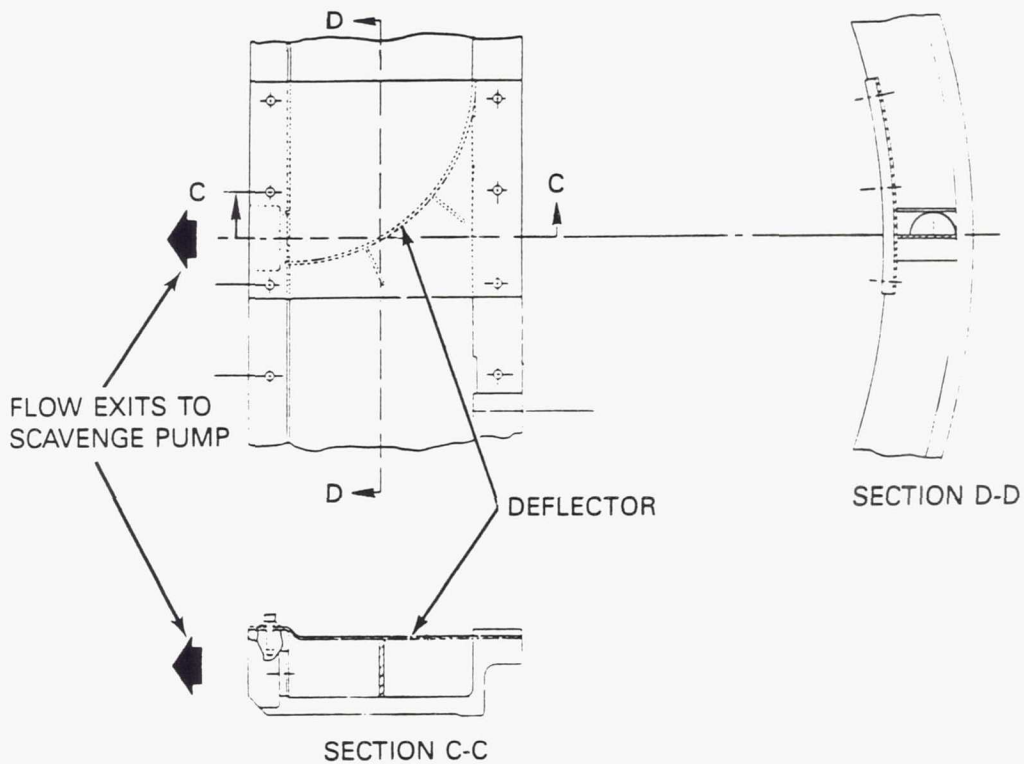


Figure 61 Scavenge Collector Cartridge Details - Deflectors direct captured lubricant into flow discharge ports.

As noted earlier, scavenging of the gear mesh system required special attention. On the one hand, oil flow into the mesh must be sufficient to provide adequate lubrication and cooling; while on the other hand, too much oil flow can result in excessive gear mesh churning losses, hydraulic losses due to oil trapped in the gear tooth root regions and excessive gear train windage losses. The windage losses can be controlled to some degree by the air/oil mixture surrounding the gear train. Consequently, provisions were made to accommodate air injection into the gearbox through the rotating distribution tubes as shown in Figure 62. The technique for injecting air into the gear mesh was investigated in the lube rig tests and found to have little if any affect on scavenge effectiveness; whereas canting the oil jets to provide an axial component to the jet impingement into the tooth mesh showed some improvement in scavenge effectiveness. Variations in the air/oil mixture also showed some reduction in windage losses. Consequently, scavenge pumps used for testing will be positive displacement, variable-speed gear pumps, with the capacity to scavenge air/oil mixture ratios in the range of 2:1 to 4:1 to enable selection of the optimum air/oil mixture.

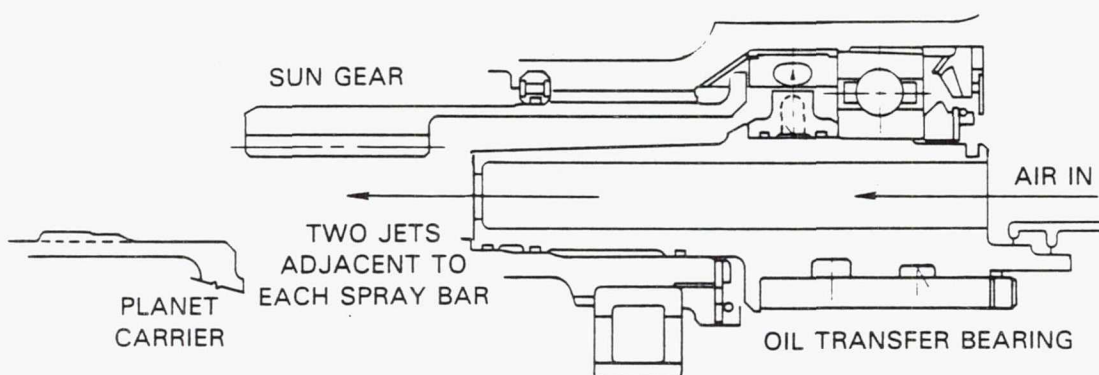


Figure 62 Scheme for Injecting Air Into the Gear Mesh - Tests showed that this had little or no effect on scavenge effectiveness.

Oil exiting the gear mesh and the number 1, 5 and 6 bearings is centrifuged along the inside walls of the front and rear ring gear housings and slung out through grooved channels in the housing outer flanges into the scavenge collector as shown in Figure 63. The effectiveness of the entire scavenge system will be monitored during the gearbox test program to identify areas where improvements may be necessary.

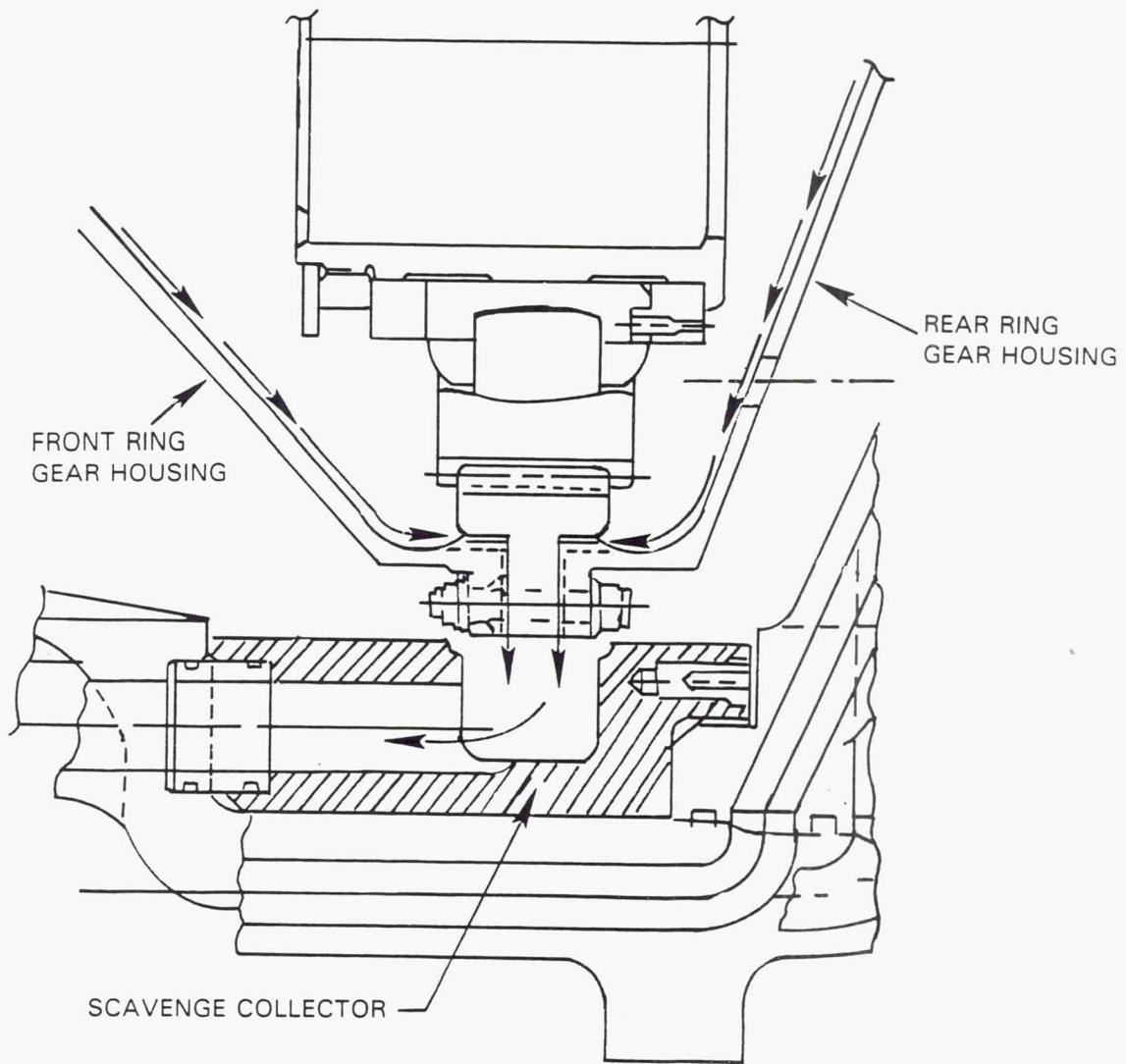
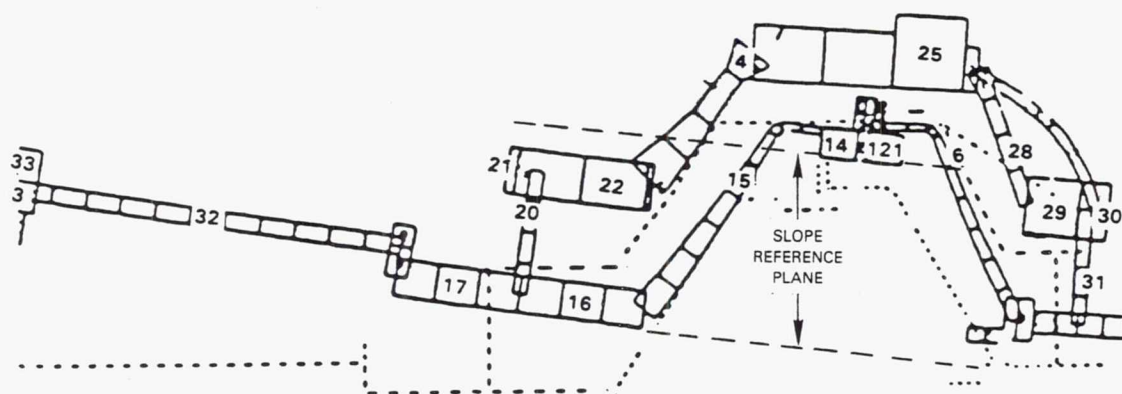


Figure 63 Scavenge Route for Oil Exiting the Gear Mesh and Number 1, 5 and 6 Bearings

#### 4.6 Shafts and Housing

During the gearbox concept studies, a structural analysis was completed on both the housing and propfan shaft of the straddle-mounted configuration to ensure control of gear mesh misalignment, minimal slope at major bearing locations and structural integrity of both shaft and housing at maximum operating load conditions. Loads considered were nominal 1.5G propeller shear and 1P pitching moment loads of 26,689 N (6000 lb), 17,083 Nm (12,600 ft-lb) gyro moment from a steady-state basis, and the loss of a single propfan blade shell and fill. Figure 64 summarizes the various load conditions and their impact on both gear mesh and bearing slopes.



$\Delta$ SLOPE-FORWARD BEARING (RAD) 0.038 cm (0.015 in)				RING GEAR		MAX HOUSING BENDING STRESS - MPa (psi)		MAX SHAFT BENDING STRESS - MPa (psi)	
LOADING	(Defl)	(Rc)	(Total)	Slope (Rad)	Defl cm (in)	Actual	Allowable	Actual	Allowable
1.5 + 1P 2721.6 Kg (6,000 lb)	0.0009	0.0009	0.00181	0.0	0.00132 (0.00052)	8.27 (1,200)	N/A	65.3 (9,470)	N/A
GYRO MOMENT 17,083.3 Nm (12,600 ft-lb)	N/A	N/A	N/A	N/A	N/A	29.7 (4,308)	N/A	206.8 (30,000)	206.8-275.8 (30-40,000)
SHELL AND FILL BLADE LOSS 9480.1 kg (20,900 lb)	N/A	N/A	N/A	N/A	N/A	42.1 (6,100)	68.9 (10,000)	332.7 (48,260)	1103.2 (160,000)

Figure 64 Deflection and Stress Analysis - The design meets structural requirements.

Several iterations were made in sizing both front and rear ring gear hubs in order to minimize prop shaft deflections. Hub stiffness was the key in controlling the slope and deflection at the ring gear; and by optimizing hub angle and wall thickness, an acceptable deflection was obtained.

A nominal load of 1.5G propeller shear plus 1P pitching moment generated a slope of 0.0009 at the forward prop shaft bearing locations. The bearing internal radial clearance created an additional slope of 0.0009. The combined total of 0.0018 is still within the acceptable level of 0.004 that bearing analyses and proven bearing experience recommend. The slope generated at the ring gear is essentially zero with reference to the mating planet gear, but the radial deflection eccentricity of 0.00132 cm (0.00052 in) is significant in that design for additional ring gear flexibility may be required to maintain load sharing among the planet gears.

The steady-state gyro moment generates a cyclic load on the prop shaft, which calculations show to be within the objective life limitations. Once per flight type loads (limit case) and major blade failure (ultimate case), in which the blade shell and filler are lost, impact both housing and shaft design. For the ultimate case, the loss of blade shell and fill, the goal is to prevent

complete destruction of the support system. This type of failure imposes a cyclic load on the housing. An 8 minute shutdown period was used as a criterion to establish life limitations for the housing. This is equivalent to 1000 cycles or a 68.9 MPa (10,000 psi) stress limitation. Calculated housing stress is 42.1 MPa (6100 psi) under blade shell and fill loss. This preliminary structural analysis indicated that severe loads imposed on the support shafts could be controlled and the deflections at the support bearings and at the gear mesh location held to acceptable levels. Having satisfied these conditions, detail design of the shafting and housing was initiated and these efforts are discussed in the following sections.

#### 4.6.1 Shafts Design

The shaft system is designed to meet three objectives: (1) to ensure structural integrity of the gear system under maximum maneuver loads and propeller blade loads, (2) to ensure that joints are free from any fretting caused by relative motion and (3) to control deflections so that bearing and gear durability is maintained. Loads imposed on the shaft system include the nominal 1.5G propeller shear and 1P pitching moment loads, a 3.2G shear load and one radian per second gyro moment load caused by a maximum maneuver, torque transfer from the engine to the propeller and blade loss imbalance loads.

The shaft system conceptual design was subjected to finite element analysis of the propeller shaft, the carrier shaft and the sun shaft. Propeller shaft analysis included the propfan mount flange and the prop shaft to ring gear connection. In addition, a pre-load analysis was conducted on each of the bearing retaining nuts. These analyses are discussed in the following sections.

##### 4.6.1.1 Propeller Shaft Analysis

The propeller shaft finite element model is shown in Figure 65. This model includes the flange where the propeller module is bolted to the gearbox, the torque tube that transfers the propeller loads to the support bearing and the cone-shaped prop-side and engine-side ring gear support shafts. Loads considered in the analysis were as described in Section 4.6-1. The criteria for life is essentially infinite life, namely greater than  $10^{10}$  cycles under normal loading conditions. The maximum maneuver loading condition rarely occurs during flight and the requirement is to maintain at least  $10^4$  cycles life in the shafting under this condition. The full gyro load for a single propeller stage was used despite the fact that with counter rotating propellers, the gyro loads counteract each other, resulting in a net load of zero at the connection to the gearbox. This is consistent with design practice and enhances shaft life with very little weight increase. The requirement for blade and shell loss was a life of 1000 cycles to insure that under this extreme imbalance condition the part would have some life margin.

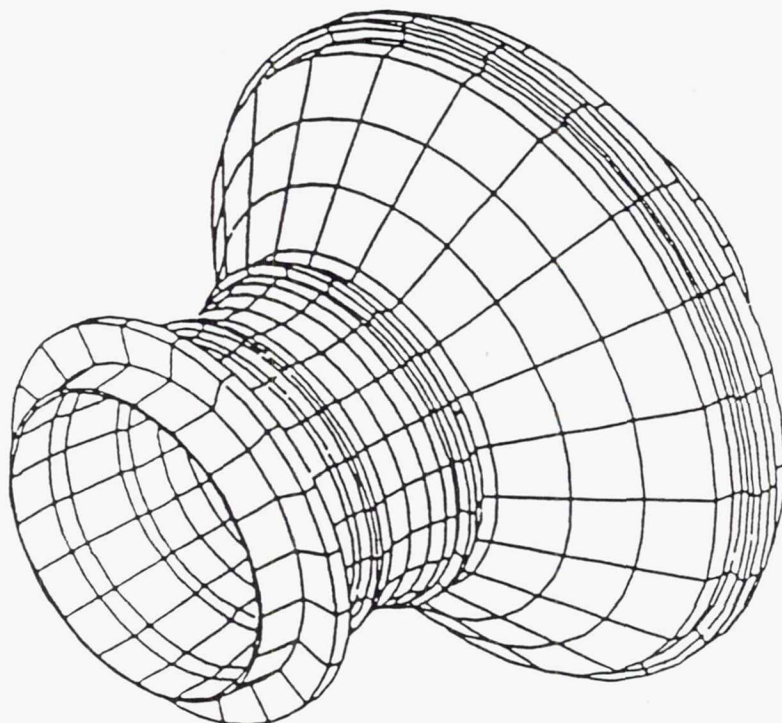
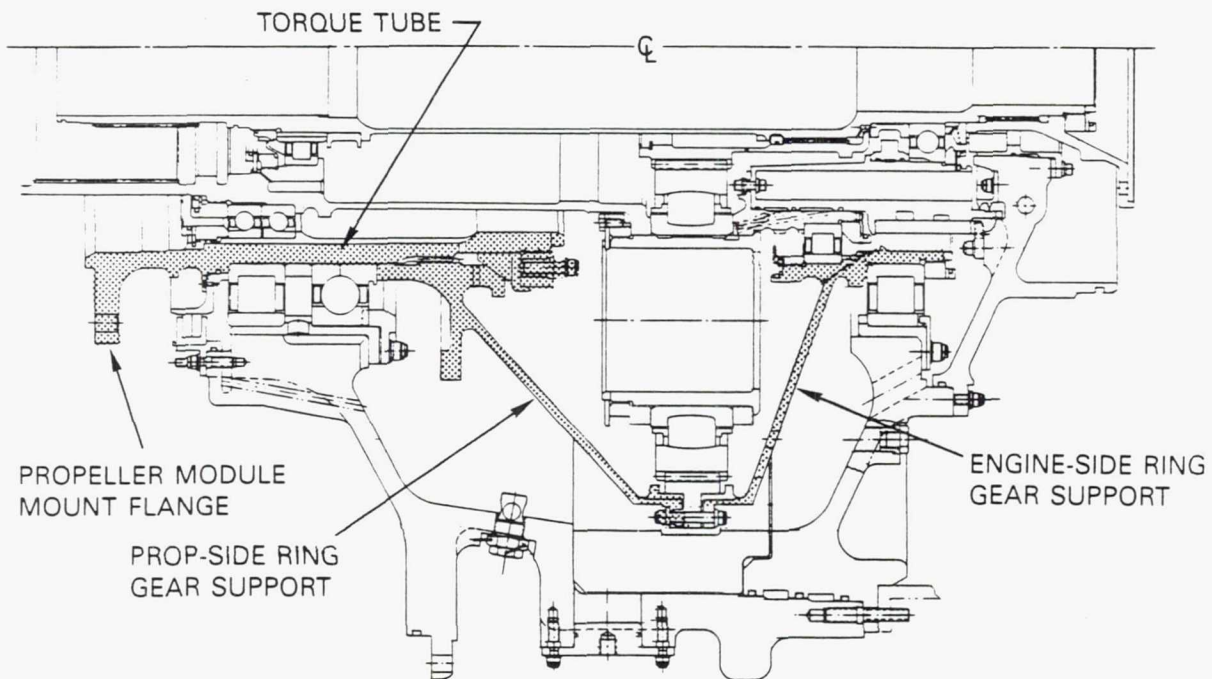


Figure 65 Propeller Shaft Finite Element Model

ORIGINAL PAGE IS  
OF POOR QUALITY

## Torque Tube Analysis

Figures 66 and 67 summarize the results of the finite element analysis at various critical locations on the prop shaft torque tube. As can be seen, all the stresses fall within the acceptable range, and acceptable part life is achieved.

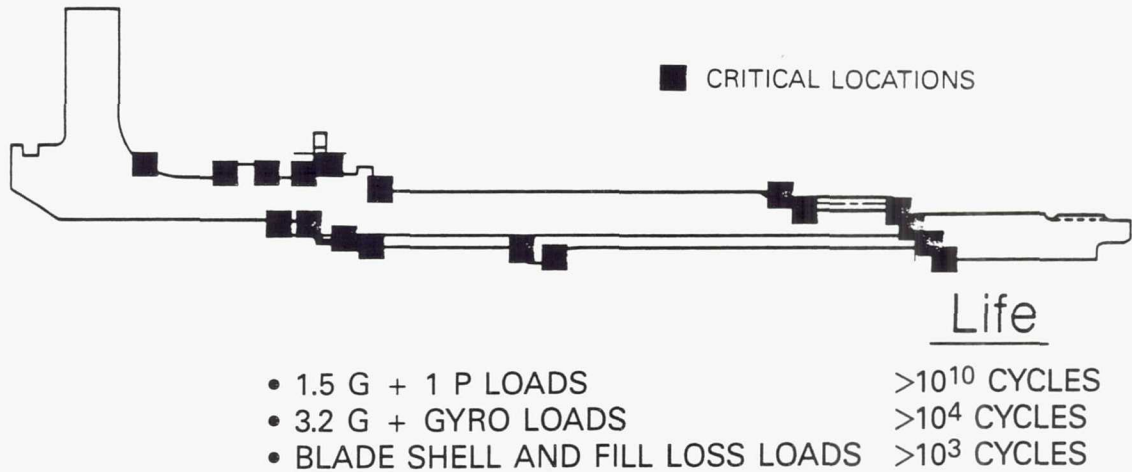


Figure 66 Torque Tube Cyclic Fatigue Results

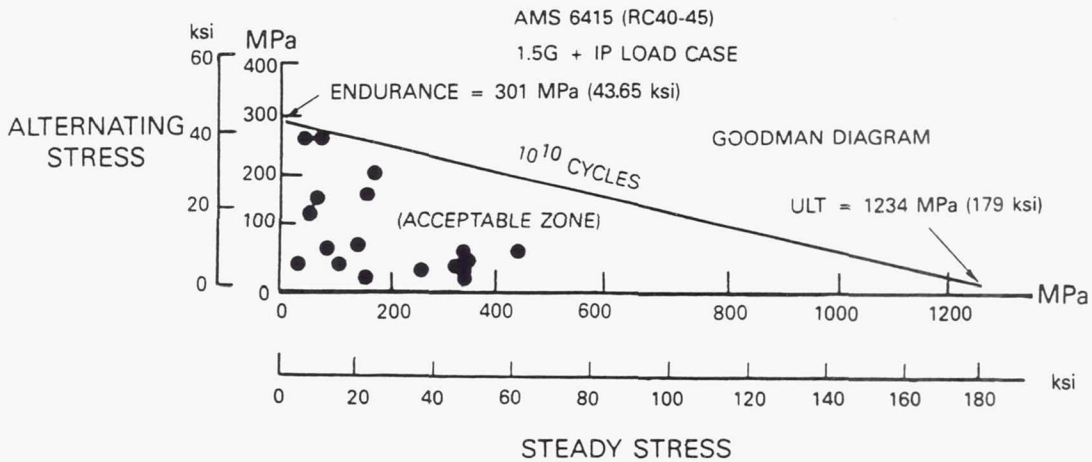


Figure 67 Torque Tube Stress Analysis Results

## Mount Flange Analysis

The prop mount flange is shown in Figure 68. The propeller module is connected to the gearbox with 32 bolts located circumferentially around this flange. In addition to the 32 bolts, 4 locating dowels provide additional alignment accuracy in connecting the propeller module to the gearbox. These dowels are equally spaced at 4 circumferential locations around the flange. Figure 69 summarizes the results of the finite element analysis of this flange at the nominal operating loads of 1.5G propeller shear combined with 1P pitching moment. Calculated bolt stresses are very low relative to the run out fatigue strength of the bolts. The bolts were also analyzed under the maximum maneuver and blade loss conditions. Results of these analyses are presented in Figure 70. Calculated stress levels were again very low for the maximum maneuver load condition and stress levels under blade shell loss imbalance loads result in part life that exceeds the  $10^4$  cycle requirement, indicating that this flange connection should be essentially fail-safe under the most extreme conditions.

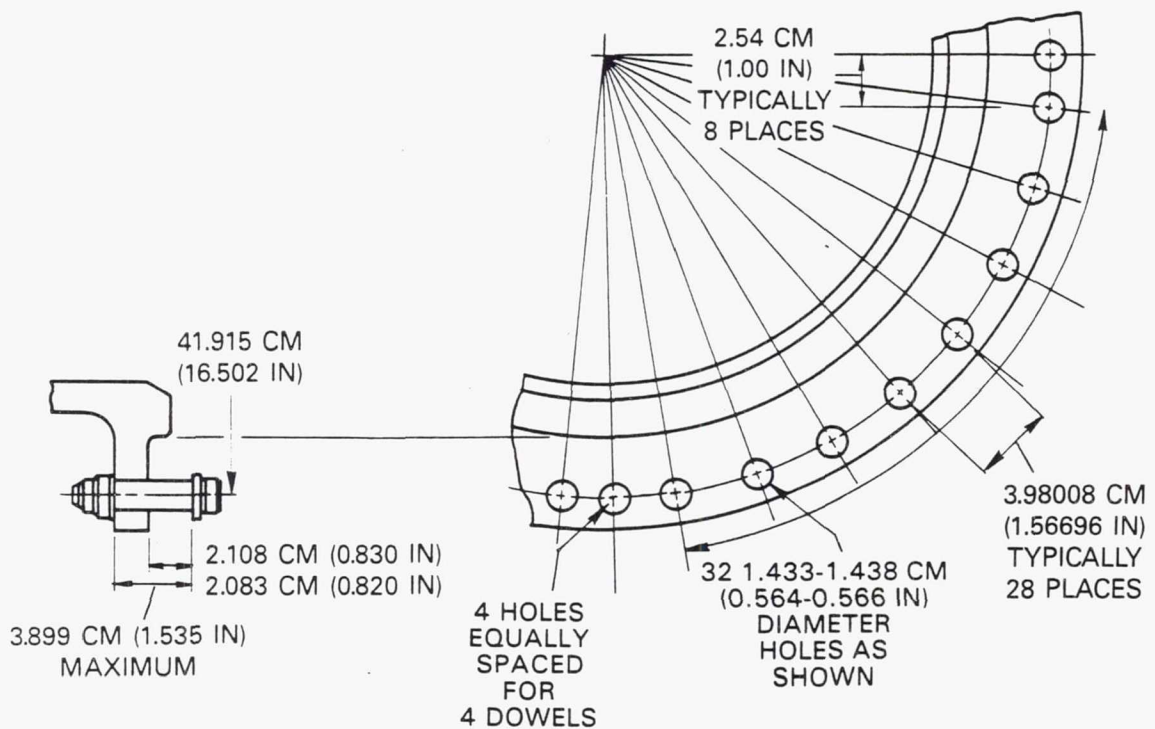


Figure 68 Prop Mount Flange Details

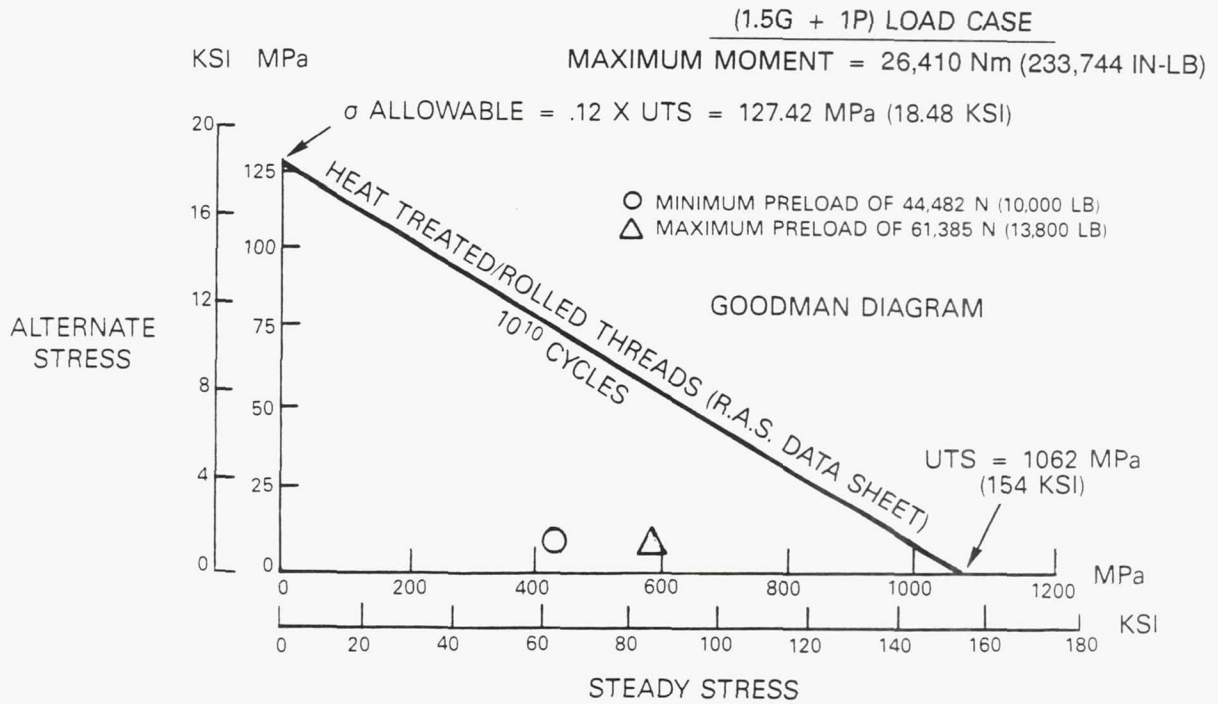


Figure 69 Mount Flange Stress Analysis Results at Nominal Operating Conditions Are Well Within Allowable Limits

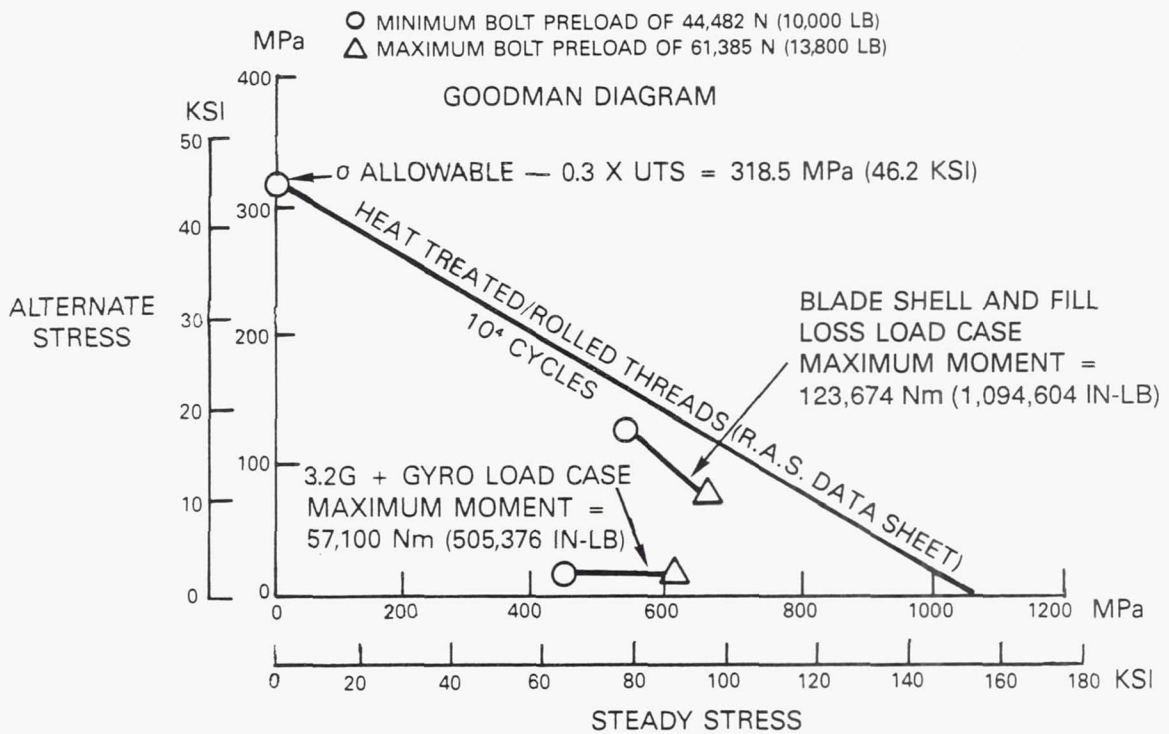


Figure 70 Mount Flange Stress Analysis Results at Maximum Maneuver and Blade Loss Conditions - Bolt stresses are within allowable limits.

## Prop Shaft to Ring Gear Connection Analysis

The connection between the prop shaft torque tube and the prop-side ring gear support shaft is shown in Figure 71. This interface was analyzed to ensure acceptable cyclic slip levels, cyclic stresses and contact stresses at the five critical locations shown in the figure. Finite element analysis results are presented in Figures 72 and 73. Figure 72 shows that acceptable cyclic slip could be achieved at the rear connection cone. Efforts to use a cone at the front end of the ring gear support cone were not successful, since cyclic slip was excessive at this location. The final design, therefore, used a cylindrical snap at the front location (see Figure 71), which resulted in acceptable cyclic slip. Results of the cyclic stress and contact stress analyses are shown in Figure 73 and indicate acceptable levels. The finite element analysis model for the prop shaft torque tube and ring gear support cones was also used to evaluate deflections at the prop shaft front and rear support bearing locations as well as at the ring gear mesh location. Results of this analysis are shown in Figure 74 and indicate that the deflection at the ring gear and the slope at the support bearings are consistent with allowable levels.

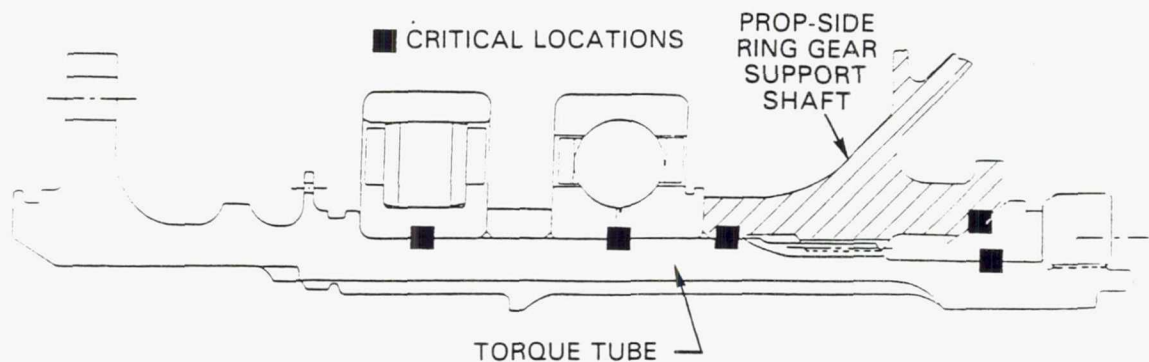


Figure 71 Torque Tube/Prop-Side Ring Gear Support Shaft Interface Showing Locations of Highest Contact Stresses

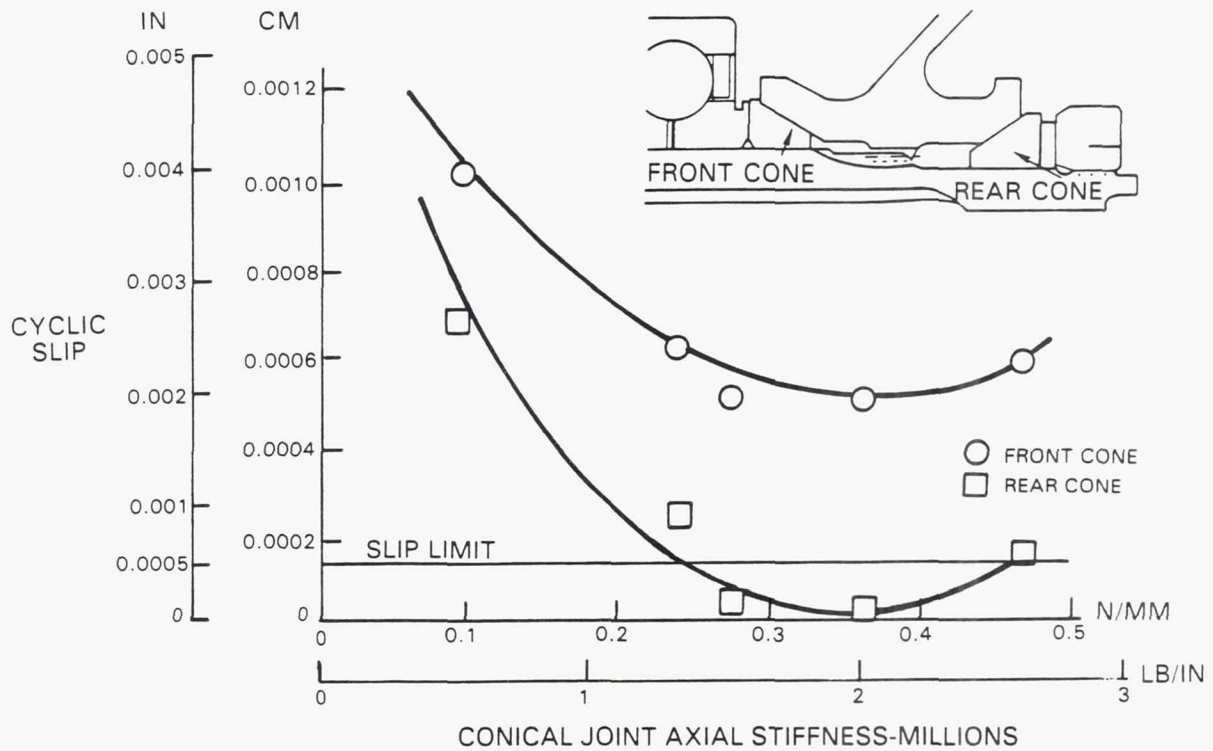


Figure 72 Cycle Slip Analysis Results for Front and Rear Connection Cones - Shows acceptable results for rear cone but unacceptable cyclic slip for a front cone design.

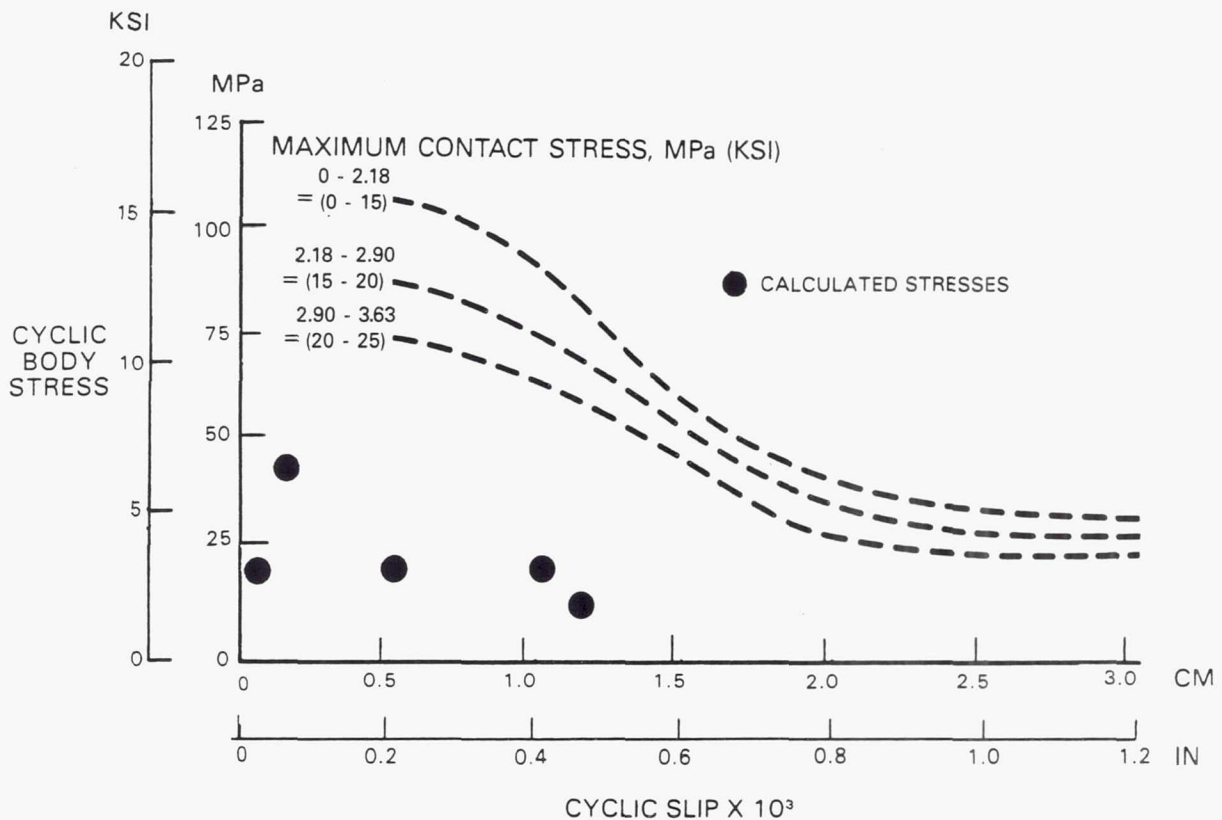


Figure 73 Cyclic Stress and Contact Stress Analyses Show Acceptable Results

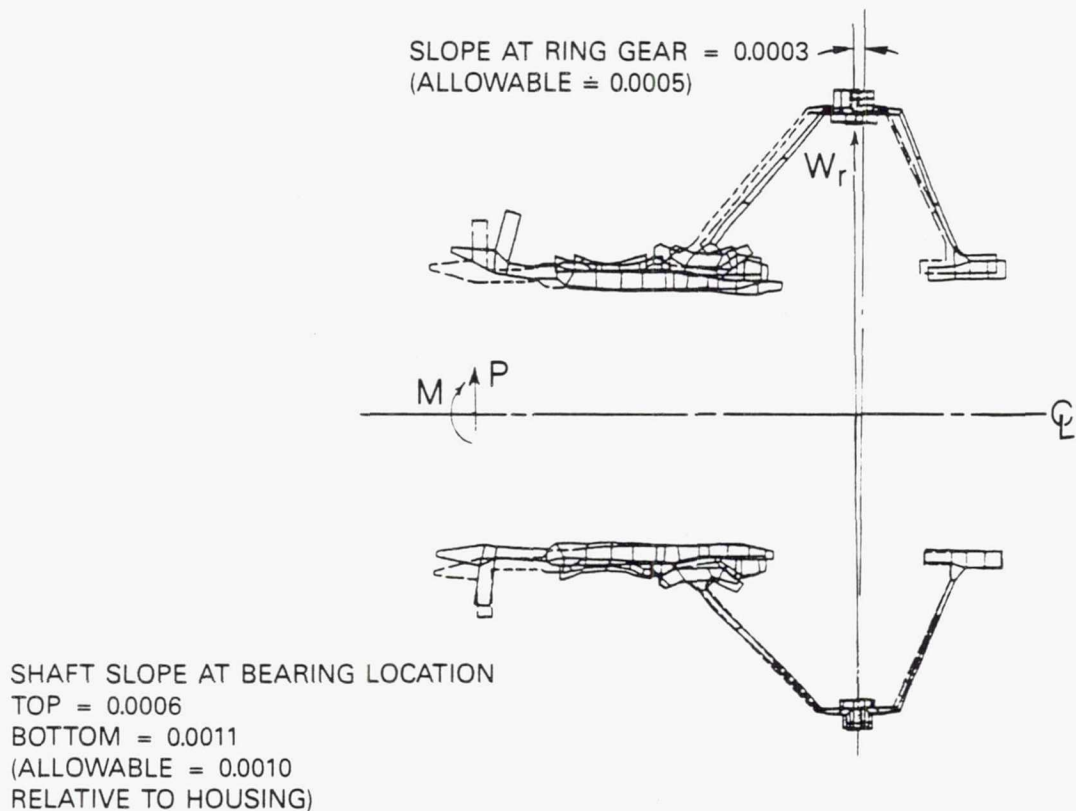


Figure 74 Propeller Shaft Deflection Analysis Results Show Deflection Consistent With Allowable Levels

#### 4.6.1.2 Carrier Shaft Analysis

The carrier support shaft assembly includes the planetary support posts, the plates that they are connected to and the cylinder that supports the carrier system through the bearings to the ring gear. Figure 75 shows the finite element model used for analysis of the carrier shaft. The analysis focused on the effects of the torsional load produced by the reaction of the planetary gear bearings against the support posts. This torsional load causes a displacement of the carrier shaft that results in a slope deflection at the planetary gear support locations. The results of this analysis are shown in Figure 76 and indicate a relatively small and acceptable slope deflection at the support posts.

ORIGINAL PAGE IS  
OF POOR QUALITY

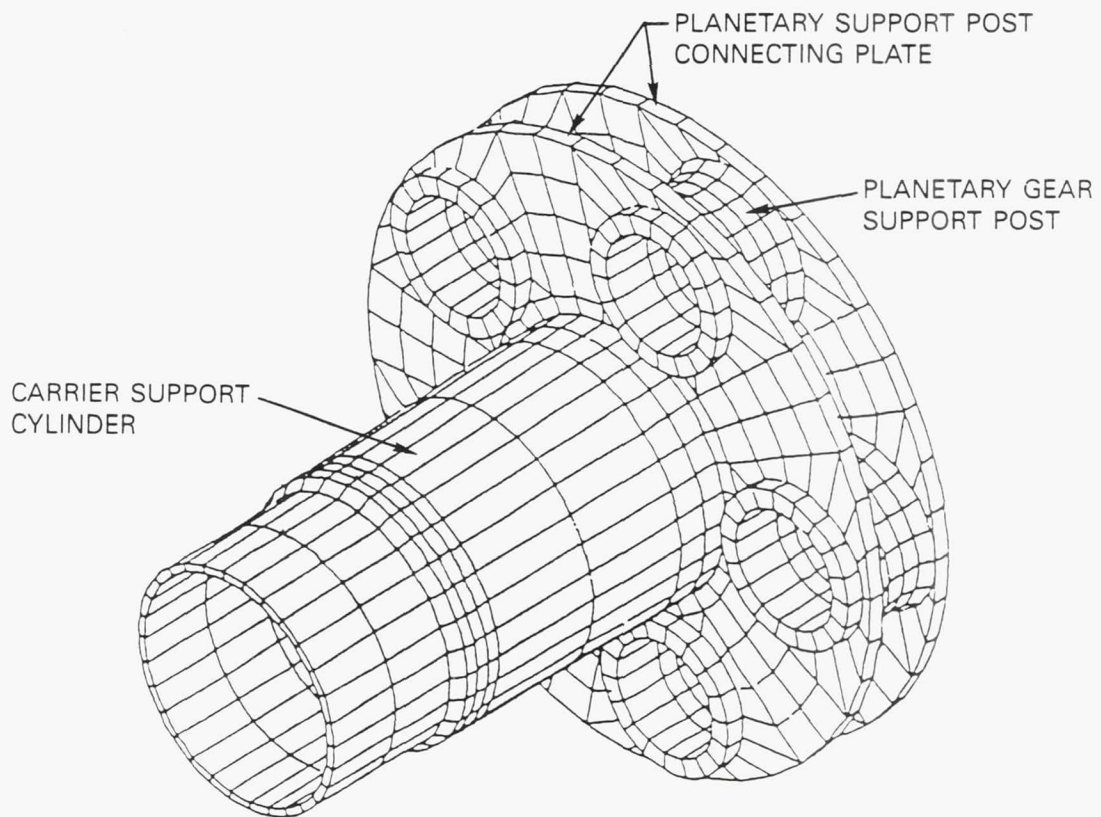
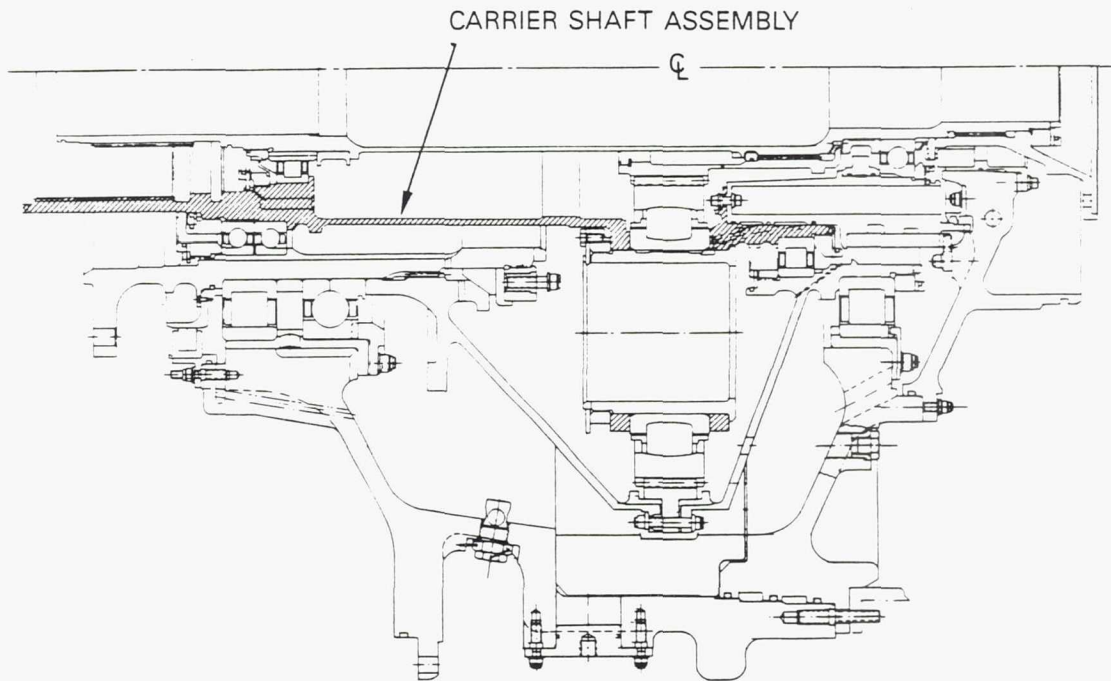


Figure 75 Carrier Shaft Finite Element Model

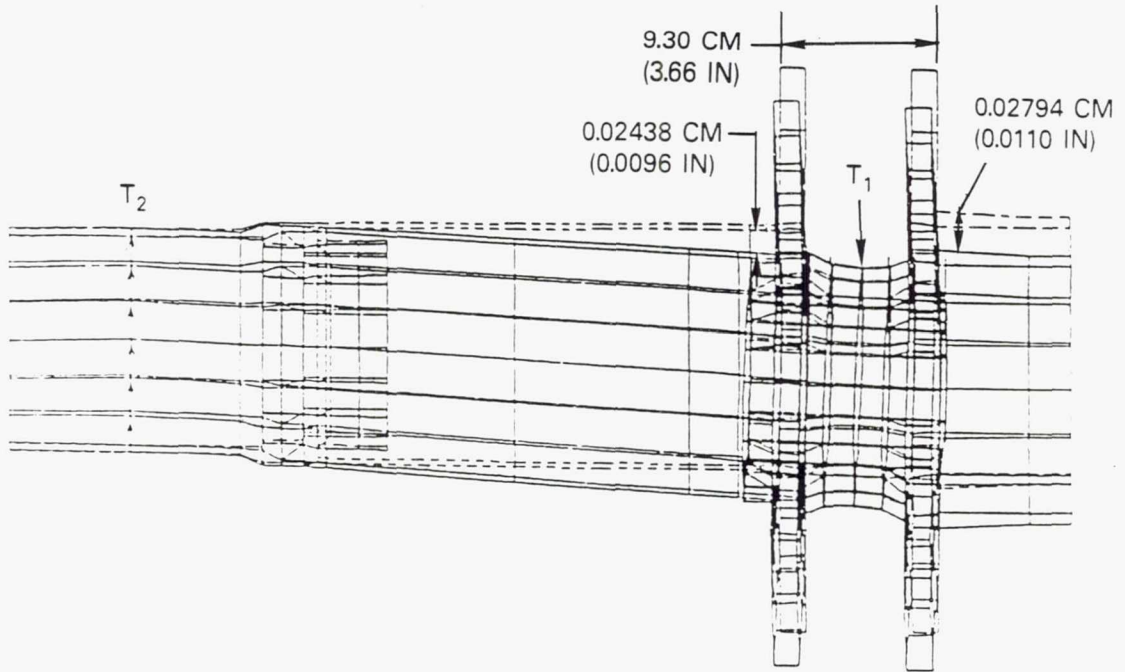


Figure 76 Carrier Shaft Deflection Analysis Results Show Acceptable Slope Deflection of 0.0004 at Planetary Gear Support Posts

Carrier shaft stresses were analyzed at the locations of potential maximum stress shown in Figure 77. The analysis considered stress concentrations at these locations and their combined effect upon the torsional stresses produced by transferring the torque through the shaft. Specifically, Goodman diagrams were constructed by first calculating the stresses associated with torque loadings, calculating the run-out fatigue strength associated with these stresses and comparing the results to allowables required to achieve design life. The results of this analysis are summarized in Figure 78, which shows that the stresses at all of the high stress locations are within the Goodman diagram allowable stress levels.

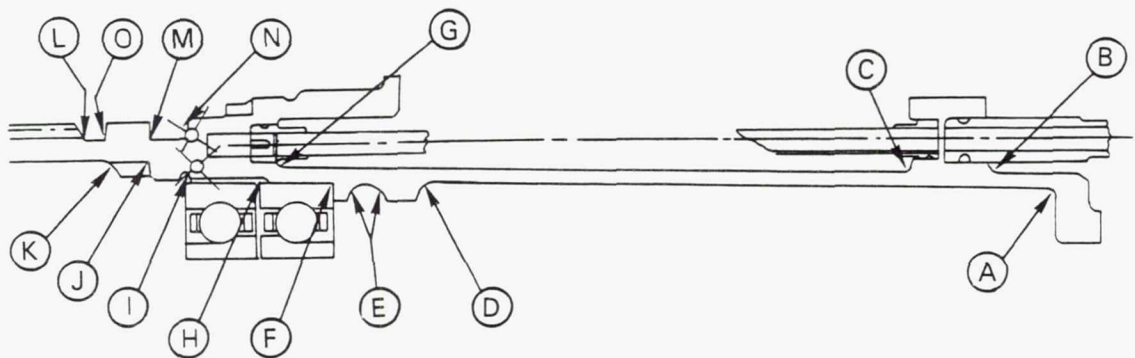


Figure 77 Locations of Potential Maximum Stress on Carrier Shaft

HCF — GOODMAN DIAGRAM  
 AMS 6415 (RC 40-45)  
 CARRIER SHAFT FATIGUE ANALYSIS  
 UNDER MAXIMUM OPERATING TORQUE

MAXIMUM NORMAL OPERATING TORQUE:  
 $T = 38,055 \text{ Nm (336,814 IN-LB)}$

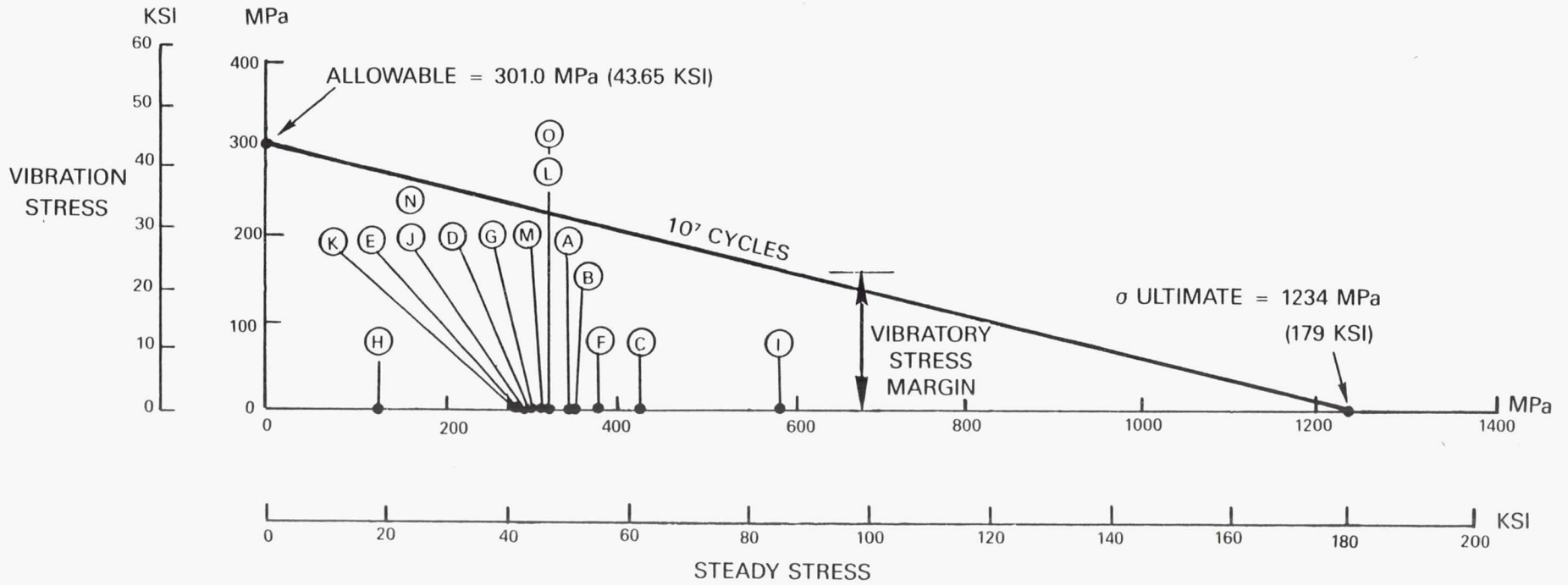


Figure 78 Carrier Shaft Stress Analysis Results Show Stresses to be Within Allowable Limits

In addition to designing the carrier shaft to accommodate torque loads, critical speed margin requirements in the sun shaft necessitated a stiff bearing support at the prop-side (number 7) roller bearing location shown in Figure 79. Carrier shaft thickness was increased by 0.254 cm (0.1 in) at this location to provide the necessary bearing support rigidity.

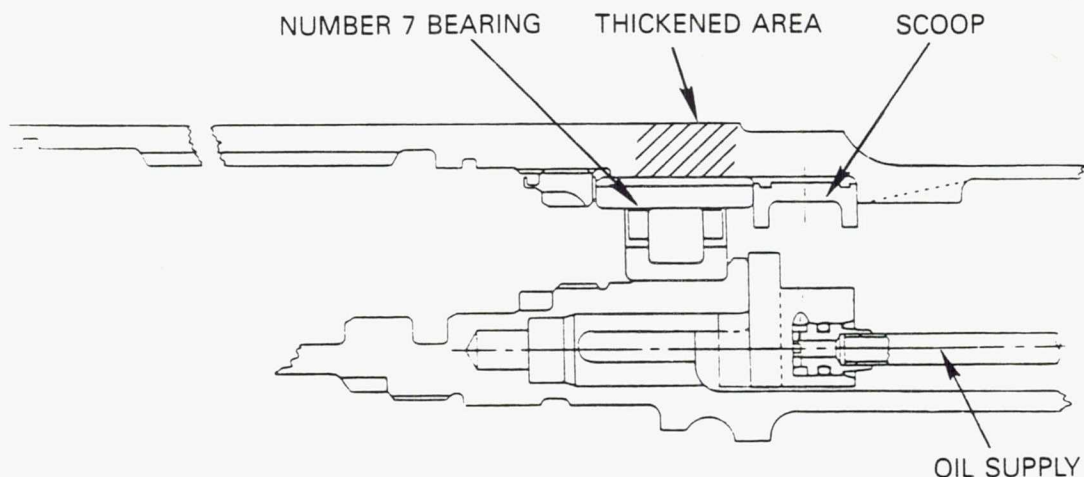


Figure 79 Carrier Shaft Showing Area Thickened to Meet Critical Speed Margin Requirements

#### 4.6.1.3 Sun Shaft Analysis

The sun shaft is designed to transfer torque from the engine drive coupling to the sun gear in the flight engine or from slave gearbox to test gearbox in the back-to-back test rig described in Section 5.0. In the latter case, this results in the extended shaft design shown in Figure 80. The design was analyzed to insure that stress concentrations in the load path were low enough to provide adequate fatigue life. Figure 80 identifies the locations of potential maximum stress where fatigue strength was evaluated. The analysis of the sun shaft followed the same procedures used for the carrier. Figure 81 summarizes the results and shows that the fatigue strength of the shaft meets the life requirements.

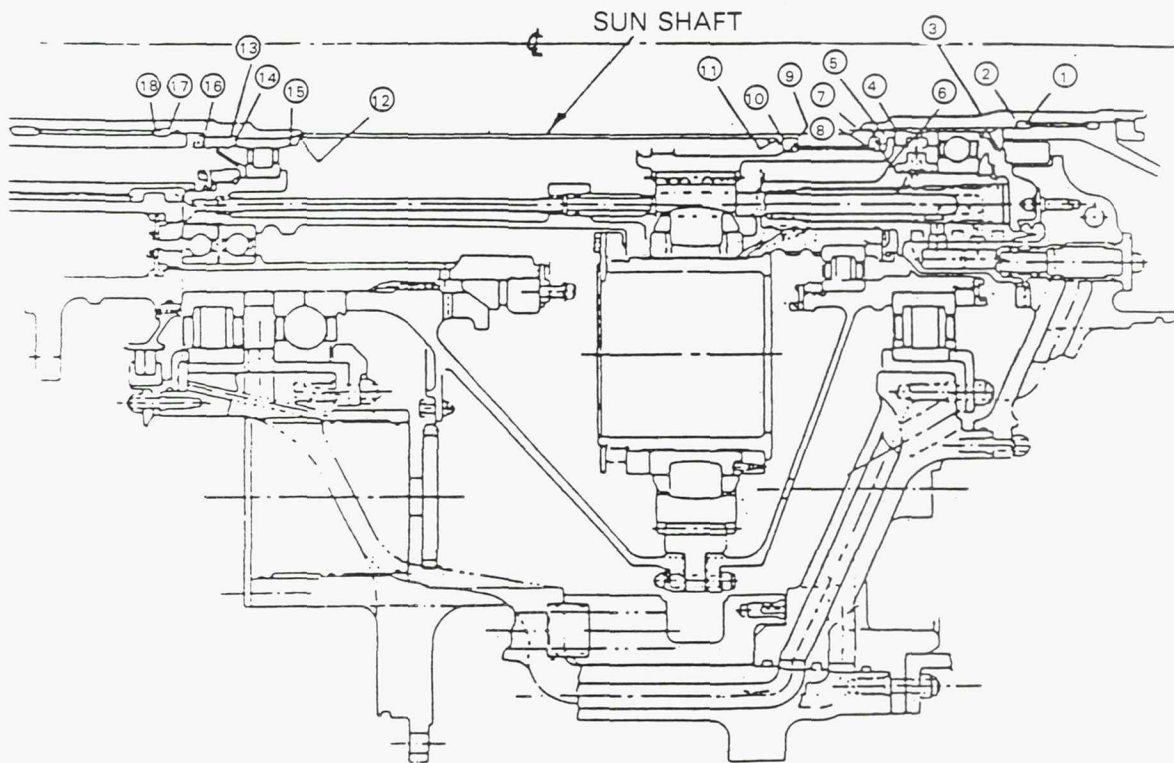


Figure 80 Sun Shaft Showing Regions of Potential Maximum Stress



#### 4.6.1.4 Bearing Retaining Nut Analysis

The bearing retaining nuts at each of the major support bearing locations were analyzed to ensure that pre-load was adequate to maintain tight bearing stacks at operating conditions. The 10 bearing retaining nuts and their locations in the gearbox are shown in Figure 82. Figure 83 shows a typical bearing configuration at the sun shaft roller bearing location. This consists of the nut, the oil scoop and roller outer ring all stacked within the housing. The maximum possible load on each nut comprises three parts; the load generated by torque, with the smallest possible friction coefficient; the load generated by the angle of turn plus the locking feature increment and the load generated by thermal expansion at the maximum operating temperature.

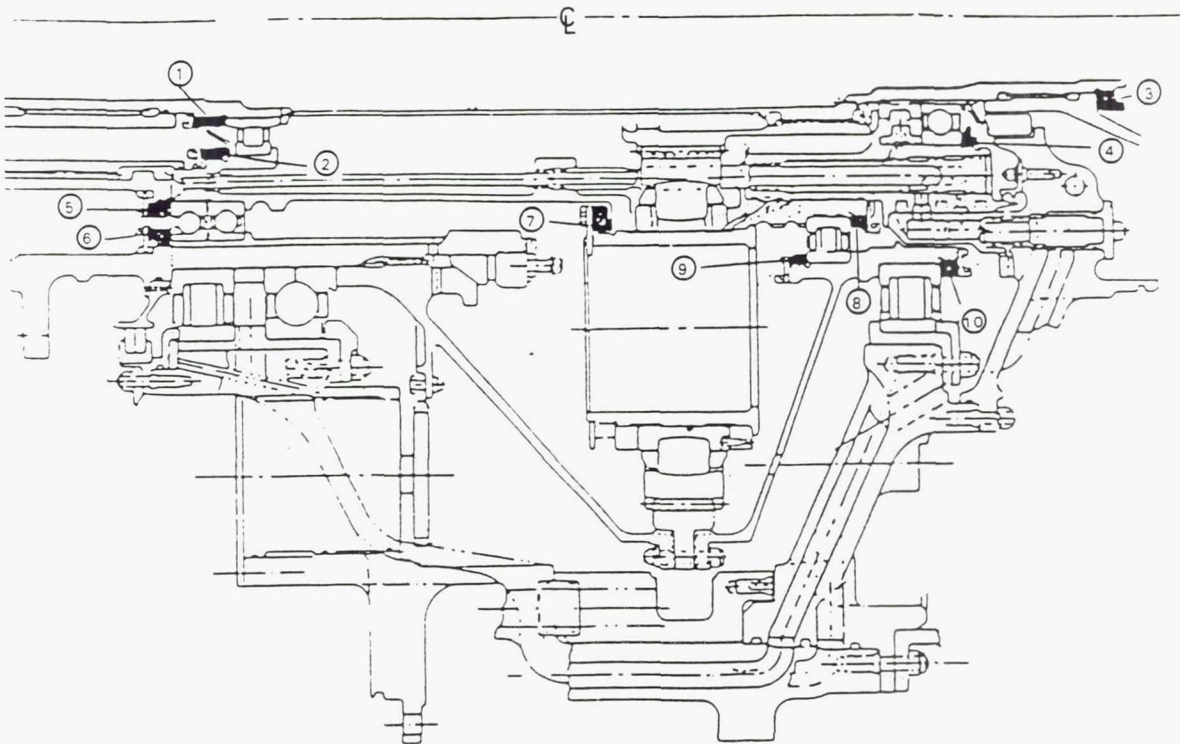


Figure 82 Gearbox Bearing Retaining Nut Locations

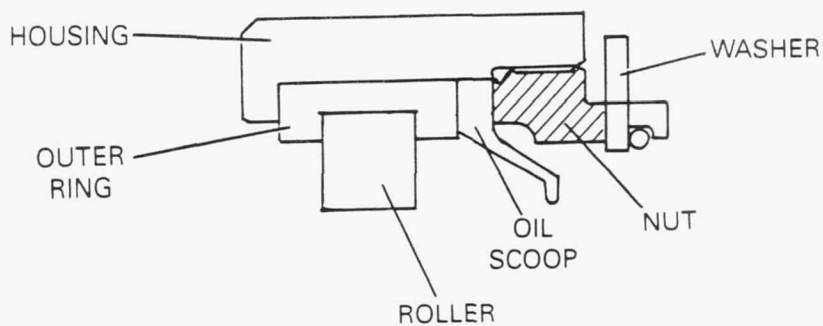


Figure 83 Typical Bearing Configuration (Location 2)

The tightening procedure for the bearing nuts requires an initial seating torque to make the joint snug followed by an angled turn to induce the stack pre-load. The angle of turn is specified such that a minimum compressive pre-load of about 44,482 N (10,000 lb) will remain on the built-up members after considering the effects of thermal expansion and applicable external loads. The initial seating torque is determined by calculating the spring rate of the whole system and assuming an initial seating pre-load of 4448-8896 N (1-2,000 lb). The angle of turn is then calculated to provide the full 44,482 N (10,000 lb) pre-load and the maximum possible load on the nut is determined. With the maximum load on the nut defined, both shear and tensile stresses in the nut are calculated, to assure that an overstress condition does not exist.

The above procedures are repeated for each of the ten different nut systems.

#### 4.6.1.5 Shaft Materials Selection

Selection of materials for the various gearbox shafts was based on meeting strength and life requirements at lowest possible cost. As a result, these components are fabricated from wrought alloy steel (AMS 6414). Advanced, high strength materials were not deemed necessary for these applications.

#### 4.6.2 Housing Design

Housing design was predicated on the straddle-mounted gearbox design concept. The general housing arrangement is shown in Figure 84. The three components of this assembly are the prop-side component, the engine-side component and the cover plate. Design of the housing considered either a tractor configuration (engine aft of the gearbox) or a pusher configuration (engine forward of the gearbox). To accommodate both configurations, the gearbox housing was designed with rails on both the prop-side and the engine-side to which mount pads could be attached. The engine-side rail provides the mount connection for the structural support member between the gearbox and the gas generator. The prop-side rail is used as a connecting mount flange to the rig test unit. Salient details of the two major housing components are described in the following paragraphs.

##### 4.6.2.1 Prop-Side Housing

The prop-side housing shown in Figure 85 is the major support member for the prop shaft support bearings. In addition, it incorporates a number of mount pads to accommodate oil supply and scavenge system pumps, oil line connections and chip detectors. The four major pump pads are shown, three of which are used and the fourth provided as a optional pad for such features as a prop brake unit or additional scavenge pump capacity, should either become necessary. Ports and a support pad for chip detector units are provided at each of the two scavenge pump locations.

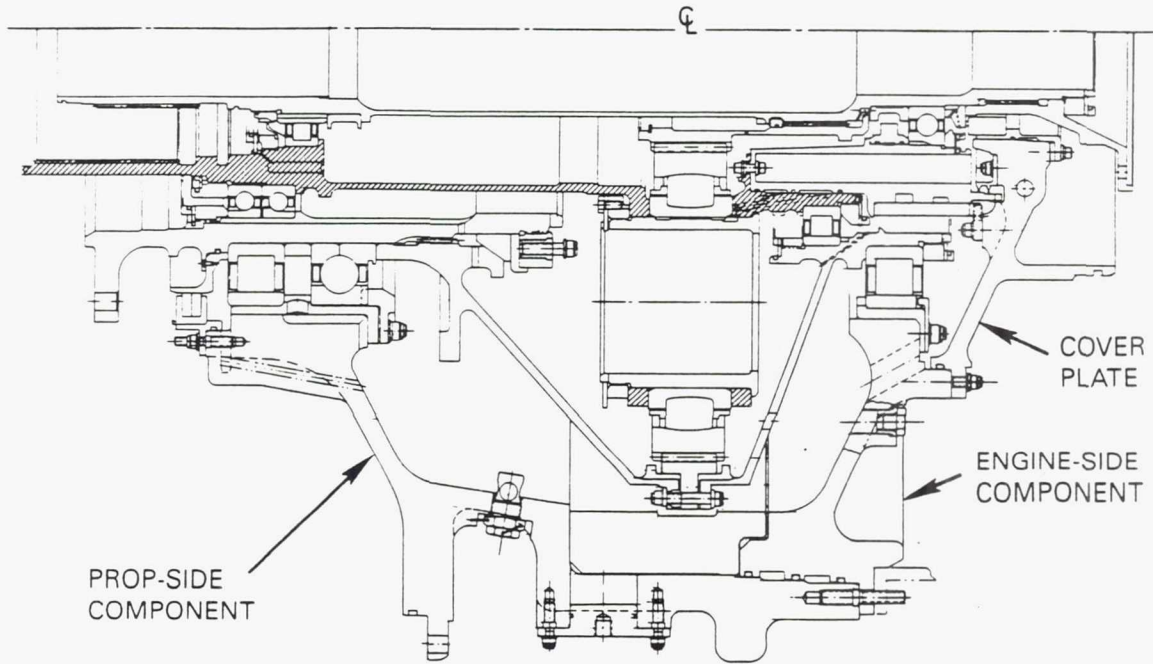


Figure 84 Gearbox Housing Assembly Showing Three Major Components

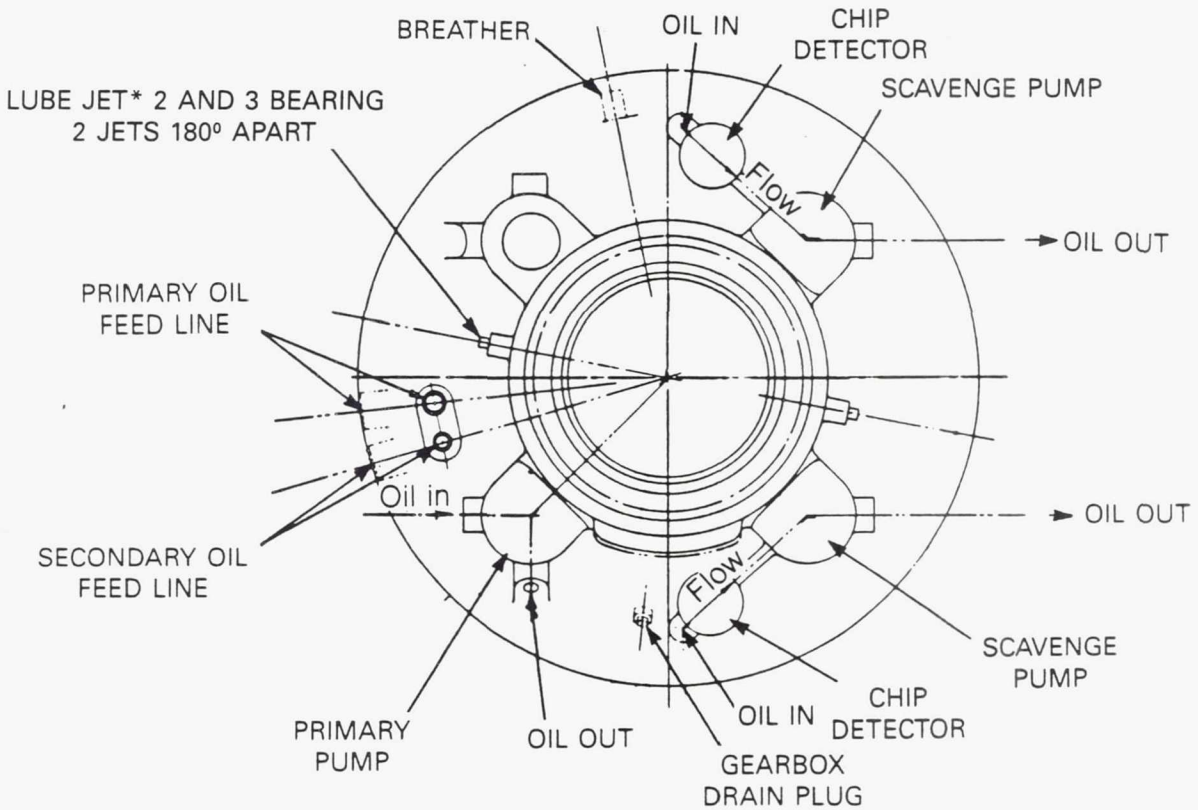


Figure 85 Prop-Side Housing Details

#### 4.6.2.2 Engine-Side Housing

The engine-side housing is shown in Figure 86. This unit provides support for the ring gear support bearing as well as providing passages for conducting lubricant into the gearbox systems. A viewing port is included for visual observation of the gear system during testing. Boroscope mounting bosses are included to enhance inspection of sun/planet and planet/ring gear meshes without having to disassemble the gearbox.

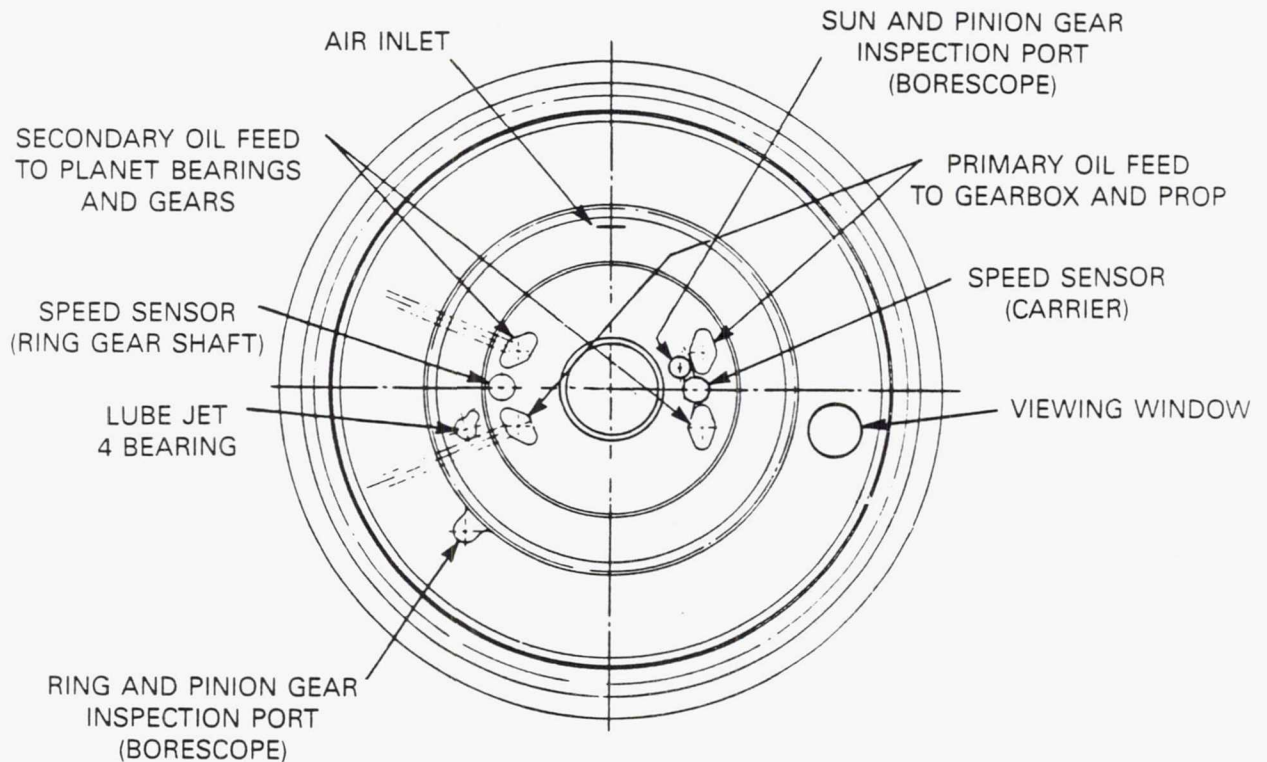


Figure 86 Engine-Side Housing Details

#### 4.6.2.3 Housing Structural Analysis

The housing system was analyzed using a finite element analysis procedure. Figures 87 and 88 show the finite element model constructed for the total housing system; including the prop-side housing, the engine-side housing and the mounting cone that connects the gearbox to the gas generator. The most limiting loading condition is the unbalance load caused by the loss of a prop shell from the propeller blade. Results of the analysis are shown in Figures 88 and 89. Figure 88 shows the range of calculated stresses at the points where maximum stress concentration would be expected to occur and Figure 89 shows that acceptable cyclic life can be achieved at these levels, even under the most limiting loading condition.

ORIGINAL PAGE IS  
OF POOR QUALITY

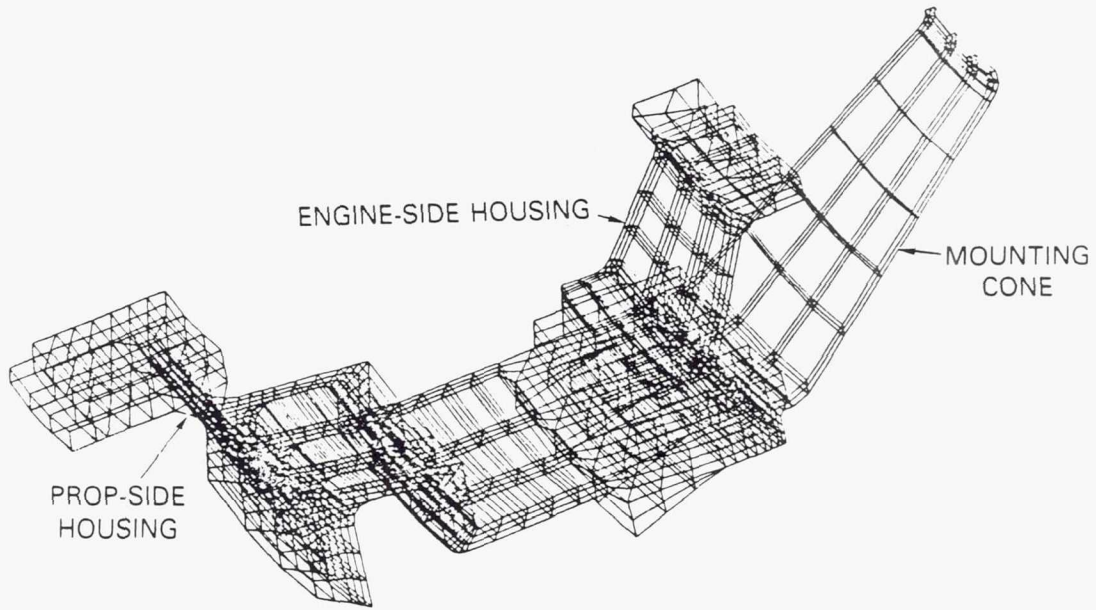
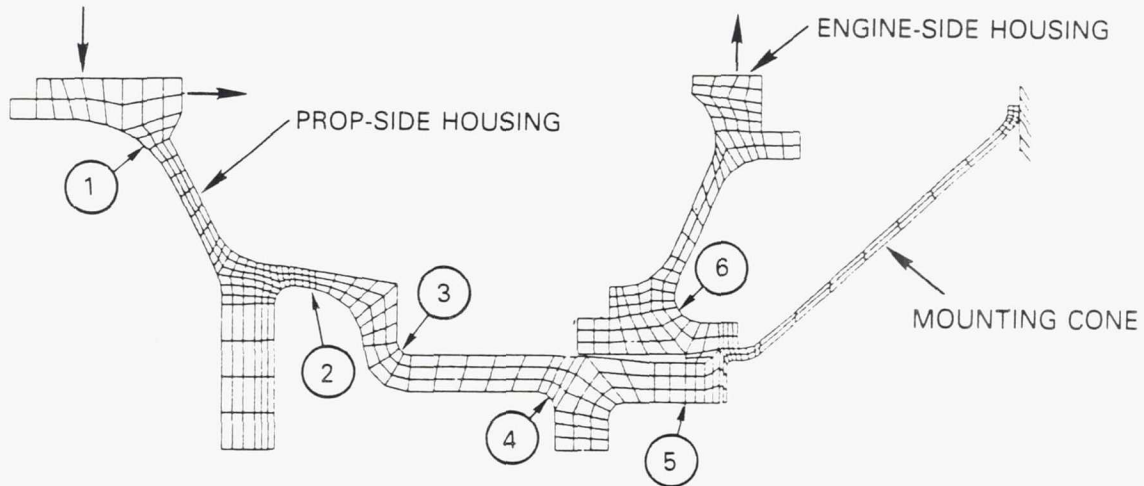


Figure 87 Housing Assembly Finite Element Analysis Model



1	-18.27 ± 40.75 MPa (-2650 ± 5910 PSI)	4	-1.38 ± 23.58 MPa (-200 ± 3420 PSI)
2	-1.17 ± 62.05 MPa (-170 ± 9000 PSI)	5	-0.48 ± 24.61 MPa (-70 ± 3570 PSI)
3	-2.28 ± 55.57 MPa (-330 ± 8060 PSI)	6	-6.96 ± 48.40 MPa (-1010 ± 7020 PSI)

Figure 88 Housing Assembly Finite Element Analysis Showing Regions of Maximum Potential Stress

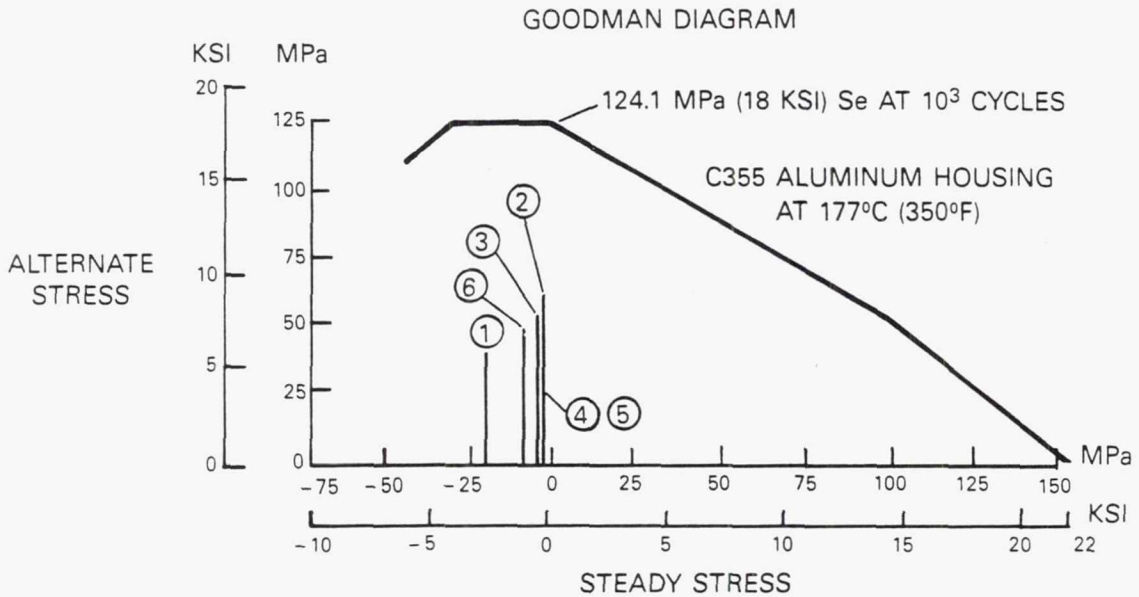


Figure 89 Housing Stress Analysis Results Show Acceptable Cyclic Life Under the Most Limiting Load Condition

#### 4.6.2.4 Housing Materials Selection

Each of the three housing components and the scavenge scroll insert were designed to be cast from AMS 4215, a high temperature capability aluminum. It is a lower cost alternative to a magnesium alloy and discussions with airline operators indicated a preference for a lightweight material that is less prone to corrosion than magnesium and has capability for weld repair. Aluminum meets these requirements.

#### 4.7 Instrumentation

Instrumentation design was an integral part of the overall gearbox design effort to properly account for instrumentation mounting and placement requirements and to provide interface definition that would facilitate ease of gearbox assembly. The objective was to provide sufficient instrumentation to accurately assess the performance and structural-dynamic characteristics of the gearbox and to provide essential on-line condition monitoring during rig operation.

Instrumentation requirements for the gearbox Build 1 test program, described in Section 5.3, are summarized in Table 23.

Table 23 Summary of Instrumentation Used in Build 1 Test Rig

	Performance	Structural	Monitoring	Total
Strain gages		32		32
Thermocouples	48	20		68
Accelerometers			4	4
Microphones	2		2	4
Pressure transducers	8	8		16
Tachometers	3			3
Flowmeters	3			3
Proximity transducers			11*	11

\* Mounted in torquer unit

Figures 90 through 92 illustrate the placement of instrumentation to monitor and record the principal test parameters. The primary parameter for measuring gearbox performance (efficiency) is temperature rise in the lubricating oil. Consequently, thermocouples are located at the oil supply and drain locations shown in Figure 90. Thermocouples mounted in the bearing races and sun/planet gear mesh cavity will serve to isolate the principal component heat generators and also serve as condition monitors for the bearings and gears (i.e., a sudden temperature rise is a sign of distress). As noted in Section 5, the test gearbox is suitably insulated to enhance accuracy of temperature rise measurements.

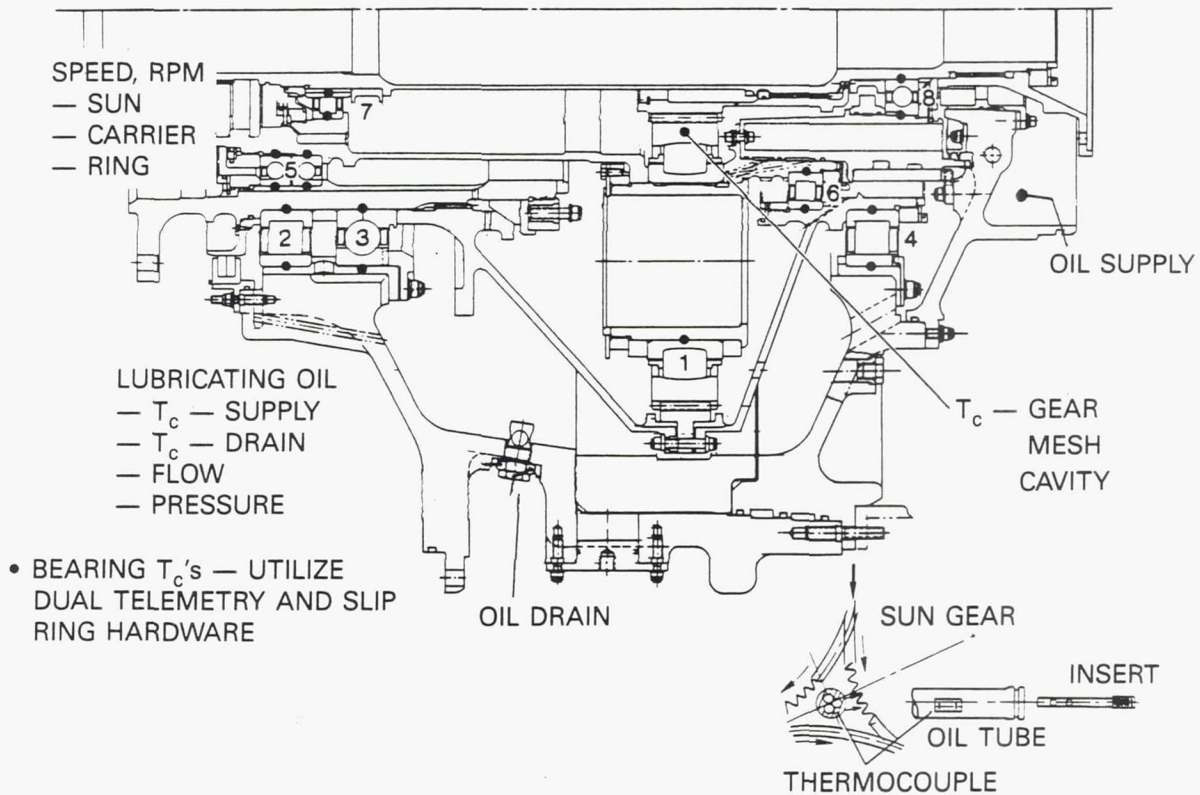


Figure 90 Location of Instrumentation Used Primarily for Performance Measurement

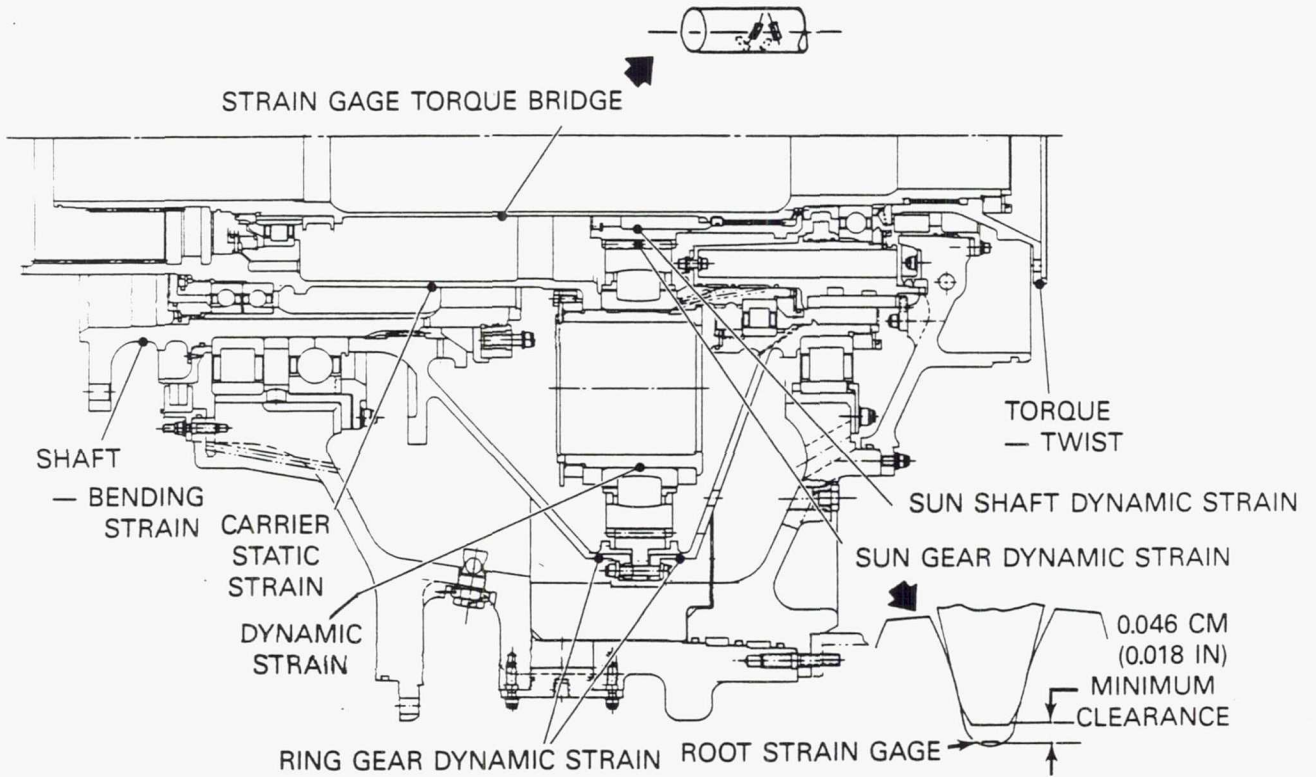


Figure 91 Location of Instrumentation Used Primarily for Structural and Mechanical Assessment

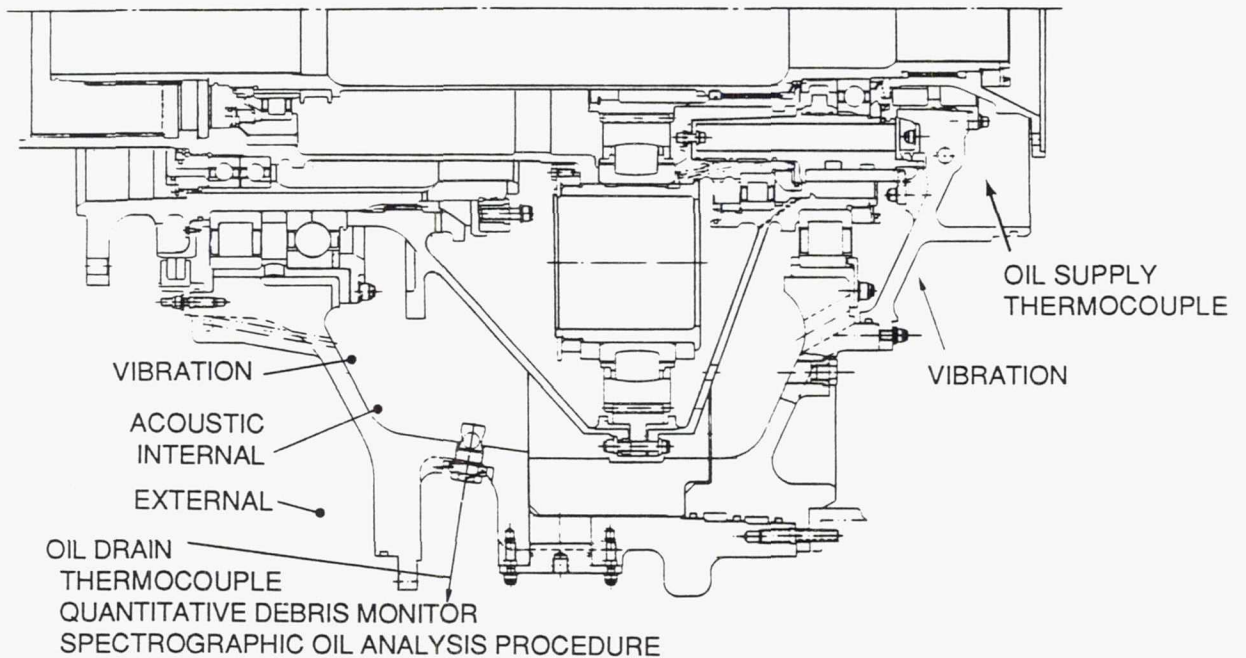


Figure 92 Location of Instrumentation Used Primarily for Condition Monitoring

Structural and mechanical load sharing characteristics of the gearbox components will be determined through use of strain gages strategically located in regions of highest anticipated stress. The most significant challenge is mounting strain gages in the location of the gear tooth root, as shown in Figure 91, to measure gear tooth stresses. The concern is that gear tooth meshing and oil entrapment characteristics may cause the gages to detach before useful data can be obtained. A standard strain gage bridge circuit was designed to enable measurement of torque on the sun gear drive shaft. Torque is also measured through use of the speed sensor signal processor to identify system 'wind up' due to torque loads. Strain gages located on the prop drive shaft are used to calibrate the shaft to simulated propeller thrust and moment loads.

The gearbox mechanical condition will be monitored during operation through measurement of vibration, noise, and oil quality. Oil quality measurements will include metallic particulate content assessment through use of a quantitative debris monitor and spectrographic analysis of the oil. As noted earlier, oil temperature rise will also be monitored for sudden changes that could indicate gearbox distress. Location of the condition monitoring instrumentation is shown in Figure 92.

Transfer of measured data from the carrier and ring shafts will be handled by two specially designed telemetry units located at the prop end of the test gearbox and shown in Figure 93. A coil set is included with each unit for power input and data signal output. A third coil set is required to access the inner (carrier) shaft. A small amount of gearbox oil is diverted for cooling of the electronic modules. Transfer of data from the sun shaft will be by a standard slip ring.

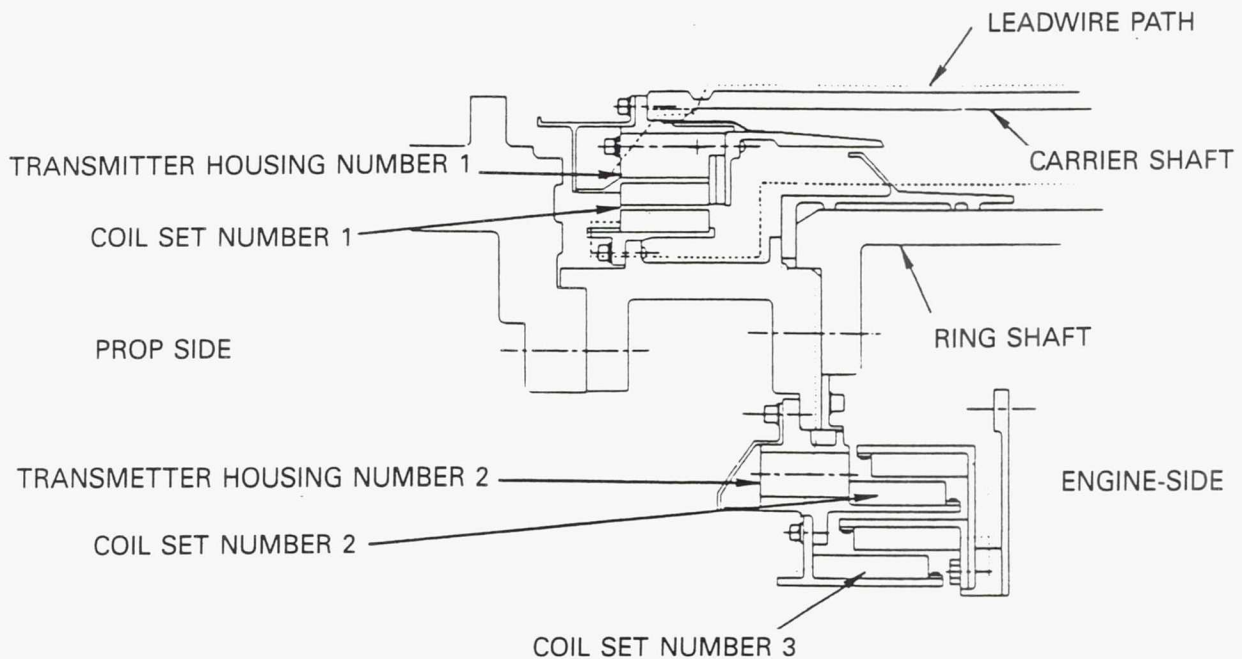


Figure 93 Rig Telemetry System

#### 4.8 Weight and Materials Summary

Since the gearbox design described in the previous sections was intended for ground-test technology demonstration only, design details and materials selection were based on meeting demonstrator requirements at lowest possible cost. For example, a 'flight-weight' design would be reduced in size and lighter-weight construction techniques and materials would be utilized, where appropriate.

Table 24 summarizes the weight and materials selected for the major gearbox components. Materials comprised basically four major categories as follows:

1. High hot hardness steel (EX-53) for the ring gear, sun gear, and planet gears (including their integral roller bearings, cages and races). This material was one of the technologies chosen for verification in the program.
2. Cast high temperature capability aluminum (AMS 4215) for the gearbox cases and scavenge scroll insert. This material was selected as a lower cost alternative to some form of magnesium alloy.
3. M-50 for all bearings other than the planet bearings.
4. Wrought alloy steel (AMS 6414) for most of the remaining components.

Weights shown are calculated based on part definition and material specifications. A final weight for the test hardware will be obtained when parts are pulled from Stores and weighed at the initiation of assembly activities. That is also the point in time when the actual part count is verified.

Table 24 Gearbox Weight and Material Summary

Part Description	Weight, kg (lb)	Material
Input flange	8.2 ( 18.1)	AMS 6414
Input shaft	12.7 ( 27.9)	AMS 6414
Sun gear	5.6 ( 12.4)	EX-53
Number 2 bearing support and lock	3.7 ( 8.2)	AMS 6414
Oil interface/rear carrier support	31.5 ( 69.4)	AMS 6414
Front planet carrier	18.2 ( 40.1)	AMS 6414
Rear planet carrier	22.9 ( 50.5)	AMS 6414
Inner planet carrier	5.0 ( 11.0)	AMS 6414
Planet sleeve	17.0 ( 37.5)	AMS 6414
Planet nut	3.8 ( 8.3)	AMS 6414
Planet outer race	28.9 ( 63.7)	EX-53
Planet inner race	12.5 ( 27.6)	EX-53
Planet rollers	11.5 ( 25.4)	EX-53
Planet roller cage	5.8 ( 12.8)	EX-53
Ring gear	16.4 ( 36.1)	EX-53
Output shaft	18.0 ( 39.7)	AMS 6414
Front hub	44.5 ( 98.0)	AMS 6414
Rear hub	30.3 ( 66.7)	AMS 6414
Output shaft (hubs)	51.1 (112.6)	AMS 6414
Output shaft nut	10.5 ( 23.2)	AMS 6414
Accessory drive gear	1.8 ( 4.0)	AMS 6414
Accessory drive	3.6 ( 8.0)	AMS 6414
Front shaft support	Not available	--
Static oil supply interface	11.3 ( 25.0)	AMS 6414
Bearing locks (number 1, 5, 6)	W/bearings	--
Bearing number 1	8.8 ( 19.4)	M-50
Bearing number 2	3.1 ( 6.8)	M-50
Bearing number 3	16.1 ( 35.4)	M-50
Bearing number 4	15.7 ( 34.7)	M-50
Bearing number 5	16.1 ( 35.5)	M-50
Bearing number 6	7.0 ( 15.5)	M-50
Bearing number 7	3.1 ( 6.9)	M-50
Front outer case	85.3 (188.0)	AMS 4215
Inner case, oil scavenge	45.8 (101.0)	AMS 4215
Rear outer case	52.0 (114.6)	AMS 4215
Rear inner case	18.6 ( 41.0)	AMS 4215
Bearing support sleeve (number 3/4)	16.6 ( 36.7)	M-50
Bearing support sleeve (number 5)	10.2 ( 22.5)	AMS 6415
Front seal support (inner)	4.0 ( 8.8)	AMS 6414
Front seal support (outer)	6.2 ( 13.6)	AMS 6414
Oil lines	1.5 ( 3.4)	Standard tube material
Subtotal	684.9 (1510.0)	
Margin 2.5%	17.1 ( 37.8)	
Total	702.0 (1547.8)	

#### 4.9 CODE DEVELOPMENT

Code development activities focused on updating existing gearbox design and analytical codes to better predict the efficiency, durability, dynamics and cooling characteristics of the AGBT design and to provide for condition monitoring of the gearbox during its operation. A code development plan was formulated and received NASA approval. The following subsections describe the basic codes and recommended modifications that were included in this plan.

##### Hamilton Standard GEARDYNMULT Program

The GEARDYNMULT code has the basic capability to determine the dynamic tooth-pair response and resulting stresses for single stage planetaries with involute spur or helical gearing. It includes options for a flexible carrier and/or ring gear, floating sun gear, center and the natural frequency solution. The approved modifications will give this code the capability to: (a) handle multiple gearing stages and/or system components, (b) represent gear mesh lubrication and temperature models currently developed, (c) optimize the gear tooth stress sensitivity formula, and (d) conduct parametric studies and establish parameter guidelines.

##### SKF SPHEREBEAN Program

The basic capability of the SPHEREBEAN code is to predict bearing life, heat generation, and internal loads and stresses (including lubrication and ring flexibility effects) for double-row spherical roller bearings. The approved modification will make this code capable of analyzing single-row spherical roller bearings in a planetary gear system.

##### SKF SHABERTH Program

The SHABERTH code is presently used to calculate complete bearing performance parameters such as stresses, deflections, fatigue life, lubrication effects and heat generation. Thermal modeling capability permits steady-state or time transient thermal analysis of an integrated single shaft housing-bearing-shaft system, including thermal interaction with bearing performance. The approved modification will enable this code to accommodate coaxial shafts.

##### NASA F78EX/IN Program

The F78EX/IN code is currently used to calculate the various losses encountered in operating gear systems. These include gear sliding and rolling losses, bearing load dependent losses, bearing viscous dependent losses and gear windage losses. These losses are subsequently combined in a gearbox overall efficiency prediction calculation. The approved modification to this code will enable the correlation of churning and windage losses with test data.

### Condition Monitoring Algorithm

This algorithm will comprise the definition of logic networks and flow diagrams for a condition monitoring computer program. The program will be planned around a variety of condition sensing devices (i.e., chip detectors, vibration pickups and thermocouples) and locations, with consideration given to sensor effectiveness based on AGBT test experience. Appropriate sensor sensitivities and normal signal levels will be identified from test experience, and a computer program structure will be created for appropriate combinations and sequences of signal deviation from the norm. The expected program output will be indications of normal or abnormal operation and warnings of impending malfunction, with the potential for predicting time remaining before part removal.

## 5.0 TEST FACILITY AND MULTIPURPOSE TEST RIG

A test facility and multipurpose test rig were supplied to the program by the Contractor at no cost to the Government. The facility and rig are capable of meeting the gearbox test program's full range of operating requirements. The following sections describe the test facility and test rig as well as the principal ingredients of a test plan that was formulated for the first build of the gearbox.

### 5.1 Test Facility

The test facility comprises a refurbished engine component test cell with an adjacent control room. The test cell houses the multipurpose test rig and drive systems, mounted on a tilting bedplate; the lube and scavenge systems for the test and slave gearboxes; the torquer unit and the step-up rig drive gearbox; and other ancillary equipment (including a 5 ton capacity manual overhead bridge crane to facilitate installation and removal of the components mounted on the bedplate). The bedplate dimensions were set to accommodate test rigs (including torquer) up to 1.22 m (4.0 ft) in diameter and 3.05 m (10.0 ft) long. A fixed grating work platform surrounds the bedplate on all sides. The control room houses the test rig and facility operating controls and the automatic data reduction equipment.

Figure 94 shows the test equipment (excluding the test and slave gearboxes) mounted on the testbed and tilted to an angle of 45 degrees during operational checkout of the facility and equipment. The bedplate can be tilted to a fully vertical position with the motor-driven chain drive shown in Figure 95. Bedplate position retention at any particular degree of tilt is achieved with the disk braking system also shown in Figure 95. Major components of the rig lube, oil and hydraulic systems are located on the floor of the test cell. Figure 96 illustrates the testbed support structure and the flexible service connections required to accommodate the tilt feature.

The main test rig drive system comprises a 600 HP DC motor coupled to a speed-increasing (step-up) gearbox (7:1 ratio). Motor speed is variable to a maximum of 1750 RPM. This correlates to a maximum test gearbox sun gear speed of 12,250 RPM. The step-up gearbox is the offset parallel shaft type with its own dedicated lubrication and vibration monitoring systems. The auxiliary drive is also a variable speed DC motor delivering 600 HP up to 1750 RPM. This motor is also capable of operating as an electric brake, with a braking capacity of up to 40 percent of rated power. Load banks (180 KVA) are utilized to absorb this power. The auxiliary drive connects to the test gearbox ring gear through a gear train in the torquer unit and thus imparts variable speed capability to the ring gear. This drive system arrangement permits testing of the full differential gear speed characteristics of the planetary gear system.

ORIGINAL PAGE IS  
OF POOR QUALITY

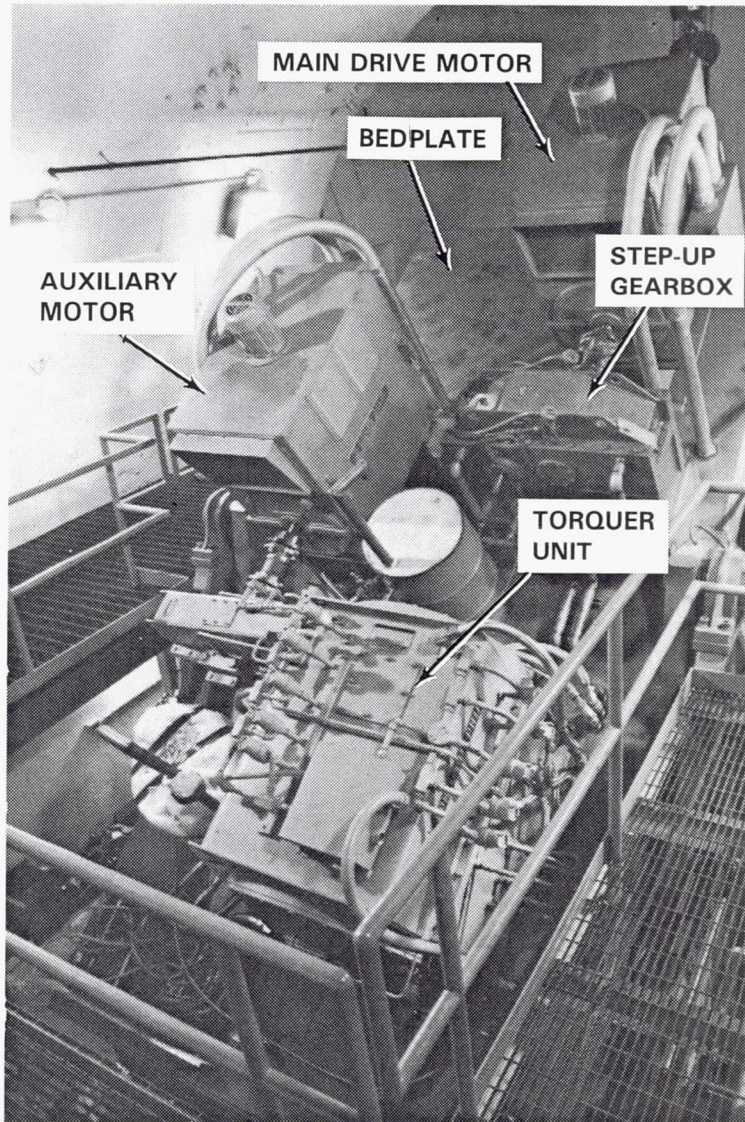


Figure 94 Advanced Gearbox Technology Test Facilities: Overall View with Rotating Testbed Tilted at a 45 Degree Angle

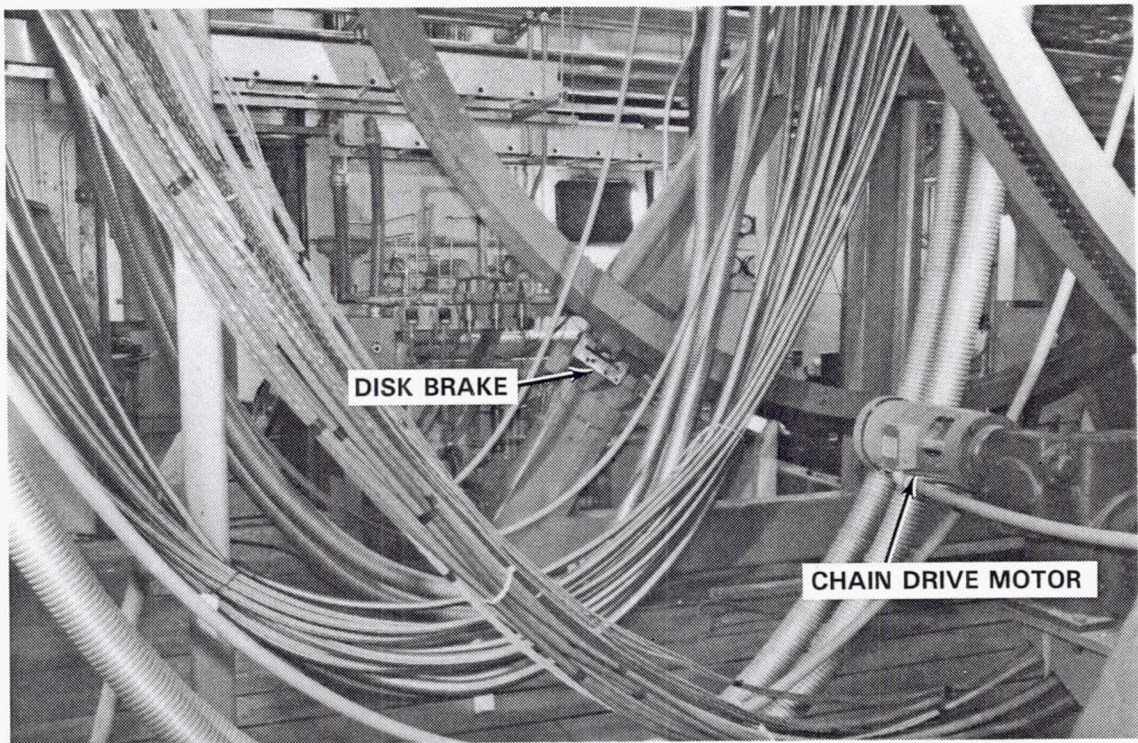


Figure 95 Rotating Testbed Drive and Braking Systems

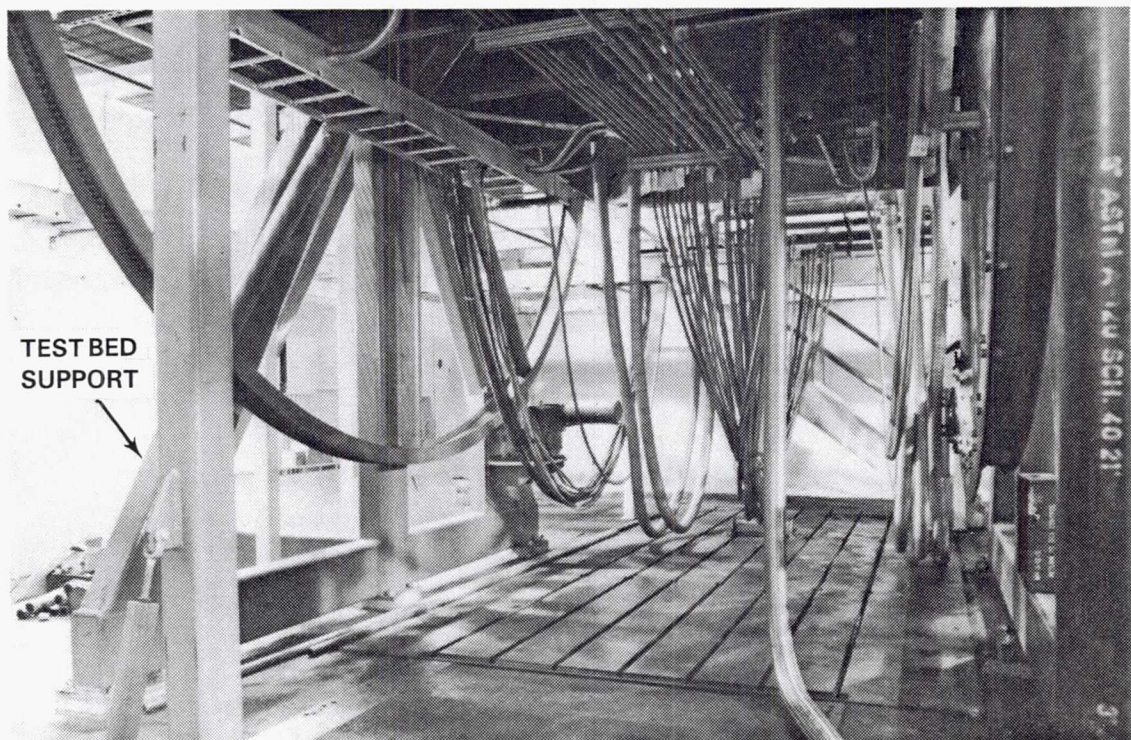


Figure 96 Advanced Gearbox Technology Test Facilities: Rotating Testbed, Bottom View

Test stand operating controls and the automatic data reduction equipment are shown in Figures 97 and 98. Controls are computer-automated with manual backup systems where appropriate. The control console has provisions to monitor a total of 20 critical rig parameters (10 temperatures, 7 pressures, and sun shaft, carrier and ring gear speeds).

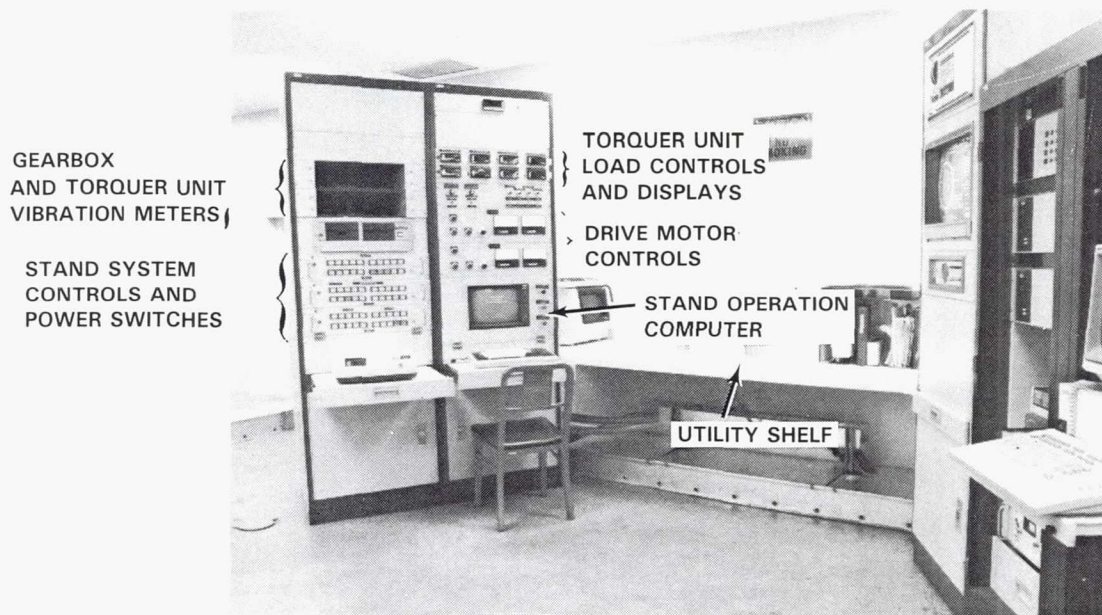


Figure 97 Advanced Gearbox Technology Test Facilities: Test Stand Computer Control System

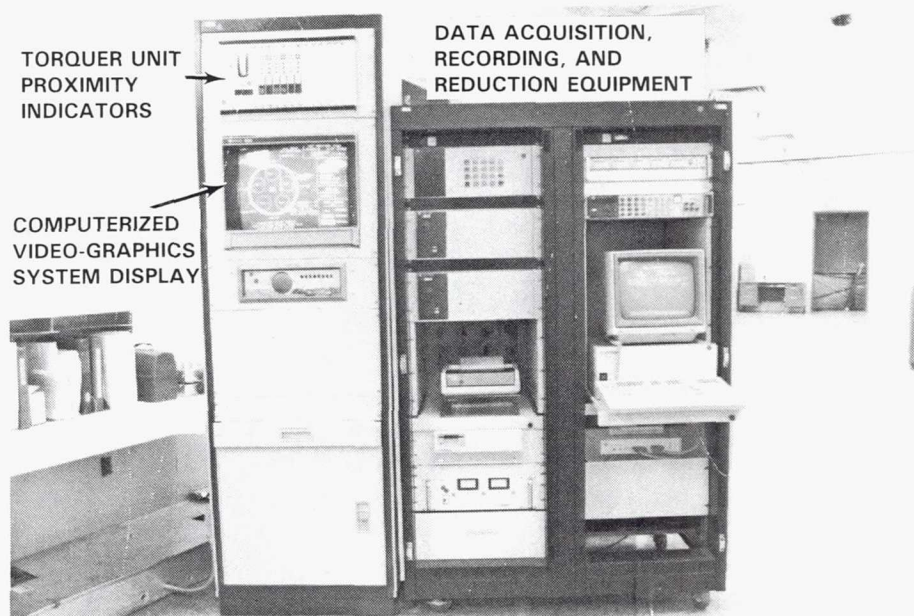


Figure 98 Advanced Gearbox Technology Test Facilities: Portable Data Recording System

The automatic data recording (ADR) system has the capability of recording and processing up to 250 inputs. Those required for initial gearbox testing included the following:

- o Two telemetry packages with 20 channels per unit
- o A 50 channel slip ring for strain gages and thermocouples
- o 50 pressures and temperatures
- o 6 oil flow rate measurements
- o 3 speed measurements
- o 8 proximity probes
- o 12 accelerometers

The system has the capability to display selected test parameters in engineering units in near real-time through use of the subsystem video display shown in Figure 98. A virtual menu of such subsystems can be developed and called up at any point in the test program. Provisions for a vibration spectrum analyzer are also included in the facility plans. This will enable real-time spectrum analysis of gearbox vibration characteristics.

## 5.2 Multipurpose Test Rig

The objective of the multipurpose test rig design effort was to provide a test rig suitable for gearbox durability evaluation and efficiency assessment over a range of applications including both fixed wing aircraft and helicopters. To accomplish this, the rig is designed to function through an attitude variation from +30 degrees to horizontal to -90 degrees (vertical). Propeller thrust, side and torque loads are simulated in the test gearbox when assembled on the rig. The test rig, as shown in Figure 99, is capable of testing gearboxes of up to 20,000 SHP, with gear unit testing capability up to 56,492 Nm (500,000 in-lb) of torque; a level chosen to accommodate accelerated gearbox endurance testing. Since efficiency will be measured from oil heat generation, heat loss control is essential. Consequently, insulation will be applied in appropriate locations to eliminate any significant heat loss. To provide for ease of installation in the test facility, quick disconnects are utilized at lubrication system and instrumentation interfaces. This feature also permits easy access to the gearboxes should maintenance be required while the rig is mounted in the test facility. Figure 100 shows the principal interfaces where quick disconnects are utilized.

The torquer unit, shown in Figures 101 and 102, is designed to test planetary transmissions by applying torque, radial loads and thrust loads to the outermost shaft of the planetary transmissions (test and slave gearboxes). The transmissions are mounted on opposite ends of the torquing elements in the torquer. Torque is created by applying hydraulic pressure to a system of sliding helical splines mated to the output shafts of the test and slave gearboxes; where the slave gearbox is required to complete the torque load circuit. In this 'back-to-back' arrangement, the only external drive power required is that necessary to overcome losses in the driven gear trains. Radial (or side) and thrust loads are imposed by hydraulic cylinders.

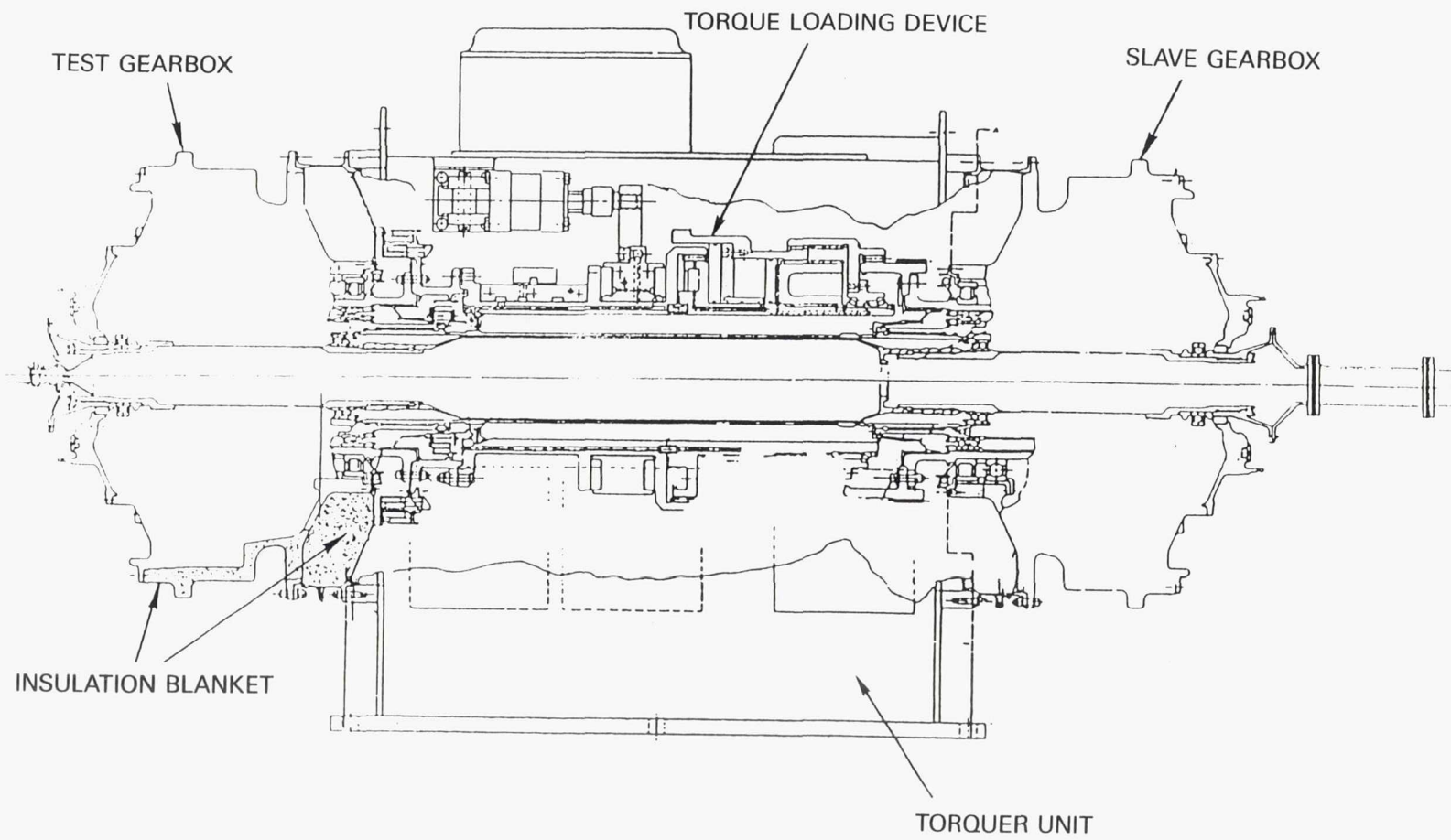


Figure 99 Multipurpose Test Rig as Assembled for Test

ORIGINAL PAGE IS  
OF POOR QUALITY

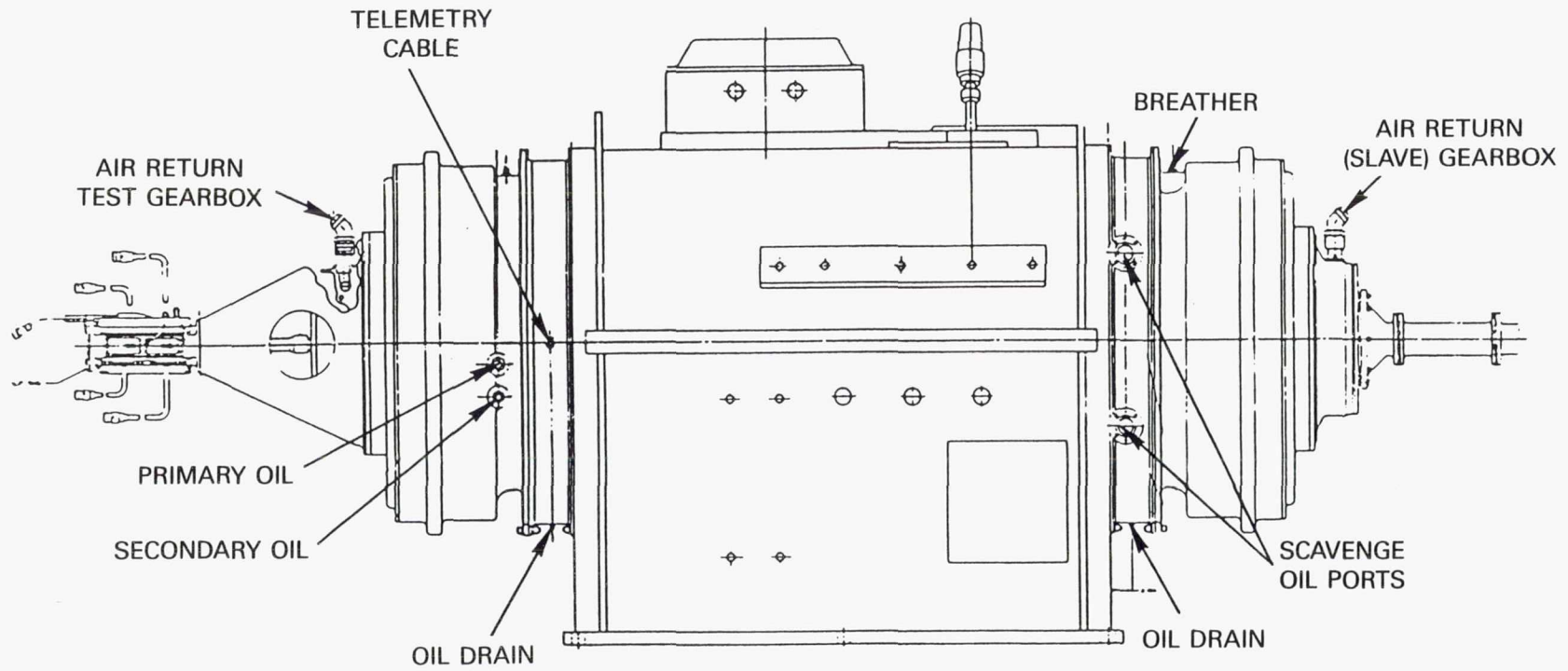


Figure 100 Test Rig Showing Principal Interfaces Where Quick Disconnects Are Utilized

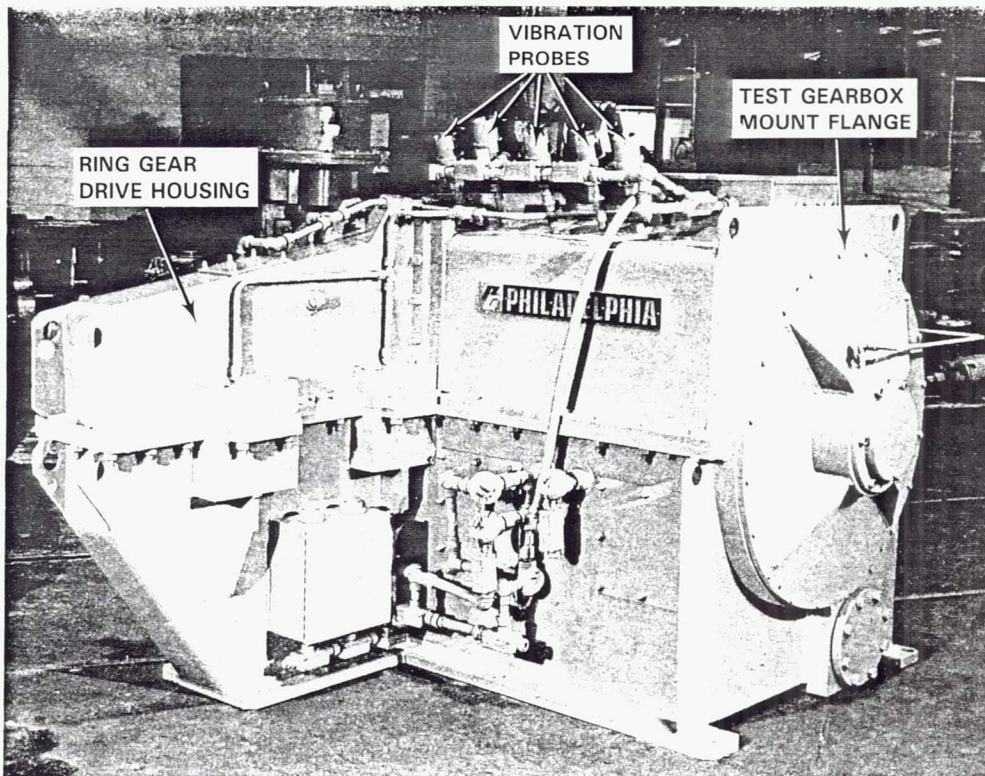


Figure 101 Torquer Unit: Test Gearbox View

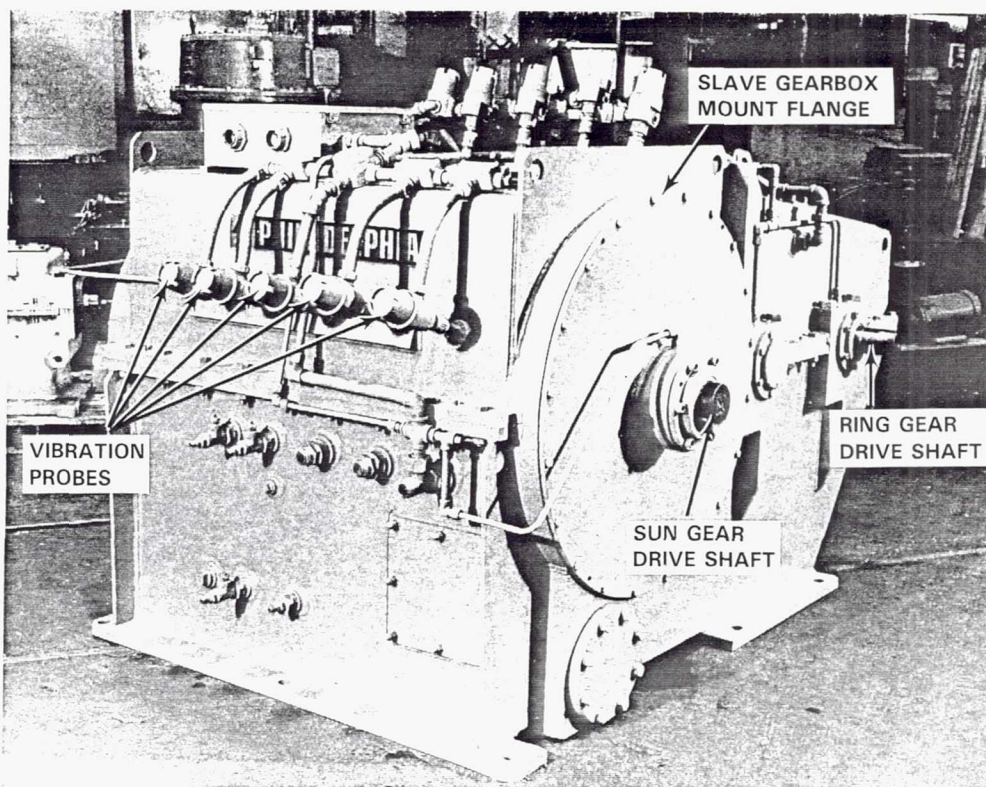


Figure 102 Torquer Unit: Slave Gearbox View

The oil used in the hydraulic systems is also used for lubrication. A lube and load console provides oil for pressure lubrication and for the hydraulic pressure to create torque. The thrust and radial actuation package provides pressure to the hydraulic cylinders which impose thrust and radial loads. An electronic controller amplifies computer signals to control the operation. A separate motor driven scavenge pump is provided.

The torquer is equipped with a ring gear drive which can be used to provide rotational speed to the torquing elements. The gear drive has been designed to allow substitution of another ratio in the future.

The gear drive shafts are mounted on double row tapered roller bearings with one bearing locked in position to take thrust and the other free to float. The torquing elements are supported by the planetary transmissions.

Thermocouples are provided in the radial and thrust bearing and the lubrication manifold and wired to a junction box mounted on the unit. Provisions for future temperature sensors are made at gear shaft bearing locations. Vibration probes are provided at the torquing elements; ten each for the rotating elements and one mounted axially at a shaft shoulder.

Figure 103 shows the multipurpose test rig arrangement.

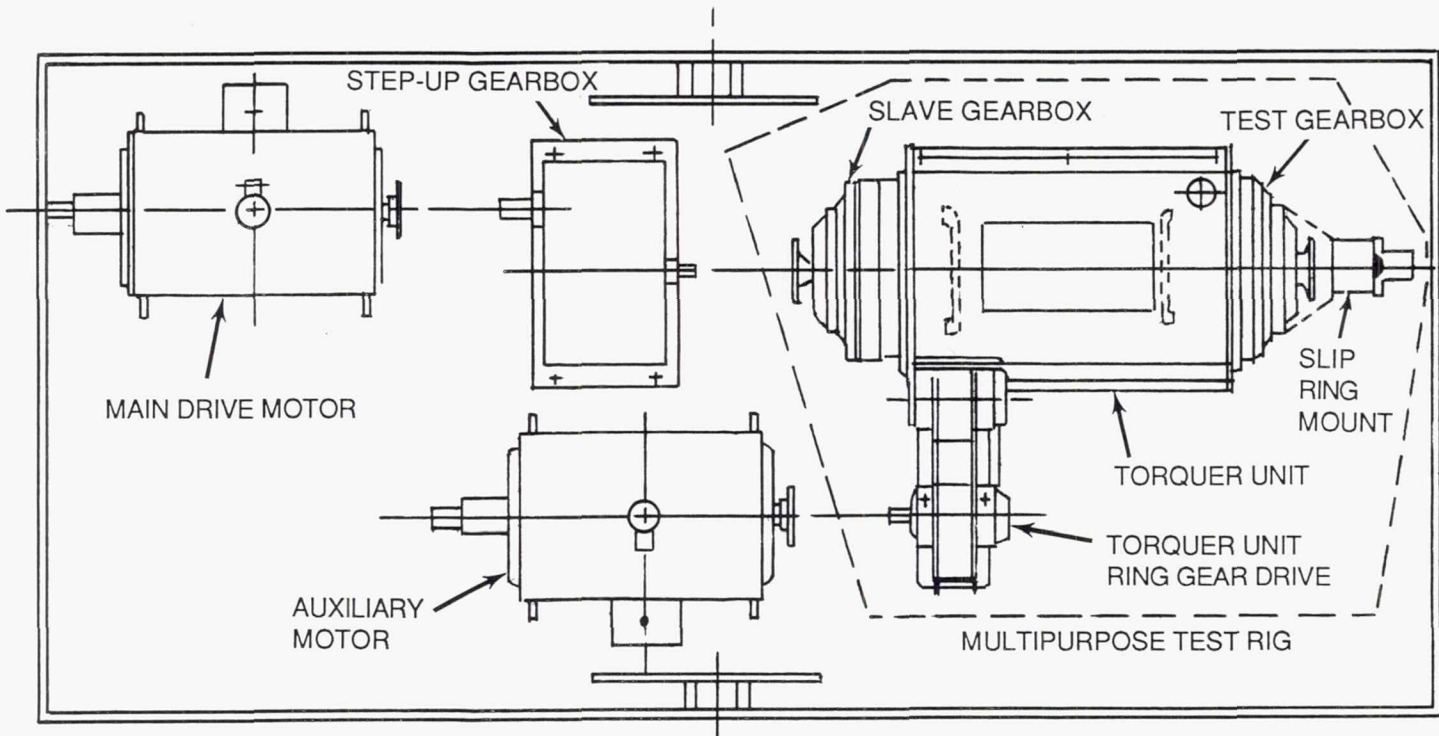


Figure 103 Multipurpose Test Rig as Mounted on Test Facility Testbed (Top View)

A limited 'shakedown' test of the test rig and associated test stand equipment was conducted to ensure that all systems were fully operational prior to initiation of AGBT gearbox testing. Elements of this test were as follows:

- o Operational checks and calibration of the stand controls and data acquisition system.
- o Operational checkout of the auxiliary drive system and the oil heating and cooling systems associated with oil temperature control.
- o Operational checks of the stand-mounted lube and scavenge systems associated with the test and slave gearboxes, the step-up drive gearbox and the torquer unit.
- o Operational checks of the torquer unit back-to-back torque load and unload system and the radial and axial load systems.

Checkout tests were conducted with the testbed in a horizontal position and tilted to 45 degrees. Approximately 10 hours of test time were accumulated at simulated test gearbox speed, load and torque conditions. Corrective action was minor in nature and the operationally-ready test rig has been 'mothballed' pending redefinition of program activities.

### 5.3 Preliminary Test Plan

A preliminary plan for testing of Build 1 of the AGBT gearbox has been formulated, which includes pretest calibrations, functional system checks and the formal gearbox test program. The objectives of the test are to: (1) verify the functional requirements of the lubrication and scavenge systems, (2) verify the performance and structural design intent for the gearbox mechanical components, (3) assess gearbox efficiency and quantify losses, and (4) assess and verify the characteristics of the primary condition-monitoring parameters associated with this gearbox design.

Pretest calibration and functional system check activities are required to prepare the various subsystems and equipment for the actual gearbox rig tests. Some of these will be accomplished during gearbox assembly and others will be accomplished after the test rig is mounted in the test facility. Table 25 summarizes these activities.

The formal gearbox test program comprises an overall system 'shakedown' test phase followed by the gearbox mechanical performance and efficiency verification tests. The principle objectives of the shakedown tests will be to: (1) verify that the rig is mechanically safe to operate, (2) obtain stress survey data in such a way as to preserve the function of the gear tooth strain gages for as long as possible and (3) provide rig operating envelope data that will facilitate more rapid data acquisition during the efficiency test phase. Efficiency testing will focus on evaluation of the lube and scavenge system performance and cooling effectiveness and identification of gearbox performance sensitivity to speed, torque and oil flow. A wide variety of parameters will be investigated and monitored during this portion of the overall test program, as shown in Table 26.

Table 25 Pretest Calibrations and Functional System Checks

At Assembly
<ul style="list-style-type: none"> <li>o Install sensors, verify and document sensor locations</li> <li>o Serialize gears and identify reference teeth; index and locate carrier journal positions with planet gears installed</li> <li>o Correlate sensor periodic waveforms with absolute positions of the carrier assembly and sun and ring gears</li> <li>o Calibrate torque characteristics of the rig sun gear shaft</li> <li>o Correlate sun and ring gear index positions with timing mark references; record planet gear positions on carrier</li> <li>o Acquire tooth contact patterns on sun gear drive tooth flanks and ring gear driven tooth flanks</li> </ul>
At Test Facility
<ul style="list-style-type: none"> <li>o Perform functional check of temperature and pressure sensors as interconnected with indicators and the data system</li> <li>o Calibrate flowmeters, pressure and differential pressure transducers</li> <li>o Perform functional checks of: <ul style="list-style-type: none"> <li>- Dynamic measuring recording instrumentation</li> <li>- Performance data recording equipment</li> <li>- Facility microprocessor and stand controls</li> </ul> </li> <li>o Check alignment of rig with stand gearbox and auxiliary drive motor</li> <li>o Perform functional check of slip ring cooling unit</li> <li>o Verify and correlate the relationship between the sun shaft, carrier and ring gear speed sensors</li> </ul>

Table 26 Test Parameters to be Investigated and Monitored During Gearbox Build 1 Testing

	Shakedown	Mechanical Performance	Efficiency
<u>Verify lubricant/scavenge system:</u>			
Blockage and leakage	X		
Flooding and surging	X		X
Oil temperature and flow within limits	X		
Attitude changes on system performance			X
<u>Assess mechanical performance:</u>			
Free rotation without load	X		
Gear tooth contact patterns	X		
Vibration	X	X	
Noise	X	X	
Bearing temperatures	X	X	
Gear tooth stress limits:			
o Load sharing between planets	X	X	
o Dynamic load effects	X	X	
o Verify tooth patterns	X	X	
o Gear mesh alignment	X	X	
Particulates in oil	X	X	
Thrust and side load effects on gear mesh		X	
Seal operation		X	
Teardown inspection		X	
<u>Assess efficiency:</u>			
Contributions of various components			X
Speed versus torque effects			X
Variations in lube flow			X
Scavenge effectiveness			X
<u>Assess condition monitoring parameters:</u>			
Vibration signature		X	
Oil system chemistry/particulates		X	
Oil $\Delta T$		X	X
Noise signature		X	

## 6.0 SUPPORTING TECHNOLOGY PROGRAMS

Two contractor-funded supporting technology programs, a scavenge rig test program and a lubrication rig test program, were conducted to help define the scavenge and lubrication system features to be incorporated into the AGBT gearbox design described in the earlier sections of this report. Two rig configurations were used: one for the housing scavenge space, and one for lubrication of the sun/planet gear mesh. These programs are described in the following sections.

### 6.1 Scavenge Rig Test Program

The objective of the scavenge rig test program was to evaluate the potential of three scavenge configurations to reduce power loss associated with inefficient removal of oil from the ring gear compartment. The three scavenge designs investigated (shown in Figure 104) were: (1) double scroll collector, (2) louvered annulus and (3) constant volume. The double scroll and louvered annulus configurations were thought to offer potential for scavenging more effectively from the top portion of the ring gear. The double scroll design would accomplish this through an aerodynamic pumping action in the flow channels, whereas the louver design would capture and direct the flow into the annulus through louvers. The test results, however, did not bear out this potential in either of those cases; the constant volume configuration was the most efficient and was selected for the AGBT.

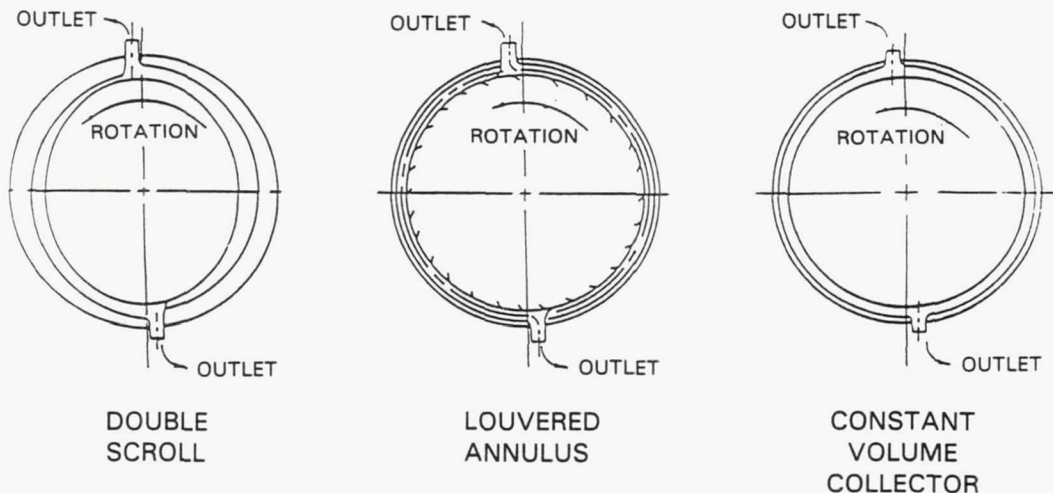


Figure 104 Collector Insert Configurations - Designs to evaluate scavenging effectiveness.

#### 6.1.1 Test Rig Description

A test rig (Figure 105) was designed and fabricated. The rig housing and bearing support were designed to accommodate a simulated ring gear rotor and scavenge compartment for scavenge tests and a sun gear/planet gear transmission for subsequent lubrication tests. Provisions for suitable instrumentation were provided, and plexiglas<sup>TM</sup> viewing ports were incorporated into the rig case design to provide visual inspection of gear train hardware and lubricant flow during testing. Air and oil were introduced through separate pipes at the rotor centerline in a range of proportions representative of anticipated flight design gearbox requirements.

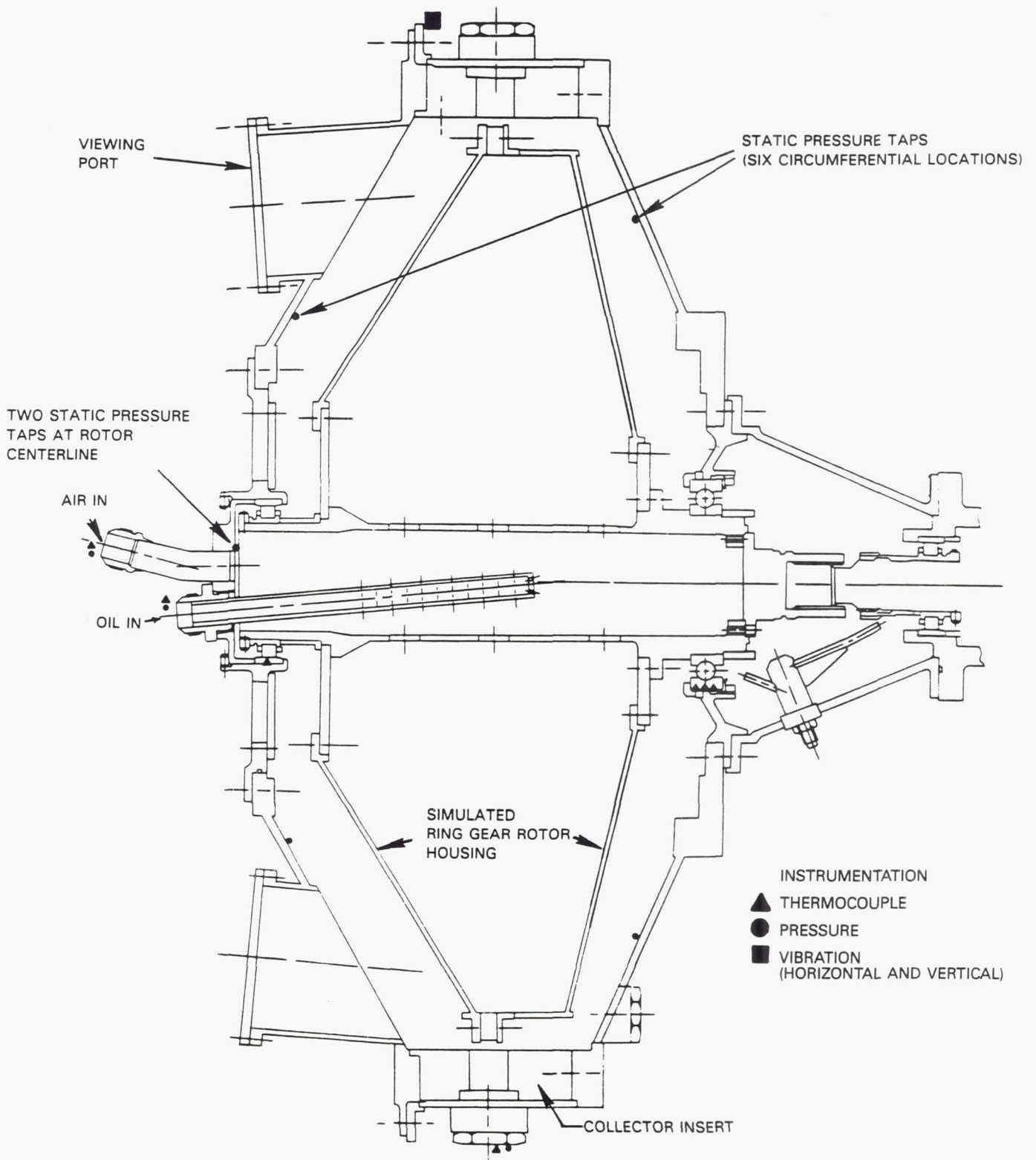


Figure 105 Test Rig - Configured for Scavenge Tests

### 6.1.2 Test Plan

A test plan was formulated to evaluate the candidate scavenge schemes. Scavenge effectiveness was measured by the amount of power required to drive the rig; the higher the power, the lower the effectiveness (and vice versa). Two oil flows were introduced: one representing the planetary gear and bearing flows (main oil flow), and the other representing the remaining lubrication requirements (auxiliary oil flow). Air was also injected to investigate its influence on power consumption. The test matrix is shown in Table 27.

Table 27 Scavenge Rig Test Plan

Test Parameter	Double Scroll	Louvered Annulus	Constant Volume
Variable ring gear speed, 600-1235 RPM	X	X	X
Variable main oil flow, 45.4-90.7 kg/min (100-200 ppm) with auxiliary oil flow at 18.1 kg/min (40 ppm)	X	X	X
Variable main oil flow only, 45.4-90.7 kg/min (100-200 ppm)	X		
Variable injection airflow at 1235 RPM; main oil flow = 90.7 kg/min (200 ppm), auxiliary oil flow = 18.1 kg/min (40 ppm)	X	X	X

ppm = pounds per minute

### 6.1.3 Test Results

Results from the scavenge tests (presented in Figures 106 through 109) show power consumption increases with ring gear speed as expected.

Figure 106 also shows that when 18.1 kg/min (40 ppm) auxiliary oil was introduced independent of ring gear speed, power consumption increased about 15% in the double scroll configuration.

Data (Figures 107 and 108) show that the constant volume configuration had the highest scavenge effectiveness (lowest power consumption) over the range of test parameters evaluated. Adding the double scroll or louvered collector inserts appears to have impeded aerodynamic scavenging and decreased the effective flow discharge area, providing a more restrictive scavenge flowpath to the lubricant discharge ports.

The addition of air at the maximum ring gear speed of 1235 RPM (Figure 109) had no beneficial effect on power consumption.

As a result of these tests, the constant volume collector design was chosen for the AGBT.

## 6.2 Lubrication Rig Test Program

The objective of the lubrication rig test program was to optimize the approach to lubrication of the planetary gear system in order to minimize both wear and heat generation. The focus of the test effort was on the potentially high loss scavenge region in the triangular spaces enclosed by the sun gear and two adjacent planet gears (Figure 110).

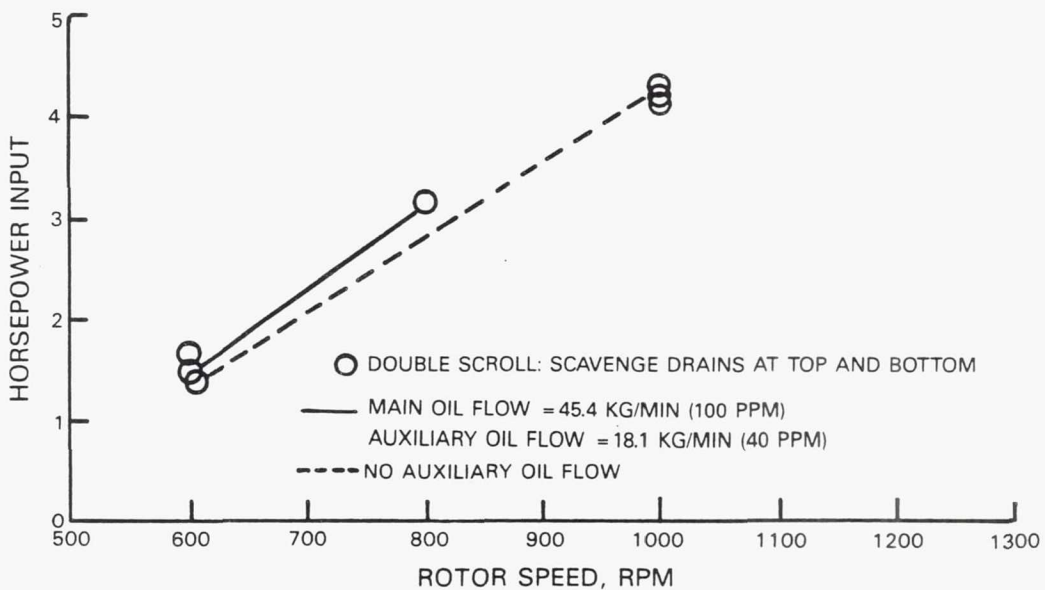


Figure 106 Power Consumption Versus Oil Flow - Power increased 15% when 18.1 kg/min (40 ppm) auxiliary oil was introduced into the double scroll configuration.

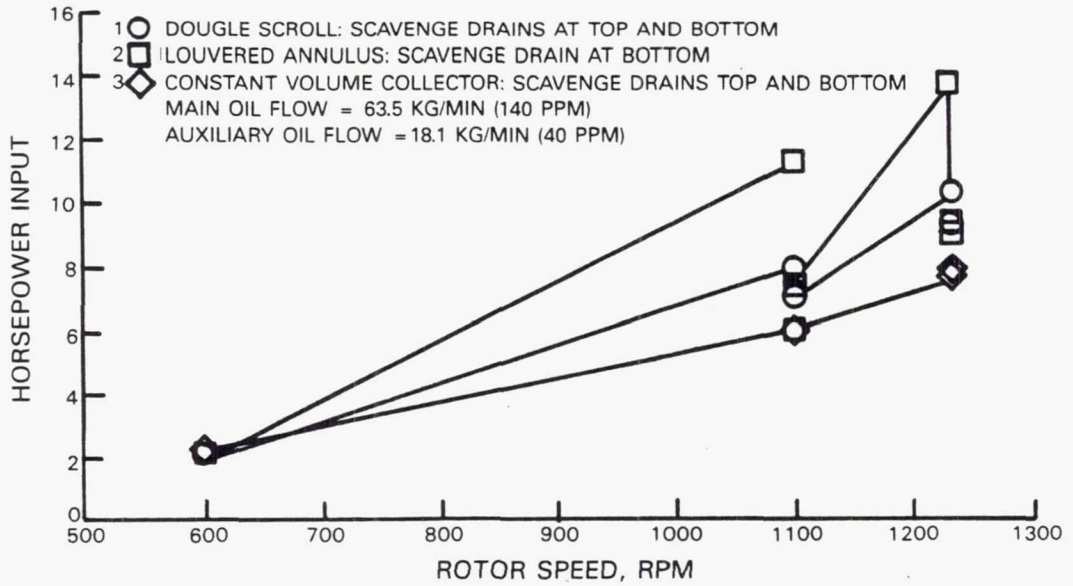


Figure 107 Oil Scavenge Design Effectiveness - Constant volume collector configuration was best.

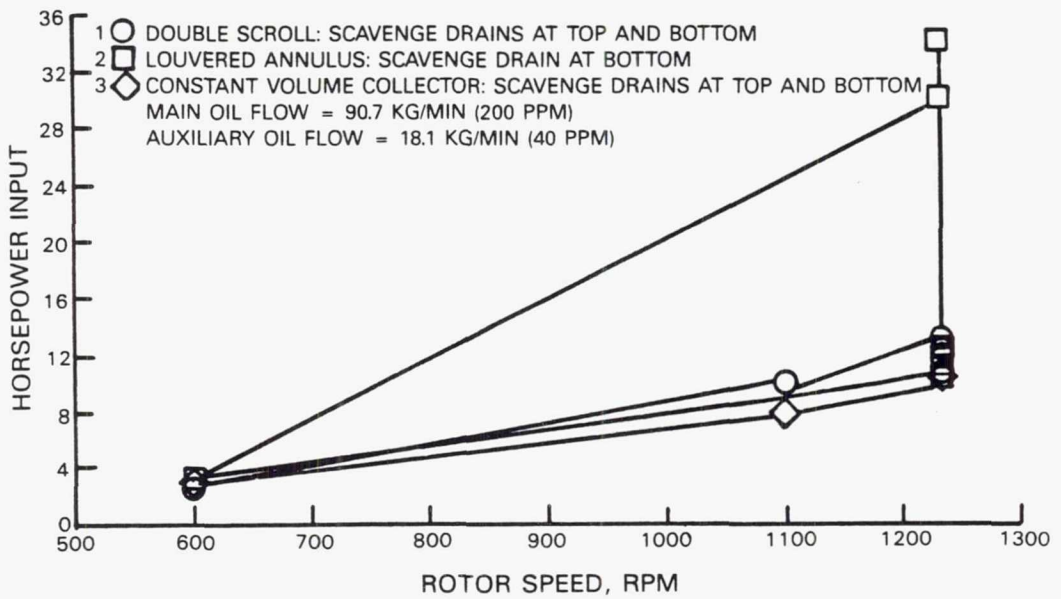


Figure 108 Oil Scavenge Design Effectiveness - Constant volume collector configuration was best.

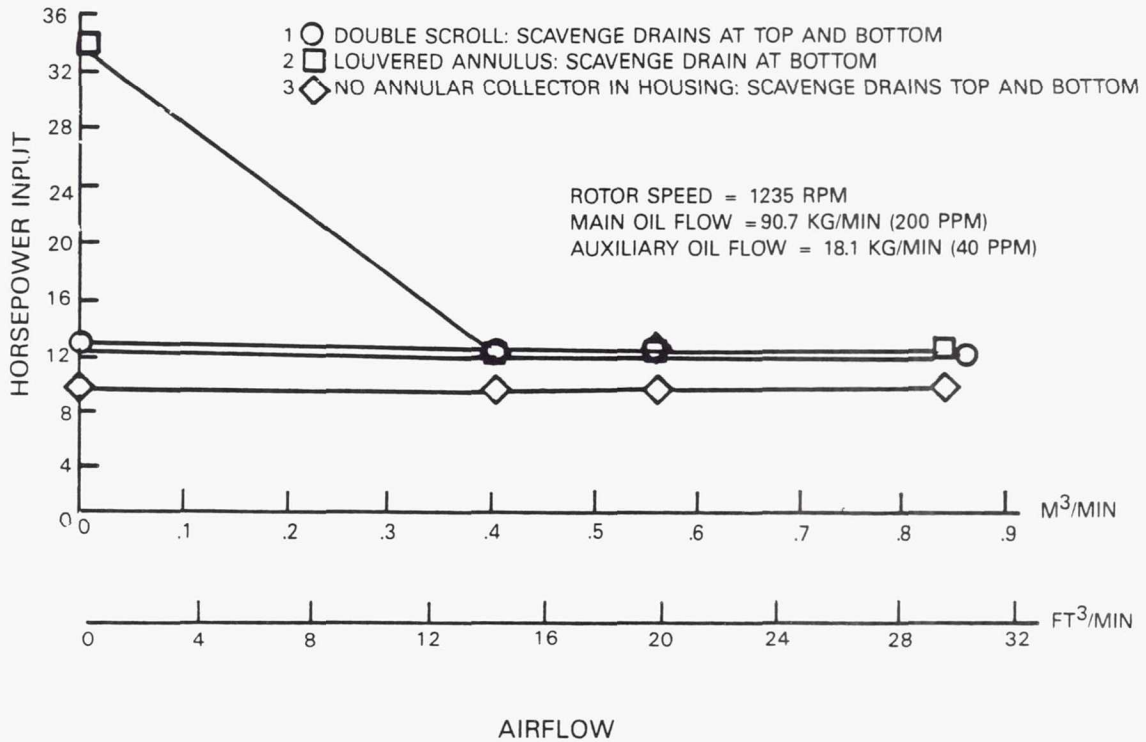


Figure 109 Power Consumption with Added Air - No impact on scavenge effectiveness.

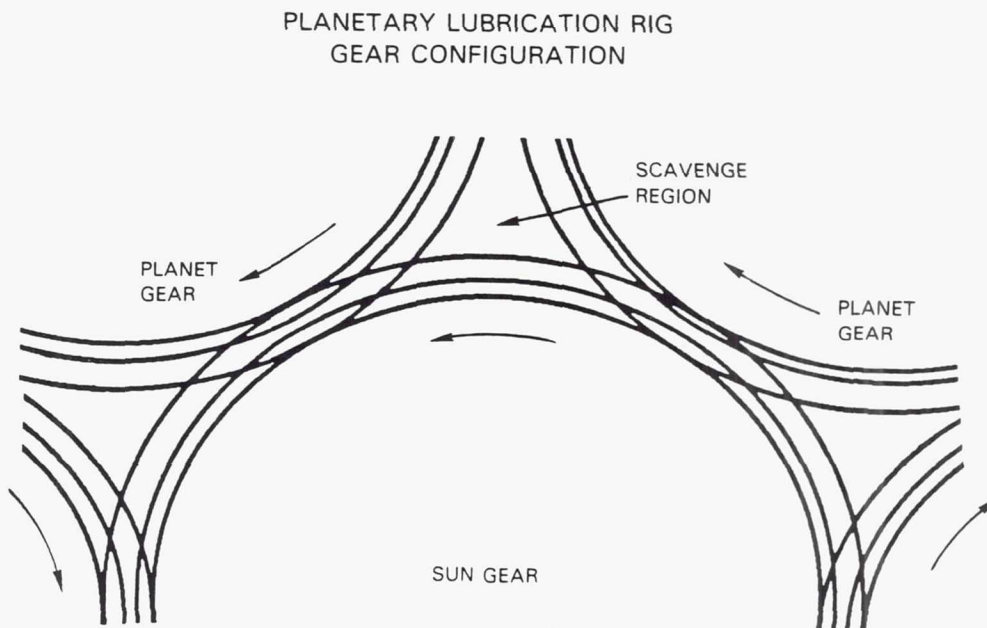


Figure 110 Planetary Lubrication Rig Gear Configuration

### 6.2.1 Test Rig Description

The test rig utilized in the scavenge rig test program was modified for lubrication testing as shown in Figure 111. The ring gear rotor assembly was removed and replaced by a sun/5 planet gear assembly. The housing was modified to provide for mounting oil supply tubes necessary to service the pinion bearings and the gear mesh triangle being investigated during the tests. Existing gears were utilized for the tests. The planetary gears were fixed in their circumferential positions (i.e., not free to rotate around the sun gear), and no external load was applied to them. This meant that power required to drive the rig was basically limited to that necessary to overcome bearing and gear tooth friction losses, oil churning losses and gear windage losses. The sun gear was mounted to the drive shaft through a 'loose' spline coupling and was cantilevered from the drive shaft. This arrangement was designed to accommodate load sharing between the sun and planet bearings. Power input to the rig was measured by a torque meter mounted on the rig drive shaft.

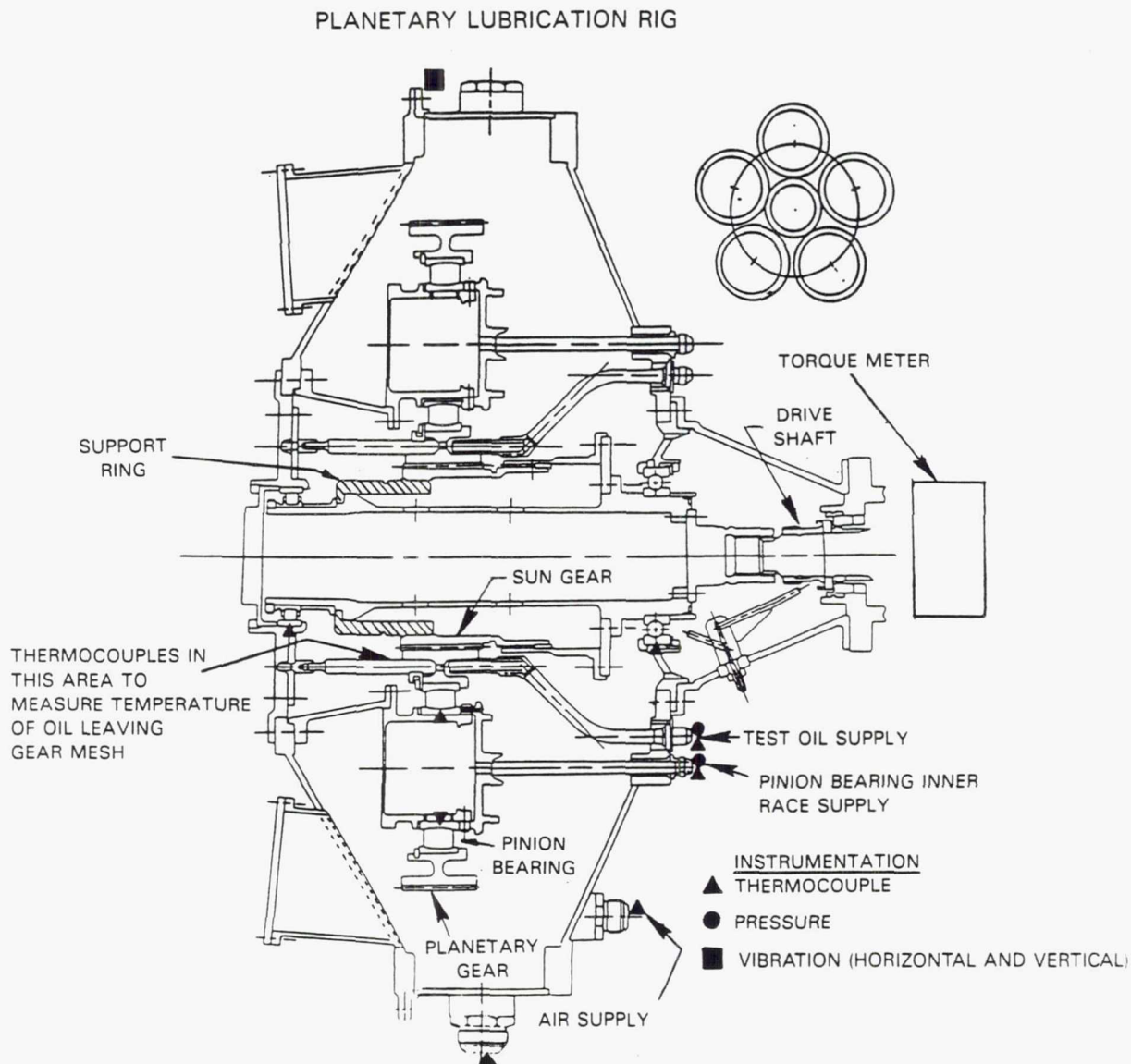


Figure 111 Test Rig as Configured for Lubrication Tests

During the initial rig shakedown test, high vibration was encountered which investigation attributed to a 'bounce' mode set up between the sun and planet gears in the lightly-loaded gear train. The solution was to modify the sun gear drive from a flexible mount to a rigid mount. This was accomplished by tightening the spline fit and adding a support ring between the ring gear and the drive shaft (Figure 111). The rig ran smoothly with these modifications.

Shakedown testing also showed that no benefit was achieved by the addition of airflow in the triangular scavenge space to enhance oil outflow from these spaces. Consequently, airflow variation was deleted from the test plan.

Instrumentation was provided to measure oil flow rates and temperature rise during testing and to monitor bearing temperatures and rig vibration.

### 6.2.2 Gear Lubrication Test Plan

The test plan outlined in Table 28 was formulated to assess the effectiveness of several oil spray configurations to reduce the losses associated with oil scavenging in the triangular spaces between the sun gear/planet gear (see Figure 112). To conduct these tests, the test rig was fitted with primary and secondary flow spray bars (Figure 112). Sun gear speed was varied to a maximum of 9035 RPM (design speed), and oil flow included rates typical of gearbox requirements at cruise power 11.8 kg/min (26.0 lb/min) and takeoff power 31.4 kg/min (69.3 lb/min). Oil supply temperature for all tests was held constant at 93°C (200°F) and oil flow to the planet bearings was held constant at 6.8 kg/min (15.0 lb/min).

Three spray bar configurations were investigated, with oil flow directed out-of-mesh relative to gear rotation. The first configuration incorporated both primary and secondary spray bars with the oil flow directed radially into the gear (Figure 112A). The second configuration incorporated only the secondary spray bar to determine whether or not increasing the available triangular space area would enhance oil scavenging in the gear mesh (Figure 112B). In the third configuration, the primary and secondary spray bars were modified (Figure 113C) to direct the oil flow onto the gear face with an axial component to enhance outflow from the mesh. Pressure transducers were mounted in line with the sun gear root-planet gear tip clearance area and displaced about 0.318 cm (0.125 in) from the sun gear face (Figure 114) to measure the pressure of the oil exiting the gear mesh. This measurement provided a qualitative indication of relative velocity of the oil exiting the mesh, and therefore the work generated by the process of gear tooth pumping in the gear interface region.

### 6.2.3 Gear Lubrication Test Results

The gear lubrication test results are shown in Figures 115 through 118. Input power consumption is plotted versus sun gear speed for several out-of-mesh oil spray configurations in the triangular spaces between the sun gear/planet gear mesh.

Table 28 Gear Mesh Scavenge - Phase I Test Plan (Oil Supply Temperature = 93 C (200 F))

Spray Bar Configuration	Oil Flow, kg/min (ppm)			
	Primary Spray Bar	Secondary Spray Bar	Total Gear	Planetary Bearings
1) Primary and secondary spray bars in place				
<u>Test Sequence:</u>				
Reference Baseline	0	0	0	0
Test number 1	0	0	0	6.8 (15.0)
Test number 2	11.8 (26.0)	0	11.8 (26.0)	6.8 (15.0)
Test number 3	11.8 (26.0)	9.8 (21.5)	21.5 (47.5)	6.8 (15.0)
Test number 4	11.8 (26.0)	19.6 (43.3)	31.4 (69.3)	6.8 (15.0)
2) Primary spray bar removed				
<u>Test Sequence:</u>				
Test number 1	0	0	0	6.8 (15.0)
Test number 2	0	11.8 (26.0)	11.8 (26.0)	6.8 (15.0)
Test number 3	0	21.5 (47.5)	21.5 (47.5)	6.8 (15.0)
3) Primary and secondary spray bars in place; angled jets				
<u>Test Sequence:</u>				
Test number 1	11.8 (26.0)	0	11.8 (26.0)	6.8 (15.0)
Test number 2	11.8 (26.0)	19.6 (43.3)	31.4 (69.3)	6.8 (15.0)

PLANETARY LUBRICATION RIG  
 SPRAY BAR CONFIGURATIONS

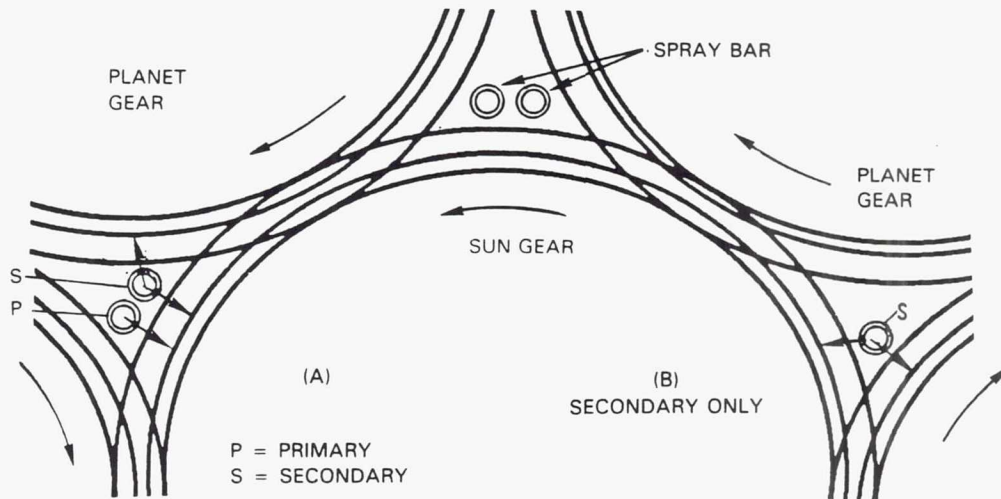


Figure 112 Planetary Lubrication Rig Spray Bar Out-of-Mesh Configurations - For testing effectiveness in reducing losses in triangular spaces between gears.

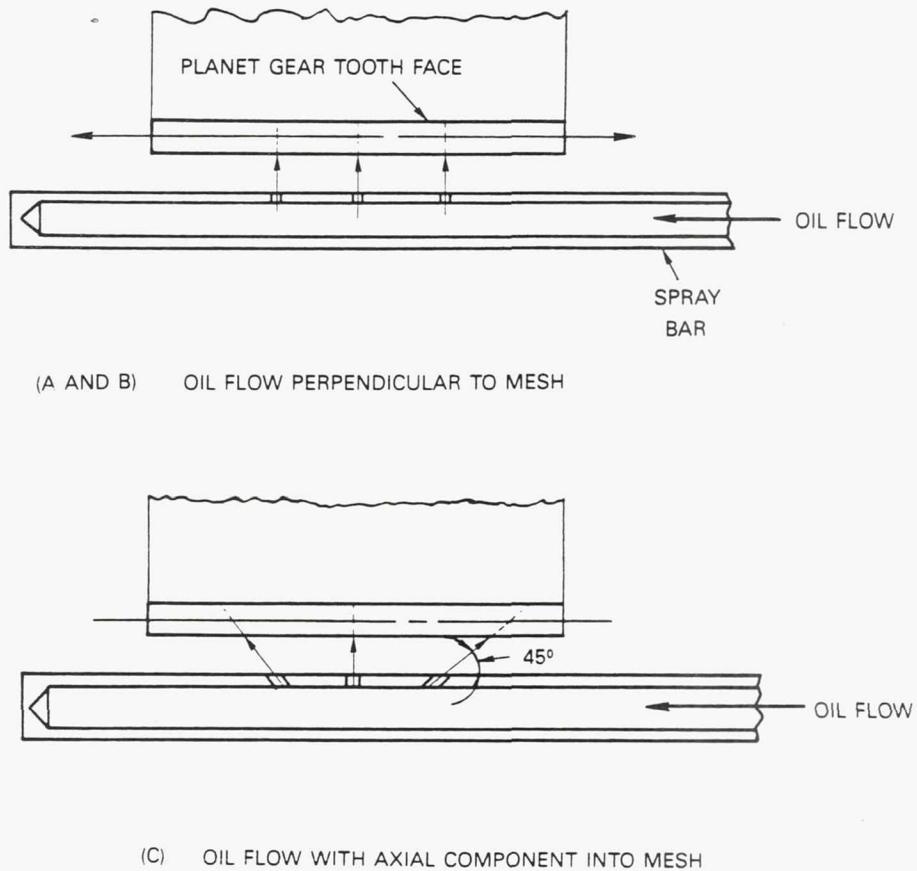


Figure 113 Lubrication Spray Angle Test - To evaluate effectiveness of an axial component of flow.

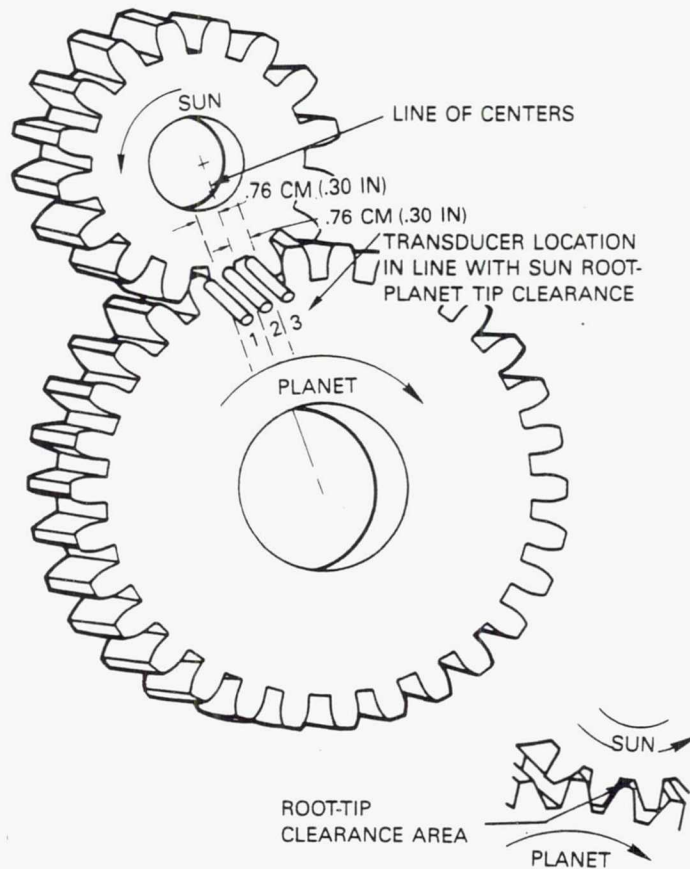


Figure 114 Pressure Transducer Locations for Gear Mesh Scavenge Oil Pressure Measurements - Provides an indication of gear tooth pumping work.

In Figure 115, test data show power consumption increases by 30% when secondary oil flow is added to simulate takeoff conditions; 31.4 kg/min (69.3 lb/min), relative to the use of primary oil flow only required for the cruise power condition; 11.8 kg/min (26.0 lb/min). These data support the use of a two-position modulated lubrication system, which takes advantage of lower power loss (i.e., greater efficiency) by shutting off the secondary oil supply at low power conditions where it is not required.

A series of test points was taken to investigate the effect that a two spray bar configuration (one supplying primary oil and one supplying secondary oil) has on increased drag and power consumption. The results of this testing, shown in Figure 116, indicated relative insensitivity in power consumption to removal of the primary spray bar. Further, the results were inconclusive; in one comparative set of data (lower set shown) removal of the primary spray bar caused a small increase in power consumption, whereas in the other set (upper curves) the removal caused a slight decrease in power consumption. The design configuration for the AGBT uses a single spray bar incorporating both primary and secondary flow jets.

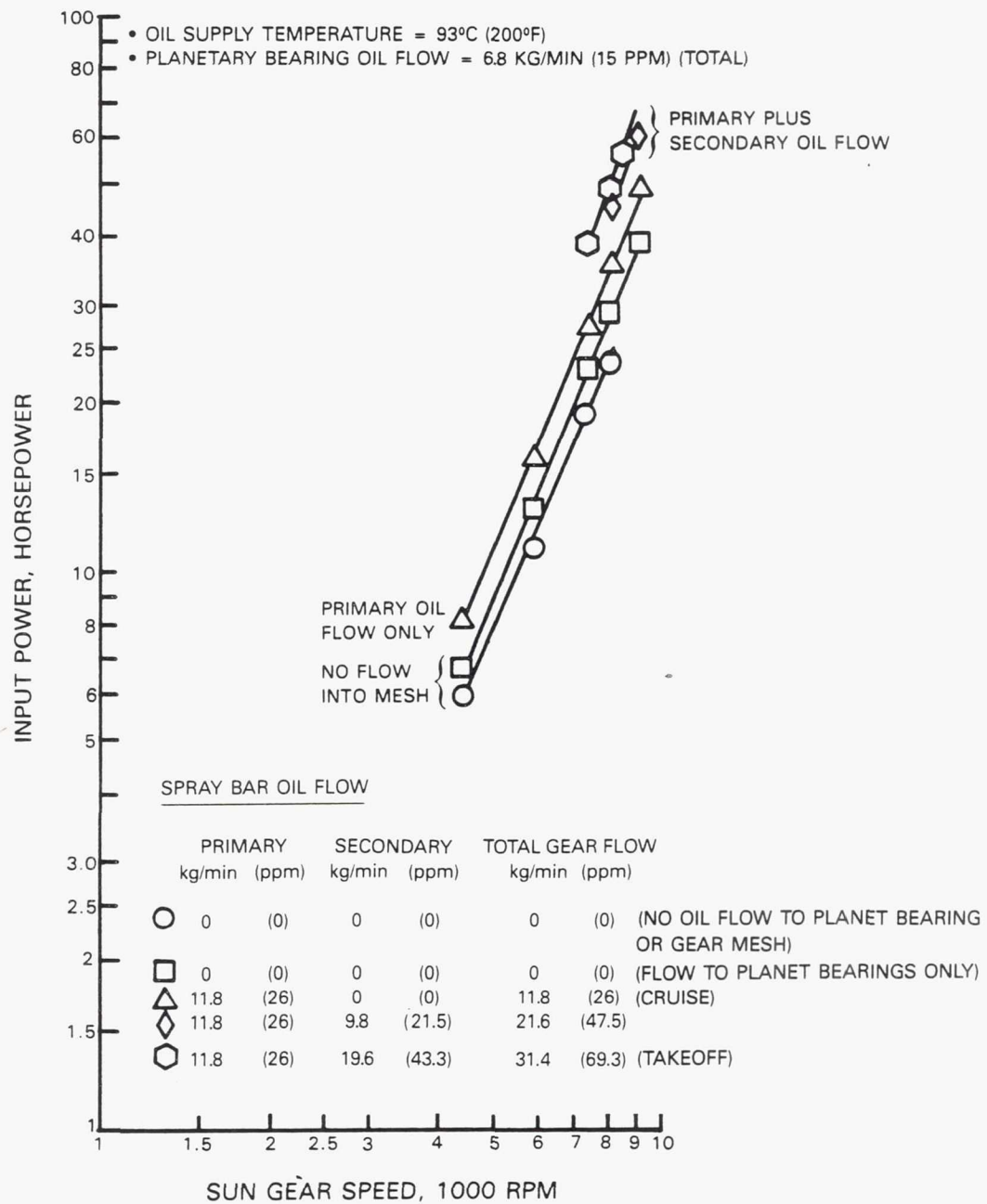


Figure 115 Planetary Lubrication Rig: Input Power Versus Sun Gear Speed; Primary and Secondary Spray Bars Installed - Power consumption increases by 30% at takeoff oil flows.

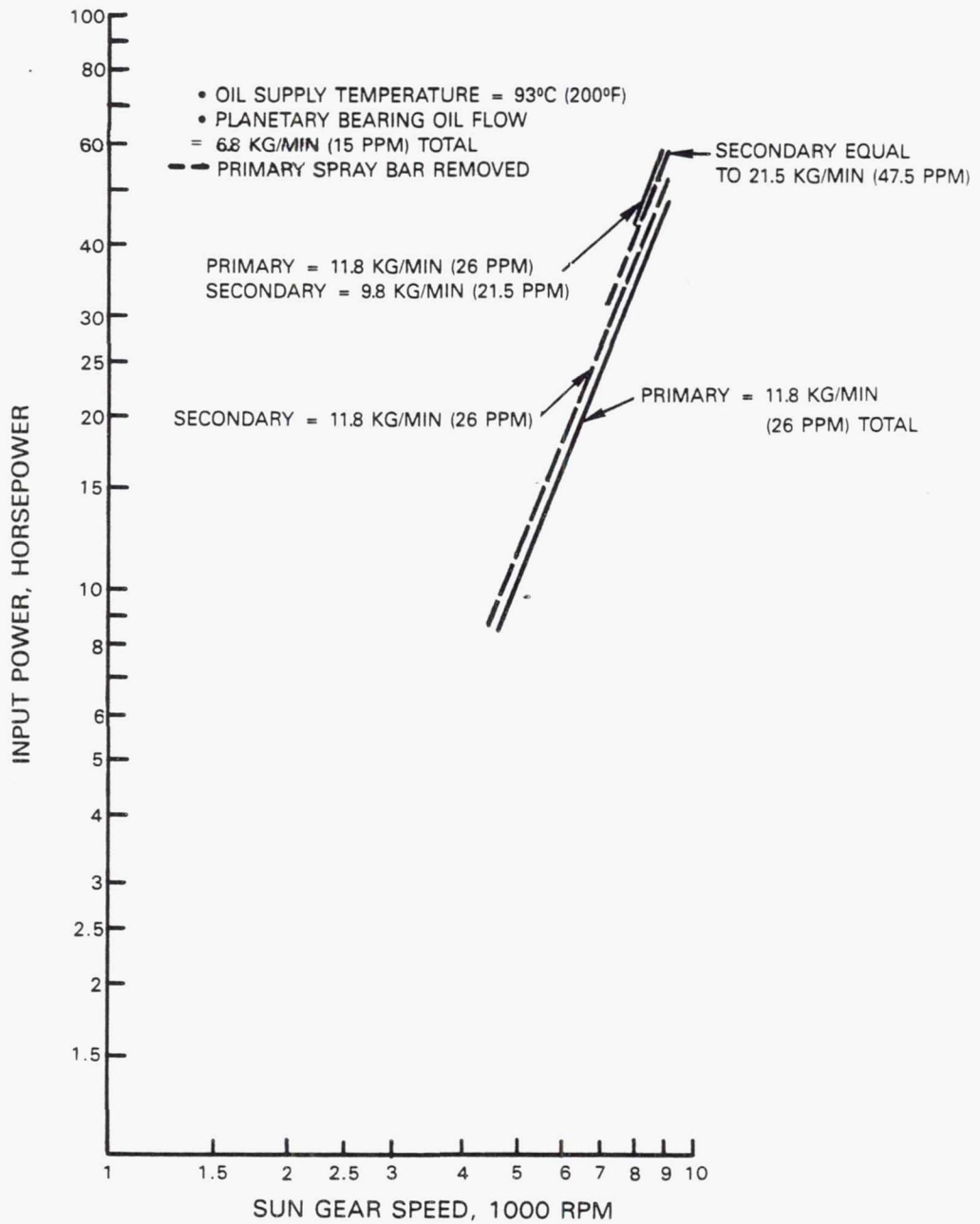


Figure 116 Planetary Lubrication Rig: Comparison of Results With and Without Primary Spray Bars Installed - Power consumption was relatively insensitive to removal of the primary spray bar.

Figures 117 and 118 show the results of testing with the angled oil jets. These data show no significant benefit was obtained with the angled oil jets at a primary-only oil flow of 11.8 kg/min (26.0 lb/min). The addition of 19.6 kg/min (43.3 lb/min) secondary flow increased overall power consumption, but the angled oil jets provided a nominal 10% reduction in power consumption at a total spray bar oil flow of 31.4 kg/min (69.3 lb/min). This suggests a relationship between gear mesh scavenge effectiveness and axial impingement angle that is flow dependent. Further testing is required to fully understand this relationship.

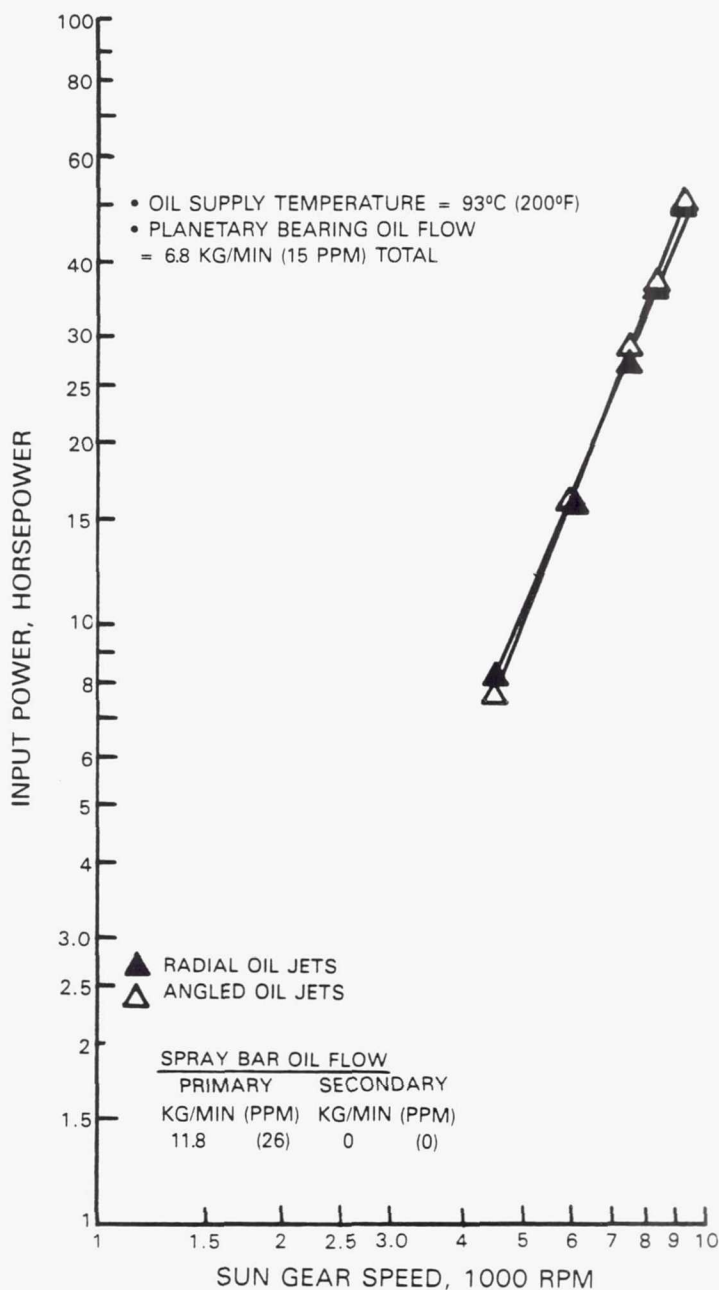


Figure 117 Angled Oil Jets Versus Radial Oil Jets - No change is evident with primary oil flow only.

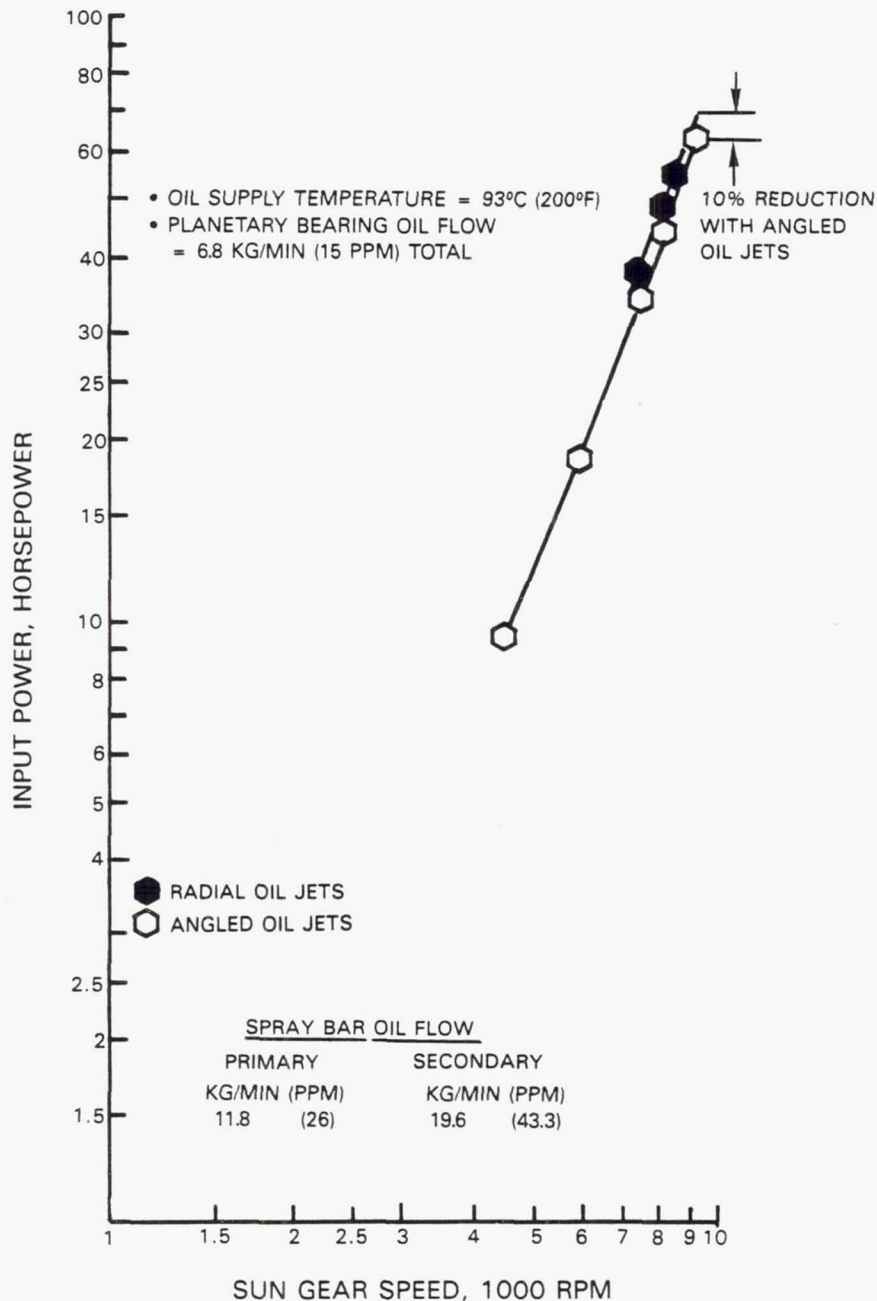


Figure 118 Angled Oil Jets Versus Radial Oil Jets - A 10% reduction in power consumption is achieved with angled jets when secondary flow is added.

Data taken from the three kulite pressure transducers (locations shown in Figure 114) showed pressure exceeding the 1.38 MPag (200 psig) range of the transducers. Post test calibration of the transducers showed no damage had been sustained during the test, adding confidence to the indication of high static and dynamic oil pressure exiting the sun/planet mesh. This test, while failing to obtain quantitative results, nevertheless showed the value of instrumenting for pressure measurements in this area, since power required is a function of gear mesh exit oil pressure.

A general observation from these tests is that oil flow rates required for lubrication and cooling of the sun/planet gear meshes should not produce excessive churning in the AGBT tests.

#### 6.2.4 Windage Loss Test Plan

The objective of this test was to obtain a preliminary indication of the magnitude of windage losses in the gear train and to assess their sensitivity to lubricant air/oil mixture ratio. To accomplish this, oil flow to the rig was reduced to zero, and tests were conducted over a sun gear speed range with rig gear compartment pressure at ambient and subsequently reduced by vacuum to a level of 0.05 MPaa (7.5 psia). Ambient pressure is representative of an air/oil mixture containing approximately 23% oil, and 0.05 MPaa (7.5 psia) represents a mixture containing approximately 6% oil. Tests were run in rapid sequence to control bearing heat-up to acceptable levels.

#### 6.2.5 Windage Loss Test Results

Results of the windage tests are shown in Figure 119. A 15% reduction in power consumption was obtained with 37.1 cm (14.6 in) Hg vacuum (equivalent to an altitude of approximately 5486.4 meters (18,000 feet)). This beneficial effect would be present at altitude conditions in the unpressurized compartment design, and would contribute to improving efficiency above the calculated value which did not account for this effect.

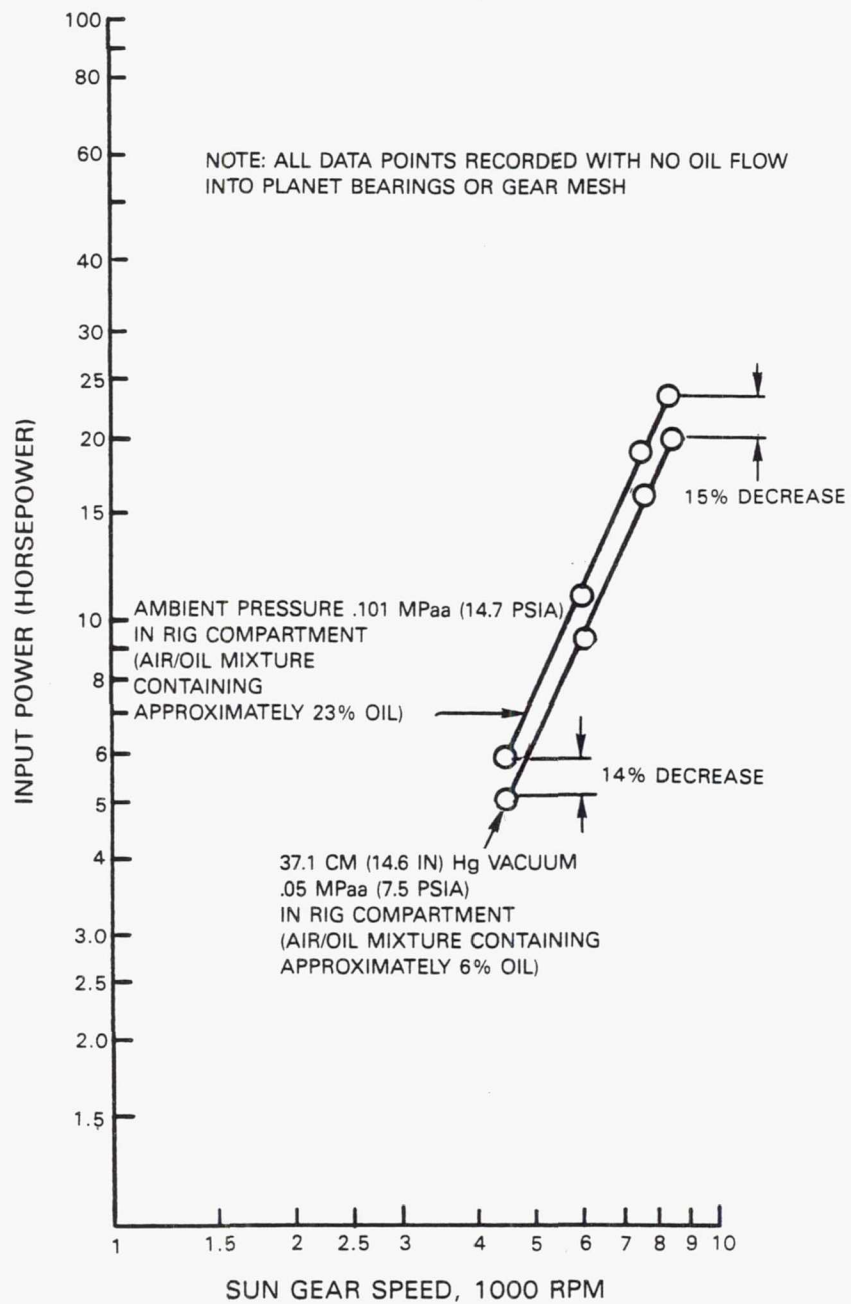


Figure 119 Planetary Lubrication Rig: Effect of Air Windage on Power Losses - A nominal 15% reduction in power consumption was achieved with 37.1 cm (14.6 in) Hg vacuum.

## 7.0 SUMMARY AND CONCLUSIONS

An advanced, in-line counter-rotating (CR) differential gearbox has been designed and fabricated to evaluate the efficiency, durability and weight characteristics of this gearbox concept as they relate to emerging propfan-powered airplane performance and flight worthiness requirements. Principal features of the design include:

- o 8.315 reduction ratio
- o Remote pitch control
- o Straddle-mounted prop shaft/ring gear support bearings
- o 5 planet gear planetary system
- o High contact ratio buttress gear tooth form
- o Single row spherical roller planet bearings integral with planet gears
- o Combination ball/roller prop shaft support bearings
- o Modulated gearbox lubrication supply system coupled to a scavenge system and separate from the engine lube system.

The test gearbox was designed for 12,000 HP (nominal) with growth capability to 15,000 HP. The principal design criteria were based on meeting a fully developed gearbox durability goal of 30,000 hours MTBUR and an efficiency goal equal to or greater than 99%. Advanced technology materials applicable to the durability goal include high strength bearing materials such as CRB7 and high hot hardness Carpenter EX-53 steel gear material. Provision has also been made for testing with advanced high temperature capability lubricants. Sufficient instrumentation is included in the test gearbox design to accurately assess the performance and structural-dynamic characteristics of the gearbox and to provide essential on-line condition monitoring during gearbox testing.

A fully automated test facility and test rig have been provided by the Contractor for future test evaluation of the gearbox. In addition, two Contractor-funded supporting technology programs provided data to assist in the gearbox design definition. The first, a scavenge test program, showed that a constant volume collector configuration had the highest scavenge effectiveness of three configurations tested, and that the addition of airflow has no noticeable impact on scavenge effectiveness. The second, a lubrication test program, showed that gearbox losses could be reduced by controlling the air/oil mixture ratio of the gearbox lubricant and by imparting an axial component to the oil jets flowing into the sun/planet gear mesh. The lubrication tests confirmed the benefits associated with a modulated lubrication supply system.

Testing of this advanced technology gearbox configuration is expected to yield an efficiency of 98.7% in the first build. Planned testing of additional builds and continuing supporting technology tests are expected to provide the data base necessary to achieve the goal efficiency of 99%+. These tests will also confirm the additional benefits of the advanced technologies incorporated into the gearbox design.

## REFERENCES

1. Advanced Propfan Engine Technology (APET) Single- and Counter-rotation Gearbox/Pitch Change Mechanism, Final Report, Volumes I and II (Contract Number NAS3-23045), NASA CR-168114, July 1985.
2. Akin and Townsend, D.P.; Lubricant Jet Flow Phenomenon in Spur and Helical Gears with Modified Center Distances and/or Addendums for Out-of-Mesh Conditions; NASA TM83723, 1984.
3. Lundberg, G., Palmgren, A.; Dynamic Capacity of Rolling Bearings; Publication Date, 1947.

### List of Symbols

ADR	Automatic data recording
AGBT	Advanced Gearbox Technology
AGMA	American Gear Manufacturers Association
APET	Advanced Propfan Engine Technology
ATP	Advanced Turboprop
BCAR	British Civil Airworthiness Requirements
Btu	British thermal units
C	Celsius
ccw	Counterclockwise
C <sub>c</sub>	Centerline
cm	Centimeter
CR	Counter-rotating
cw	Clockwise
Defl, $\delta$	Deflection
deg	Degrees
DFI	Double flange inner
DOC	Direct operating cost
DP	Diametral pitch
EFH	Engine Flight Hour
F	Fahrenheit
FAR	Federal Air Regulations
F <sub>b</sub>	Gear tooth bending stress
F <sub>c</sub>	Gear tooth compressive (hertz) stress
FEA	Finite element analysis
FPS	Feet per second
ft	Feet
ft-lb	Foot-pound
FW	Gear tooth face width
Fwd	Forward
G	Gravity
HCF	High cycle fatigue
HCR	High contact ratio
Hg	Mercury
HP	Horsepower
I	Interest
in	Inch
in-lb	Inch pound
kg	Kilogram
km	Kilometer
ksi	Kips per square inch
lb	Pound
LCF	Low cycle fatigue
m	Meter
max	Maximum
mm	Millimeter
min	Minute
Mn	Mach number
MPa	Megapascal
MTBUR	Mean time between unplanned removals
N	Newton
NASA	National Aeronautics and Space Administration
N/A	Not available

List of Symbols (Continued)

Nm	Newton meter
OD	Outer diameter
P	Propeller moment
p-r	Planet to ring
plan	Planetary
ppm	Pounds per minute
psi	Pounds per square inch
P&W	Pratt and Whitney
Qty	Quantity
R	Radius
rad	Radians
R.A.S.	Royal Aeronautical Society
Rc	Rolling contact
rms	Root mean square
RPM	Revolutions per minute
sec	Second
SHP	Shaft horsepower
SLTO	Sea level takeoff
spec	Specification
s-p	Sun to planet
std	Standard
$\Delta T$	Temperature change
Tc	Thermocouple
TH	Maximum continuous thrust
TR	Reverse thrust
UTS	Ultimate tensile strength
$\phi$	Gear tooth pressure angle
$\sigma$	Stress